An adaptive D-STATCOM control scheme utilising impedance estimation

Christopher James Rose, BEng.

Thesis submitted to The University of Nottingham
for the degree of Doctor of Philosophy

September 2015

Abstract

Concerns for energy security and the environment are driving significant changes in the way electrical power is generated and distributed. In many parts of the world, electrical power systems are gradually changing from centralised systems with a small number of large generators and substations performing most control operations to distributed systems, with a large number of devices providing control at a local level. Power electronic converters have an increasingly important role to play in modern electrical power systems. One example of power electronics in such systems is the STATCOM, a power electronic device which can be used to provide an efficient and effective means of controlling power system voltages. This thesis presents an investigation into STATCOM voltage control for distribution level power networks.

In this work, a STATCOM voltage control structure is proposed and an impedance estimation algorithm is used to tune the controller gains in order to achieve the desired dynamic performance. This work demonstrates that the use of impedance estimation for controller tuning allows the STATCOM dynamics to remain consistent when installed on different systems or if the system impedance should change. In addition to proposing the voltage control structure, this thesis also proposes improvements to an earlier impedance estimation method, taking into account changes in converter structures and control methods since the method was first proposed.

Acknowledgements

I would like to begin by thanking my supervisors: Professor Mark Sumner, Professor Dave Thomas and Dr Ed Christopher. Their advice, guidance and support throughout this project has been invaluable and I have benefited enormously from their combined knowledge and experience.

I would also like to thank all other academics and researchers within the PEMC group, both students and staff, who have helped or contributed to this work in any way. There are too many people to name individually but I would particularly like to thank those I have worked closely with at one time or another: Richard Davies and Seksak Pholboon and everyone else in the "FlexElec" lab, Ke Jia, Saul Lopez Arevalo, Jing Li, Yang Cao, Ewan Farr and David Hind.

The technical support provided through the tireless work of Colin Blackburn and his team has been a great help in allowing this work to be completed. I would therefore like to offer my thanks to Colin and all the other technicians who have helped with this work in any way.

Thank you to my parents for allowing me to be a student for far too long. Thank you to my partner, Eleanor, for tolerating me and offering her love and support when it was most needed. Finally, the cats, Versace and Marie, for their nonsense contributions and friendly bites reminding me to work and not play ...

Contents

List of Figures

List of Tables

Publications by the author

The work detailed in this thesis has resulted in the publication of a number of papers by the author:

1. C. Rose, D. Thomas, M. Sumner, E. Christopher and S. L. Arevalo, "Intelligent impedance based fault location for zonal power systems", 12^{th} *IET International Conference on Developments in Power System Protection (DPSP)*, April 2014

2. C. Rose, M. Sumner, D. W. P. Thomas and E. Christopher, "Impedance sensitive STATCOM control for systems supported by renewable generation", 3^{rd} *IET International Conference on Renewable Power Generation (RPG)*, September 2014

3. C. Rose, D. W. P. Thomas, M. Sumner and E. Christopher, "Development and testing of an experimental power system fault demonstrator", *IET International Conference on Resilience of Transmission and Distribution Networks (RTDN)*, September 2015

Chapter 1

Introduction

Electrical power systems have developed over nearly 150 years in to large networks predominantly powered by a few high capacity generators. The networks as a whole have been clearly separated in to distinct subsystems: generation, transmission and distribution. In the past, generation has mostly been sourced from large, centralised power stations using fossil or nuclear fuels. The power has been fed into the transmission system which in turn feeds the distribution system. Consequently most of the system control functions are performed either in large power stations or at substations connected to the transmission system [1].

Many networks have not undergone any significant modernisation for many years. This, coupled with increasing environmental concerns and deregulation in many parts of the world, has resulted in a need for change. The

United Kingdom and all other European Union members currently have a target of producing 20 % of electricity from renewable sources by 2020 [2]. Currently, the UK produces about 15 % from renewable sources [3]. To further complicate matters demand for electrical power is increasing.

The next generation "Smart Grid" is expected to consist of a large number of semi-autonomous networks with their own energy producing capabilities connected together and working cooperatively [4, 5]. Effectively, the importance of the distribution networks increases, while the transmission system becomes less important. The Institute of Engineering and Technology [1] has predicted that in the United Kingdom the number of generators providing grid control functionality could increase from 10–15 at present (all on the transmission system) to as many as 600,000 (connected to both transmission and distribution systems), and voltage regulating devices could increase from about 10,000 devices to almost one million. A simplified illustration showing some of the changes that may occur in power systems is shown in Figure 1.1.

Some of the major changes expected to occur over the coming decades are:

- A substantial increase in the number of distributed energy resources (DERs), including renewable generation and energy storage, connected to the grid [6, 7].
- An increase in the number of devices actively controlling the power system voltage and frequency [1, 4, 5].
- The increased formation of "islands" (isolated areas of the network, continuing to operate using local generation) [8, 9].

These structural changes create a number of engineering challenges which must be addressed. This thesis intends to contribute to the existing work in this field by addressing effective voltage control on electrical distribution systems, which, as has already been highlighted, is becoming an increasingly important issue.

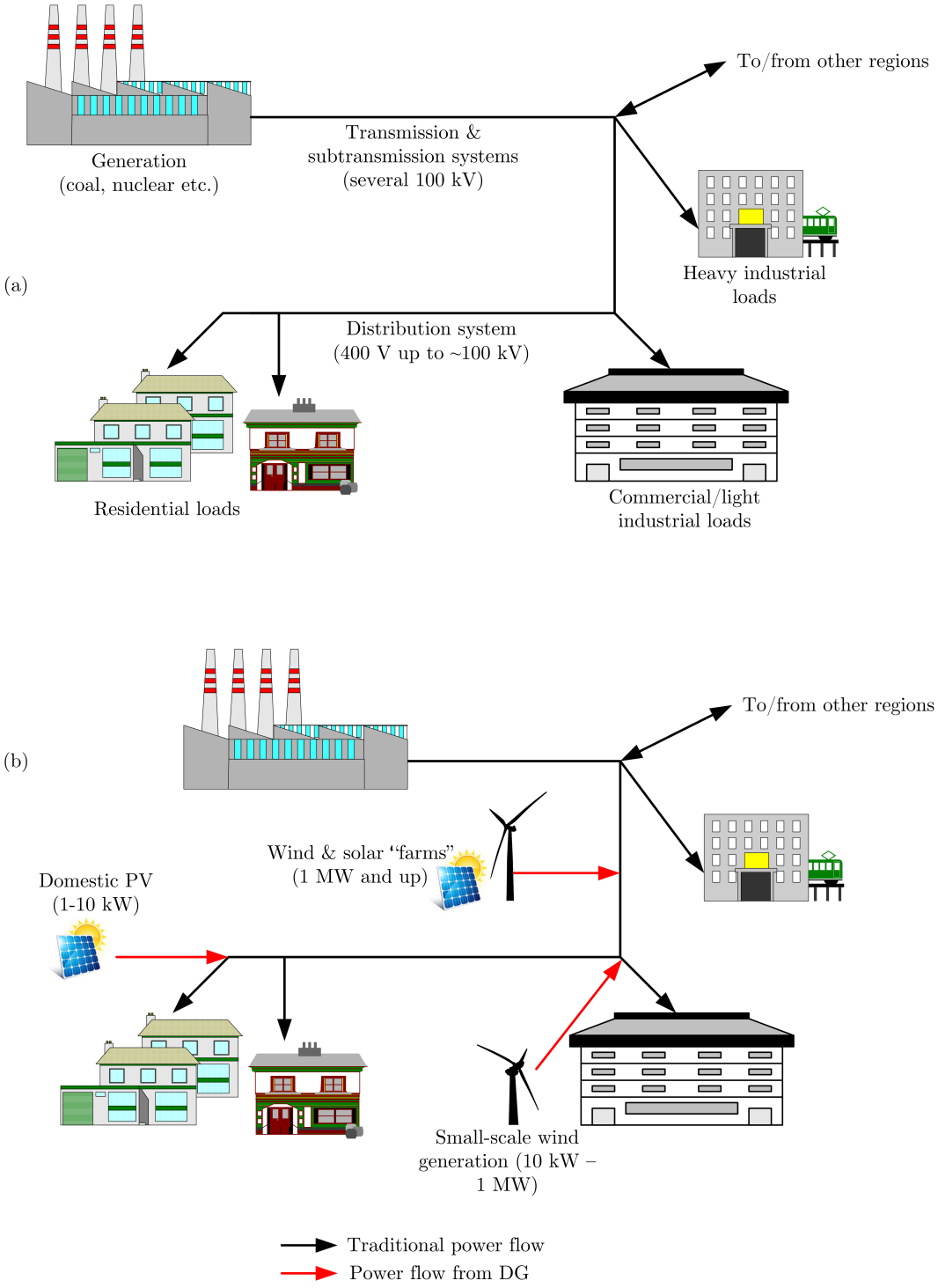

Figure 1.1: An illustration of (a) a traditional power system, and (b) the same power system with distributed generation at various levels.

1.1 Power system voltage control

Voltage control is typically employed in order to maintain the steady-state system voltage within specified limits. Voltage control may also be employed to address power quality issues associated with voltage, including dips, swells and flicker. Some of the common power quality issues associated with steady-state and transient voltage are [10]:

- *Undervoltage:* a voltage reduction of greater than 10 % below nominal for more than one minute.
- *Overvoltage:* a voltage rise of greater than 10 % above nominal for more than one minute.
- *Dips:* a voltage reduction of between 10 % and 90 % below nominal for a duration between one half-cycle and one minute.
- *Swells:* a voltage rise of between 10 % and 90 % above nominal for a duration between one half-cycle and one minute.
- *Flicker:* random variations in the voltage between 90 % and 110 % nominal voltage. So named because it causes visible fluctuations in the output of lighting.
- *Surges:* significant but short-lived rises in voltage, typically lasting only microseconds. Generally these are caused by large inductive loads switching off or lightning strikes to exposed cables.

1.1.1 Traditional methods of voltage control

A number of methods of power system voltage control are currently in use and most have been employed for many years. At present, almost all significant voltage control is performed on the transmission system.

Primary voltage control is achieved by varying the voltage as measured at the terminals of large generators. Generator terminal voltages may be controlled by varying the current flowing in the field winding of a synchronous machine using the generator's automatic voltage regulator (AVR). Primary voltage control is fast, typically taking less than a second to respond to a change in system voltage. However, primary voltage control is only effective locally and the terminal voltages may only be varied within the stability constraints of the generator. Generator reference voltages may be obtained from a centralised secondary voltage controller, which aims to control the voltage at select points throughout the network. Secondary voltage control will typically respond to variations in system voltage over periods of several seconds.

One other common method of voltage control is to use on-load tap changing (OLTC) transformers. OLTCs are transformers with numerous tap positions on one winding and an electromechanical means of switching between taps. By changing the tap position, the winding ratio of the transformer is varied and the secondary winding voltage will vary accordingly. Electrical arcing and the resulting mechanical wear are limiting factors both to the frequency of tap-changing and the service life of OLTCs.

Mechanically switched capacitor banks and shunt reactors have also been used to control power system voltages. Both capacitor banks and shunt reactors are used to adjust the reactive power flowing in the network. Capacitor banks inject reactive power, increasing system voltage. Shunt reactors absorb excess reactive power to reduce the system voltage. Such devices are usually installed at substations or near loads which are likely to cause large voltage drops, such as large direct-on-line electrical motors.

1.1.2 Power electronic methods of voltage control

In recent years there has been an increasing interest in developing more flexible means of power system voltage control. Power electronics offers a

number of possible means of improving the flexibility of existing technologies as well as introducing new methods.

One of the simplest ways in which power electronics may be used is to replace mechanical switches with semiconductor switches, most commonly thyristors. This allows the construction of thyristor assisted OLTCs, thyristor switched capacitors (TSCs) and thyristor controlled reactors (TCRs). The use of thyristor switches allows devices to respond faster and with greater control than their mechanically switched equivalents. Mechanical wear is also reduced or eliminated, potentially increasing the usable life of equipment. The reactive power from TSCs cannot be varied. Although the output of TCRs can be varied, doing so produces large switching transients and causes substantial harmonic distortion to the grid current and voltage which should be filtered. In addition, only inductive reactive power may be injected by the TCRs.

More advanced power electronics have been deployed in the form of Static Synchronous Compensators (STATCOMs) and Unified Power Flow Controllers (UPFCs). In both cases, power electronics and some form of energy storage, normally a large capacitor, is used to emulate one or more voltage sources, which may then be used to either source or sink reactive power (in the case of a STATCOM and a UPFC) or to reroute real power (in the case of a UPFC). The reactive power can be continuously varied over the operating range of the device and may be either inductive or capacitive. Using a STATCOM or UPFC to control reactive power may be used to indirectly control the system voltage. STATCOMs and UPFCs use more advanced switching devices than TSCs and TCRs, typically gate turn-off thyristors or IGBTs depending on the required power level. These devices allow more flexible control and can simplify the filtering of harmonic distortion, although the cost is higher for similarly rated devices and losses may also be higher. The control requirements for the STATCOM and UPFC tend to be more complex. This is because the devices must emulate a sinusoidal voltage source by switching multiple times per fundamental grid cycle, whereas the TSCs and TCRs only require switching, at most, once per half-cycle. In addition,

the STATCOM and UPFC must also control the energy storage components used, which is not a concern with TSCs and TCRs.

1.2 Objectives of this work

The importance of effective voltage control on distribution systems is increasing. The aim of this thesis is to investigate how STATCOM controllers may be affected by distribution system parameters, particularly the supply impedance and how any changes to the impedance may be identified, and how the information may be used to optimise control performance.

This work shall investigate the use of impedance estimation in power network voltage control using a STATCOM. The motivation for this work came from previous works on power quality improvement, which demonstrated that impedance estimation may be an effective means of tuning controller gains and others which have considered effective control of weak and islanded systems. In order to achieve the stated aim, a number of specific objectives have been identified:

1. To develop an AC voltage control strategy for STATCOMs installed on distribution networks using impedance estimation to tune the controller dynamics to the rest of the system.
2. To demonstrate the method both through simulation and experimentally.
3. To illustrate the applicability of this adaptive control scheme to a representative system which includes backup generation for use in times of power outages.

Both simulation and experimental work have been performed to address these objectives. Simulations were performed using MATLAB/Simulink,

with the aid of the PLECs blockset. Experimental verification of the simulations was performed using a 90 kW Triphase power converter and a 45 kVA experimental power network constructed as part of this work.

1.3 Novel elements of this work

In order to complete the objectives outlined, this work makes a number of novel contributions. First, on-line impedance estimation has been used to tune the STATCOM AC voltage controller. To the author's knowledge, impedance estimation has not already been used for this purpose. Second, novel modifications have been made to the impedance estimation algorithm used, specifically, the method has been changed to account for the control behaviour of the power converter used for impedance estimation in order to improve the quality of the results. Third, testing of the impedance estimation algorithm, both experimentally and through simulation, has resulted in some unexpected findings with regards to the interaction between the impedance estimation and nearby controlled sources and loads, as well as highlighting some of the limitations of the impedance estimation method used when implemented on a power converter with an LCL filter structure. Finally, the control behaviour of a STATCOM in the presence of a backup generator after a loss-of-mains incident has been investigated. As far as the author is aware, this is also a novel contribution to knowledge.

1.4 Outline of the thesis

This chapter has attempted to outline the motivation for and to state the key objectives of this work. The remainder of this thesis consists of six additional chapters.

Chapter 2 presents a review of the relevant existing literature. This re-

view discusses methods of identifying power system impedance, detecting changes in system impedance, existing methods of controlling distribution system voltages.

Chapter 3 introduces the STATCOM controller design, the simulation models used and the hardware used to implement the STATCOM for the experimental portion of this work. The design of the AC voltage controller is described.

Chapter 4 describes a method of power system impedance estimation. The method described is based on creating transient current disturbances and measuring the resultant voltage disturbance. The impedance estimates may then be used to tune the STATCOM controller.

In Chapter 5 a number of simulated case studies are described. This chapter introduces the simulated power system and studies simulated behaviour of the STATCOM control. System behaviour with a variety of load types is studied, as well as the behaviour of the system when local generation is included. Simulation results are presented and discussed.

Chapter 6 presents experimental results to validate the work presented in previous chapters. The experimental power system is described and experimental results are presented for the tests performed. The results are discussed with reference to simulated and theoretical behaviour of the system.

In Chapter 7 the applicability of STATCOM controller returning to electrical systems with backup generation is considered. The transition from normal supply to backup supply is described and the effect of the change on the system impedance is considered.

Chapter 8 concludes the work. In this chapter, the key findings of the work are highlighted and the work completed is evaluated against the objectives stated. In addition, the key limitations of the methods used are described and the practical effects explained. Proposals are made for potential future work in the field.

Chapter 2

Background and existing work

This thesis is concerned with the challenges of effective voltage control for modern electrical power distribution systems. Chapter 1 describes how modern distribution systems are rapidly evolving and some of the challenges accompanying the change. In this chapter a review of existing literature is presented to further elaborate on the problem of distribution level voltage control, especially in the presence of distributed energy resources (DERs). This chapter contains two main sections. First, the need for distribution level voltage control and existing methods of controlling distribution level voltage are considered. This section will also discuss the importance of knowing the grid impedance in order to achieve effective control. Second, some grid impedance estimation methods are discussed. The findings of this chapter will then be used to better define the issues this work hopes to address.

2.1 Voltage variation at distribution level

As was explained in Chapter 1, demand for energy security accompanied by environmental concerns is driving a general trend away from centralised, primarily coal-fuelled electricity networks towards more distributed, more renewable energy systems. This is a major structural change to systems that have remained almost untouched for decades and a number of challenges arise as a result [1]. One of the key issues that must be addressed is maintaining the stability of distribution system voltages and frequencies with high levels of DER penetration. A considerable body of literature is available discussing these issues and a sample has been reviewed within the context of this work.

2.1.1 Steady-state voltage variation

First, steady-state variations in distribution system voltage are considered. Voltage rise may be caused by high levels of distributed generation and may last for several hours. These long-term voltage variations are a concern because the voltage may rise above statutory limits, resulting in damage to sensitive loads, or over-voltage trips could be triggered, causing loads to be disconnected. Alternatively, if the nominal voltage is adjusted to accommodate the high levels of DER penetration, the voltage may drop below the statutory minimum during times of high load and low generation, causing problems such as a visible drop in light levels from electric lighting, triggering of under-voltage trips and increased losses where constant power loads are present.

A substantial portion of the existing literature is concerned with high levels of photovoltaic (PV) generation being installed on distribution networks. A 2008 review paper by Ropp et al. [11] outlines some of the key findings from a number of studies and attempts to draw conclusions regarding the maximum level of PV penetration that may be achievable on any given feeder.

One of the most common problems reported was voltage fluctuations due to changes in PV output and system loading. The literature reviewed gave maximum PV penetration levels from 5 % to greater than 50 % of feeder peak load before problems were reported. Unfortunately the wide range of reported upper limits for PV penetration makes it difficult to draw conclusions without closer inspection of the original sources, a selection of which are considered below. This paper also asked a number of engineers from various utility companies in the USA about their concerns regarding high PV penetration and found that voltage regulation was one of the more common responses.

As early as 1988 studies were made to investigate voltage regulation issues in the presence of high PV penetration [12]. Simulation studies were presented investigating the impact of cloud transients on feeder voltage regulation and power swing in the South Tulsa area of Oklahoma. The paper concluded that at times of light load significant effects begin to be observed at 15 % penetration level. Power swing problems at this level of penetration were observed but the authors concluded that the issues were solvable and could be addressed through proper planning. Although penetration levels above 15 % were not considered in this study the authors did note that higher levels were likely to be found in the future.

In 1989 Garrett and Jeter authored another early study of particular relevance to this work [13]. Their work was concerned with modelling the interactions between on-load tap changing (OLTC) transformers and systems with a high-level of PV penetration. Through simulation, the authors found that fluctuations in PV output could cause excessive operation of the OLTCs. It should be noted that the study was theoretical in nature. Experimental data was not used and the simulated PV penetration level was described as "high" without more detail being given.

More recent publications include a 2007 study by Thomson and Infield with particular relevance to the UK [14]. The authors noted that voltage rise is often a cause for concern and considered the probability distribution of volt-

ages for an 11 kV feeder and associated 400 V and 230 V circuits when various levels of PV penetration are considered. A test network was modelled using unbalanced load-flow analysis. The authors reported that high penetration levels of PV can cause voltage rises at the point of common coupling (PCC) but that the effect is usually small. Furthermore, it was noted that strict interpretation of the relevant UK and European standard [15] would result in a PV penetration limit of about a third of feeder capacity. This limit was a result not only of the rise in voltage caused by the PV, but the combination of the voltage rise and the high supply voltage, which was already approaching the allowed upper limit. Feeder voltages are often set above the nominal value in order to allow for the increased voltage drop at times of heavy load and it is therefore not unusual to find voltages approaching the allowed maximum during periods of light load. A similar paper presented by Hou et al. [16] in 2014 considers the modelling of a portion of the Swedish grid with high levels of PV. Their results show considerable variation in the system voltages, although the voltages never exceed the statutory limit of 10 % above nominal. However, it is noted that the voltages are low to begin with; most are below 1 p.u. most of the time and the lowest voltage is almost 10 % below the nominal (the lower statutory limit). In addition, the authors note that the area considered has a wide variation in load types; therefore, the low consumption that may be expected in residential areas during the day when PV generation is high is offset by nearby industrial and residential loads.

Modelling of voltage profiles when PV penetration is high was also performed by Tonkoski et al. [17], with an emphasis on residential areas. It was found that rural areas were likely to be the most affected by voltage rise due to PV because of the greater length and therefore impedance of the lines. This is important as both Thomson [14] and Hou [16] considered urban areas in their studies. In addition the authors highlighted the importance of transformer and line impedance in determining the likely voltage rise due to PV. A paper by Canova et al. [18] came to similar conclusions regarding the differences between urban and rural systems, although the authors did

highlight that the effect on urban networks is not negligible.

A paper by Masters et al. [19] modelled a 450 MVA power system with up 8 MW of wind generation connected. Similar to the work presented by Thomson and Infield for PV generation in [14], the statistical distribution of voltages was considered and the likelihood of exceeding voltage limits calculated. The authors found that at low wind penetration the system voltage typically remained below 1 p.u. and there was little need for concern. When the full 8 MW of possible generation was considered the likelihood of an overvoltage event occurring increased substantially. The probability of exceeding 1 p.u. was found to be greater than 50 % under certain conditions. It was also found that under the same conditions, the probability of exceeding 1.1 p.u. overvoltage was greater than 20 % and there was a 5 % chance of greater than 1.15 p.u. overvoltage. The figures presented by the authors show that the possibility of DG induced overvoltage is not insignificant and cannot be disregarded.

A 2010 paper by Vittal et al. [20] analyses the steady-state voltage stability of networks with high wind penetration using a variety of methods. The authors were interested in examining the worst-case scenarios, but found that the conditions required to create such scenarios were not always obvious; in particular, the expected peaks and troughs in demand did not necessarily correspond with times of worst-case voltage stability, which was more closely correlated with instantaneous wind power production. The results presented by the authors suggest a significant probability of overvoltage events occurring. In addition, it is shown that the increased voltage may propagate from the low-voltage and distribution networks onto the transmission system.

Trichakis et al. [21] considered a number of technical challenges associated with high DG penetration on low-voltage networks. This paper was particularly interested in the impact of a large number of small embedded generators being connected to the system. The authors simulated two different 11 kV/400 V networks intended to be representative of parts of the UK

and European distribution networks. A number of possible factors limiting the allowable level of penetration were identified and these included voltage rise and voltage regulation. Analysis was used to calculate the expected voltage rise as a result of a given amount of generation and the calculated figures were then confirmed through simulation. The voltage rise figures were then used to calculate a maximum allowable level of penetration. Voltage rise was found to be the factor which most limited the allowable DG power for the UK network, except when voltage unbalance caused by connecting all the DG to a single phase was considered. For the European network, voltage regulation was found to be the most important constraint.

A simulated study of steady-state voltage stability on transmission systems by Eftekharnejad et al. [22] found that bus voltage rise peaked when PV penetration is between 20 % and 30 % before beginning to fall again. The peak rise in bus voltages was found to be between 4 % and 7 %. The authors of this study found that in some cases the rise in voltage as a result of high PV penetration was significant enough to require preventative action in order to keep the voltage within allowable limits; their suggested actions were to disconnect shunt capacitors and to adjust the terminal voltages of conventional generation.

The effect of high levels of DER penetration on distribution system steady-state voltages has been considered in this section. Although it is difficult to give a precise limit for the allowable levels of penetration before corrective action must be taken, from the literature reviewed it would appear that problematic voltage rise is likely to start to be seen when penetration approaches approximately 30 % of circuit capacity. It therefore seems reasonable to conclude that some voltage control is likely to be required on distribution systems with levels of DER penetration greater than about 25 % of circuit capacity, particularly if the level of penetration is likely to rise in future.

2.1.2 Transient grid voltage variation

In this section the transient stability of voltages when DER penetration is high is considered. Transient rises and falls in voltage may be caused by cloud movement causing changes in PV output power or a sudden change in wind direction or speed. Regardless of the cause, fluctuations in DER output power may result in system voltages briefly dropping below or rising above statutory limits. Although these voltages may only be present for a few seconds and are unlikely to cause significant damage to the system or any connected loads, they may cause nuisance problems such as lighting flicker, or have serious side effects such as tripping of the DERs, which could result in a cascade failure scenario if alternative generation is not available to compensate.

In the previously mentioned paper by Eftekharnejad et al. [22] the transient stability of systems with high levels of PV is also considered. A three-phase fault was applied at various locations on the simulated system and the transient behaviour of generators on the system observed as the system recovered. Results were variable; in some cases the high levels of PV appear to aid the system recovery, in others recovery times and oscillatory behaviours seem to increase as a result of PV on the system. The authors observe that a variety of factors affect the system transient behaviour and that the level of PV penetration, system topology and the type and location of disturbances are all influential.

Transient voltage stability is studied by Kawabe and Tanaka [23]. A six-bus system was considered, although all of the load and PV generation was connected to only one bus. As in the previous paper a three-phase fault was considered. The authors considered the ability of the system to recover from the fault when the time taken for the PV output current to return to the pre-fault level was varied. It was found that the system could recover if PV was disconnected or when the PV recovery time was limited; however, if recovery time of the PV was increased too much, the system was unable

to recover from the fault. Similar to findings of Eftekharnejad et al. [22], the conclusions drawn from this work were that while it is possible that PV may be able to improve system transient stability, it is also equally possible for it to have a detrimental effect.

Similar work was carried out by Yagami et al. [24], who performed simulations of a 9-bus system to study the transient stability of systems with a high level of PV penetration. Again, recovery from a three-phase fault was considered. In this paper the synchronisation of a synchronous generator connected to the system on a bus near to the PV connected bus was considered. The PV and synchronous generator were both rated at 500 MVA. Initially the authors considered an ideal case where the system was supplied from an "infinite bus." In this case, the risk of instability was low regardless of whether the PV was allowed to remain connected during the fault and the probability that the generator remained synchronised to the grid was high. The authors then considered the case of a power system with limited capacity and PV capacity of comparable size. In this case, it was found that the risk of the generator losing synchronisation was high if the PV was disconnected during the fault, but decreased if the PV continued to supply power while the system recovered.

A paper considering the impact of irradiation variance as a consequence of varying cloud cover have been published by Tan and Kirschen [25]. This paper highlights the issue of under and over-voltage trips, which are typically required to prevent islands forming. The work presented illustrates that it is possible for the inverter's protective circuitry to undesirably trip as a result of transient voltages caused by sudden changes in PV output. Alternatively, transient voltages on the system could cause the inverter to trip. When considered within the context of the various works on transient stability above this is a particularly concerning finding. The tripping of the PV inverters has the potential to exacerbate transient effects and cause additional instability.

Modelling of a 69-bus test system was performed by Hossain et al. [26] in order to study transient voltage stability of systems with high levels of wind

generation. Comparisons were drawn between a system supplied entirely using synchronous generators and the same system with 60 % of the demand supplied by DFIG wind turbines. The results presented in this paper show a substantial difference between the two cases; the response of the system with high levels of wind is slower and more oscillatory than the system with only synchronous generators. Similar to the conclusions drawn regarding system stability and PV in [22–24], the authors note that disconnection of the wind generation during system faults can exacerbate rather than mitigate stability issues.

In a 2010 conference paper presented by Feng and Wei [27] the effect of DG on voltage quality is investigated. The authors considered three types of DG: an asynchronous wind turbine coupled directly to the grid, a synchronous generator and an "inverter-based DG." The authors considered transients caused by switching of both DG and loads. Their results show that as the ratio between DG power and power imported from the network increases the transient response becomes more oscillatory. The authors also presented results showing steady-state voltages; however the DG penetration ratio was varied by adjusting the power available from the network and not DG production, making the results difficult to interpret.

A 2008 paper by Kasmas and Papathanassiou [28] considered the switching transients associated with DG and the effect this has on system voltage. The authors considered the example of a small synchronous generator used in a hydroelectric plant. The generator and synchroniser dynamics were modelled in detail. The results presented show that the initial transient caused by connection of the DG causes a step-like drop in voltage and that recovery from this drop can be quite oscillatory. Steady-state changes in voltage were not considered in this paper.

This section has considered the transient impact that high levels of DG penetration can have on distribution system voltages. Voltage transients caused by DER power swings can have a severe impact on power systems; undervoltage and over-voltage tripping caused by sudden rises or drops in volt-

age may result in cascade failure. It has also been seen that fault ride-through capabilities may be improved if DG remains connected rather than disconnecting during transient faults. Since the problems highlighted in this section may only take a few seconds, or even less, to appear, fast control is required to compensate for them.

There is a general consensus in the literature reviewed so far that DG and DERs in general can cause variations and fluctuations in the supply voltage in some circumstances. There is still some debate about the level of DER penetration that may be reached before voltage rise becomes a significant problem. The limits of DER penetration would appear to be case specific, although it is seen in the literature that problems tend to be most likely to occur in rural areas where the supply impedance is relatively high and at times when demand is low. In addition to voltage rise, the problem of voltage fluctuations as a result of variations in output power of the DERs has also been highlighted by a number of authors and it has been suggested that the consequences of such fluctuations can be severe. Fast voltage control is required to mitigate many of the transient problems caused by high levels of DER penetration. A number of proposals have been made in an attempt to address the concerns regarding DERs and system voltage. These shall be considered in the following section.

2.2 Distribution level voltage control

A selection of papers was reviewed in the previous sections in order to show that system voltages can vary as a result of the presence and fluctuating output of DERs. Chapter 1 gave a brief overview of how power network voltages have been controlled in the past and some of the shortcomings of these methods were highlighted. In this section the role of modern power electronics in regulating power systems voltages is to be discussed.

Various papers highlight that problems may be caused as a result of inter-

actions between DERs and some existing voltage regulation devices, particularly on load tap-changing transformers (OLTC) [13, 29–34]. Accelerated wear as a result of increasing frequency of operation is one of the motivations given for a number of pieces of research. Another motivation for the research is the failure of OLTCs to correctly regulate voltage as a consequence of the line-drop compensation used, which assumes no reverse power flow. Finally the slow operation of OLTCs and similar electromechanical regulators is considered a significant drawback by some authors [35, 36].

Since the 1990s there has been increasing interest in the role of power electronics in transmission system control [37]. This has led to the development of Flexible AC Transmission System (FACTS) technologies. Many of the FACTS technologies are now beginning to be considered for use at distribution level. Vazari et al. [36] considered the performance of a Static VAr Controller (SVC) on the distribution system and compared their results to the performance of an OLTC. SVCs (see Figure 2.1) are FACTS devices consisting of inductors, capacitors or both controlled using power electronic switches, usually thyristors, and are an example of a device which controls reactive power flow in order to indirectly regulate voltage. The authors concluded that the SVC gave superior voltage control and a faster response when compared to the OLTC.

Tsunedomi et al. [38] also considered an SVC on the distribution system. Experimental results for a 400 kVAr SVC installed adjacent to a wind farm with 1,700 kW capacity on a rural feeder were presented. Three different control structures were considered; the first was intended to regulate the voltage as close to the reference voltage as possible, the second to suppress voltage fluctuations over several minutes and the third to suppress short term fluctuations. In all regulation modes the authors reported an improvement in voltage. It should be noted that the results for the no SVC case were calculated using the SVC reactive power and system parameters and not experimentally recorded. However, the work does demonstrate that there is some justification for the installation of FACTS devices, specifically SVCs,

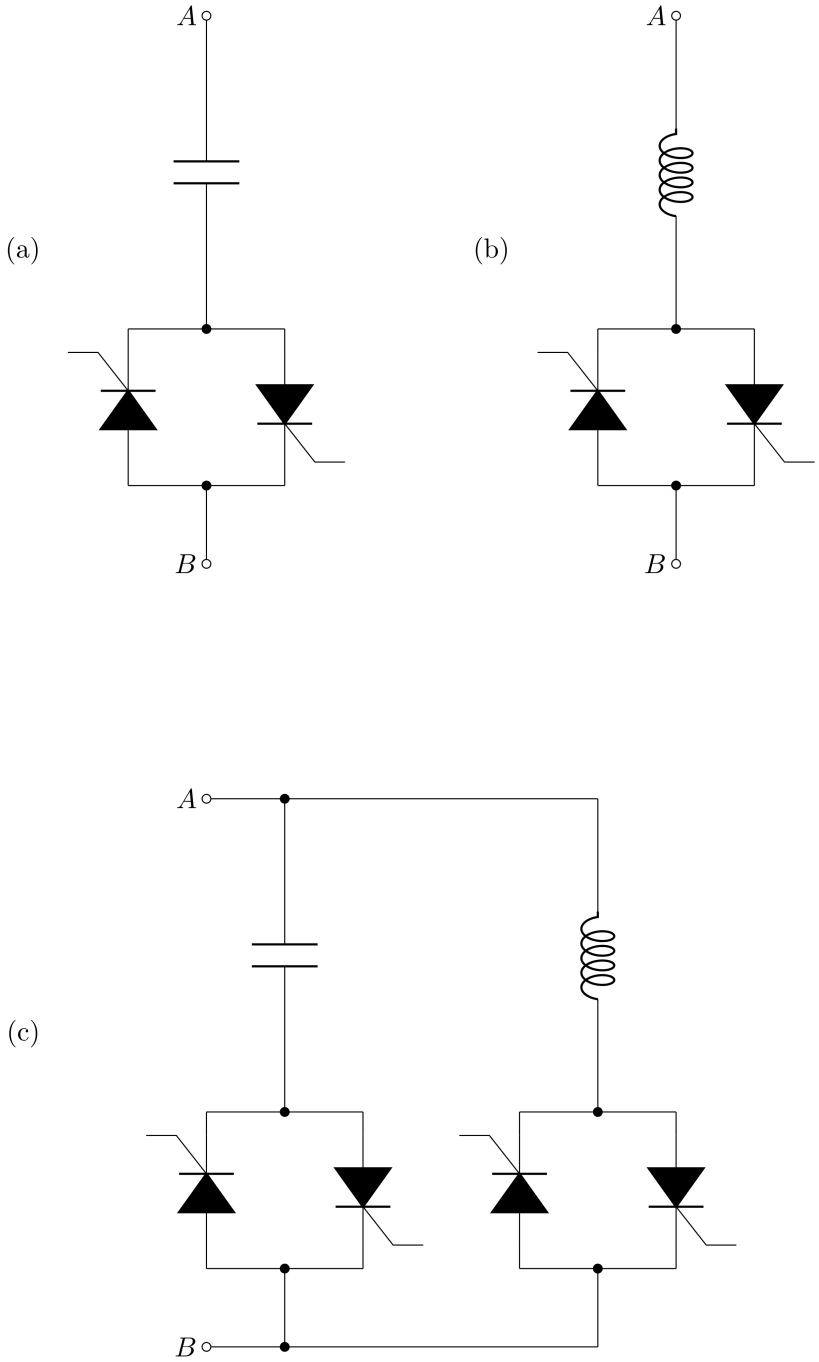

Figure 2.1: Three types of SVC: (a) Thyristor switched capacitor (TSC), (b) thyristor controlled reactor (TCR) and (c) both combined to form a TSC-TCR.

on distribution networks.

Wong et al. [39] authored a paper proposing SVCs as a potential solution to voltage fluctuation problems on distribution networks. The authors considered the transient voltages seen on the system as a result of motor starting events. First it was demonstrated that switched capacitors could mitigate the voltage drop during motor starting. Considerable fluctuations in the voltage remained however and it was demonstrated that this could be almost entirely compensated for using the SVC. The conclusions presented in this paper highlighted some features of SVCs which the authors considered particularly advantageous. These were fast control, small physical size and flexibility of location.

The previously described papers demonstrate that SVCs can be a useful technology for regulating voltage. This demonstrates the principle of using reactive power control to manage distribution system voltages. However, it should be noted that there are some significant disadvantages to using SVCs. The current that the SVC is able to sink or source is proportional to the system voltage [40]. As a consequence, the operating capacity of the SVC is reduced during undervoltage conditions when reactive power is most needed. The use of thyristor switches results in SVCs creating significant harmonic distortion which may be undesirable or may require additional filtering [41]. The creation of resonances may also be a concern. The static synchronous compensator (STATCOM) is a FACTS device which offers some solutions to the limitations of SVCs. STATCOMs are an inverter-based reactive power compensation technology, as can be seen in Figure 2.2. The V-I characteristics of a STATCOM are shown in Figure 2.3 with the V-I characteristics of an SVC for comparison. It can be seen that the STATCOM is capable of sinking or sourcing the same current regardless of the system voltage. The use of IGBT switches allows a higher switching frequency and finer control than is possible with thyristors, resulting in reduced harmonic distortion from the STATCOM compared with the SVC and therefore simpler filter requirements. A number of authors have considered the STATCOM for use on distribution systems. The name D-STATCOM is used in

some of the literature in order to differentiate from STATCOMs found on transmission networks.

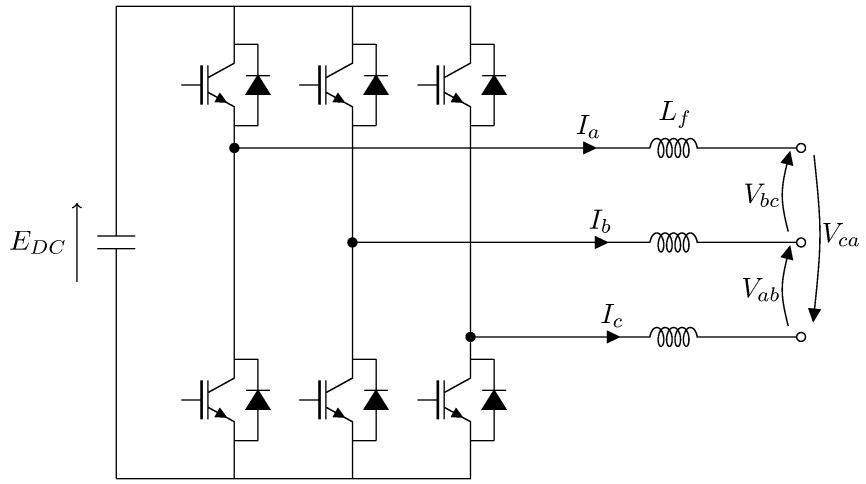

Figure 2.2: Simplified schematic of a D-STATCOM based on an IGBT inverter.

A STATCOM is considered to address the issue of voltage sag in a 2012 paper by Mahyavanshi et al. [42]. The paper is concerned with voltage quality issues found in many industrial and commercial settings. Simulations were performed on a simple three-phase system with both linear and nonlinear loads. A STATCOM is used to regulate the voltage at the point of common coupling (PCC). The results presented show that the STATCOM is able to regulate the system voltage successfully, mitigating a voltage drop of almost 70 V. The overall system power factor is also improved and a the current drawn from the supply reduced, a result of the STATCOM providing most of the load reactive power.

Freitas et al. [43] studied the dynamic performance of induction generators connected to the distribution system and supported with a STATCOM. A 7-bus system was simulated which included a STATCOM and an induction generator. Two methods were considered for generating the STATCOM reactive power demands; a voltage control method and a power factor control method. Simulations were performed for each control strategy with a fault imposed on the system. When the power being supplied by the genera-

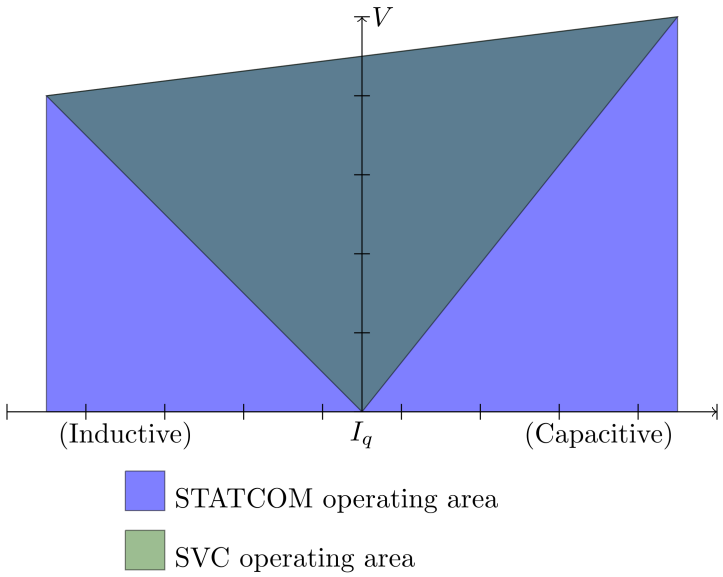

Figure 2.3: *V-I* operating area of SVCs (TSC-TCR topology) and STATCOMs. The STATCOM may operate up to rated current regardless of voltage. The SVC output current is limited at reduced voltages.

tor was moderate, both the voltage control and power factor control methods showed improved performance when compared with the no STATCOM case. When the generator power was increased, only the voltage-controlled STATCOM was stable. In addition the reactive power injected by the STATCOM in power-factor control mode showed oscillatory behaviour.

A 50 MVA ship power system including a STATCOM was simulated by Mitra and Venayagamoorthy [44]. The ship power system is a useful example of an isolated system, which may exhibit similar behaviour to isolated microgrids or so-called "weak-grids" with local generation. An artificial neural network is used for the STATCOM controller in this paper. A variety of loads are considered, including a pulsed load and a 36 MVA propulsion motor, both of which may be expected to have a significant impact on the supply voltage. Simulations with the STATCOM included show greatly improved transient performance in the presence of the pulsed load. Time taken to recover from the transients is reduced and the oscillatory behaviour of the system is efficiently damped.

A few authors have published results from STATCOM installations. Grünbaum published one such paper where the use of a STATCOM (termed "SVC Light" in this paper) is used to address the problem of voltage flicker in an industrial environment [45]. The STATCOM was installed in order to mitigate voltage fluctuations caused by an electric arc furnace at a Swedish steel mill. The results presented demonstrated a substantial reduction in the level of voltage flicker caused by the erratic nature of the loads. This paper also considers fluctuations caused by wind generation and notes that the deployment of a STATCOM may be beneficial to power quality. Clouston and Gurney also considered the ability of STATCOMs to address voltage flicker [46] caused by industrial wood chippers installed at a mill and also concluded that there was considerable improvement after commisioning of the STATCOM. Simulation and experimental testing was carried out by Muni et al. [47]. A 500 kVAr STATCOM was developed and tested. As with the previous two examples, the STATCOM was installed in an industrial environment with rapidly fluctuating loads causing considerable voltage distortion. The authors note that the installation of the STATCOM did not require any substantial work to be carried out on the substation to which it was connected.

2.2.1 Design of STATCOM AC voltage controllers

The literature reviewed in the previous section shows that there is considerable interest in deploying STATCOMs on the distribution system. STATCOMs offer faster voltage control than OLTCs, are unlikely to create new resonances – which is a potential problem with SVCs – and cause lower levels of harmonic distortion than SVCs. However, while surveying the literature it was found that there is a very limited amount of information regarding the controller design and particularly the tuning of controllers. The need for fast control was highlighted when the transient impact of DERs was considered. In order to operate quickly and reliable, a properly tuned controller is required. Many authors have used PI controllers, yet few state

the gains used or how the values were calculated and those that do have often used trial and error. A number of papers use particle swarm optimisation or similar methods. Such methods take considerable time in order to reach a final control value and can be very computationally intensive.

One example of PI controllers being used is found in [48]. In this paper the authors are concerned with the control of a STATCOM under unbalanced conditions. Simulations were performed on a 9-bus power system. A five-level converter was used to model the STATCOM. PID controllers were used to regulate both the positive and negative sequence currents and voltages. The controllers were implemented in a rotating (dq) frame of reference aligned to the grid voltage vector; however, the emphasis of the paper was on the control structure and the authors did not state how they calculated the controller gains. Wang [49] considers a control structure intended to provide improved damping of power system oscillations. PID controllers are used, but as with the previous paper, the emphasis is on the control structure and the calculation of gains is not presented.

Some authors have considered biologically inspired methods of tuning controllers, such as Safari et al. [50], who considered using honey bee mating optimisation (HBMO) in order to find an optimal controller gains and compared results for controllers tuned using a genetic algorithm (GA). Simulation results were presented showing that both methods could be used to find suitable controller gains, with the HBMO control gains showing slightly better performance. Implementation of both GA and HBMO retuning requires that a large number of possible controller gains are evaluated and compared. They are therefore computationally intensive methods and potentially slow. In addition, the use of random values for the initial population used in the algorithms means that consistent results cannot be guaranteed.

Kumaravel and Kumar [51] used a bats echolocation algorithm to tune STATCOM PI controllers. The authors successfully used simulations to demonstrate that they could retune controllers using the echolocation algorithm. The motivation given for the work in this paper is that fixed controllers were

found to give performance which varied considerably with system loading. The authors note the importance of system impedance, particularly the variable load impedance, on the controller gains. As with the GA and HBMO controller tuning methods, the echolocation method requires evaluation of a large number of possible controllers which is a computationally intensive process. Only simulation results have been presented and it is therefore unclear if such methods could achieve similar performance when used in a real-time control environment, where the tuning time and computational power required may make the method impractical.

A paper by Xu and Li [52] highlights the lack of literature on STATCOM control and states that this is a significant motivational factor for the work presented. A review of other works highlighting the lack of literature on STATCOM controller design is presented and this is followed by original work demonstrating a controller retuning method. The method presented involves comparing the step-change response of the STATCOM with a reference response curve and uses the difference between them to calculate a new set of controller gains. Simulation results are presented which show desired operation for small changes in operating conditions and an improvement over a static controller. Although the results demonstrate that the method presented can give the desired performance it is noted that it requires a step-change in load in order to retune the controller and therefore the retuning may not be performed at any time. In addition a considerable amount of calculation is required in order to perform the retuning. Finally, all the disturbances simulated are small; it is therefore unclear whether the control retuning will behave as desired with large disturbances or in the presence of significant noise.

A paper by Wang presents a model of a power system with a STATCOM installed [53] based on the Phillips-Heffron model, originally proposed for modelling of synchronous generators [54]. Wang's paper is of interest for three reasons. First, the model presented shows that the STATCOM and power system behaviours are both non-linear and highly interdependent. Second, it can be seen that the interactions between the STATCOM and

power system are highly dependent on the system operating point and that the modelling relies on linearisation of equations about an assumed operating point. Third, it shows that a direct comparison may be drawn between STATCOM control and synchronous generator control. This is a useful comparison to make, since similar difficulties to those encountered with STATCOM controller design are reported when generator control is considered [55–57]. Although these papers are not directly applicable to this work, they do offer some insight into the problem of STATCOM voltage control and will therefore be briefly considered. Bollinger and Lalonde [55] state that the automatic voltage regulators (AVR) used in generators are often tuned open circuit, effectively assuming that the generator does not operate under load, with retuning rarely performed, even when system oscillations are encountered. The authors recommend retuning the controllers for more realistic operating conditions, but also caution against the use of complex and impractical high-order controllers in an attempt to compensate for the interdependency of system parameters. Ibrahim et al. [56] and Finch et al. [57] also comment on the unsatisfactory performance of fixed gain controllers. In both of these papers, an adaptive control scheme based on parameter estimation is proposed to overcome the problem of AVR tuning.

The reviewed literature has revealed that there is no standard way in which to determine the controller gains for a STATCOM. The high level of interdependency between multiple system variables and the variability of performance at different operating points makes the design of a generic STATCOM voltage controller difficult. Manually tuning the controllers when connecting the STATCOM is only a viable solution if only a small number of installations are required, since it requires a skill and experience in order to be performed correctly and is therefore unlikely to be useful if a large number of devices are installed on the distribution system. It has also been found that statically tuned controllers can give poor performance with varying load conditions. The use of particle swarm optimisation and similar methods has been proposed because of their usefulness in finding work-

ing solutions from a large initial set of options; however, these methods are computationally intensive and therefore may take a very long time to complete and this may also make them unsuitable for use in an embedded system. Furthermore, depending on the precise method used, consistent results cannot be guaranteed and the final result produced by the algorithm may not be the optimal solution. The method proposed by Xu and Li [52] seems to offer a possible solution, since it is not as computationally intensive as many of the other proposed methods, nor does it use static PI controller gains. However, it is far from clear that the performance shown in simulation could be replicated on a real system, given the ideal conditions used to demonstrate the method. Since STATCOMs use reactive power injection to control system voltage, the relationship between reactive power and voltage will briefly be considered.

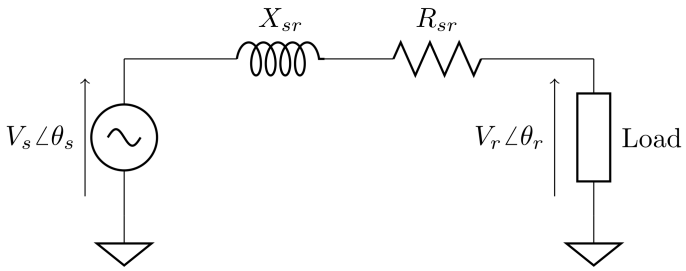

Figure 2.4: Simplified power system model used to analyse basic real and reactive power flow.

For a simple power system with impedance $Z = R + jX$ between the supply and load, as shown in Figure 2.4, the real and reactive power at the load end of the line can be calculated:

$$P_{rs} = R\frac{V_r^2 - V_r V_s \cos(\theta_r - \theta_s)}{R^2 + X^2} - X\frac{V_r V_s \sin(\theta_r - \theta_s)}{R^2 + X^2} \tag{2.1}$$

$$Q_{rs} = -R\frac{V_r V_s \sin(\theta_r - \theta_s)}{R^2 + X^2} - X\frac{V_r^2 - V_s V_r \cos(\theta_r - \theta_s)}{R^2 + X^2} \tag{2.2}$$

For transmission systems it is usual to assume that the resistance is much

smaller than the reactance. However, for distribution systems this is often not the case. For a short distribution line the two ends may be assumed to be almost in phase so that $\theta_r \approx \theta_s$, allowing some simplification of the equations. Considering only the reactive power:

$$Q_{rs} \approx X\frac{V_s V_r - V_r^2}{R^2 + X^2} \tag{2.3}$$

The change in reactive power caused by a change in receiving end voltage may therefore be found by differentiating Q_{rs} with respect to V_r:

$$\frac{\partial Q_{rs}}{\partial V_r} = X\frac{V_s - 2V_r}{R^2 + X^2} \tag{2.4}$$

If it is assumed that the voltage drop is small and therefore that the sending and receiving end voltages are almost equal then the equation may be simplified further and knowledge of the supply voltage is no longer required:

$$\frac{\partial Q_{rs}}{\partial V_r} = \frac{-XV_r}{R^2 + X^2} \tag{2.5}$$

Let $\alpha = R/X$. The result in (2.5) may then be simplified further:

$$\frac{\partial Q_{rs}}{\partial V_r} = \frac{-V_r}{X(1 + \alpha^2)} \tag{2.6}$$

Using similar analysis for real power:

$$\frac{\partial P_{rs}}{\partial V_r} = \frac{\alpha V_r}{X(1 + \alpha^2)} \tag{2.7}$$

From the analysis above it can be seen that it is possible to calculate the reactive power required to vary the system voltage by a given amount using knowledge of the system impedance. For transmission systems it is assumed that the effect of resistance may be ignored. For distribution systems,

resistance may be significant. As the X/R ratio decreases the required reactive power will rapidly increase. Comparing (2.6) and (2.7) it can be seen that if the X/R ratio falls below unity then it becomes more effective to inject real power to regulate voltage, although this is not necessarily a more practical option.

In the past the fundamental impedance of low-voltage networks was calculated using short-circuit currents. This may not always give sufficiently accurate results [58] and therefore a more reliable method is desirable. In addition, the method also relies upon the assumption that the impedance is time invariant. The accuracy of the time invariant supply model is questioned in [59]. Experimental measurements presented in [60] and [61] provide some evidence that the grid impedance can vary with time, including at frequencies near to the fundamental.

There are many possible reasons for changes in the system impedance. Load, generation and other infrastructure changes may all cause the impedance to vary with time, particularly in weak systems. Similarly, changes in tap-changer and capacitor bank settings could also cause changes in the system impedance. Larger changes to the grid impedance may be caused by power system faults [62, 63] and loss-of-mains (islanding) on systems supported by distributed generation [64, 65]. Impedance estimation has proved useful in identifying such changes in system configuration in the past. The potential for the system impedance to vary makes it likely that a one-off estimate of the impedance would be inadequate for reliable control purposes and therefore an on-line method of impedance estimation is required. This is particularly true if the controller is expected to cope with scenarios such as islanding, where large changes in impedance may be expected. It has already been seen that fast voltage control is likely to be required when DER penetration is high. In order for a fast controller to behave correctly, it must be properly tuned to the system. Given the relationship between reactive power, voltage and system impedance, tuning the controller using on-line impedance estimation is proposed as part of this work.

It is often assumed that the distribution system may be treated as being supplied from an "infinite bus" with zero supply impedance and infinite capacity. This model relies on the transmission system having far greater capacity than any individual part of the distribution system. In a distributed grid the transmission system is likely to become weaker while variations in load and generation on the distribution system are likely to have a far greater impact. The use of on-line impedance estimation in order to tune the STATCOM controller has therefore been considered as an alternative to using fixed controller gains based on the limited information provided by one-off measurements. In the next section a selection of impedance estimation methods are to be considered.

2.3 Grid impedance measurement methods

In the previous section it was found that reactive power may be used to effectively address voltage control issues on distribution systems. Reactive power control through the use of STATCOMs was considered particularly effective. It was also found that there is a lack of literature discussing how STATCOM controllers may be designed. Consideration of the relationship between reactive power and voltage reveals that for a desired change in voltage, the required reactive power is dependent on the system impedance. There is evidence within the literature to suggest that the impedance of power systems may vary with time, even when operating normally. Given the wide range of possible operating conditions that may be encountered in the future, a STATCOM controller that is capable of dealing with these changes in system impedance is required. Changes in system impedance may cause significant changes in the controller performance and therefore impedance estimation has been proposed as a means of tuning the STATCOM AC voltage controller.

For the purpose of this review, impedance estimation methods have been divided into three categories: "passive"; "active, steady-state"; and "active,

transient". The passive methods analyse the currents and voltages already present on the system in order to estimate impedance; the active methods create a disturbance in order to measure the impedance. Steady-state methods analyse the system while the voltages and currents have near-constant amplitude and phase; transient methods take advantage of short-term disturbances to the system. Examples of these types of methods and their applications are given in this section.

2.3.1 Passive impedance estimation

The most basic method of impedance estimation involves monitoring of the voltages and currents at the point of interest, usually the PCC or point-of-connection. Once voltages and currents have been measured at two operating points, the supply impedance, Z_S, at the fundamental frequency may be calculated using (2.8), where I_1 and I_2 are steady-state currents at the two operating points and V_1 and V_2 are the corresponding steady-state voltages. In addition the load impedance at any given operating point may be calculated using only a single measurement by taking the ratio of measured voltages and currents.

$$Z_S = \frac{V_1 - V_2}{I_1 - I_2} \tag{2.8}$$

It may also be possible to estimate the harmonic supply impedances using this method; however, this is entirely dependant on harmonic content being present during the measurement period.

The most common variant of this method was described by Crevier and Mercier in 1978 [66]. In their paper, the authors used the switching of a shunt capacitor to create the required change in operating point. Practical tests were carried out in a 12 kV substation and the results compared with other available data. The results were deemed to be acceptable by the authors. The use of capacitor switching has subsequently been used

by others [67, 68]. The popularity of using capacitor bank switching may be attributed to the use of capacitor banks for reactive power support and power factor correction on distribution systems. By continually monitoring the system to detect when capacitor switching has occurred there is no need to create any additional disturbances to the system. Capacitor bank switching is discussed by Oliveira et al. [68]. The authors note that the method may be generalised so that any switching event may be used. Switching of a non-linear load is suggested as this creates additional frequency content which may be used to estimate the impedance at harmonic frequencies.

The use of the capacitor switching transients for wideband impedance estimation has also been considered [69–72]. In these papers the wide range of frequencies present during the initial inrush resulting from the connection of capacitor banks is used to estimate the system impedance. An alternative method to using capacitor switching for impedance estimation was proposed by Palmer and Ledwich [73]. They investigated the use of transformer tap-changing as an alternative to capacitor switching, reasoning that tap-changing transformers are more readily available than capacitor banks, although the disturbance created by tap-changing is often smaller than for capacitor bank switching. Although the smaller disturbance may well be desirable for the normal operation of the system, it results in reduced resolution and poor noise performance from an impedance estimation perspective. The authors performed impedance estimation on an 11 kV distribution system using both tap-changing and capacitor switching and compared results from both methods. They found them to be consistent despite the greater noise in the tap-changing results. In another paper by Xie et al. [74] transformer inrush currents are investigated as a means of impedance estimation.

Analysis of other power system transients can be used to estimate impedance as demonstrated in [75, 76]. The authors were investigating two methods of using passive impedance estimation to locate faults. Simulation and experimental results are presented demonstrating that the impedance over a wide range of frequencies (from DC to 3 kHz in the results presented) may

be estimated using fault transients. Impedance estimates using the fault transients were compared with calibrated measurements and found to be consistent. The main disadvantage of this method is the large transients required. In the case of the papers cited, a fault transient was used, although it may be possible to use transients caused by transformer or capacitor inrush currents.

The impedance estimation methods discussed so far use disturbances that naturally occur on power systems and therefore do not require the creation of an additional disturbance. The main disadvantage of these methods is that the impedance cannot be estimated as desired. This could be overcome by forcing a disturbance, but such an approach could have undesirable consequences such as the creation of resonances caused by capacitor switching or the change in voltage resulting from OLTC transformers. If a disturbance is not forced, it is also necessary to continuously monitor the system in order to know when new information is available. To address this a number of active methods of impedance estimation have been developed which can be activated when required with limited impact on the normal operation of the system. A selection of these shall be reviewed in the next section.

2.3.2 Active, steady-state estimation

In 1994 Harris et al. [77] described a method for line impedance estimation using a signal generator and network analyser. Rhode et al. developed a similar method in [78] and [79]; a single portable unit was developed as an alternative to using several pieces of commercially available equipment, as was done in the previous paper. In both cases, the impedance was estimated at inter-harmonic frequencies by injecting a sinusoidal waveform. A resolution of 10 Hz was used and it was found that the impedance could be identified over a wide range of frequencies using this method. A notch filter tuned to the fundamental frequency was connected to the equipment, both to protect the equipment and remove any influence the fundamental

may have on the results. No estimation was therefore performed at the fundamental. Unsuccessful attempts were made to estimate the impedance at harmonic frequencies; it was found that the influence of existing harmonic content was too great for the results to be useful. Interpolation was therefore used to calculate the impedance at the fundamental and harmonic frequencies.

Asiminoaei et al. [65, 80–83] developed a method for impedance estimation for embedding into photovoltaic (PV) inverters. A near-fundamental inter-harmonic current was injected onto the grid using the inverter. The method was first described in [80] where a 1.5 A, 75 Hz injection was injected for two fundamental cycles (0.04 s). Both simulation work and experimental verification was conducted with acceptable results. The work was further developed in [81] where the effect of changing various injection parameters was examined in detail. Further work by the authors focused on practical implementations of the method. In [82] a number of implementation issues and their solutions are explored and further experimental verification is conducted. It was found that the precision of this method was affected considerably when the inter-harmonic injection frequency was already present on the grid [83]. To address this the authors proposed a method for avoiding injection conflicts and erroneous results in situations where multiple PV inverters are running in parallel.

This section has described some active methods of impedance estimation which inject a steady-state signal onto the system in order to measure the response. The disadvantage of these methods is that they are only able to estimate the impedance at a single frequency at any one time. Wideband impedance estimation is possible, but it requires a large number of injections. Wideband estimation is therefore unacceptably time consuming for more than a few frequencies.

2.3.3 Active, transient estimation

The final methods of impedance estimation to be considered have been labelled as "active, transient" methods. These methods aim to estimate the impedance at a wide range of frequencies using short-term non-sinusoidal injections. Various works on transient injection based impedance estimation can be found in [59, 64, 84–86]. In these papers, a semiconductor switch consisting of two back-to-back thyristors is used to connect a load to the system. By activating the thyristors shortly before the zero-crossing a narrow current spike may be created. The current spikes and resulting transient voltages may be analysed to estimate the system impedance at a wide range of frequencies.

In 2000 Palethorpe et al. [87] first described a method of on-line, real-time impedance estimation using controlled injections from a three-phase converter. The method was intended to be implemented on an active shunt filter and used to optimise harmonic cancellation for non-linear loads. An injection was created by directly manipulating the PWM switching pattern of the power converter. Simulation results showed that the technique could be used to estimate linear impedances with a high degree of accuracy. The method was further studied in [88–91]. The technique was experimentally verified in [88] with the experimental results confirming the high accuracy of the method. In their previous work the authors had used an 160 mS injection which they considered too long for some circumstances. Therefore further experimental work was conducted, this time using a 800 μS injection. The two injection lengths were termed "medium term" and "short term" respectively. The short term injections were shown to give a similar quality of results to the medium term injections used previously, but with considerably less disturbance to the system.

A 2014 conference paper presented by García et al. studies a variation of Palethorpe's method [92]. Unlike earlier work, where it was assumed that the converter would use a purely inductive filter to couple to the grid, a

power converter having an LCL type filter is used to perform the injections. LCL filters are increasingly being used on converters due to their superior performance when compared to L and LC filters. Results presented in this paper show a significantly attenuated current injection when compared to earlier work, despite the injection length being increased. The results suggest that it is still possible to use the method for impedance estimation, however, it should be noted that the injections were performed continuously, occurring at each voltage zero-crossing. It took several injection cycles for the impedance estimates to converge on a suitable estimate, however, this is likely due to the iterative estimation method employed by the authors rather than inherently poor results.

A novel impedance estimation method was introduced by Neshvad et al. [93] in 2014. The method is designed to be implemented on a power converter by creating a small transient injection at the end of each PWM switching cycle. The polarity of the injections is determined by a pseudo-random binary sequence (PRBS), resulting in a apparently noise-like injection with a number of useful properties [94]. The use of a PRBS allows the injections to have a low amplitude while also having a high signal-to-noise ratio, since the actual grid disturbances may be correlated with the expected injection pattern. The work is experimentally demonstrated in a paper by Tewari et al. [95], although only a single result is given. The work presented in these papers is of particular interest as it may be adapted to allow multiple parallel units to implement impedance estimation simultaneously, provided that suitable sequences are chosen for each inverter. This functionality has not been explored by the authors.

2.4 Summary

In this chapter a review of existing literature has been used to show that there is cause for concern regarding the control of voltages on the distribution system, especially when DERs are used to supply a significant pro-

portion of the system demand. The literature shows that concerns have been raised with regard to both steady-state and transient voltage behaviour. Traditionally distribution systems have regulated voltage through the use of electromechanical tap-changing transformers. Some important limitations to the use of tap-changers have been found while reviewing the literature and three key reasons for considering an alternative, or at least supplementary, means of voltage regulation can be identified:

1. To reduce the impact of short-term voltage quality issues on the system, improving transient stability of the system.
2. To reduce wear on traditional electromechanical means of voltage control caused by an increase in contact switching events.
3. To mitigate poor regulation caused by reverse power flows, which OLTCs and similar devices were not designed to accommodate.

The literature on distribution system voltage control shows that there is an increasing need for more advanced methods of voltage control than tap-changing transformers at distribution level. In particular, the literature has shown that fast control may be required. Reactive power control has been demonstrated as a fast and stable means of voltage control on distribution systems, and STATCOMs provide a flexible and effective means of reactive power control. It has also been found that a consistent method of tuning STATCOM controllers is required and that the system impedance can be expected to have an impact on the controller dynamics. Consistent controller dynamics are particularly important when attempting to mitigate the transient impact of DERs. Methods of impedance estimation were therefore considered as an aid to adaptive, self-tuning controller design.

The literature shoes that even during normal operation, the system impedance may be expected to change with time and this shall, in turn, change the dynamics of the STATCOM AC voltage controller. A number of impedance estimation methods have been reviewed. Passive methods are considered to be of limited relevance to this work as the impedance cannot be

estimated at an arbitrary time. Active methods have therefore also been considered. The key advantage of active methods of impedance estimation when compared to passive methods is that they can estimate the impedance when required and at any frequency of interest, not just those already present on the system. One disadvantage of such methods is that they create a disturbance which may impact on normal operation of the system. In addition, they require the use of additional hardware to create and record the disturbance. Some active methods have been implemented using power converters and these are of particular interest.

Chapter 3

The STATCOM control scheme

This chapter shall introduce the STATCOM controller design used in this work. The purpose of the new controller design is to adapt to changes and reconfigurations of the surrounding power system in real time. In the proposed method, impedance estimation is used to evaluate the system and calculate new controller gains to match the current configuration. Changes in system impedance may occur when new power lines are installed, or old ones decommissioned, when local generation is activated or deactivated, and, for weak power systems where supply impedance may be comparable to load impedance, when a large load is switched on or off. Such changes to the system configuration are also likely to affect local system voltage, making it important to identify and compensate for them.

3.1 Proposed control structure

In this section, the STATCOM control design is considered. It was seen in Chapter 2 that there is no standard method for the design of STATCOM controllers. The proposed controller uses knowledge of the system impedance to determine the controller gain. For the purposes of this chapter, it is assumed that the system impedance is already accurately known. The impedance estimation and controller retuning part of this work will be presented in Chapter 4.

The STATCOM hardware consists of a three-phase grid connected inverter with appropriate measurements and a suitable controller. A simplified diagram of the STATCOM, showing only one of the three phases, is shown in Figure 3.1. The control structure consists of three parts: a DC-link voltage controller, an AC voltage magnitude controller and an AC current controller. The AC voltage controller and the DC link voltage controller are together referred to as the "outer, voltage control loop" and the AC current controller is referred to as the "inner, current control loop." The controller is said to have a nested structure. This is shown in Figure 3.2. The outer control loop calculates current references from the voltage errors, which are fed to the inner current control loop.

If a rotating reference (dq) frame is used for control, then the AC and DC voltage controllers may be designed independently of each other; assuming that the controller is synchronised to the AC system voltages, the DC-link voltage may be controlled by varying only the d-axis (in phase) component of the current, while the AC voltage magnitude may be manipulated by varying the q-axis (90° out of phase) current component. PI controllers may be used for the DC-link voltage controller and the AC current controller and these may be optimally designed based on the size of the components used in the STATCOM using standard design methods [96]. The real and reactive power of the STATCOM can be calculated in the dq reference frame using (3.1) and (3.2).

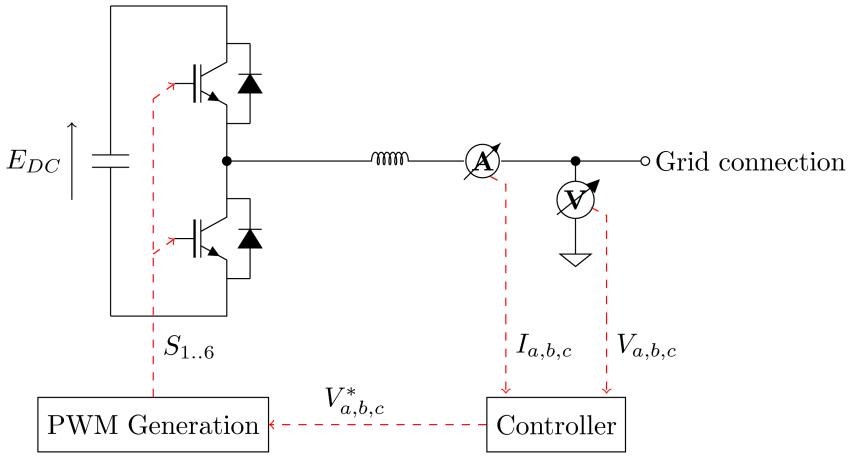

Figure 3.1: A simplified diagram of the STATCOM hardware, showing one leg of a three-phase converter, the required measurements and controller.

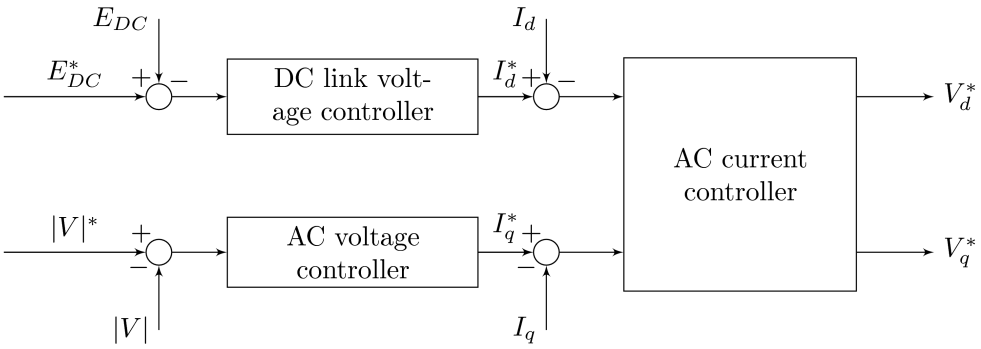

Figure 3.2: A simplified diagram of the STATCOM control structure.

$$P = V_d I_d + V_q I_q \tag{3.1}$$

$$Q = V_d I_q - V_q I_d \tag{3.2}$$

Grid synchronisation is achieved using a phase-locked loop, which is described in more detail in Appendix A. The STATCOM is synchronised to the supply voltage vector and therefore the q-axis component of the voltage should be zero. For the simulations performed in this work the STATCOM was assumed to be ideal. Specifically, it was treated as being 100 % efficient and therefore $P = 0$. It can therefore be seen that the d-axis current must also be zero. For this reason the DC-link controller is not considered in simulation.

The inner current control loop is designed to control the current flowing through the STATCOM output filter. The STATCOM filter inductance would ideally be minimised in order to reduce the required converter voltage at any given operating point. However, reducing the filter inductance will increase the current ripple due to the switching of the power electronic devices within the STATCOM. Using a higher switching frequency and higher control bandwidth does reduce the switching ripple, although it is still common to find LCL output filters on power converters to attenuate the switching ripple further. For the simulations performed in this work a purely inductive filter was used, and this was done to simplify the control design. This was acceptable because of the linearised STATCOM model used. The current control structure is shown in Figure 3.3. The controller consists of two identical PI controllers. The measured supply voltage is added to the output of the d-axis controller. The cross-coupling terms are included to improve the dynamic performance of the controller.

In order to allow the control loop to be implemented efficiently in software, the controllers were converted to an equivalent discrete form using the bilinear transform method and a pair of difference equations describing their

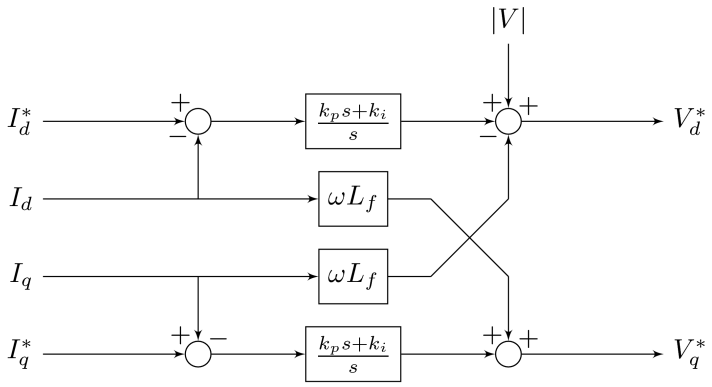

Figure 3.3: The dq current controller.

Parameter	Value
E_{DC}	900 V
L_f	750 μH
F_s	16 kHz
ω_0	800 Hz
ζ	0.8
k_p	6.032
k_i	18950

Table 3.1: Parameters used to model the STATCOM.

behaviour was derived. The circuit and control parameters used to model the STATCOM are listed in Table 3.1. F_s is the converter switching frequency and the sampling frequency of the control loop. ω_0 and ζ are the control loop bandwidth and damping factor respectively. Although the DC link voltage, E_{DC}, is not used directly in the simulations, which do not model the DC side of the STATCOM, it is used to determine the limits of the STATCOM converter voltages, which are confined to the range $\pm E_{DC}/2$.

The filter inductance, L_f, has been chosen based on the desired maximum reactive power capability of the STATCOM. The 750 μH inductor used allows approximately 530 A of peak reactive current to flow when connected to a 400 V system operating at nominal voltage. In this work, the actual maximum peak current is limited to 400 A which ensures that the STAT-

COM remains stable, even when the system voltage is high. The simulated STATCOM uses a linearised model and therefore the attenuation of switching ripple has not been considered when choosing a suitable inductance.

The controller proportional and integral gains, k_p and k_i, have been calculated to give the desired controller bandwidth, ω_0, and damping factor, ζ. The controller bandwidth was chosen to give a fast current response, but not so fast that the sampling delay had to be considered when designing the controller. A high controller bandwidth is desirable as it will improve both the overall dynamic response of the STATCOM and also improves the quality of the current [97]. The bandwidth has been limited to $F_s/20$ in order to ensure that the controller behaves as expected and is not affected by the control loop sampling delay. The damping factor has been chosen so that the controller is almost ideally damped ($\zeta = 0.707$), but with a small amount of additional damping so that the controller should not begin to resonate as a result of interactions with the system to which the STATCOM is connected.

3.1.1 Design of the AC voltage controller

As was discussed in Chapter 2, the design of the AC voltage magnitude controller is not so well documented; although PI controllers may be used, the actual gains are often fixed, having been set during commissioning of the system. It was also shown that the reactive power required to cause a change in voltage, ΔV, is dependent on the system impedance and the system voltage magnitude, V [10, 40]. The relationship is shown in (3.3), where $\alpha = R/X$.

$$\Delta Q \approx -\Delta V \frac{V}{X(1+\alpha^2)} \tag{3.3}$$

The required change in reactive current, ΔI_q, may then be calculated by dividing by V,

$$\Delta I_q = \frac{-\Delta V}{X(1+\alpha^2)} \tag{3.4}$$

If ΔV is taken as the instantaneous error between desired system voltage and measured system voltage, $V^* - V$, then using (3.4) it is possible to easily calculate an estimate of the required reactive current to regulate the voltage to the desired value. Integrating (3.4) with respect to time, (3.5) is obtained.

$$I_q^*(t) = k \int \frac{V(t) - V^*}{X(1+\alpha^2)} \, \mathrm{d}t \tag{3.5}$$

The parameter k is a fixed gain and is used to determine the time taken for a correctly tuned controller to respond to a disturbance. Specifically, the rise time, τ, of the controller is equal to $1/k$ seconds. Therefore, the value of k is chosen to give the desired controller rise time, which will be application specific. However, k must be limited so that τ remains larger than the system fundamental period (0.02 S for a 50 Hz system) or the controller may become unstable. In this work the value of k is fixed at 20; this allows for some error in the variable controller gain without compromising controller stability.

The performance of the controller may be evaluated by comparing the measured voltage following a disturbance with the expected value. Assuming that the voltage is initially equal to V^* then if a step change in voltage of magnitude ΔV, occurs at time $t = 0$ then the voltage at time $t = \tau$ may be found using (3.6):

$$V(\tau) = V^* + \Delta V \, \mathrm{e}^{-1} \tag{3.6}$$

The controller structure is shown in Figure 3.4. The input voltage, $|V|$, is the RMS voltage as measured at the STATCOM terminals. Calculation of the grid voltage is described in Appendix A. The measured voltage is first passed through a first-order low-pass filter. The cut-off frequency of this filter is 50 Hz. This frequency was chosen in order to attenuate any harmonic

voltages that may be present while still allowing reasonably rapid fluctuations in voltage to be detected. The calculation of the voltage magnitude effectively results in all harmonic frequencies being down-shifted by 50 Hz. The low-pass filter will therefore attenuate all frequencies beyond the second harmonic. The second harmonic will not be significantly attenuated, however, the level of second harmonic voltage, if present at all, should be low as a high level would imply asymmetry in the voltage waveforms. The voltage error is calculated as the difference between the measured system voltage and the demand voltage. The voltage error is then used to calculate the instantaneous reactive current demand. The final reactive current demand is calculated by integrating the instantaneous demands.

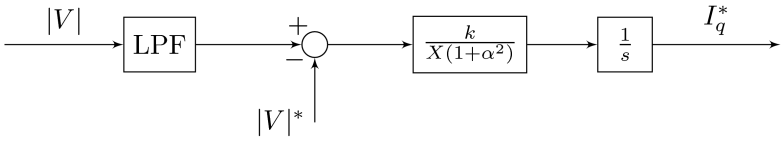

Figure 3.4: Block diagram of the AC voltage controller.

Simulations were performed on a very simple power system so that the controller design could be assessed. Both steady-state and dynamic performance of the controller are considered. The sensitivity of the controller to errors in the gain set using the system impedance is also considered. For the simulations, the power electronic components and the DC side of the STATCOM were ignored; the inverter was treated as three ideal, controllable voltage sources coupled to the grid through an inductive filter. A single line diagram of the simulation model used is shown in Figure 3.5. Initially the total supply impedance for these simulations is 0.1 Ω. The X/R ratio is initially set to 2.5, which was chosen as it is recommended as a test value in G83/2, the DG grid-connection standard for low voltage systems [98]. For the simulations presented in this section, the STATCOM reactive current was limited to ±400 A.

The first simulation was performed in order to observe both the steady-state and basic dynamic performance of the STATCOM AC voltage controller. Initially the supply voltage is 1 p.u. After 1 s a step decrease occurs so that

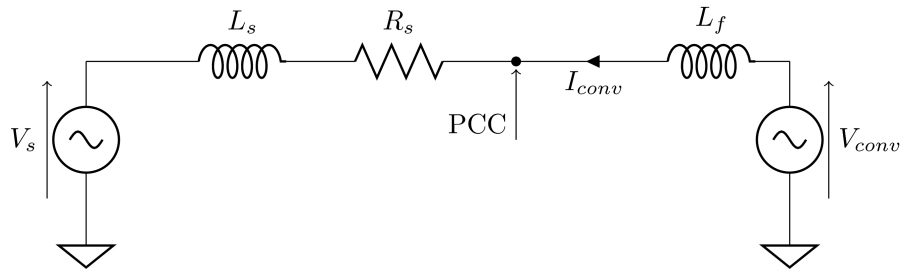

Figure 3.5: Single line diagram representing the simulated system used to demonstrate the controller behaviour.

the supply voltage becomes 0.95 p.u. For this simulation, the controller gain was set to exactly match the system impedance values. The fixed controller gain was set to give a controller rise time of 0.05 s. The voltage should therefore take 0.05 s to reach 0.98 p.u. after the initial disturbance. The simulation was repeated with the impedance estimates changed. The reactance estimate was initially set 50 % above the actual value, resulting in a reduced controller gain. The simulation was then repeated with the reactance estimate set 50 % below the actual value, resulting in an increased controller gain. Results of the simulations are shown in Figure 3.6.

It can clearly be seen that increasing the controller gain reduces the time taken to respond to the disturbance. The tuned controller reaches 0.98 p.u. approximately 0.054 s after the change in supply voltage. This is slightly later than expected and is most likely due to the voltage after the transient initially dropping as low as 0.94 p.u., below the expected minimum of 0.95 p.u. For comparison, the controller with the gain set high reaches 0.98 p.u. after 0.043 s and the controller with the gain set low reaches 0.98 p.u. after 0.067 s.

Simulations were performed in order to observe the sensitivity of the controller to a variation in supply resistance. As before, a step decrease in supply voltage was applied after 1 s. In this case, the reactance remained constant and the X/R ratio was varied from 1 to 5 by changing the resistance without adjusting the AC voltage controller gain to compensate. The results

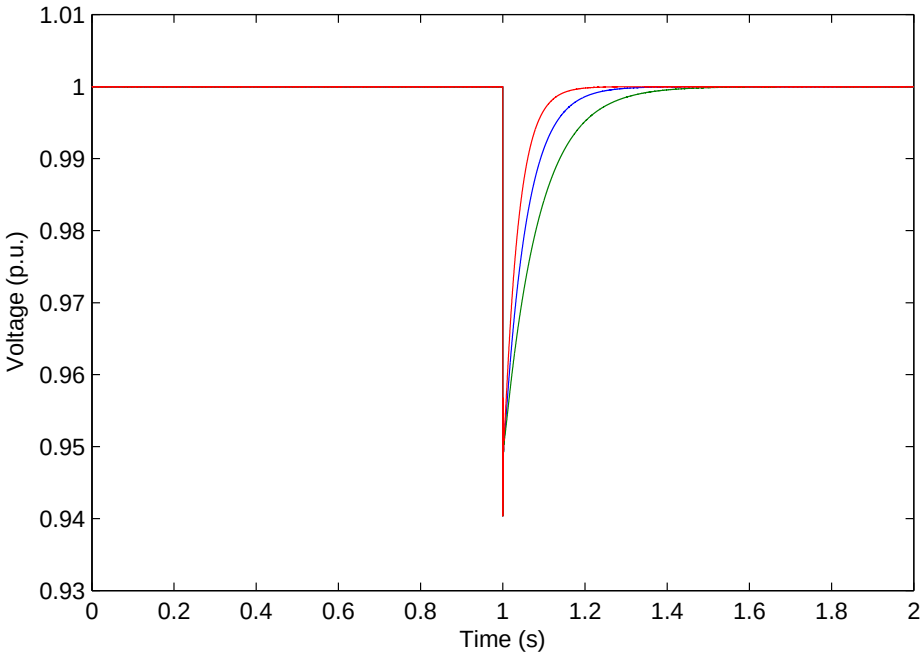

Figure 3.6: Controller response to a step change in supply voltage as the controller gain is varied. Nominal gain is shown in blue, high gain is shown in red and low gain in green.

are shown in Figure 3.7. Additional simulations were performed with very low X/R ratios. Figure 3.8 shows the results when the X/R ratio is varied from 1 to $^1/_3$.

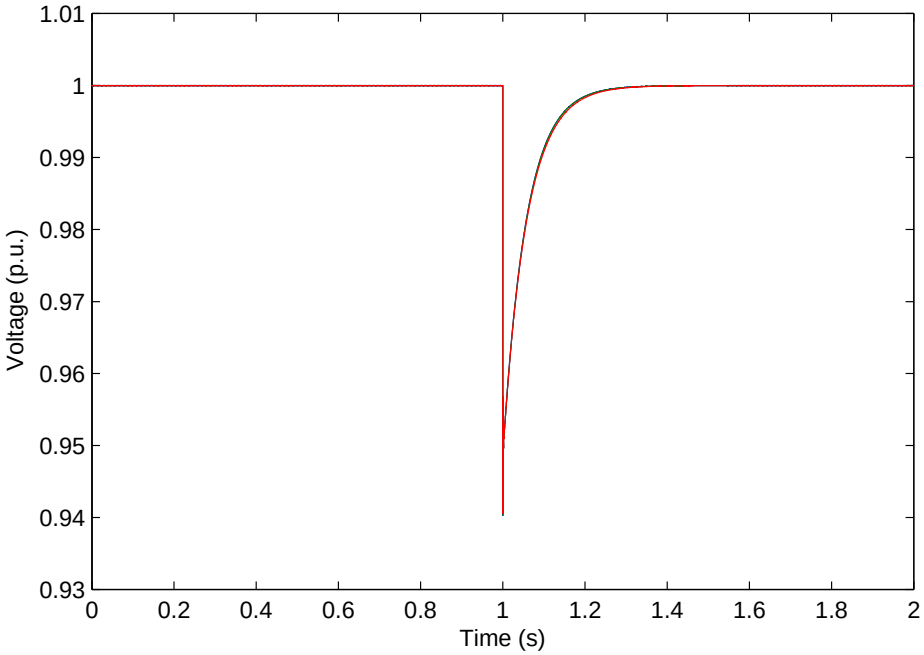

Figure 3.7: Controller response to a step change in supply voltage as the supply resistance is varied and reactance is held constant. X/R ratios of 1 (blue), 3 (green) and 5 (red) are considered.

It can be seen that when the X/R ratio is unity or greater the variation in resistance has a negligible effect on the controller dynamics. This result suggests that the effect of resistance on the controller dynamics may be ignored. The increase in resistance only slightly increases the amount of reactive power required to regulate the voltage. When the X/R ratio is 5, the reactive power required to maintain the voltage at 1 p.u. is 121 kVAr. When the X/R ratio is 1, this increases to 125 kVAr.

For X/R ratios less than one, the results are quite different. There is a noticeable difference between the response of the controller when the X/R ratio is $^1/_2$ compared with when it is 1, although the difference is still small. When the X/R ratio is further reduced to $^1/_3$ the system becomes unstable

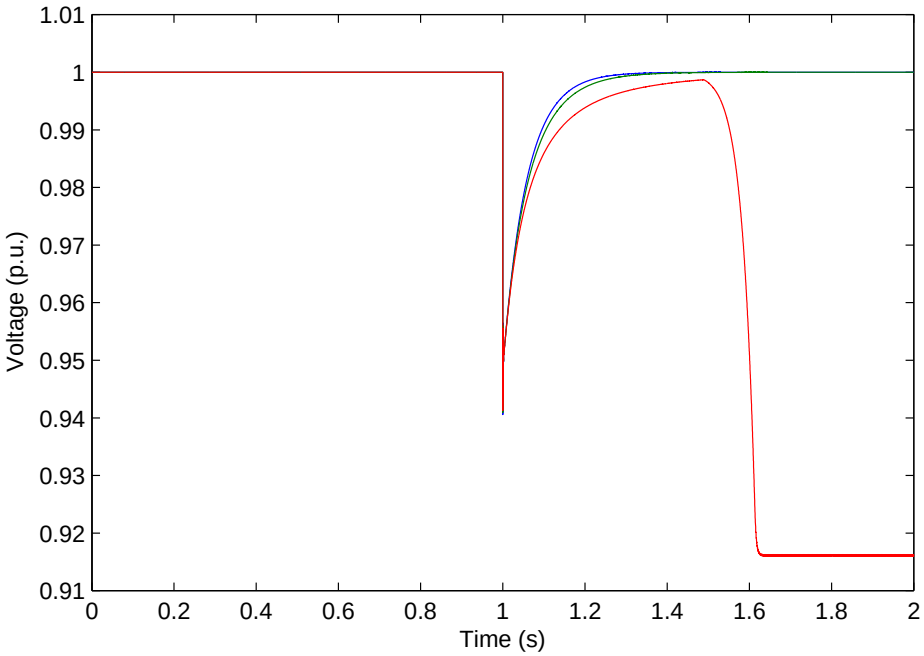

Figure 3.8: Controller response to a step change in supply voltage as the controller resistance is varied and reactance is held constant. X/R ratios of 1 (blue), $^1/_2$ (green) and $^1/_3$ (red) are considered.

and the voltage collapses. Voltage collapse occurs when the output of the STATCOM current control loop saturates. The risk of STATCOM instability when the X/R ratio is very low limits the applicability of this work to systems where the resistance is not significantly larger than the reactance and for this reason the remainder of this work is concerned only with systems having an X/R ratio greater than one. Determining a typical X/R ratio for distribution systems is difficult because the exact value is dependent on a number of factors, particular the type and length of cable and transformers used, the proximity to the nearest transformer and the circuit voltage. Consideration of a number of sources suggests that the X/R ratio is likely to be in the range 0.3–6 for 400 V and 11 kV networks [99–103], with the higher values typically found near substations and transformers, and on circuits with higher power capacities. If the STATCOM is installed close to a transformer then it is unlikely that the X/R ratio will be less than unity.

From the power flow equations it was predicted that the resistance would affect the controller dynamics. From the results presented this does not appear to be the case. To explain this discrepancy, it is observed that the power flow equations describe real and reactive power flow between the two ends of the line. If the reactive power at one end of the line is changed, then the reactive power at the other end of the line does not change by an equal amount. This is illustrated for a system with an X/R ratio of 2.5 in Figure 3.9 and for a system with an X/R ratio of 1 in Figure 3.10. The impedances, and therefore the voltage drop between the two ends of the line, has been exaggerated for clarity.

Initially the current at the receiving end of the line is $I = 0.4 + j0.12$ p.u. The real power at the receiving end of the line is equal to $P_r = VI\cos(\theta)$ and the reactive power is equal to $Q_r = VI\sin(\theta)$. At the sending end of the line the real power is equal to $P_s = VI\cos(\theta + \delta)$ and the reactive power is equal to $Q_s = VI\sin(\theta + \delta)$. The real power at the sending end of the line is therefore less than would be predicted if δ was neglected while the reactive power is greater than would be predicted.

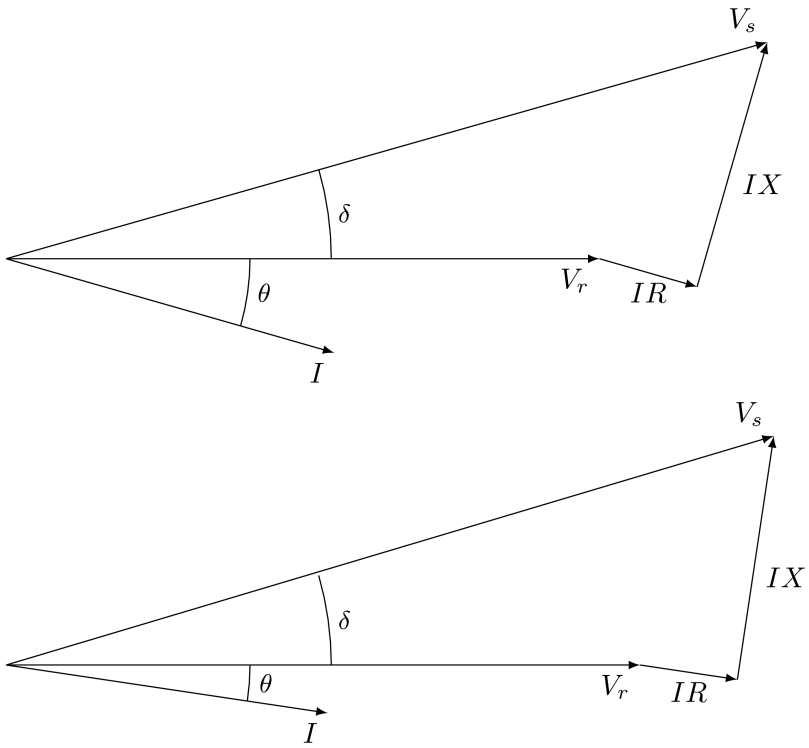

Figure 3.9: Phasor diagram showing the effect of varying reactive power at the receiving end of the line for a system with an X/R ratio of 2.5.

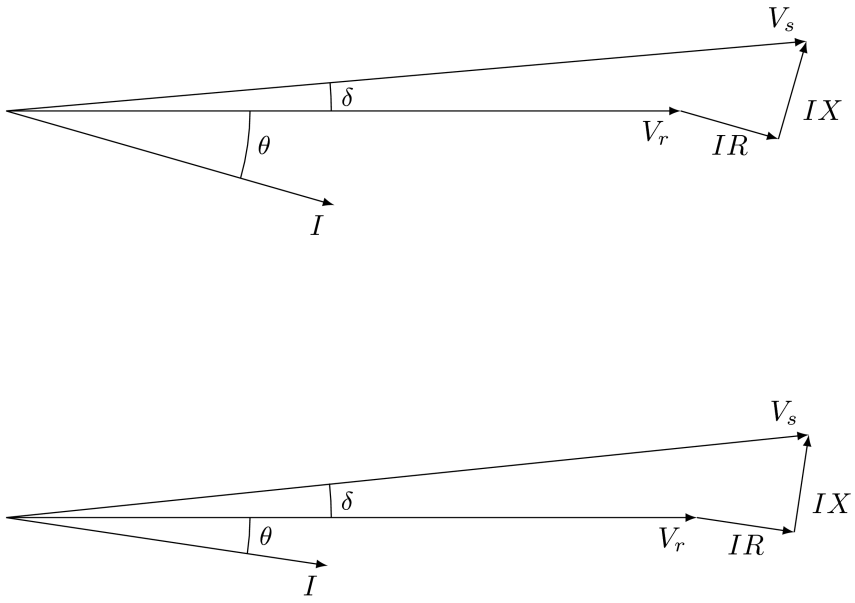

Figure 3.10: Phasor diagram showing the effect of varying reactive power at the receiving end of the line for a system with an X/R ratio of 1.

The reactive current is halved and therefore the overall current is reduced to $I = 0.4 + j0.06$ p.u. It can be seen from the phasor diagrams that the change in reactive current only slightly changes the absolute magnitude of the current, although it does have a significant effect on the angle, θ, between the receiving end voltage and the load current. Similarly, the magnitude of the voltage drop between the sending and receiving ends of the line remains almost constant, but rotates relative the receiving end voltage phasor. At the receiving end of the line, the change in reactive current, I_q, results in a significant change in reactive power and a small change in real power, which is caused by the change in receiving end voltage and may be assumed to be almost zero. At the sending end of the line, both real and reactive power change significantly. Although only reactive power has varied significantly at the load, both the real and reactive power flowing in the line have varied considerably as a result.

The voltage drop phasor, $\Delta\mathbf{V}$, may be calculated from the load current, I

and the complex line impedance, Z:

$$\Delta \mathbf{V} = IZ \tag{3.7}$$

The apparent power, S, at the sending end of the line is equal to:

$$S = P_s + jQ_s = V_s I^* \tag{3.8}$$

Where I^* is the complex conjugate of the current, I. Combining (3.7) and (3.8), the voltage drop may be calculated from the sending end real and reactive power using (3.9):

$$\begin{aligned} \Delta \mathbf{V} &= \frac{SZ}{|V_s|} \\ &= \frac{(P_s - jQ_s)(R + jX)}{|V_s|} \\ &= \frac{P_s R + Q_s X}{|V_s|} + j\frac{P_s X - Q_s R}{|V_s|} \end{aligned} \tag{3.9}$$

Assuming δ is small, the difference in voltage magnitude between the sending and receiving end voltages may be approximated by calculating only the real part of the voltage drop, as in (3.10):

$$\Delta V \approx \frac{P_s R + Q_s X}{|V_s|} \approx \frac{P_r R + Q_r X}{|V_r|} \tag{3.10}$$

This approximation is widely used when resistance is not negligible and δ is small [10, 103]. It is clear from these results that the controller design should be revised so that the resistance is not considered, since only reactive power is varied by the STATCOM. The revised controller design, once the terms involving resistance have been removed from the control equations, is shown in Figure 3.11.

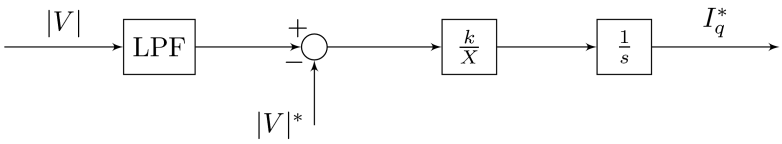

Figure 3.11: Block diagram of the revised AC voltage controller.

A final series of simulations was performed in order to observe the sensitivity to a variation in reactance. For these simulations, the resistance was kept constant and the X/R ratio was again varied from 1 to 5. The controller gains were kept constant as in the previous simulations. Results are shown in Figure 3.12.

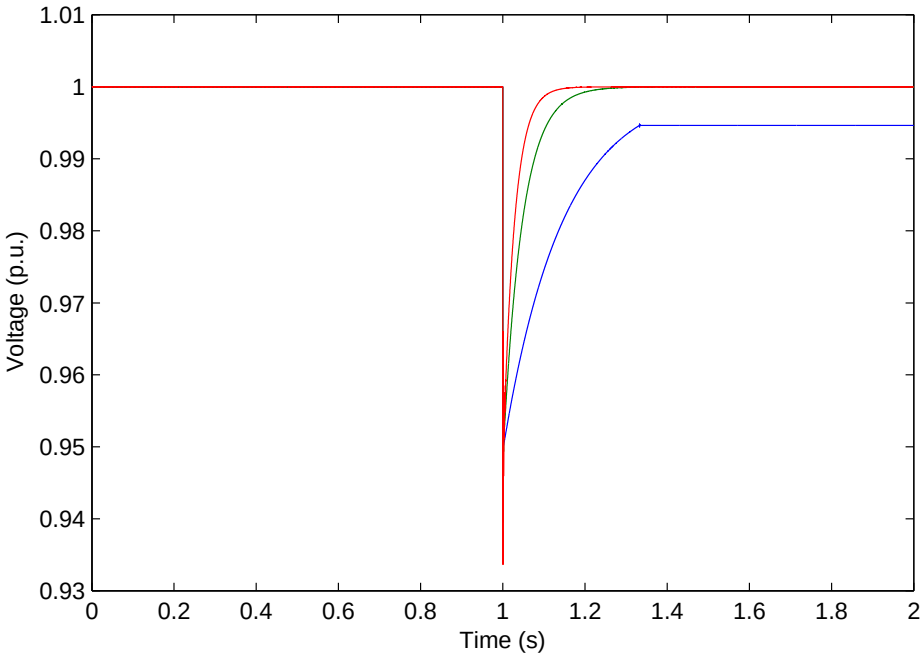

Figure 3.12: Controller response to a step change in supply voltage as the supply reactance is varied and resistance is held constant. X/R ratios of 1 (blue), 3 (green) and 5 (red) are considered.

When the X/R ratio is 1 it can be seen that the voltage does not return to 1 p.u. This is because the AC voltage controller saturates before the voltage has reached the desired level and therefore the STATCOM is not able to supply the required reactive power. Unlike saturation of the STATCOM current controller, this does not cause voltage instability. As expected, the response

time of the controller can be seen to decrease as the supply reactance increases. The reactive power required to control the voltage also decreases with increasing supply reactance. When the X/R ratio is 1 the STATCOM supplies 276 kVAr and the output of the AC voltage controller saturates. Only 60 kVAr is required to return the voltage to 1 p.u. when the X/R ratio is 5.

3.1.2 Variation in displacement angle

The analysis presented has so far ignored the effect of reactive power injection on the displacement angle between the supply and the STATCOM, δ. The displacement angle is normally small and may therefore be disregarded in order to simplify calculations. It is also disregarded for practical reasons: in order to calculate δ it is necessary to have knowledge of the instantaneous voltages at both the supply and STATCOM terminals and the required measurements may not be available. Despite this, variations in displacement angle may have an impact on the effectiveness and stability of the STATCOM. For low X/R ratio systems the displacement angle is dependent on both real and reactive power flow, unlike transmission systems where it is normally assumed that displacement angle is almost exclusively dependent on real power flow [40]. The variation in displacement angle caused by the reactive power supplied by the STATCOM will now be considered.

When only reactive power flow is considered the displacement angle, δ, may be calculated using (3.11):

$$\delta = -\arctan\left(\frac{I_q R}{V_r + I_q X}\right) \tag{3.11}$$

Assuming that the change in voltage resulting from injection of reactive power is small, then for the 400 V system with a supply impedance of 0.1 Ω and X/R ratio of 2.5 used in the previous simulations the estimated change in δ is less than 0.01° per kVAr of injected reactive power. This change is

small and is not considered to be a significant concern. Simulations were performed on the system described to evaluate the accuracy of this approximate analysis. The injected reactive power was varied in steps. At each step the displacement angle and injected reactive power were recorded. The injected reactive power was then used to estimate the displacement angle. The results of both the calculations and the simulations are listed in Table 3.2.

Some difference is seen between the estimated values and those obtained through simulation. However, it should be noted that the estimated values do not take into account the variation of voltage caused by the injection and absorption of reactive power and therefore some difference between the two sets of values is to be expected. Both the estimated and simulated values of δ remain small. In practice, the actual value of δ may not be 0 when the STATCOM is not supplying reactive power, since any loads on the system will also cause the phase displacement to vary. Since the variation is non-linear, as can be seen in Table 3.2, these results should be interpreted with care. What can be inferred from these results is that provided δ is small, then the STATCOM itself is unlikely to cause a significant change in the phase displacement between the supply and PCC.

Injected Q(kVAr)	Estimated δ	Simulated δ
-100	0.75°	0.89°
-50	0.38°	0.46°
-20	0.15°	0.17°
-10	0.08°	0.09°
0	0°	0°
10	−0.08°	−0.10°
20	−0.16°	−0.19°
50	−0.39°	−0.48°
100	−0.80°	−0.93°

Table 3.2: Estimated and simulated change in δ for various levels of reactive power injection.

The simulation was repeated for a system with a unity X/R ratio. The over-

all impedance of the system remained the same. The results from this simulation and the estimated values of δ are shown in Table 3.3. As with the previous set of results, both the estimated and simulated values of δ are small. Some discrepancy is seen between the two sets of values, but as before, the estimated values do not take into account the change in voltage caused by the change in reactive power. The results for the supply with the lower X/R ratio show that the change in δ has increased. This is to be expected as the change in displacement angle caused by a change in reactive power is dependent on the supply resistance, which has been increased.

Injected Q(kVAr)	Estimated δ	Simulated δ
-100	1.44°	1.74°
-50	0.73°	0.88°
-20	0.29°	0.36°
-10	0.25°	0.18°
0	0°	0°
10	−0.25°	−0.18°
20	−0.30°	−0.36°
50	−0.75°	−0.91°
100	−1.51°	−1.86°

Table 3.3: Estimated and simulated change in δ for various levels of reactive power injection for a low X/R ratio system.

This section has described the STATCOM control structure and proposed an AC voltage controller to generate the reactive current demand. Basic simulations have been presented to validate the proposed AC voltage controller. Calculations and simulations have been performed in order to demonstrate that the STATCOM is unlikely to cause a significant change in displacement angle between the system supply and the point of common coupling. In the next section, droop modifications to the AC voltage controller, allowing parallel operation of multiple STATCOMs, will be described and validated.

3.2 Operating units in parallel

In a large and complex electrical system it is likely, if not inevitable, that two or more sources, of either real or reactive power, will end up competing to regulate voltage. It is possible for devices capable of regulating voltage to be connected in parallel if they are controlled correctly and the following conditions are met [10]:

1. The terminal voltages of the regulating devices must be equal.
2. The phase sequence of the regulating devices must be the same.
3. The regulating devices must be operating at the same frequency.

In the case of STATCOMs operating in parallel, conditions 2 and 3 above are achieved through synchronisation to the grid and for this reason are not an issue. Therefore, this section is concerned with how condition 1 is achieved. It should be noted that condition 1 may not be met if each device attempts to control the voltage independently; it is necessary that the devices cooperatively manage the voltage and this is only possible if the voltage set-point is allowed to vary, i.e. absolute voltage control must be sacrificed to allow flexibility and future expansion of the system.

3.2.1 Droop control

In the context of this work, droop control is applied to the AC voltage controller and is used with the intention that:

1. Two or more STATCOMs may be operated in parallel if desired.
2. Reactive power is shared between parallel units proportional to the maximum ratings of each unit.

The steady-state terminal voltage, V_T, of each device is adjusted depending on the reactive current being supplied by that device, as in (3.12). D_Q is referred to as the "droop constant" and is calculated as shown in (3.13). When per-unit quantities are used, the droop constant may be expressed as a percentage or per-unit value, and is equal to the voltage drop relative to the nominal system voltage, as measured at the device terminals, when operating at full load.

$$V_T = V_{nom} + D_Q I_q \tag{3.12}$$

$$D_Q = \frac{V_{nom} - V_{min}}{\hat{I}_q} \tag{3.13}$$

Figure 3.13 aims to give a graphical explanation of droop control. Two sources with different ratings are supplying reactive power to a system at voltage V_T. If the voltage changes to V_T' then the reactive power supplied by the two sources will also change. The new system voltage may be used to find the new reactive power supplied by the two sources, as shown by the dashed lines. Provided the droop constant and the nominal voltage of both sources is the same, the ratio of Q_1 and Q_2 remains the same at the new operating point and therefore the load is shared proportionally between the two sources.

In addition to allowing multiple devices to operate in parallel, using a droop-controlled voltage regulator has an additional benefit: continuously adjusting the voltage reference means that the operating range of the STATCOM is effectively increased and that the overall current demand on the STATCOM at a given system operating point is reduced. The current rating may therefore be reduced for a droop-controlled STATCOM compared to a fixed-reference STATCOM. Regulations allow for some voltage variation [15], so the loss of absolute voltage control is acceptable in most circumstances.

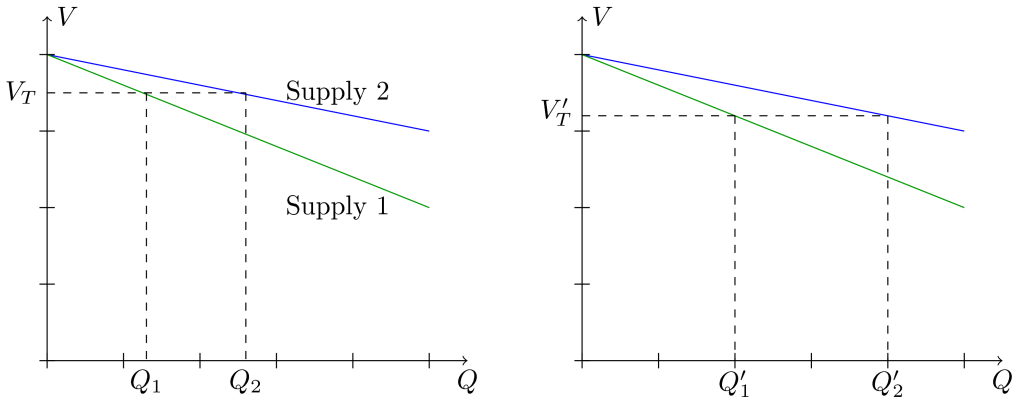

Figure 3.13: A graphical illustration of droop control showing two reactive power sources at two different operating points.

3.2.2 Controller modifications for droop control

The inclusion of droop functionality in the control loop requires a simple modification to the AC voltage controller. The reactive current demand is fed back from the controller output, scaled by the droop gain, and subtracted from the voltage reference at the input. The revised controller is shown in Figure 3.14. The additional feedback cancels the integral action of the original controller at low frequencies, causing the controller gain to be reduced. At higher frequencies the controller gain is unaffected by the droop feedback and the ability of the droop controller to respond to transients is therefore not compromised. The feedback gain is set according to the desired droop constant and the rating of the STATCOM. For the STATCOM described in the previous section, with a 400 A rating and a droop constant of 5 %, the droop constant is 0.0425 VA^{-1}. It should be noted that since positive reactive current causes a drop in system voltage and since an increase in reactive current demand now results in a proportional increase in the STATCOM AC voltage demand, the time taken for the controller to reach a new steady-state operating point is reduced. This is shown for a single droop controlled STATCOM in Figure 3.15. The response of the STATCOM without droop control is shown for comparison. It can be seen that the droop-controlled STATCOM has a time-constant which is approximately

half the time-constant of the original controller, or 0.025 S.

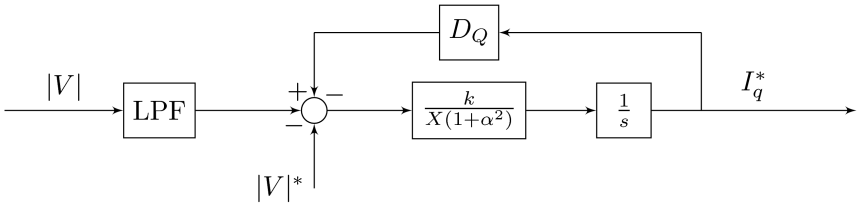

Figure 3.14: The voltage controller with droop feedback.

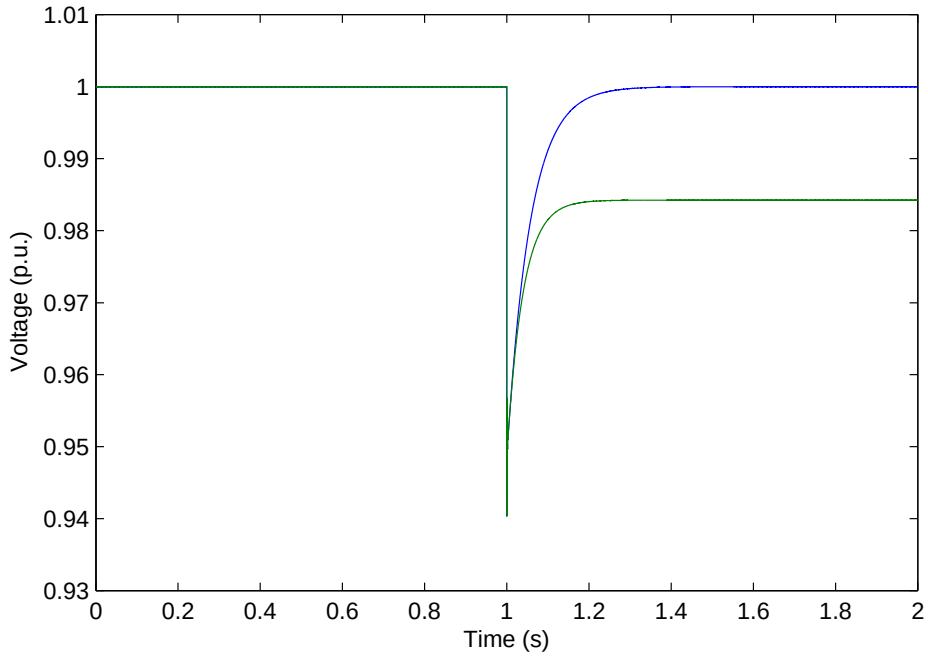

Figure 3.15: Response of the droop controller (green) compared with the original controller (blue).

In order to demonstrate that the droop controller behaves as expected, simulations were performed with a second STATCOM with the same current rating as the first present. The STATCOMs were connected in parallel. Both STATCOMs had correctly tuned controllers and the droop constant for both was set to 0.0425 VA^{-1}. A small additional impedance had to be placed between the STATCOMs for the simulation to run correctly; when this was not done, the system voltage failed to converge on any realistic value. The additional impedance was provided through a 10 μH inductance in series

with each STATCOM. Results showing the system voltage are shown in Figure 3.16 and the reactive currents provided by each of the STATCOMs are shown in Figure 3.17.

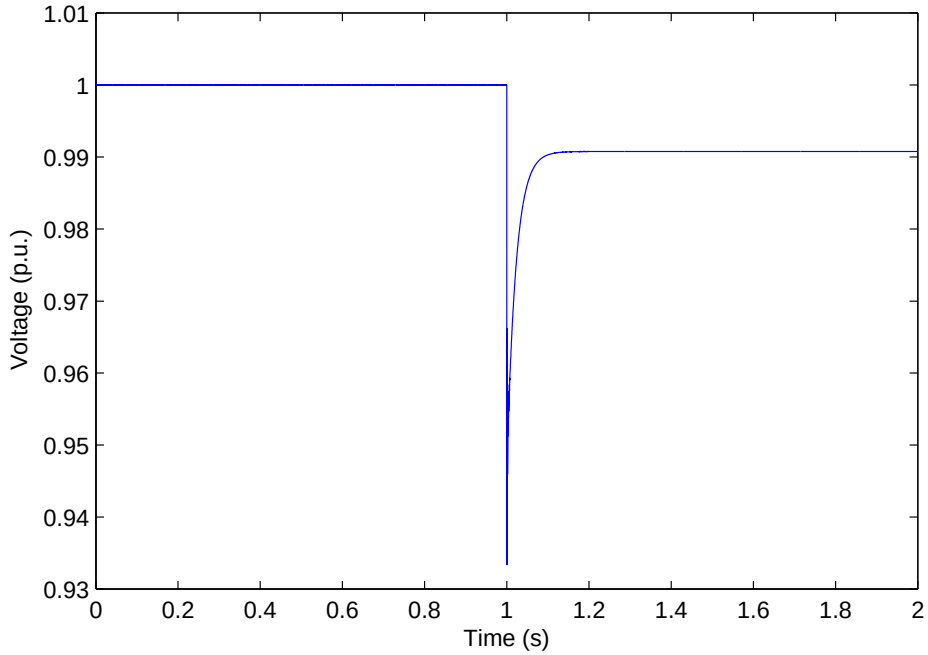

Figure 3.16: PCC voltage of the system when two droop controlled STATCOMs with equal ratings are controlling the voltage.

The new steady-state voltage is slightly above 0.99 p.u. This is only marginally lower than the original value of 1 p.u., although the new voltage will vary with load. The two current curves cannot be distinguished from each other, which shows that the two STATCOMs share the load equally between them and the control response for both STATCOMs is the same. The reactive current provided by each STATCOM is approximately 72 A, which gives 144 A total. For comparison, a single droop controlled STATCOM with the same ratings as the two used in these simulations regulates the voltage to approximately 0.985 p.u.and requires almost 120 A to do so. In the case of a single STATCOM without droop control, the current required to regulate the voltage to 1 p.u.is approximately 170 A.

The simulation was repeated with two STATCOMs having different droop

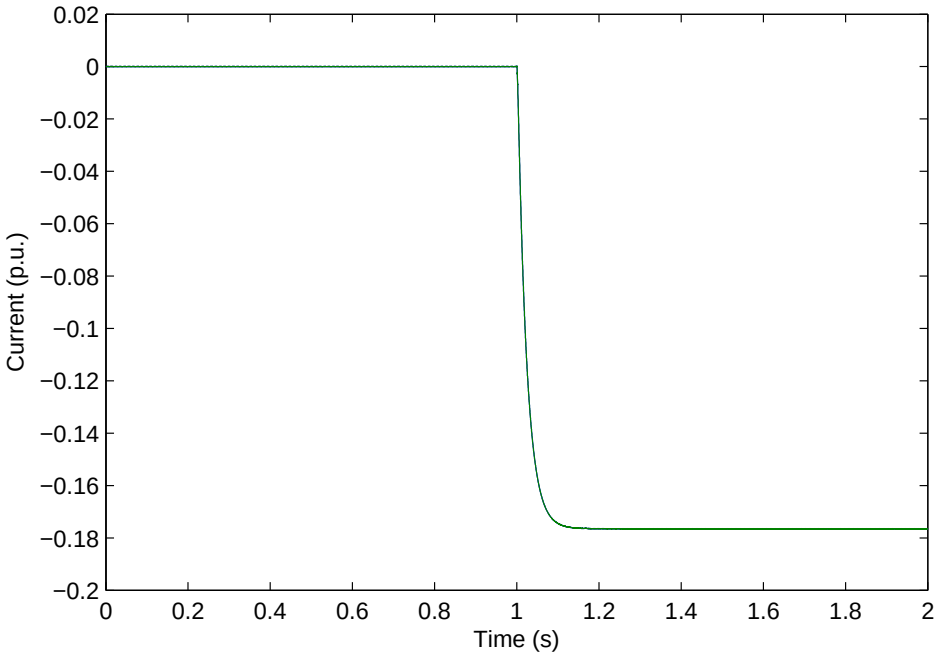

Figure 3.17: Reactive currents supplied by the two STATCOMs.

constants and maximum current ratings. In this case one STATCOM, referred to as STATCOM 1 for clarity, has a droop constant of 0.0567 VA^{-1} and a current rating of 267 A. The other, referred to as STATCOM 2 for clarity, has a droop constant of 0.0283 VA^{-1} and a current rating of 533 A. The system voltage is shown in Figure 3.18 and STATCOM reactive currents are shown in Figure 3.19.

As was the case when two identical STATCOMs were used, the voltage is controlled to approximately 0.99 p.u. once it has returned to steady-state. Once ins steady state, STATCOM 1 supplies approximately 48 A while STATCOM 2 supplies approximately 93 A. In both cases, when the respective STATCOM current rating are taken as the base current, the per unit current is close to 0.18 p.u., although it can be seen that STATCOM 1 provides a slightly larger share than STATCOM 2. This result, although not ideal, is not entirely unexpected as imperfect load sharing between droop controlled sources has been reported by a number of previous authors [104–106].

In this section, modifications to the AC voltage controller have been made

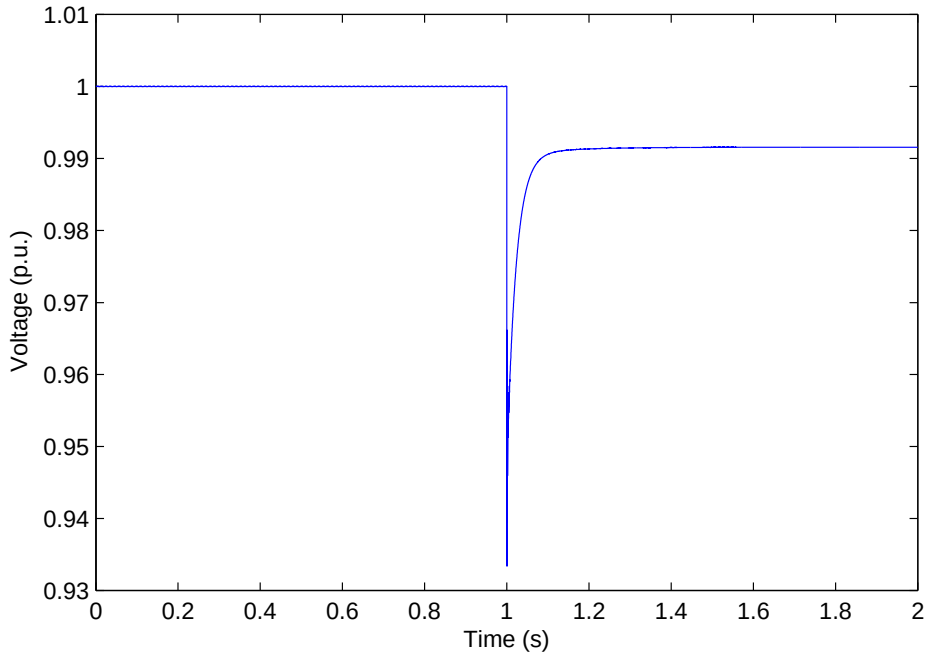

Figure 3.18: PCC voltage of the system when two droop controlled STATCOMs with different ratings and droop constants are controlling the voltage.

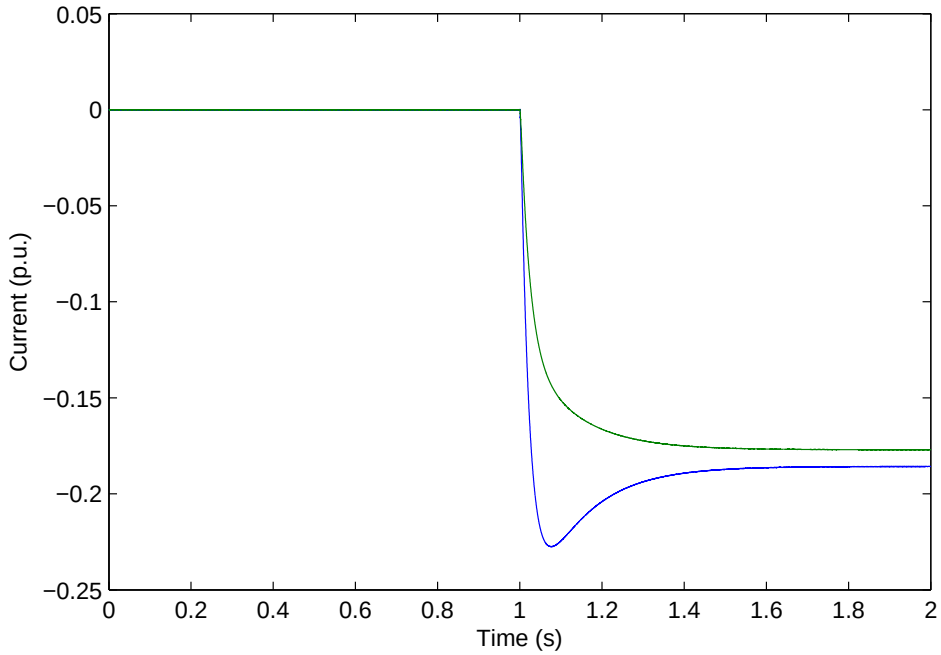

Figure 3.19: Reactive currents supplied by STATCOM 1 (blue) and STATCOM 2 (green).

in order to allow multiple STATCOMs to operate in parallel. Simulations have been used to demonstrate the behaviour of the revised controller and the operation of multiple parallel STATCOMs. Study of the droop controlled STATCOM does not form a major part of this work, but has been included for completeness and to demonstrate that the proposed controller with droop modifications is suitable for deployment on systems where multiple devices may be installed in parallel or where future expandability is desirable.

3.3 Summary

This chapter has introduced the STATCOM control scheme used throughout the rest of this work. The control scheme works by continually estimating the reactive current required to reach the desired system voltage and adjusting the output of the STATCOM accordingly. Simulation has been used to demonstrate that the controller functions as expected. The behaviour of the controller when the system X/R ratio is small, as is typical on distribution systems, has been considered. Unexpectedly, it was found that the supply resistance does not have a significant impact on the controller dynamics when the supply X/R ratio is greater than one.

Droop control modifications required to operate STATCOMs in parallel have been described and it has been demonstrated through basic simulation that, with the appropriate modifications to the control structure, parallel operation of multiple STATCOMs is possible, with reactive power shared between them.

Knowledge of the system impedance is required for the controller described to function correctly. In this chapter it has been assumed that the impedance of the system is known and fixed controllers have been used based on this assumption. The impedance of the system may not already be known or it may change from time to time. In the next chapter the applicability of im-

pedance estimation to tuning the STATCOM controllers will be discussed.

Chapter 4

Impedance estimation

The impedance estimation method used in this work needed to be one which could be implemented using a power electronic converter, therefore allowing it to be an added function of the STATCOM control. In addition, it had to be possible to estimate the impedance when desired, without having to wait for a significant grid event. Ideally the method would allow the impedance over a range of frequencies to be calculated. Finally, although the method had to be invasive (in order to meet the previous requirement) the disturbance created by the method should be kept to a minimum. In order to meet these requirements, an impulse injection method was chosen.

4.1 Fully controlled injections

Palethorpe et al. [87] proposed an impulse injection method which is referred to as Active Impedance Estimation (AIE). This method has been described in more detail in Chapter 2 and uses a power electronic converter to inject a small disturbance on to the grid. The PWM switching pattern of the power electronic converter is manipulated in order to give an injection of the desired length and with approximately the shape and amplitude intended. This method was initially considered for the impedance estimation portion of this work, however some limitations of the method were identified and in order to overcome these some modifications to the technique are proposed in this section. For the purposes of this work, the original AIE method is referred to as "feed-forward AIE" and the modified AIE method is referred to as "fully-controlled AIE."

The key disadvantage of the feed-forward method and the main motivation for modifying the scheme is the distortion of the injection caused by the current control loop in the power converter. This is illustrated in Figure 4.1, where an "ideal" 2 mS, 20 A injection is shown and compared to the same injection when the response of the current controller is taken in to account. As can be seen, the amplitude of the injection is reduced and the shape has changed substantially. The frequency content of both injections is also shown, with the amplitude normalised to the reference injection. It can be seen that the frequency content has also changed considerably, especially at low frequencies.

The length of the "ideal" injection was chosen to allow good impedance estimation at low frequencies. For the 2 mS injection used, most of the injection energy is concentrated at frequencies below 1 kHz. The attenuation of these frequencies is therefore a particular concern for this work. The wavelength of the injection at 1 kHz is approximately 300 km, which is likely to be greater than most lengths of cable found on distribution systems and therefore line length is not considered to be an issue for this work. The pulse

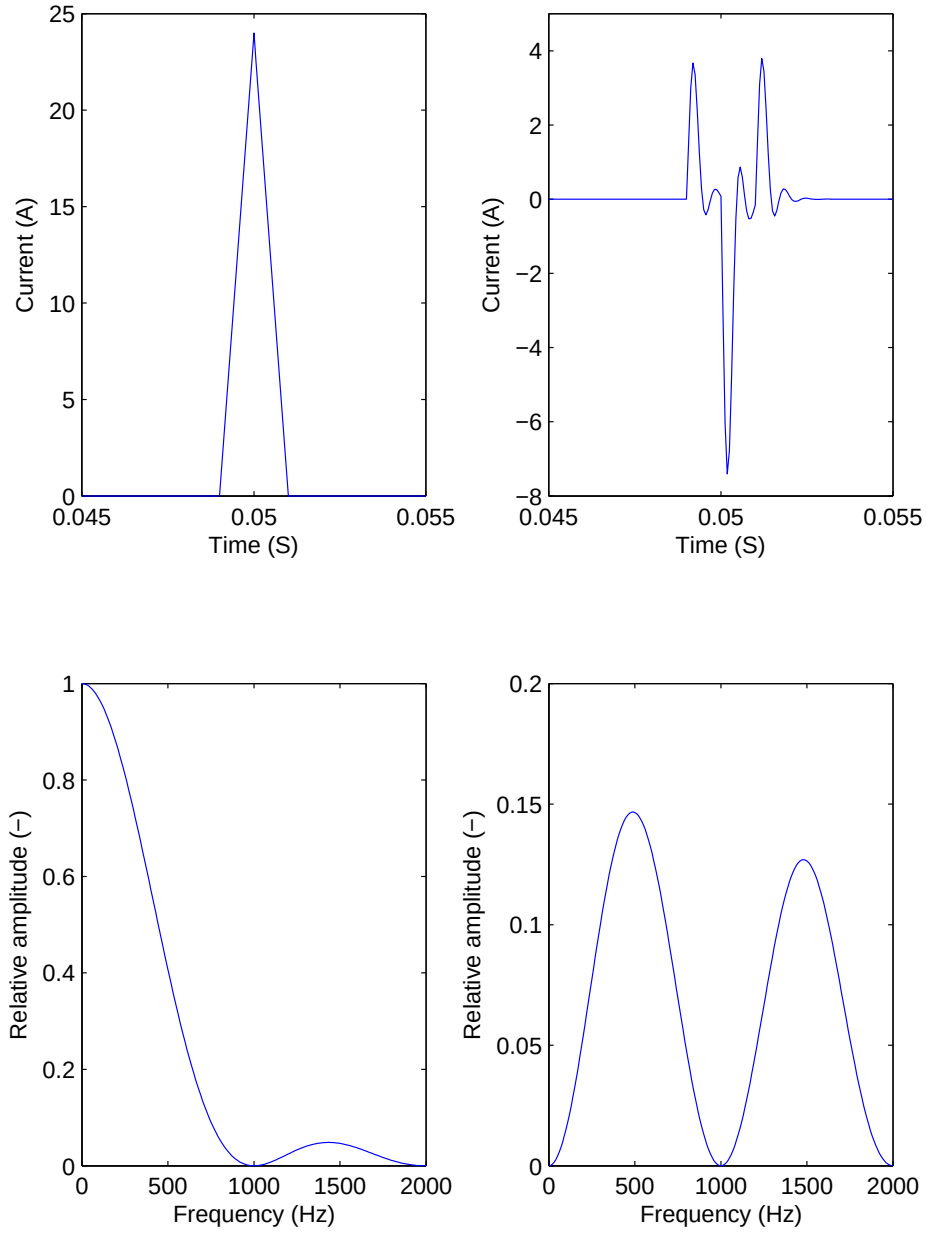

Figure 4.1: Reference current injection (left) compared to the actual current injection (right) when the control dynamics are considered in both the time and frequency domains.

amplitude for the "ideal" injection was chosen as a compromise between injection strength and the size of the disturbance caused; a larger injection amplitude will improve results but also increase the disturbance a 20 A injection for 2 mS is unlikely to cause a disturbance significant enough to effect nearby loads or generation.

Rather than manipulating the PWM signals directly, the fully-controlled injection method uses a high-bandwidth current controller and varies the current demands in order to create the injection. The injection current demands are generated in the stationary reference frame and then translated to the rotating dq reference frame. The injection current demands are then added to the usual current demands, I_d^* and I_q^* to produce revised demands, $I_d^{*'}$ and $I_q^{*'}$ which are then supplied to the current controller. This is illustrated in Figure 4.2. For this work, a converter with a 16 kHz switching frequency and 800 Hz current controller bandwidth as described in the previous chapter was simulated. The current controller bandwidth is high enough to allow the injected current to be controlled to the level required to produce an injection that resembles the "ideal" injection, as can be seen in Figure 4.3. It can be seen that the controlled injection resembles the reference injection reasonably well and that the frequency content of the two injections is similar, particularly at low frequencies, which are of the greatest importance to this work.

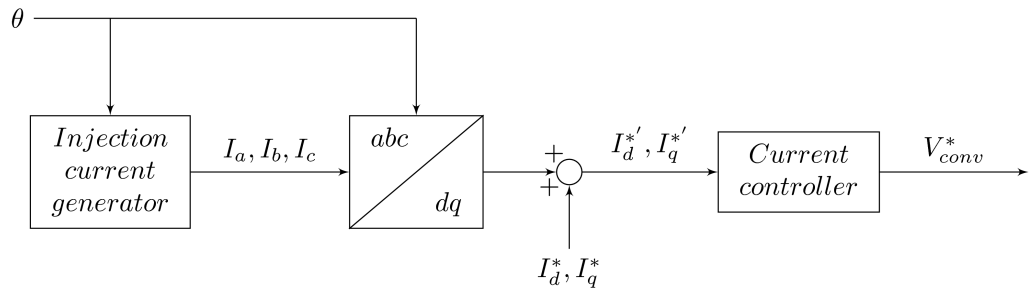

Figure 4.2: The converter current control loop, modified to allow controlled current injections.

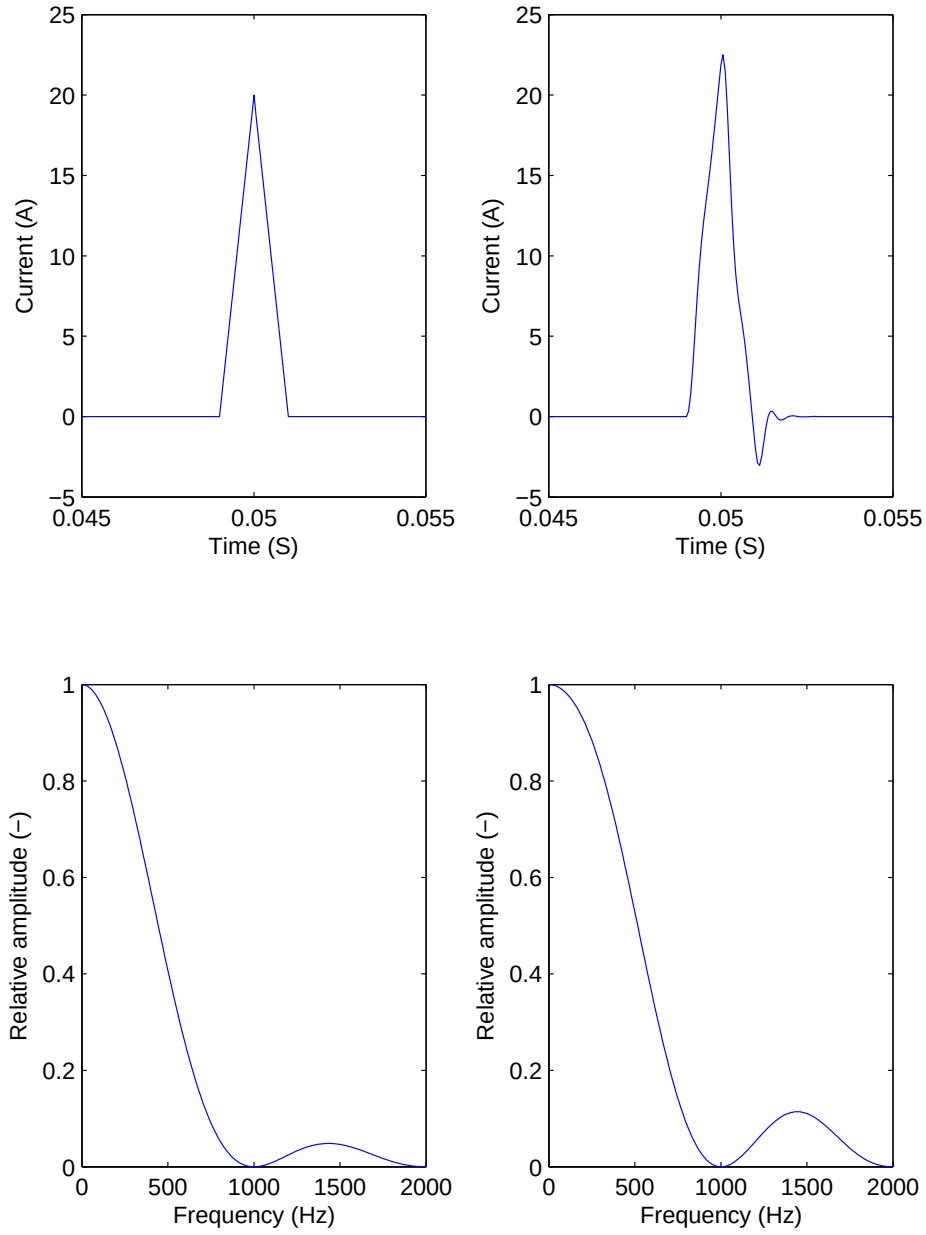

Figure 4.3: Reference (left) and fully controlled (right) injections compared in both the time and frequency domain.

4.2 Signal processing method

Once the transient voltages and currents have been captured some processing is required in order to estimate the system impedance. The recorded voltage and current data will invariably contain a significant component at the system fundamental frequency and several harmonics thereof. The fundamental and harmonic content are a significant source of error in the impedance estimates if not addressed. Prior to using the recorded data for impedance estimation, a number of steps may be taken to mitigate the effect of the steady-state frequency content.

The steady-state components of the signal may be removed by subtracting a time-delayed copy of a signal from itself. This is described mathematically in (4.1) and (4.2), where $v'(t)$ and $i'(t)$ are the processed voltage and current measurements to be used for impedance estimation, t is the current time and T the amount of time by which the copied signal is delayed. If translated to the frequency domain, this method is equivalent to having notch filters tuned to $\frac{1}{T}$ and all its harmonics and is known as comb filtering. The simplest discrete implementation of a comb filter is shown in Figure 4.4. The constant, n, is chosen so that $n = \frac{T}{T_s}$, where T_s is the sampling period of the delay. The filter frequency response is shown in Figure 4.5.

$$v'(t) = v(t) - v(t - T) \tag{4.1}$$

$$i'(t) = i(t) - i(t - T) \tag{4.2}$$

If T is chosen to be exactly equal to one fundamental period then the fundamental and harmonics will be exactly cancelled. The effectiveness of this method is dependent on how closely matched the comb filter tuning is to the system fundamental. T could actually be equal to any number of fundamental periods; however, as T is increased, the effect of errors caused by small deviations in fundamental frequency also increases. In practice, significant

attenuation of the steady-state signal is achievable, but complete cancellation is not. In the United Kingdom the grid frequency should be maintained between statutory limits of 49.5 Hz and 50.5 Hz [107]. The ideal comb filter gain at these frequencies is 0.063, which would result in unacceptably poor cancellation. In practice the grid frequency is maintained within a narrower range during normal, steady state operation to ensure that the limits are not exceeded. It is also possible to measure the grid frequency and adjust the filter delay time to match the grid fundamental period.

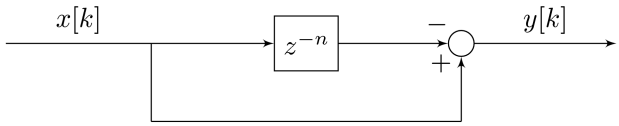

Figure 4.4: A comb filter implemented as a discrete transfer function.

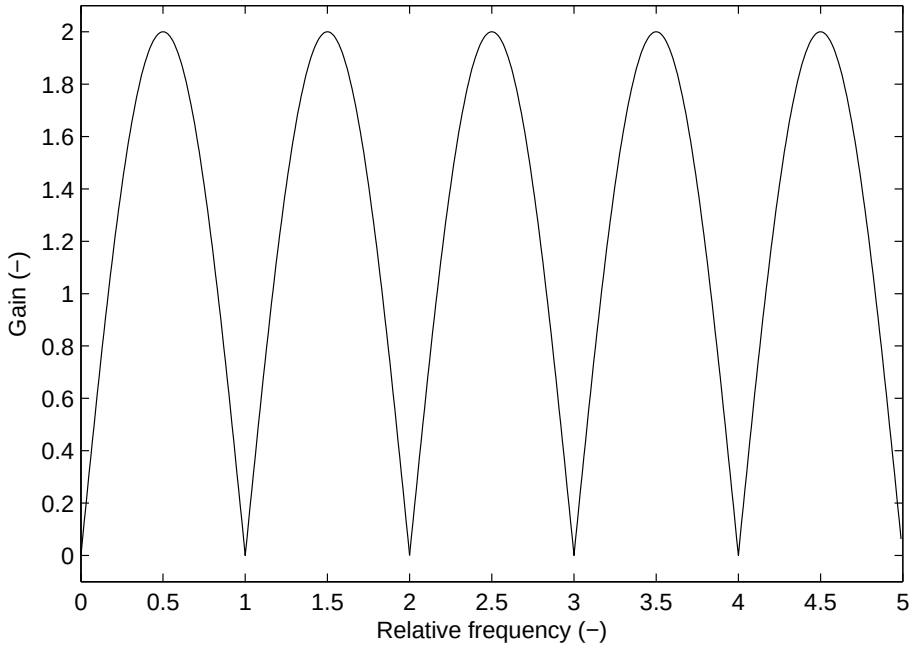

Figure 4.5: Gain of the comb filter plotted against frequency.

The comb-filter will create a delayed and inverted image of the injection transients. The method described therefore requires that the injection be performed towards the end of the data capture so that the image does not

affect the results. As a result, a rectangular window is used in the signal processing. This has the potential disadvantage of poor suppression of spectral leakage, although windowing is theoretically not necessary with impulse type signals [108]. Other windows which may offer improved characteristics are possible by either shortening the length of the data capture or increasing the delay time of the comb filter, although the first option will reduce the frequency resolution of the results and the second is likely to result in reduced suppression of the steady state voltages and currents and stricter synchronisation requirements between the grid and comb filter.

Once pre-processing has been applied, the impedance is calculated by applying Goertzel's algorithm [109] to the voltage and current transients and dividing the results, as in (4.3)—(4.5), where ω denotes the frequency of interest in radians, t is the current time and T is the window length in time. It is noted that Goertzel's algorithm is equivalent to calculating the DFT of the signal for a single frequency. It is therefore a computationally efficient means of frequency-domain analysis when only a few frequencies are of interest.

$$V_\omega = \sum_{t=0}^{t=T} v(t) e^{-j\omega t} \tag{4.3}$$

$$I_\omega = \sum_{t=0}^{t=T} i(t) e^{-j\omega t} \tag{4.4}$$

$$Z_\omega = \frac{V_\omega}{I_\omega} \tag{4.5}$$

Even after pre-processing, some steady-state frequency content is likely to remain. As a result, it is highly unlikely that attempting to estimate the fundamental impedance directly will yield acceptable results. Therefore, a pair of frequencies for impedance estimation are chosen and the fundamental impedance is then extrapolated from the available information. The

choice of frequencies used for impedance estimation is important. Frequencies close to the fundamental will be the most affected by spectral leakage and should therefore be avoided. The chosen frequencies must also be close enough to the fundamental that they are unlikely to have a significantly different impedance. The 50 Hz impedance was therefore extrapolated from impedance estimates at 80 Hz and 120 Hz. Averaging the imaginary parts of two values gives an estimate of the reactance at 100 Hz. This may then be halved to obtain an estimate of the 50 Hz reactance. The resistance is assumed to be constant with frequency and is calculated by finding the average of the real parts of the two values. Where wideband impedance information is required it may be obtained by calculating the FFT of the voltage and current data and dividing, as in (4.6) ($\mathcal{F}$ denotes the Fourier transform):

$$Z = \frac{\mathcal{F}(v(t))}{\mathcal{F}(i(t))} \tag{4.6}$$

In this work, wideband data is used to provide additional verification of the method. Wideband impedance estimation may also be of interest in other applications. Wideband impedance estimates were not used for controller tuning in this work for two reasons. First, implementing an FFT on the hardware used to for the practical STATCOM was found to be too time consuming to run in parallel with the other control software. Second, the impedance was only needed at the fundamental and extrapolating from frequencies significantly above this may not yield accurate results. Where wideband impedance estimates are available the accuracy of results may be improved by curve fitting the results, although care should be taken when choosing the curve fitting algorithm.

4.2.1 Generalisation of the method

Discussion so far has been concerned with the case of a single-phase system, where only one impedance needs to be estimated. For the majority of this

work a balanced three-phase system was considered. When a three-phase system is balanced, the single phase analysis may be applied directly to the three-phase system. In principle a single injection could be used to estimate the impedance of all phase simultaneously. However, for an unbalanced three-phase system a complete impedance matrix $\mathbf{Z}$ is required to describe the system.

$$\mathbf{Z} = \begin{pmatrix} Z_{aa} & Z_{ab} & Z_{ac} \\ Z_{ba} & Z_{bb} & Z_{bc} \\ Z_{ca} & Z_{cb} & Z_{cc} \end{pmatrix} \tag{4.7}$$

The full impedance matrix is shown in (4.7). The three elements on the leading diagonal, Z_{aa}, Z_{bb} and Z_{cc} are the self impedances of the three phases. The other six elements of the matrix are the mutual impedances which describe the coupling between phases. Although the matrix has nine elements only six of them are unique since the coupling between phases is generally assumed to be symmetrical, i.e. $Z_{ab} = Z_{ba}$, $Z_{ac} = Z_{ca}$ and $Z_{bc} = Z_{cb}$. A minimum of three injections are required to identify all elements of the impedance matrix. However each injection must be unbalanced and independent of the other two.

The above analysis assumes negligible neutral impedance. In practice this is never the case. Inclusion of the neutral impedance will add an additional row and column to the impedance matrix. It is not possible to fully identify all elements of the impedance matrix when the neutral is included. In addition, the power converter used for impedance estimation may not have a neutral connection, as is the case for the converter used in this work. Due to the difficulties associated with completely populating the impedance matrix this work assumes that the system may be treated as a balanced three-phase system with equal impedances for each phase allowing the mutual impedance terms to be disregarded. In situations were the unbalance is so great as to make this assumption invalid, it is recommended that the system be treated as three independent single-phase systems. Some consideration is

given to the effect of unbalance on the efficacy of the impedance estimation algorithm in Chapter 5, however, an in-depth analysis of unbalanced systems is outside of the scope of this work and therefore has not been considered, although it has been identified as an area of potential future study.

Although in this work it has been assumed that the supply is a provided by a balanced three-phase system, three injections are still performed during each impedance estimation cycle in an attempt to improve accuracy. The injections are performed at successive phase-neutral voltage zero crossings. A positive current of amplitude $\hat{I}$ is injected in to the phase passing through zero. Negative currents of amplitude $\frac{\hat{I}}{2}$ are injected in to the other two phases. The impedance of each phase is then taken to be equal to the average of the three estimated impedances.

4.3 Injection triggering

The previous section described the impedance estimation algorithm used throughout this work. The method uses current injections and is therefore invasive. As a result of this it is desirable to have a suitable means of triggering the injections so that the impact of the injections on the system may be limited. In this section, methods of triggering the impedance estimation algorithm are considered. This section is included for completeness and the methods described are not further explored in this work.

One of the most basic methods of triggering the impedance estimation algorithm would be to use a fixed delay and periodically perform injections. Although this method is simple and will result in very deterministic injection times, it has several disadvantages. First, no consideration is given to whether the current impedance estimate requires updating or not and therefore the injection, and the accompanying disruption caused to the system, may not be necessary. Second, if the quality of one impedance estimate is poor – which may be the case if, for example, the injection is performed

during a grid transient – it will be necessary to wait until the next injection time to correct the erroneous values. Third, any event causing a change in impedance may go undetected until the next injection time. Finally, a clear procedure would be required to determine the time between injections and this would probably have to be determined on a case-by-case basis.

For the STATCOM considered in this work, an alternative to the timer-based triggering method would be to compare the response of the STATCOM when a large voltage transient occurs to the expected response. This method has the advantage of being able to detect an incorrectly tuned controller in some circumstances. However, a sufficiently large transient is required so that the transients may be reliably compared and the injections are not triggered unnecessarily due to noisy measurements. In addition, the expected STATCOM response must be known, which is likely to limit the applicability of this method to step changes in voltage. However, many significant events that are likely to change the system impedance, such as faults on a nearby circuit, may well result in a step change in voltage and therefore this method may be well-suited in some circumstances.

The final method of triggering the impedance estimation algorithm to be considered here is to inject after the power converter used is switched on. This method provides "plug-and-play" functionality: when first powered, the device implementing impedance estimation will inject and identify the system impedance. The impedance estimates may then be used to tune the STATCOM AC voltage controller. The unit will only inject again following recovery from a loss of supply. This method has the advantage that the number of injections performed is minimised during normal operation and that it does not require the additional signal processing associated with the transient comparison method. However, like the timer based method, there is no way to correct for a change in supply impedance. This method is useful in situations where the system may switch between two alternative supplies, such as the standby generation scenario described in Chapter 7.

In practice, a combination of the methods described in this section could

be used to provide various means of determining when to inject. Injections could be periodically triggered at intervals of an hour or more in order to continuously monitor the impedance without causing an excessive disturbance to the system, while significant grid events resulting in a change in impedance will trigger the impedance estimation algorithm using the second method described. The third method would guarantee that the impedance is estimated following an outage. Alternatively, a less accurate, passive method of impedance estimation may be used in order to continuously check for changes in the impedance, although such an approach requires additional signal processing. This type of approach has been previously considered by Diana et al [110].

4.4 Demonstration through simulation

This section presents simulated results to demonstrate that the injection method can aid identification of the system impedance. The simulation results presented in this chapter are intended to demonstrate that impedance estimation using these methods is possible and not to analyse the quality of the results, which shall be considered later in the experimental section of this work. Simulations were carried out in MATLAB/Simulink with the aid of the PLECS blockset.

The current and voltage results presented in this section are all for Phase A of a three phase system. In each set of results, three injections can be seen. The largest of the three injections is the injection on Phase A. The two subsequent smaller injections are the result of Phase A providing a return current path for injections on Phases B and C. The impedance estimation results shown are calculated based on the average of the estimated impedances for all three phases. Figure 4.6 show an the three-phase converter currents during an injection cycle. The injection performed on each phase has been labelled so that it can be clearly identified. It can clearly be seen that each injection creates an additional disturbance on the other two phases.

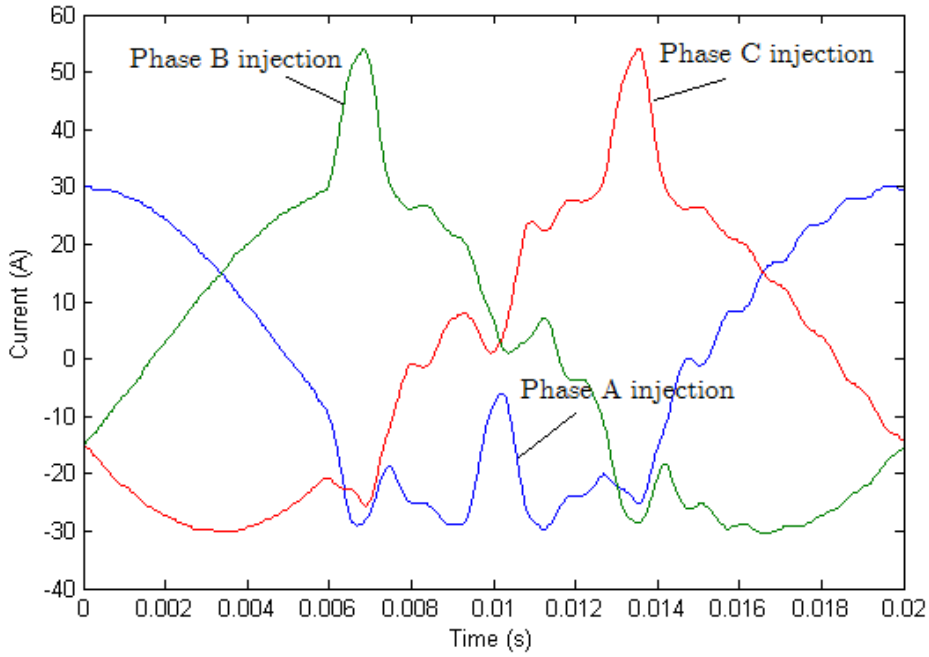

Figure 4.6: Three-phase converter currents during an injection cycle.

Two linear grid impedance models were considered and these are shown in Figure 4.7. In the first model the supply is treated as an inductance in series with a resistance. The second model adds a capacitor and resistor in parallel with the supply. Using these models allows an "ideal" impedance to be easily calculated for comparison with the simulation results.

Simulations were performed for each of the supply models using a converter with an inductive filter to couple to the grid, as described in Chapter 3. The simulated voltage and current measurements were sampled at a rate of 16 kHz and quantised so that the results would be representative of what may be achieved using an analogue to digital converter (ADC). The quantisation interval for the voltage measurements was set to 0.20 V. The quantisation interval for the current measurements was set to 0.28 A. These figures are equivalent to using 12-bit ADCs for sampling, with input ranges of $\pm$400 V and $\pm$580 A for voltage and current measurements respectively. The input ranges were chosen to be similar to the ratings expected for a medium sized STATCOM on a 400 V system.

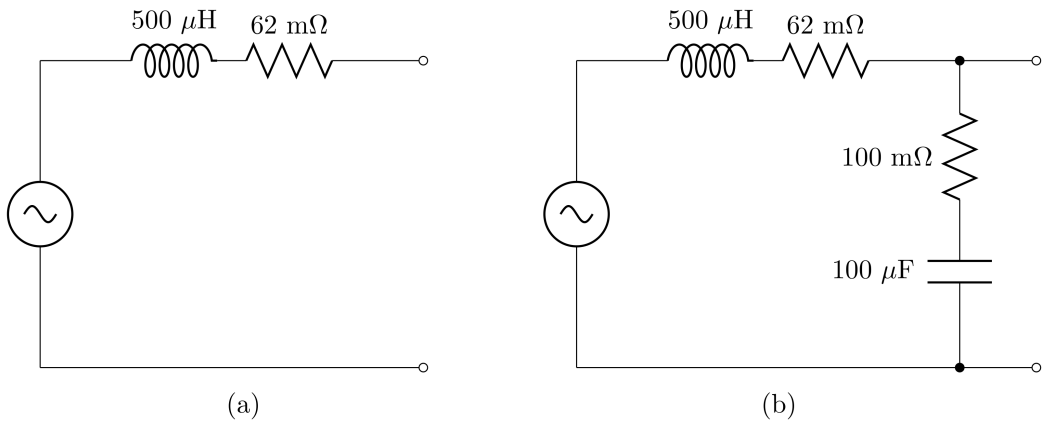

Figure 4.7: Models used to represent different grid impedances in simulation.

Initially the supply voltage was set to zero. Results are shown in Figure 4.8 for the first supply model. Results for the second supply model are shown in Figure 4.9 for the simulations where the supply voltage and frequency may be ignored entirely. Figures 4.10 and 4.11 show results for the system with a 50 Hz supply frequency. The fundamental and harmonic components of the current and voltage waveforms have been suppressed using a comb filter as has already been described. Results for the system with a 49.5 Hz supply are shown in Figures 4.12 and 4.13. As with the 50 Hz results, a comb filter has been used to suppress the fundamental and harmonic voltages and currents. To demonstrate the effect of spectral leakage on the results when the system fundamental and comb filter frequencies do not match, the comb filter is still tuned to 50 Hz. In practice, retuning of the comb filter to the actual, rather than nominal, system frequency should be performed in order to minimise spectral leakage. In all of these results, ideal impedances are shown using a dashed line for comparison to the estimated values.

First the results for supply model (a) are considered. All of the results show that the reactance estimates are more accurate than the resistance estimates, particularly at high frequencies. At high frequencies, the strength of the current injection is reduced compared to low frequencies and therefore it is expected that the accuracy of the results will be reduced. In addition, the

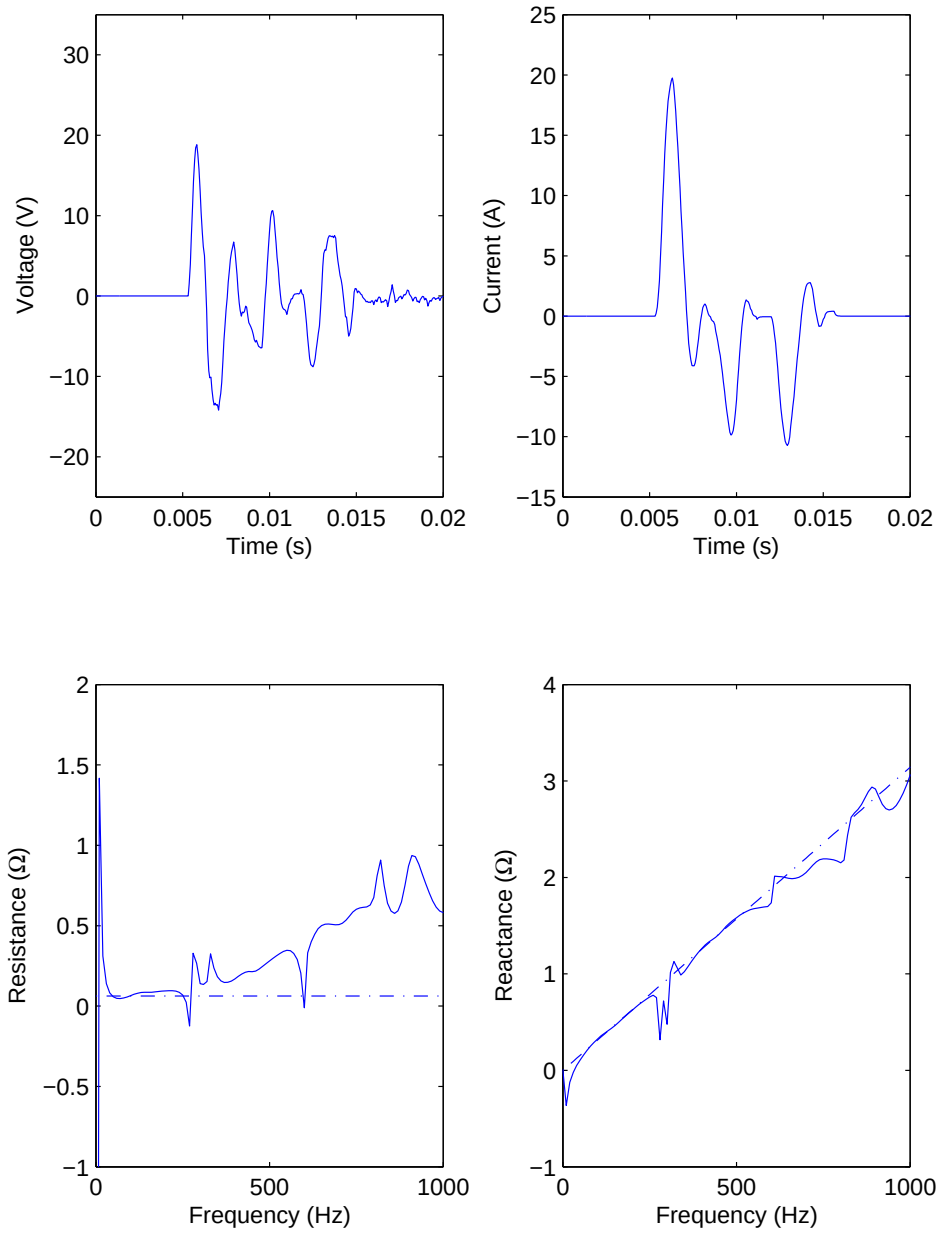

Figure 4.8: Impedance estimation results for supply model (a) with no supply voltage.

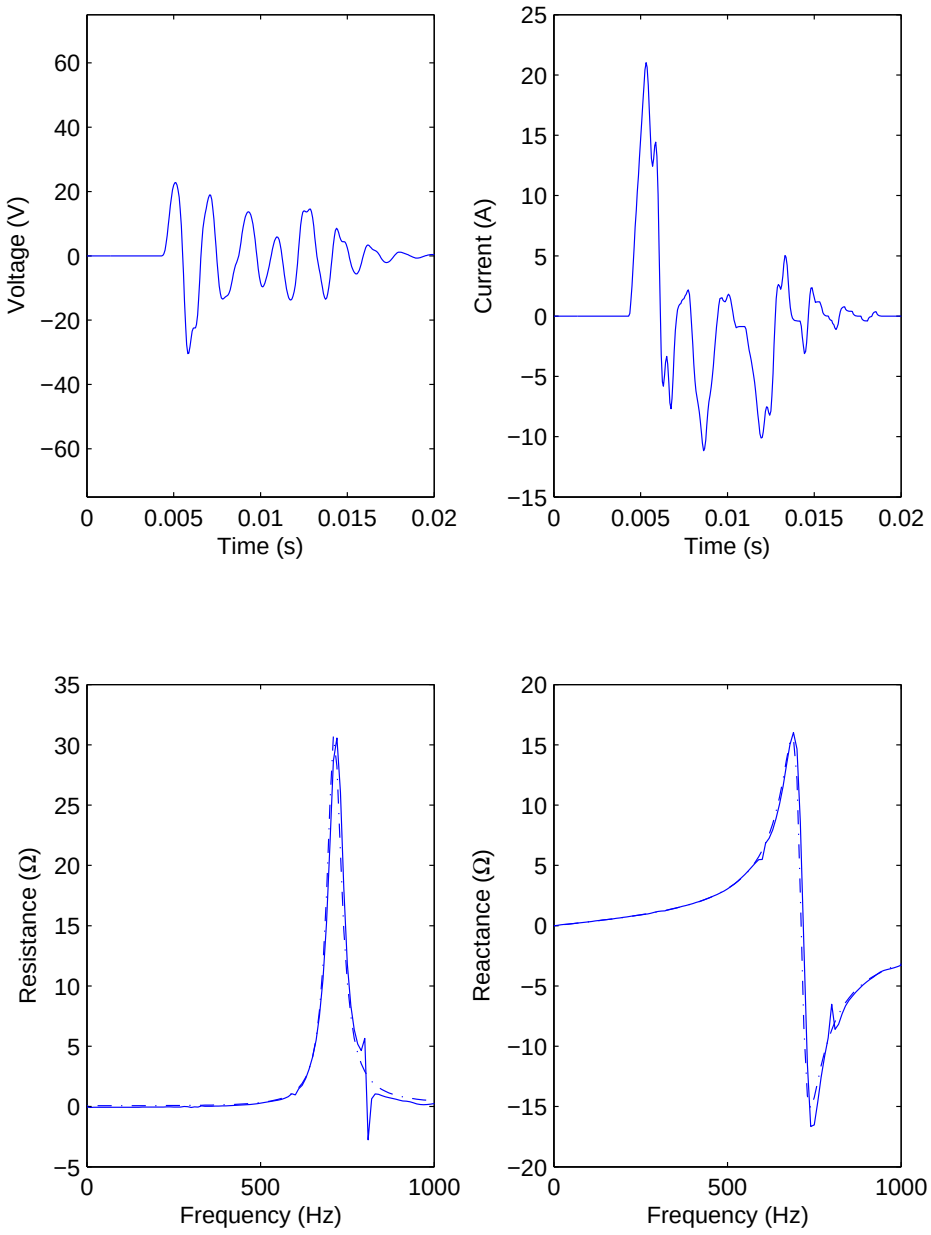

Figure 4.9: Impedance estimation results for supply model (b) with no supply voltage.

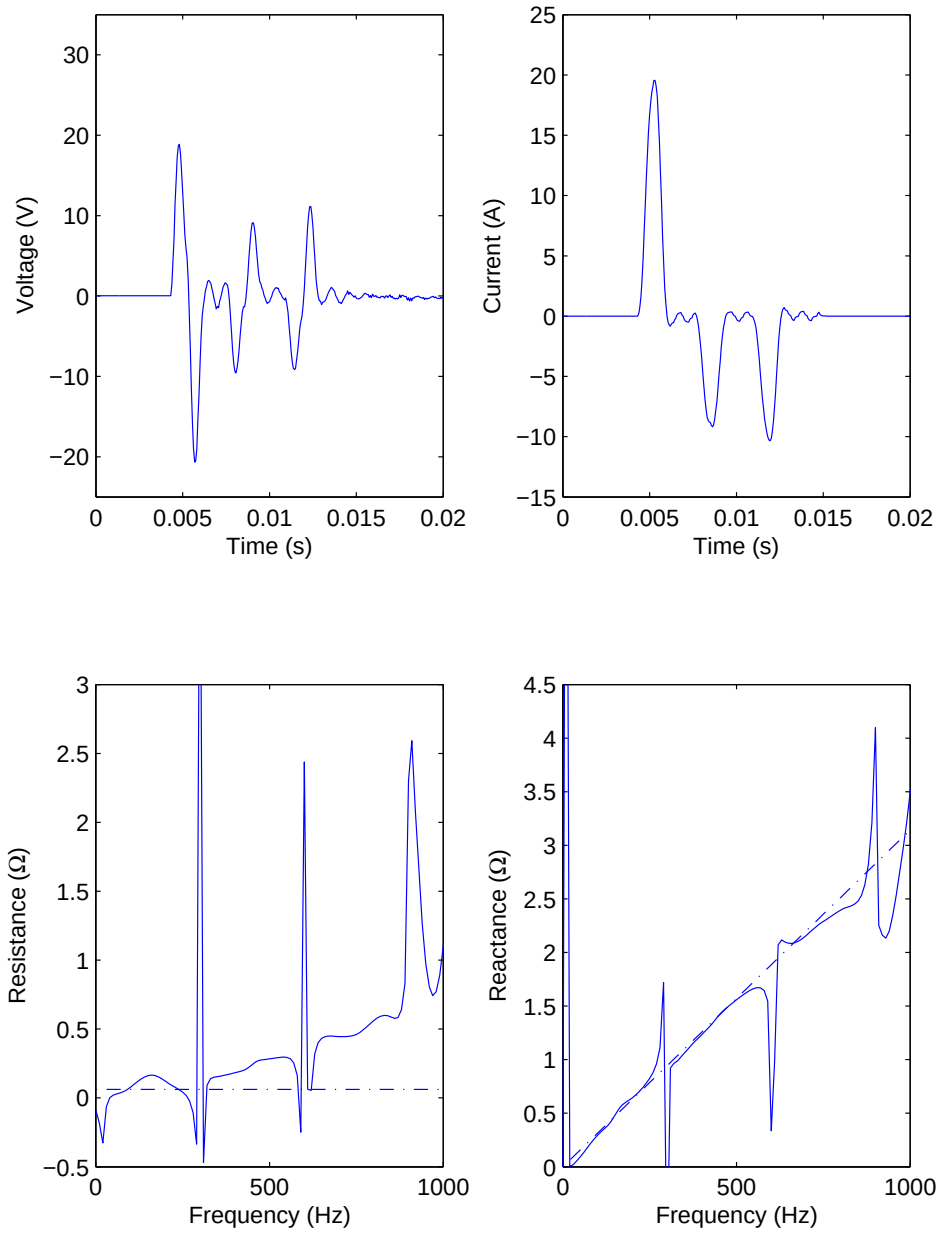

Figure 4.10: Impedance estimation results for supply model (a) with a 400 V, 50 Hz supply voltage.

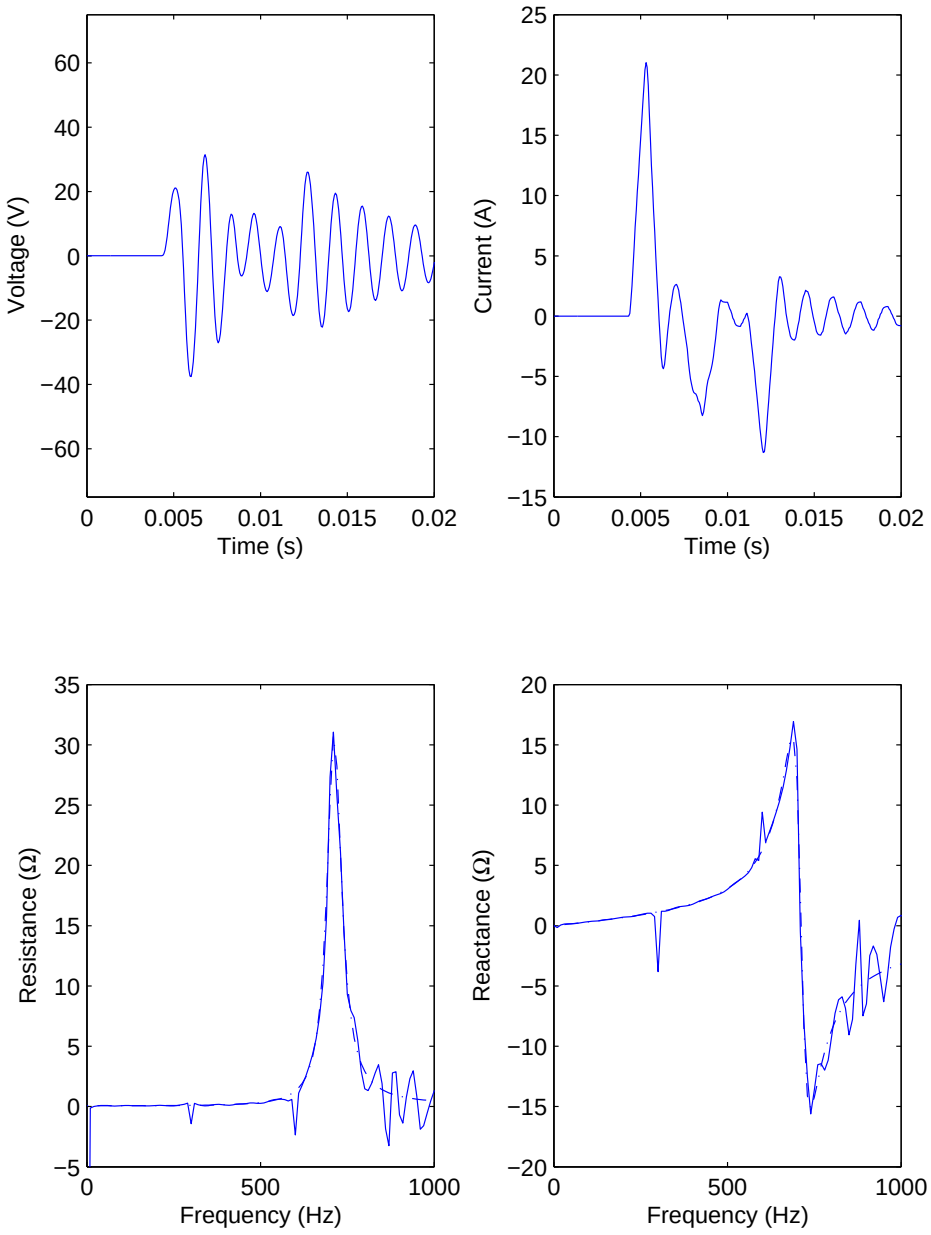

Figure 4.11: Impedance estimation results for supply model (b) with a 400 V, 50 Hz supply voltage.

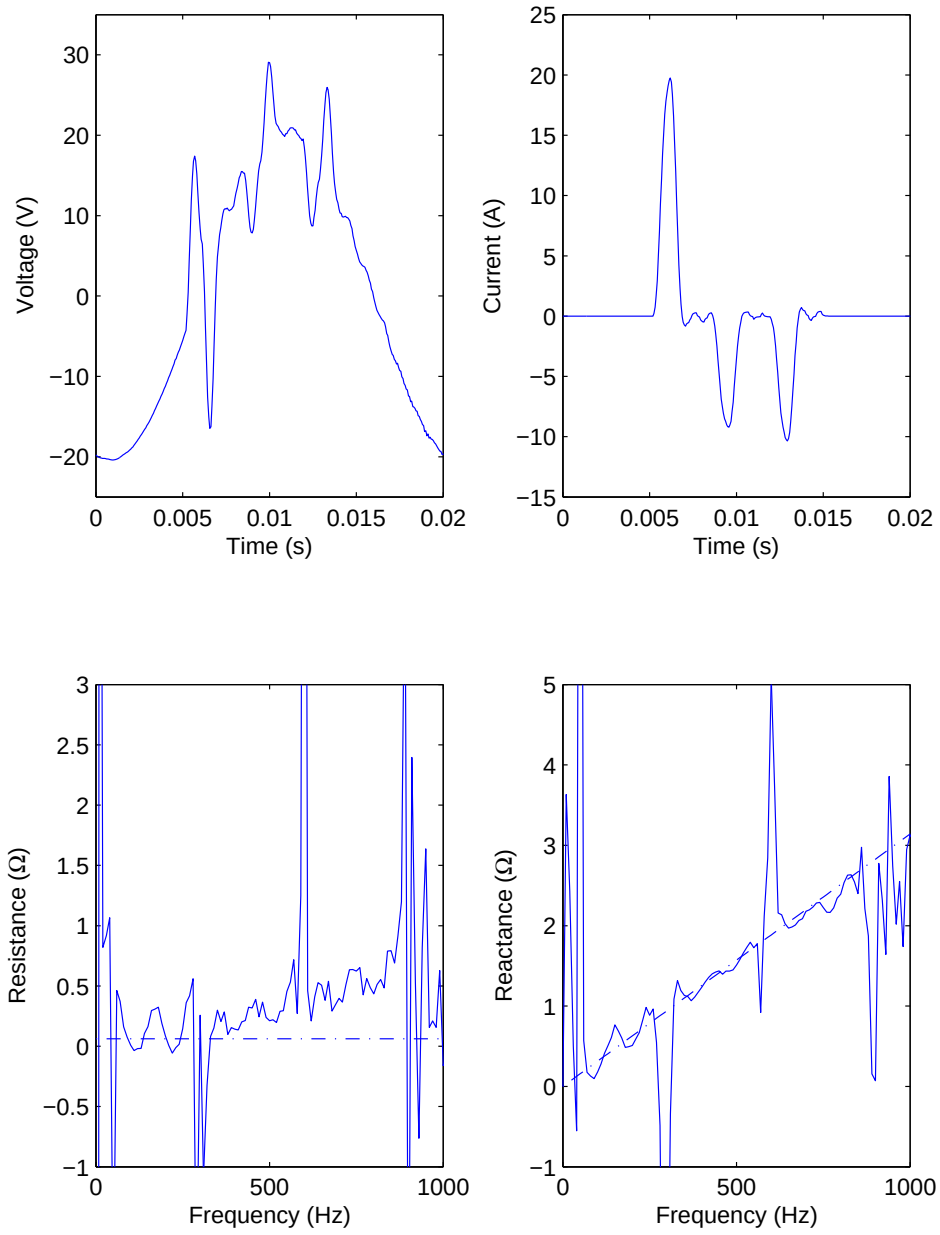

Figure 4.12: Impedance estimation results for supply model (a) with a 400 V, 49.5 Hz supply voltage.

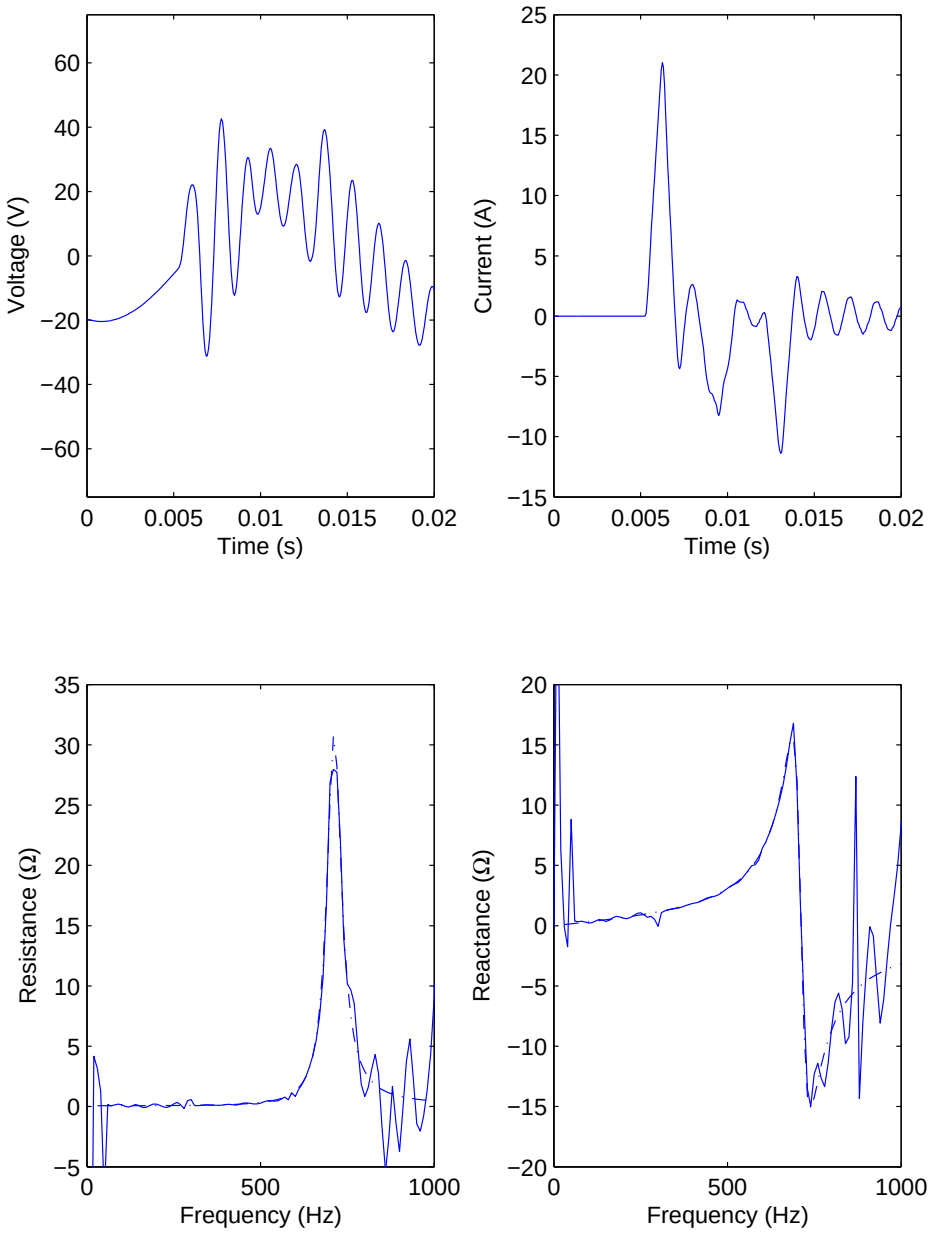

Figure 4.13: Impedance estimation results for supply model (b) with a 400 V, 49.5 Hz supply voltage.

X/R ratio increases with frequency and therefore the effect of inductance on the high frequency components of the voltage disturbance is greater than that of the resistance. All the results also show discontinuities in the results at 300 Hz, 600 Hz and 900 Hz. This is a result of injecting on each phase at successive zero crossings. The injections are 3.33 mS apart, corresponding to a frequency of 300 Hz. In the frequency domain, the injections cancel each other at 300 Hz and subsequent harmonic frequencies and the result is deterioration of the results at and around these frequencies. When the supply is not considered, the estimate for the 50 Hz resistance is 63 mΩ and estimate for the reactance is 0.162 Ω, equivalent to an inductance of 516 μH.

Results for the 50 Hz supply frequency are of a similar quality to the results when the supply is not considered. However, an increase in estimation error can be seen below 20 Hz, and at 300 Hz, 600 Hz and 900 Hz. The very low frequency errors, which are also present on the other results, are a result of the lack of significant content in the voltage disturbance at these frequencies. The single-frequency estimated resistance at 50 Hz is 64 mΩ. The estimated reactance is 0.150 Ω, equivalent to an inductance of 477 μH.

As was expected, spectral leakage causes errors across the full frequency range for the results of the 49.5 Hz supply. The fundamental can clearly be seen in the voltage waveform and the effect is clearly visible in the graphs showing the impedance estimates. However, it can seen that, other than at the fundamental and other frequencies already mentioned, the reactance results are generally a reasonable match to the ideal values. In addition, the system frequency in this case is unusually low and represents a worst-case scenario. During normal network operation in the United Kingdom, the actual fundamental frequency will typically be within 0.2 Hz of the nominal value [107]. The single-frequency estimated resistance at 50 Hz is 56 mΩ. The estimated reactance is 0.171 Ω, equivalent to an inductance of 544 μH.

The most immediately obvious feature of the results for supply model (b) is that the injection causes excitation of the LC supply resonance. This can be seen in both the current and voltage disturbances from all of the simulations

and is reflected in the impedance estimation results. The results show the resonant frequency of the supply to be approximately 700 Hz; the frequency at which resonance is expected to occur is 711 Hz.

The results for supply model (b) share many features with the results for supply model (a). As before, the results when the supply voltage is set to zero appear to be the most accurate, while results for the 49.5 Hz supply appear to be the least accurate. Increased errors can be seen at 300 Hz, 600 Hz and 900 Hz. However, unlike the results for supply model (a), the results for supply model (b) appear to show reactance and resistance estimates of similar quality for each of the supplies. The presence of significant capacitance appears to improve the resistance estimates considerably. This is due to the capacitance causing a reduction of X/R ratio at higher frequencies so that the estimates of the real part of the impedance are not so disproportionately affected by measurement or calculation errors, as was the case for supply model (a). As with supply model (a), the single frequency impedance estimates were calculated for 50 Hz. When no supply was considered, the resistance was 67 mΩ and the reactance was 0.160 Ω (509 μH). For the 50 Hz supply the resistance was 73 mΩ and the reactance was 0.157 Ω (500 μH). For the 49.5 Hz supply the resistance was 50 mΩ and the reactance was 0.169 Ω (538 μH).

4.5 Experimental demonstration

In order to validate the simulation results presented in the previous section, an experimental demonstration of impedance estimation was carried out using a Triphase power converter [111], implementing the necessary control software and connected to the main laboratory power bus through a variable inductor. The inductor could be varied between 0 mH and 1 mH in steps of 250 μH. Due to the controller used with the Triphase converter it was not possible to implement full wideband impedance estimation in real-time and therefore only fundamental impedance estimation using Go-

ertzel's algorithm at selected frequencies (80 Hz and 120 Hz) was implemented for processing in real-time. However, the voltage and current transients were recorded and processed in MATLAB after the experiments had been completed to give the wideband impedance estimates.

Typical wideband results for each setting of the supply inductors are shown in Figure 4.14—4.18. In each case, three injections are made, one at each phase-neutral voltage zero crossing, similar to the simulation results presented in the previous section. Each injection is 2 mS in duration and is limited to 25 A maximum amplitude. The fundamental and harmonic frequencies have been removed using a comb filter. An ideal impedance is included for each of the impedance estimation results and this is shown as a green line. It should be noted that this ideal value has been calculated using the averaged values for resistance and inductance at 50 Hz given in Table 4.1 and is not based on an independent measurement of the supply impedance over the full frequency range. For this reason, any discrepancy between the estimated and ideal values should be interpreted with care.

Some spectral leakage is clear at frequencies close to 50 Hz although the suppression of the fundamental and harmonics is sufficient to yield usable results. Anomalous results can also be seen at and around 300 Hz, 600 Hz and 900 Hz. As was explained for the simulated results, the zero crossings are 3.3 mS apart, which causes partial cancellation of the injections at 300 Hz and subsequent harmonic frequencies.

It can be seen that as the added supply impedance increases, the useful bandwidth of the impedance estimation decreases. Initially, results are reasonable across most of the spectrum up to 1000 Hz. For the 1 mH supply, the useful bandwidth of the estimates is limited to frequencies below 500 Hz. The limits correspond reasonably well with the resonant frequency formed by the grid-side inductor and capacitor of the PWM output filter of the Triphase power converter combined with the supply impedance: 1000 Hz for the 250 μH supply, 820 Hz for the 500 μH supply, 710 Hz for the 750 μH supply and 640 Hz for the 1 mH supply. Allowing for some tolerance in

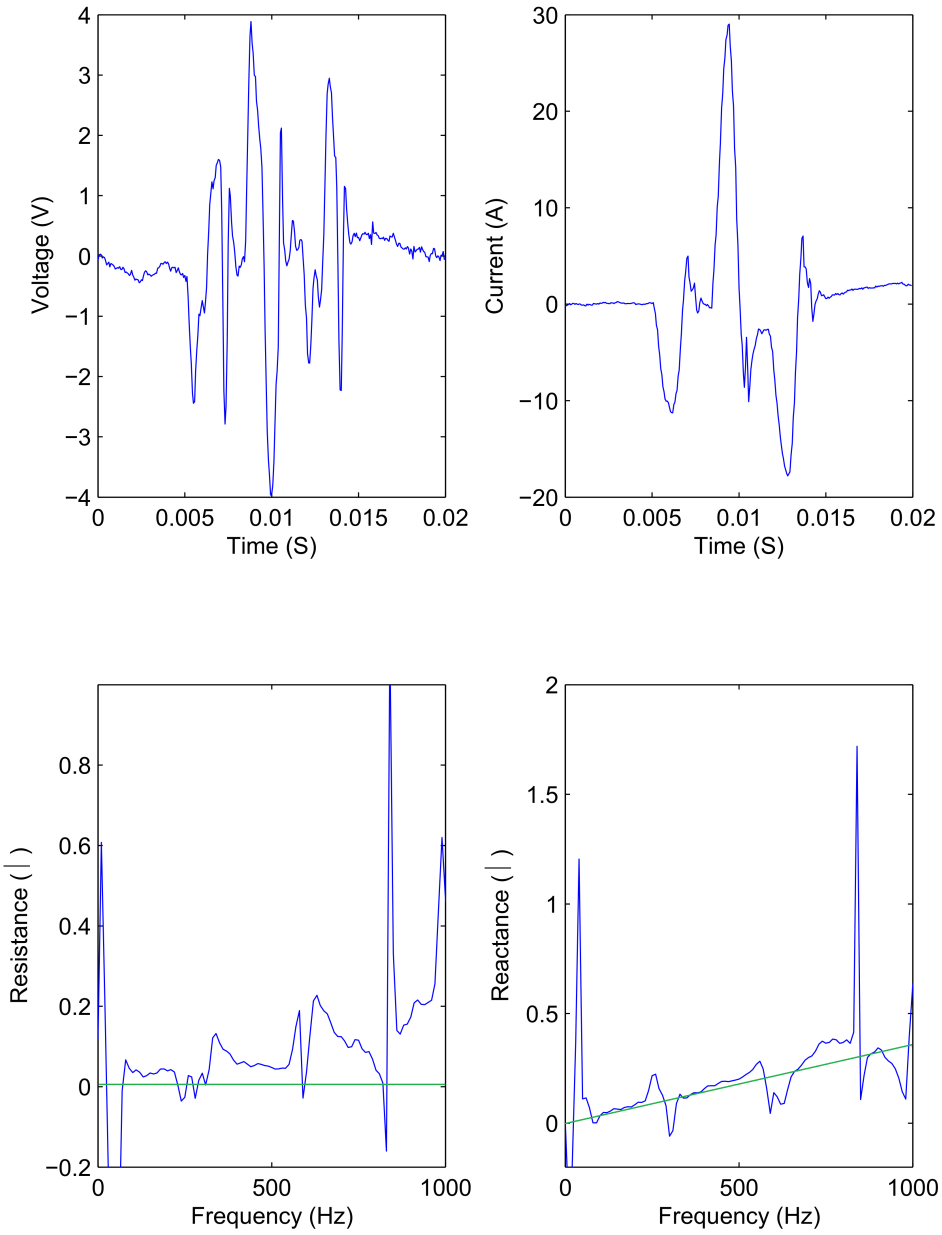

Figure 4.14: Injection shape and impedance estimates for the supply when no inductance is added.

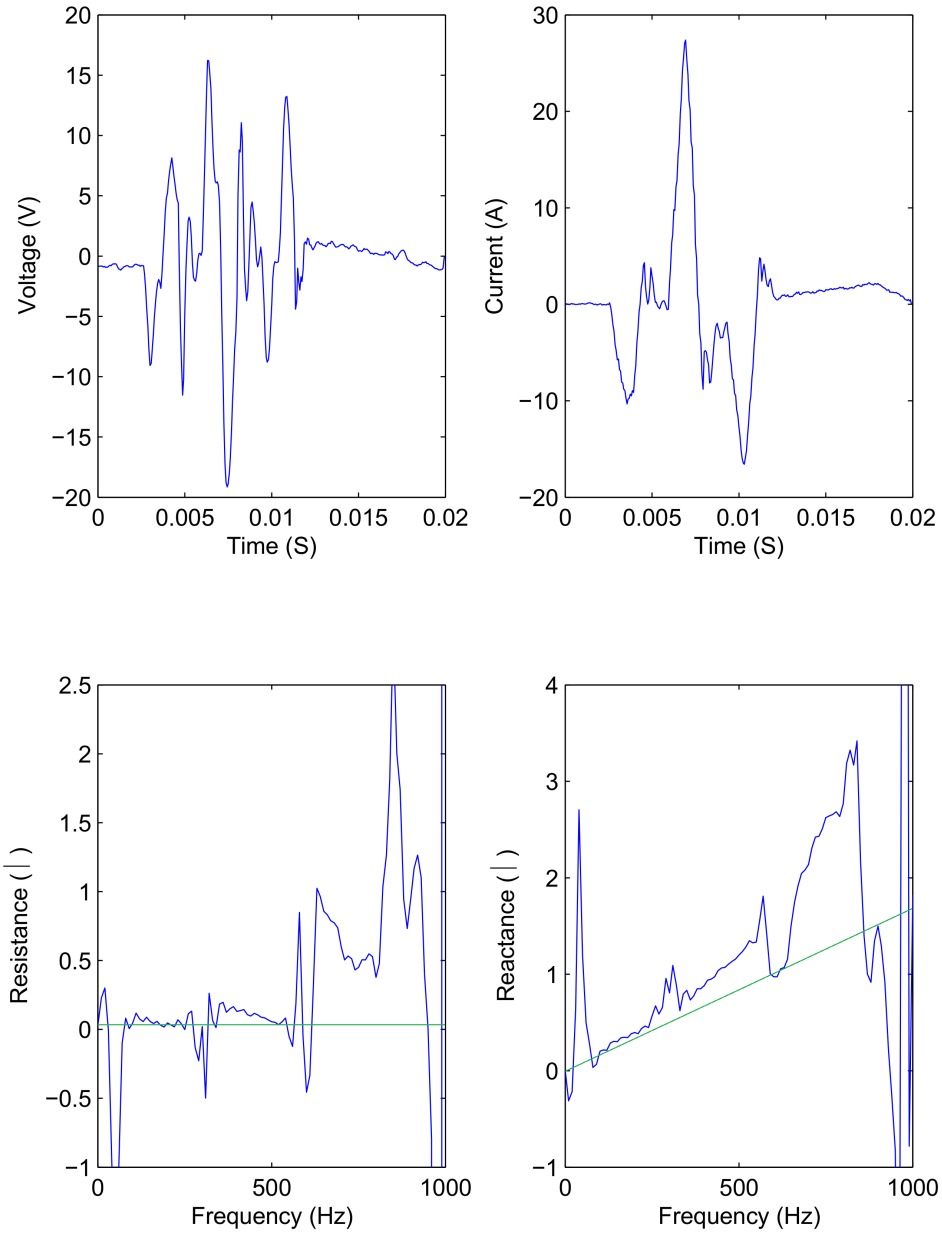

Figure 4.15: Injection shape and impedance estimates for the supply when 250 μH of inductance is added.

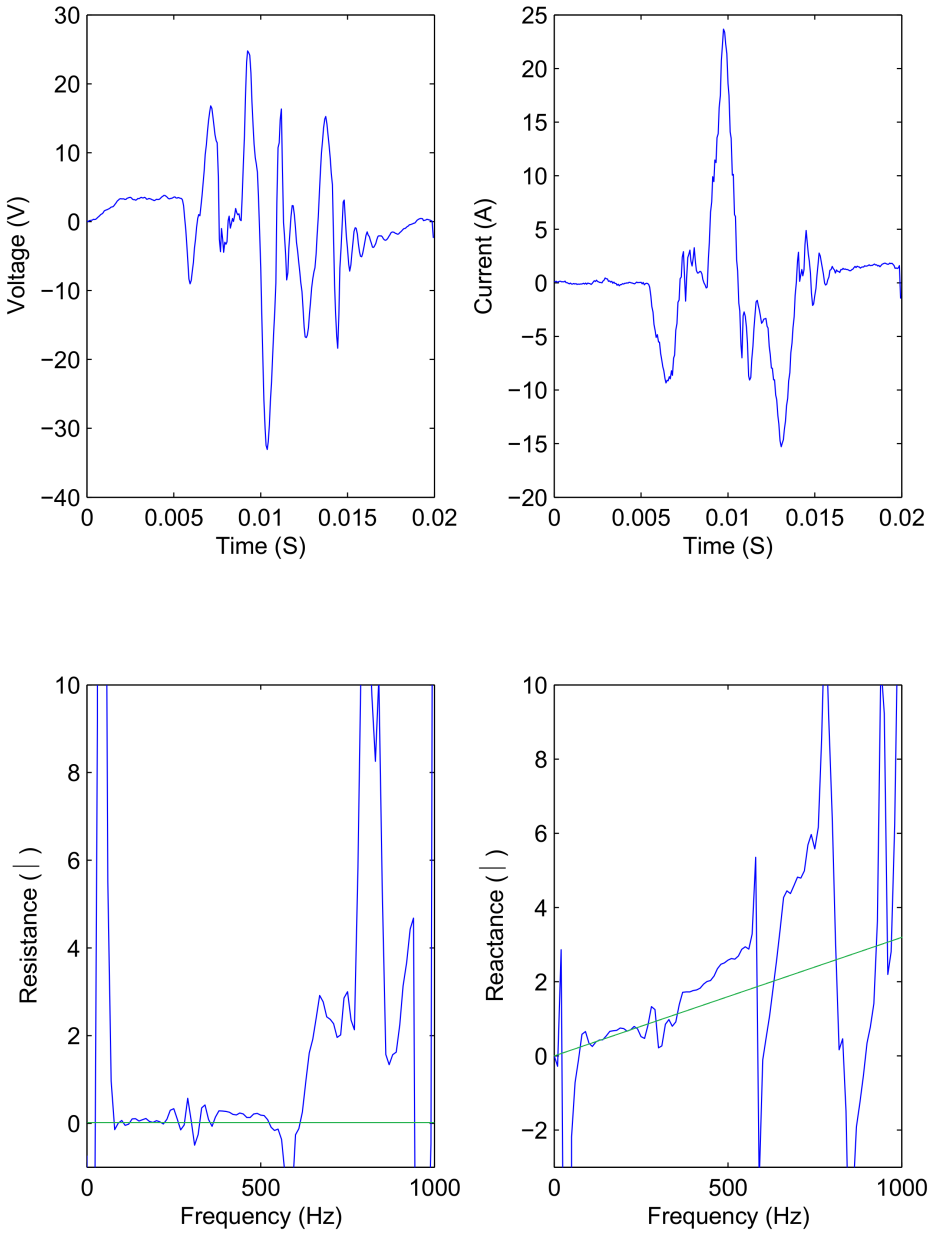

Figure 4.16: Injection shape and impedance estimates for the supply when 500 μH of inductance is added.

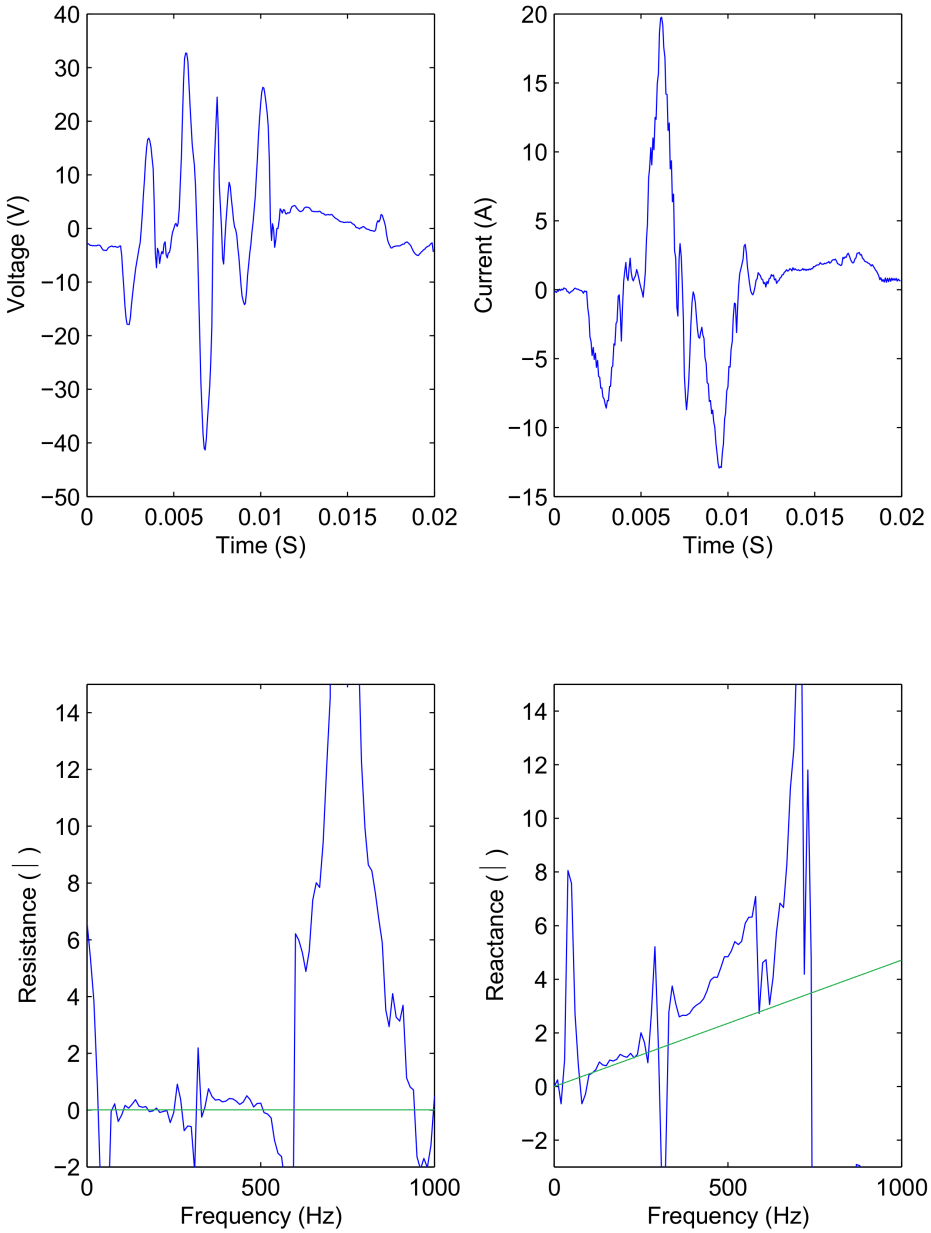

Figure 4.17: Injection shape and impedance estimates for the supply when 750 μH of inductance is added.

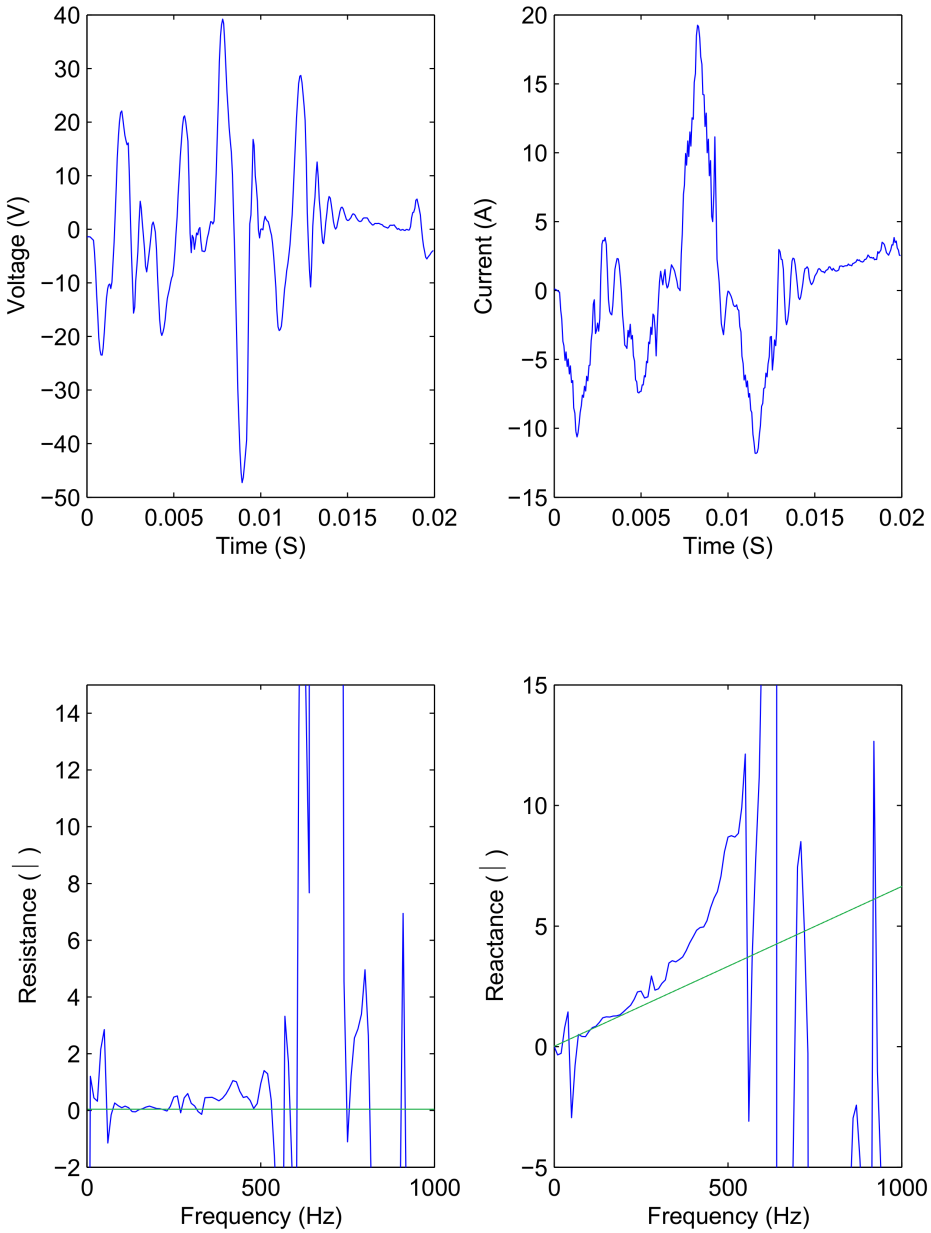

Figure 4.18: Injection shape and impedance estimates for the supply when 1 mH of inductance is added.

component values it seems reasonable to conclude that the filter causes degradation of the quality of results at frequencies above the resonant frequency of the filter formed by the supply impedance and the grid-side inductor and capacitor of the power converter's PWM filter. At higher frequencies the filter capacitor presents a lower impedance to the injection than the combined impedance of the supply and grid-side inductors. As a result, the injected current on one phase flows to the other phases through the PWM filter capacitor rather than through the supply, suppressing the injection before it causes a disturbance to the grid. It is also noted that some ringing is visible on the voltage and current waveforms at higher supply impedances; this is caused by the filter resonance. This result was not expected and could have some considerable practical significance, although for this work it is not seen as a major problem since the frequencies of interest are still well below the resulting bandwidth limit. It is also worth noting that the larger supply impedance values were chosen because of the availability of suitable inductors and not because they are considered representative of the expected supply impedance.

The overall accuracy of the method was evaluated by considering the average and standard deviation of a sample of 100 estimates using Goertzel's algorithm for each supply setting. The results are listed in Table 4.1.

L setting	$\overline{R}(\Omega)$	$\sigma_R(\Omega)$	$\overline{X}(\Omega)$	$\sigma_X(\Omega)$	$\overline{L}$(mH)
0 mH	0.0161	0.0067	0.0160	0.0069	0.051
0.25 mH	0.0258	0.0151	0.0832	0.0087	0.265
0.5 mH	0.0368	0.0275	0.1511	0.0166	0.481
0.75 mH	0.0467	0.0375	0.2233	0.0249	0.711
1 mH	0.0529	0.0447	0.3007	0.0262	0.957

Table 4.1: Statistical summary of impedance estimation results.

From Table 4.1 it would appear that the resistance estimates are more variable than the reactance estimates in most cases, the notable exception being the case when no inductance is added to the supply, where the variation in estimates is approximately equal regardless of whether resistance or reac-

tance is being estimated. The impedance estimates show the X/R ratio of the supply as being close to unity when no impedance is added, whereas X/R ratios of the other supply impedances, based on the impedance estimates, is between 3 and 6. The average estimates for the inductances, $\overline{L}$, are given for comparison with the nameplate values of the inductors. The discrepency between the "ideal" and actual values should not be interpreted as measurement error, however, since the nameplate values are design values only and subject to a tolerance, typically between 10 % and 20 % [112–114], although the actual tolerances for the inductors used is not available.

4.6 Summary

This chapter has described an impedance estimation method and demonstrated the method using both simulation and experimentation. The method is based on an earlier transient injection method, which has been termed "feed-forward injection" for the purposed of this work. The method described in this chapter, "fully controlled injection," improves on this earlier method by using a high-bandwidth current controller to shape the injection as required. This avoids suppression of the low frequencies by the power converter's current controller. The results presented show that the method can be used to identify the impedance of the system at the fundamental frequency with reasonable accuracy. These impedance estimates may then be used to set the gains of the STATCOM AC voltage controller.

Chapter 5

Simulation case studies

This chapter introduces a number of simulation case studies which have been performed as part of this work. These simulations have been designed to evaluate the performance of AIE-based STATCOM control. The work in this chapter is split into numerous sections, beginning with studies verifying that the proposed control scheme works for a single-source, balanced linear system and later studying the effects of multiple sources, unbalance and harmonics. A system having a single droop-controlled STATCOM is also considered and the analysis of this may be extended to a system having multiple STATCOMs operating in parallel.

This chapter starts by introducing the base power system model, which is used in all simulations. In each subsequent section, the modifications to the model are described and results for the specific simulations performed are

presented and discussed.

5.1 Description of the simulated power system

The base model for the simulated power system consists of a supply and a single feeder having four load "zones" distributed at equal distances along the length of the line, referred to as Zones 1—4. Additionally, there is a fifth zone (Zone 0) at the point of common coupling (PCC) and an optional sixth zone (Zone 5) at the end of the line. The base simulation model is illustrated as a single-line diagram in Figure 5.1. As shown, the STATCOM may be connected to the system at either the PCC or at the end of the line, although in this work, only one of the two possible locations is used at any one time. The STATCOM measures the local voltage wherever it is connected. Therefore, when the STATCOM is connected at the PCC, the PCC voltage is controlled. When connected at the end of the line, the end-of-line voltage is controlled.

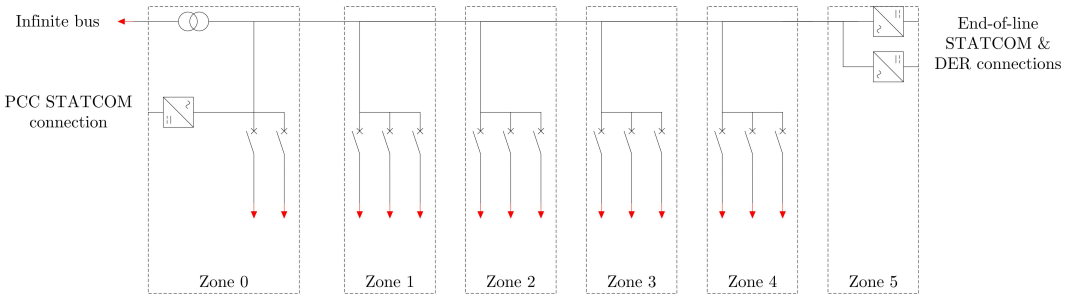

Figure 5.1: The simulated power system represented as a single line diagram.

Zone 0 is intended to be representative of the large loads that may be found near the PCC; for example, a plant room containing large motors to supply heating and ventilation to a rest of the building. Half of the loads in Zone 0 are considered to be permanently connected and the other half may be switched. In addition, Zone 0 may also contain harmonic filtering and power-factor correction equipment. Zone 5 is intended to represent an extension to the original system; for example, the roof of a multi-storey building, where a PV array would be connected.

Transformer rating	Inductance, L	Resistance R
100 kVa	250 μH	16 mΩ
200 kVa	125 μH	8.0 mΩ
315 kVa	80 μH	5.1 mΩ
500 kVa	50 μH	3.2 mΩ
800 kVa	32 μH	2.0 mΩ
1000 kVa	25 μH	1.6 mΩ

Table 5.1: Some common LV transformer ratings and approximate output impedances.

Each of the Zones 1—4 in the base model consists of three individually switched loads. Except where stated, these are balanced three-phase loads, and within a zone, each of the loads is equally sized. The loads are linear, passive loads and may be configured as a combination of resistance, inductance and capacitance. Between each of the zones some impedance is included to represent impedance of the cable runs between the zones.

It is assumed that the main incoming supply to the power system is fed from a transformer, which is itself fed from an effectively ideal supply. Therefore, the source impedance is assumed to be dominated by the winding resistance and leakage reactance of the transformer's secondary winding.

The typical impedance for a transformer is about 5 % of the per unit system impedance and primarily inductive [115]. Low-voltage (400 V) distribution transformers are typically rated between 100 kVA and 1000 kVA [116], which gives a range of source inductances between approximately 25 μH and 250 μH. Assuming that the winding resistance is about 1 % p.u. then the source resistance may vary between approximately 16 mΩ and 1.6 mΩ. It is assumed that for 400 V systems the supply impedance is dominated by the output impedance of the transformer, since the power available from the rest of the grid will far exceed the power requirements of the 400 V system.

Table 5.1 lists some common low-voltage transformer ratings and the estimated supply inductances and resistances corresponding to these ratings,

calculated based on the assumptions above. The simulations presented in this chapter have been performed on 100 kVA, 200 kVA and 315 kVA systems using the appropriate estimated transformer impedances. The per-unit length cable impedances used in simulation are based on the required cable sizes for a 315 kVA supply and assuming that approximately 33 % of the total system load is located in Zone 0. The cable impedance is based on using 95 mm^2 SWA cable [117], giving a resistance of 0.43 $m\Omega m^{-1}$ and an inductance of 0.414 μHm^{-1}.

In this work it is assumed that the when first used, no effort has been made to tune the STATCOM AC voltage controller. A default AC voltage controller gain of 3.18 has been used for the untuned STATCOM. This is equivalent to a STATCOM tuned to a 1 mH supply reactance. 1 mH may be considered a very large supply reactance for most distribution systems. Although this means that the AC voltage controller response will be slow, it should ensure that the system remains stable when the STATCOM has not been tuned. The fixed gain of the controller, k, is set to 20 throughout all the simulations in this chapter. This gives an ideal controller time-constant, τ, of 0.05 s.

5.2 Simulation of a single-source system

Initial simulations were performed for a single-source, linear system. The purpose of these simulations is to verify the operation of the control strategy. In addition, the sizing of the STATCOM relative to the rating of the power system is investigated. This is done for a single STATCOM regulating the system voltage to a fixed set-point and for a droop-controlled STATCOM. Simulations were also performed to investigate the effect of changing where along the feeder the STATCOM is positioned.

5.2.1 Fixed-reference STATCOM

The proposed control and tuning method was initially demonstrated using simulations of a single STATCOM controlling the grid voltage to match a fixed reference. The control was evaluated on a number of systems to demonstrate the efficacy of the retuning method. Initially, the STATCOM was used to regulate the PCC voltage; in later simulations, the STATCOM was moved to Zone 4 for comparison. Table 5.2 shows the real and reactive powers for each of the zones. The loads have be chosen so that the load power factor for each zone is 0.9 and the total apparent power is 90 % of the rated system power.

Figure 5.2 shows the measured voltage at various points along the feeder for 100 kVA, 200 kVA and 315 kVA systems operating at full load with no STATCOM voltage support, voltage support at the PCC and voltage support at the end of the line. For these simulations, no limits were applied to the STATCOM current controllers; as a result, the STATCOM will always regulate the voltage, even when the required reactive current exceeds the rated current of the system. It can be seen that the inclusion of voltage support does not significantly change the overall voltage profile, but increases the system voltage regardless of where the STATCOM is connected.

In Figure 5.3 a load step change from no load to full load is applied and the reactive current required to regulate voltage at the PCC is compared with the reactive current required to regulate voltage at the end of the line for a 100 kVA system. It can be seen that regulating voltage at the end of the line requires substantially more reactive power than regulating the voltage at the PCC, with the required reactive current reaching almost 1 p.u. For the 200 kVA and 315 kVA systems, although the reactive current required at the PCC remained at about 0.7 p.u., the reactive current required at the end of the line exceeded the rated current of the system. In all cases, the voltage in each zone remains within the allowed limits of 1 p.u. +6 %/-10 %.

The results presented above all use fixed controller gains, chosen to give

100 kVA system		
Zone	Real power, P	Reactive power, Q
0	23.7 kW	11.5 kVAr
1	14.3 kW	6.91 kVAr
2	14.3 kW	6.91 kVAr
3	14.3 kW	6.91 kVAr
4	14.3 kW	6.91 kVAr
Total	80.9 kW	39.1 kVAr
200 kVA system		
Zone	Real power, P	Reactive power, Q
0	47.4 kW	23.4 kVAr
1	28.6 kW	13.8 kVAr
2	28.6 kW	13.8 kVAr
3	28.6 kW	13.8 kVAr
4	28.6 kW	13.8 kVAr
Total	161.8 kW	78.6 kVAr
315 kVA system		
Zone	Real power, P	Reactive power, Q
0	75.0 kW	36.3 kVAr
1	45.0 kW	21.8 kVAr
2	45.0 kW	21.8 kVAr
3	45.0 kW	21.8 kVAr
4	45.0 kW	21.8 kVAr
Total	255 kW	123.5 kVAr

Table 5.2: Maximum system loading for each zone of the 100 kVA, 200 kVA and 315 kVA systems.

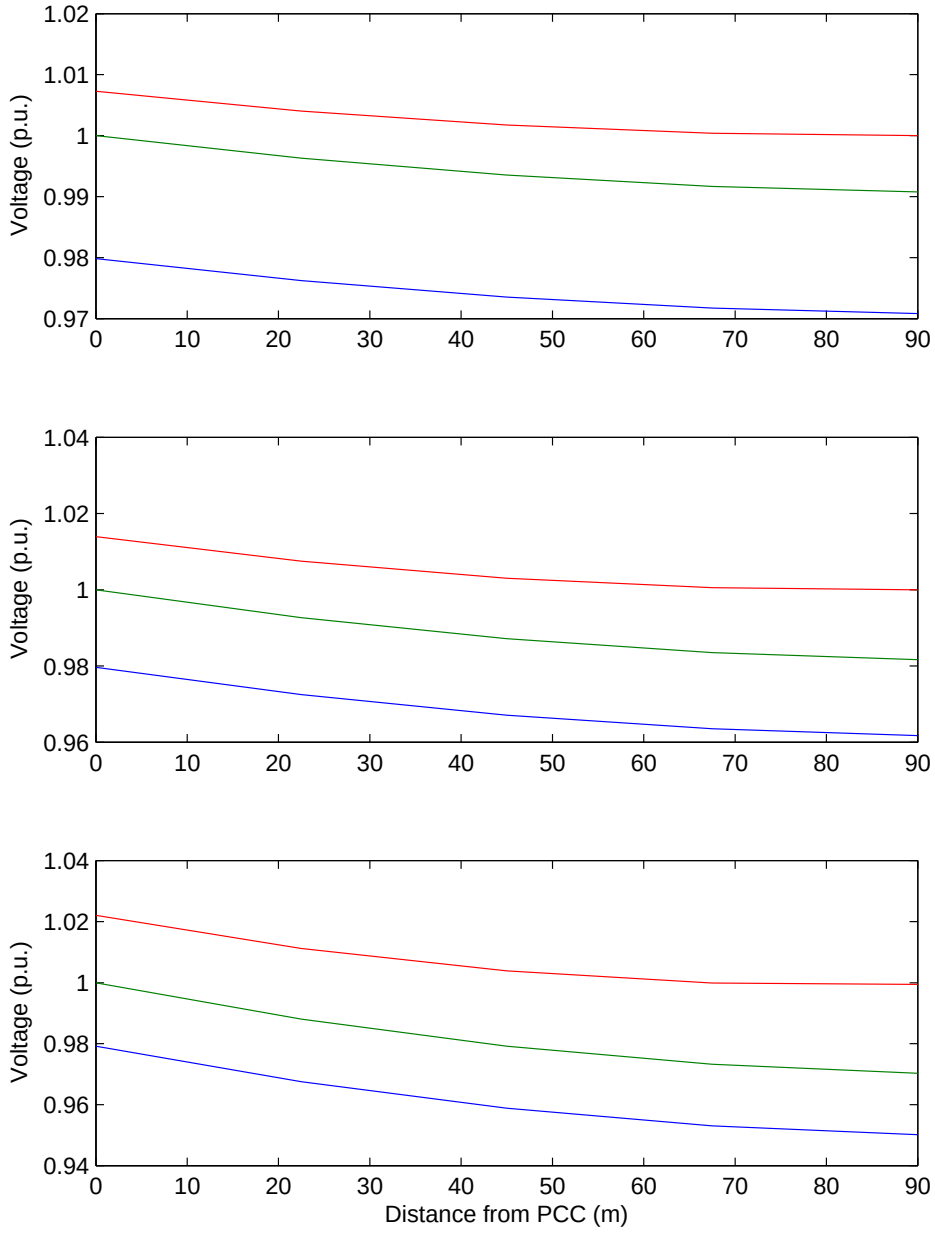

Figure 5.2: Voltage levels at different points along the line for 100 kVA, 200 kVA and 315 kVA systems with no voltage support (blue), STATCOM voltage support at the PCC (green) and STATCOM voltage at the end of the line (red).

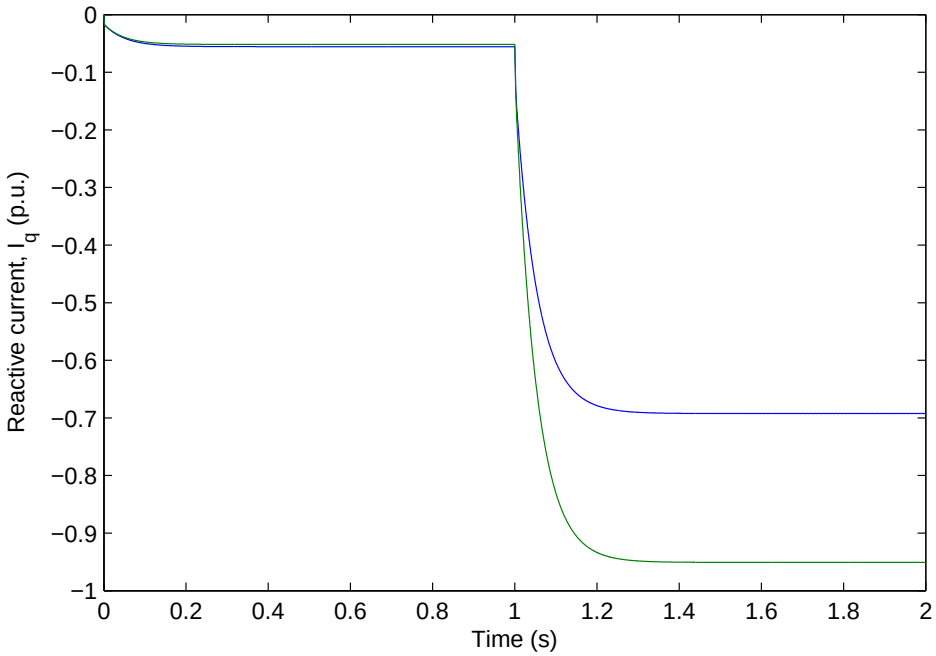

Figure 5.3: Response of the STATCOM to a step change in load when regulating voltage at the supply (blue) and at the end of the line (green) for a 100 kVA system.

a consistent response from each simulation. In order to demonstrate the impedance estimation algorithm, the estimated impedances were recorded for comparison with the "ideal" calculated system impedances. Reactance estimation results showing the full usable bandwidth are presented in Figure 5.4. The results are very close to the ideal values calculated from the component values used in simulation. The reactances calculated using only the 80 Hz and 120 Hz are listed in Table 5.3. The ideal values refer to the supply impedance only and do not take the load into account. As can be seen, the estimation errors when this method is used are small and predominantly due to neglecting the load when calculating the "ideal" impedances. However, the simulations are close to ideal and only a simple impedance is being estimated. Although quantisation errors are considered, as described in the previous chapter, the simulations do not take account of many other sources of error that are expected on real systems, such as noise or interference from the converter switching.

System	Ideal (Ω)	No load (Ω)	Full load (Ω)
100 kVA	0.0785	0.0786	0.0765
200 kVA	0.0393	0.0392	0.0380
315 kVA	0.0251	0.0251	0.0242

Table 5.3: Fundamental reactance estimates using extrapolation from 80 Hz and 120 Hz data when the system is operating at no load and full load.

To demonstrate the controller retuning method, simulations were performed with the STATCOM retuning performed part way through so that the response of the STATCOM before and after retuning could be compared. Figures 5.5—5.7 show the reactive current injected by the STATCOM for each system. In each case, the controller is initially untuned. The settling time of the untuned controller varies considerably for each system. In comparison, after tuning, the controller settling time is consistent at each power level.

Figure 5.8 shows the resultant system voltage response for each of the simulated power levels. The figure shows that the response from the tuned

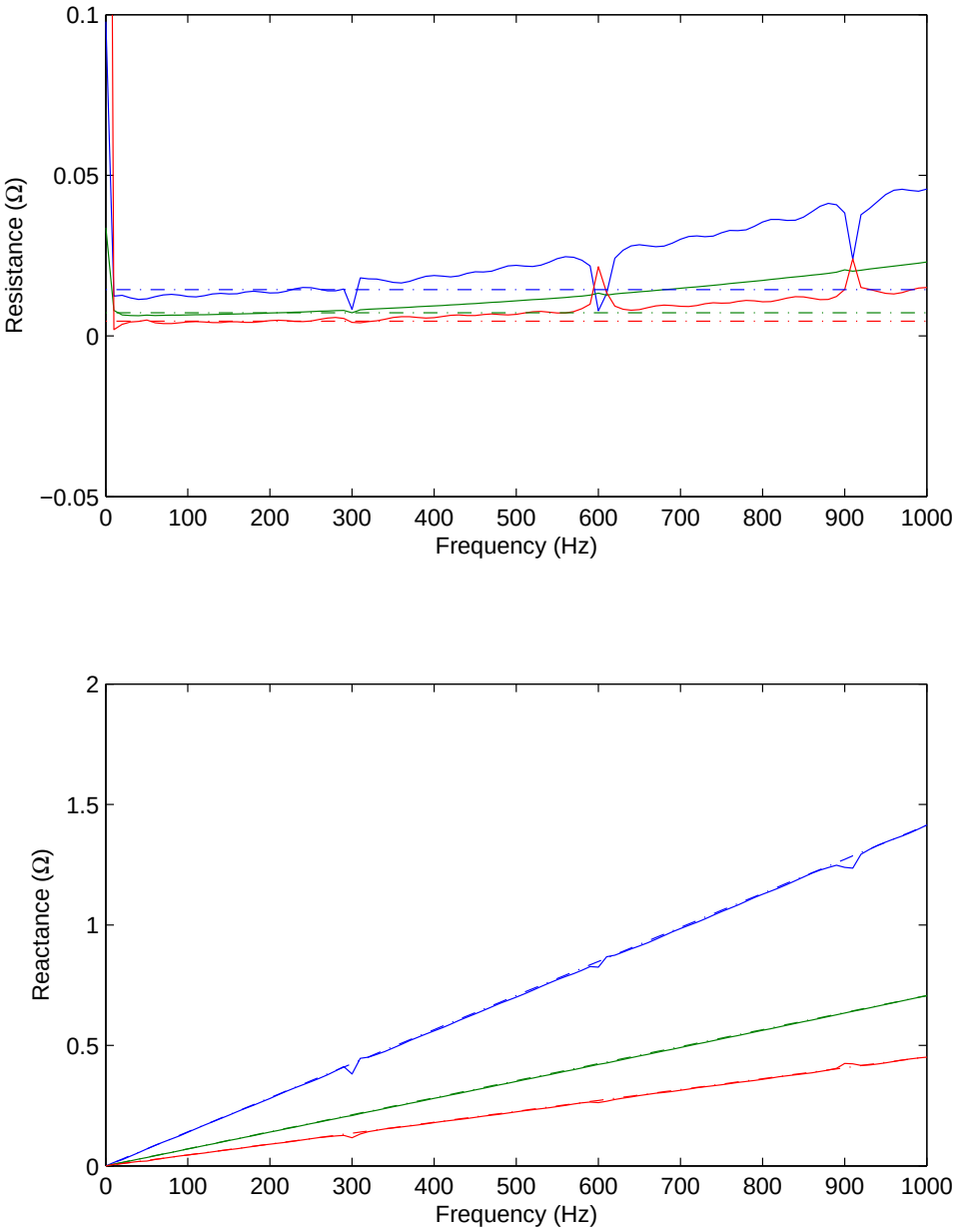

Figure 5.4: Reactance estimates for the 100 kVA, 200 kVA and 315 kVA systems, as measured from the PCC.

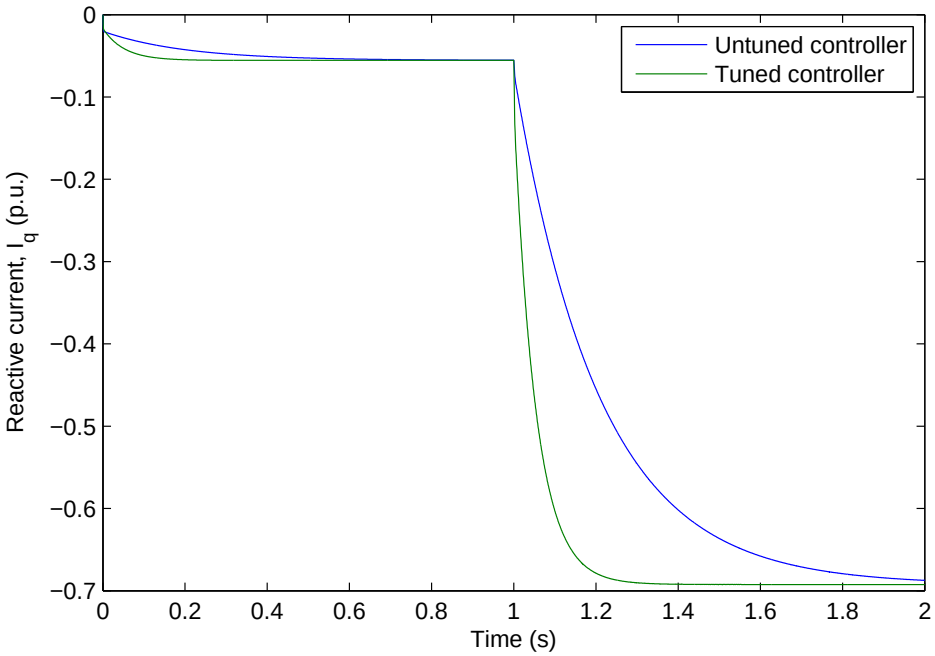

Figure 5.5: Injected reactive current step response for both a tuned and untuned controller on the 100 kVA system.

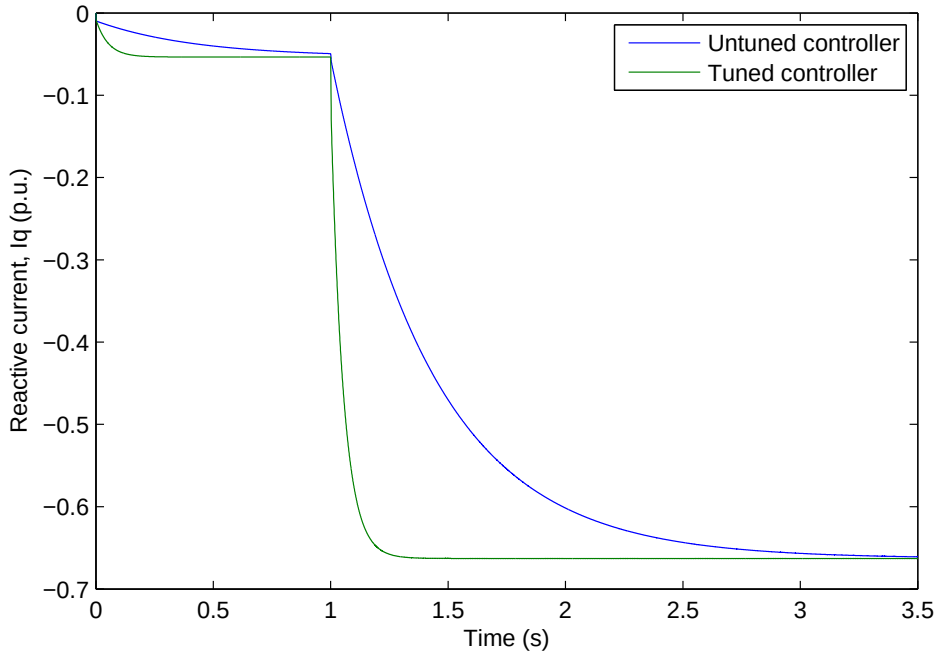

Figure 5.6: Injected reactive current step response for both a tuned and untuned controller on the 200 kVA system.

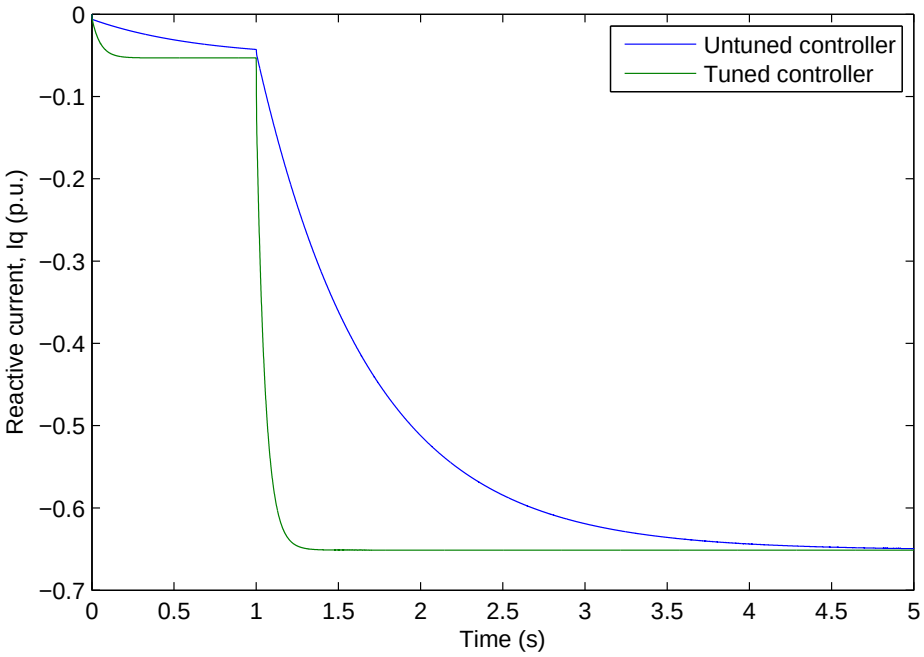

Figure 5.7: Injected reactive current step response for both a tuned and untuned controller on the 315 kVA system.

controllers is consistent, to the point where the results cannot easily be distinguished from each other, while the response from the untuned controllers varies considerably. The same results, showing the voltage transients over a shorter length of time, are presented in Figure 5.9.

Each of the tuned controllers takes approximately 0.2 s to return the system voltage to a value close enough to 1 p.u. for the system to be considered in steady-state. This is consistent with the controllers having the expected time-constant of 0.05 s. For the untuned controllers the time taken for the voltage to return to 1 p.u. is much longer: about 1 s for the 100 kVA system, 2 *textrms* for the 200 kVA and 3.2 s for the 315 kVA.

The loads used in the previous simulations consist of resistance and inductance only. Additional simulations have been performed where a capacitive load is included at the PCC, representing power factor correction equipment. The loads in each zone were adjusted so that the power factor in each zone was reduced to 0.8 while the overall apparent power of each load re-

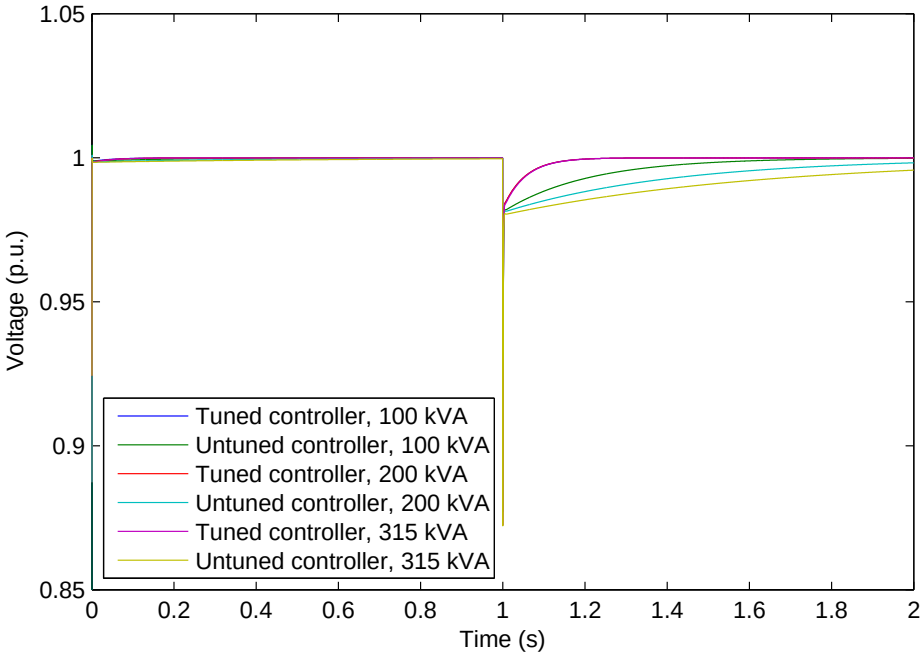

Figure 5.8: The effect of a step change in load on the magnitude of the system voltage, for both tuned and untuned controllers.

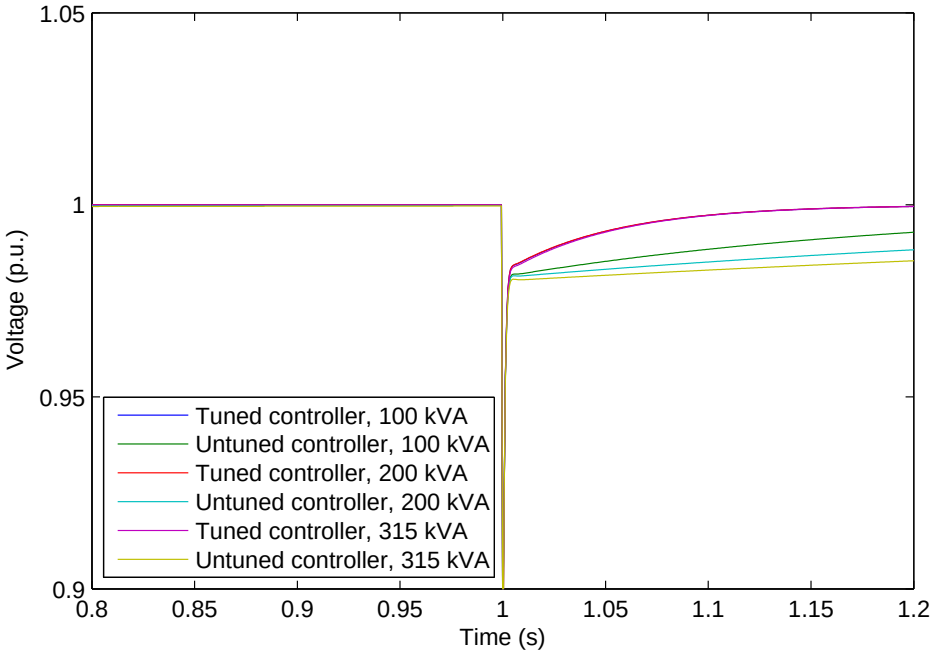

Figure 5.9: As previous figure, but zoomed on the transient.

mained the same. A mostly capacitive load was then included in Zone 0 to provide the required reactive power to reduce the overall system reactive power demand by 75 %. The installed capacitors were 830 μF, 1660 μF, 2600 μF for the 100 kVA, 200 kVA and 315 kVA systems respectively. In each case 0.5 Ω resistors were added in series with the capacitors to limit inrush currents and damp the resulting resonance.

Figure 5.10 shows the wideband impedance estimation results for systems with power factor correction capacitors at the PCC. The reactance estimation results are of a similar quality to the previous results when no capacitance was considered, as can be seen in Table 5.4. The purpose of the capacitors is to act as a source of reactive power, thereby increasing the voltage at the PCC and reducing the load on the STATCOM. The change in reactive power demand as a result of the power factor correction can be seen in Figures 5.11—5.13.

System	Ideal (Ω)	Estimated (Ω)
100 kVA	0.0800	0.0806
200 kVA	0.0400	0.0394
315 kVA	0.0255	0.0247

Table 5.4: Fundamental reactance estimates using extrapolation from 80 Hz and 120 Hz data when PFC capacitors are installed at the PCC.

It can be seen that when the system is only lightly loaded, the STATCOM must provide positive reactive power in order to reduce the voltage. This is a shortcoming of the simulations performed, which assume that the capacitors are always connected. Real power factor correction would likely be controlled so that the capacitors are disconnected when not required.

In this section simulations have been used to demonstrate that the system impedance can be accurately identified for a single-source, linear system and that the calculated impedance estimates may then be used to tune a STATCOM controller. It has been shown that using the impedance data to tune the controller allows consistent controller dynamics to be achieved

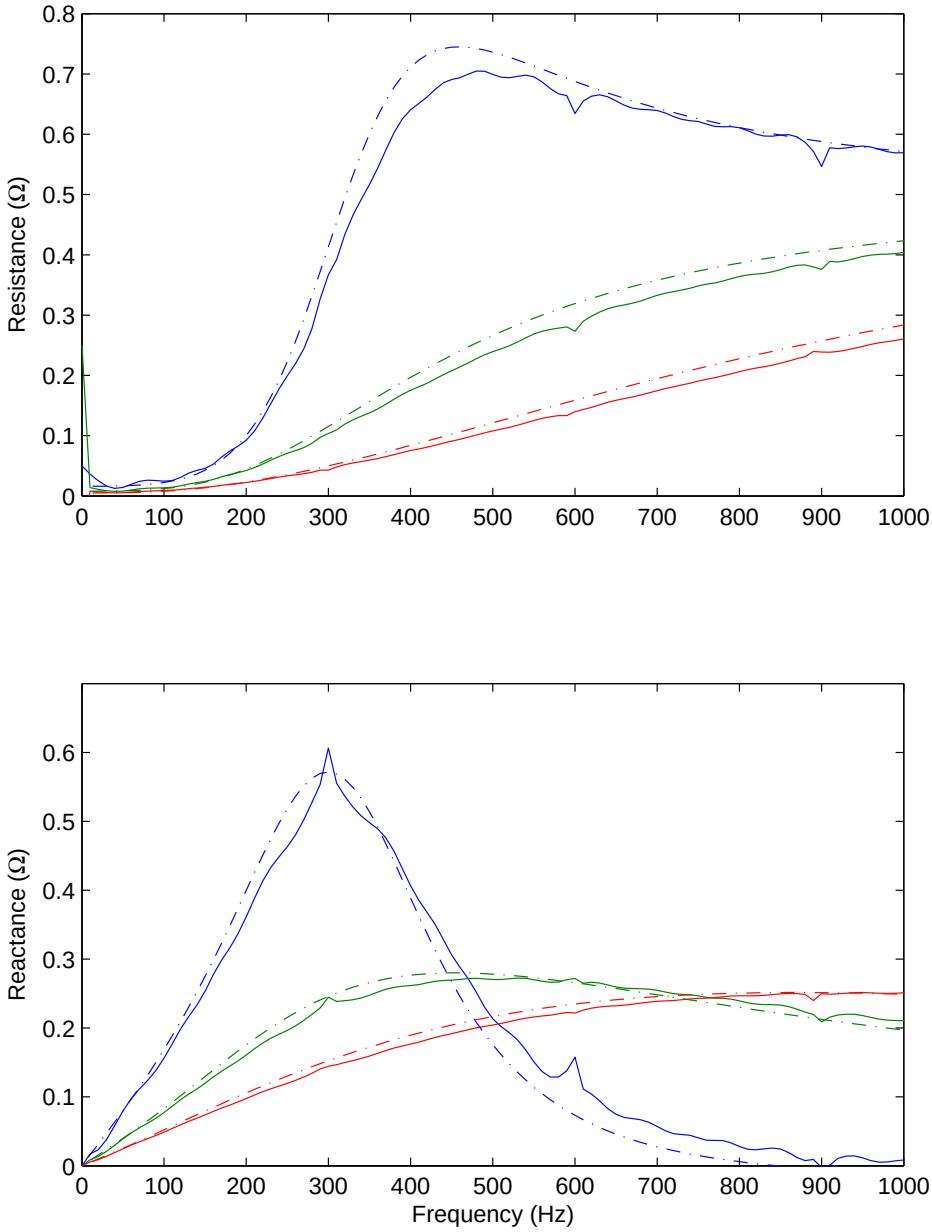

Figure 5.10: Reactance estimates for the 100 kVA, 200 kVA and 315 kVA systems, as measured from the PCC, when power factor correction capacitors are installed.

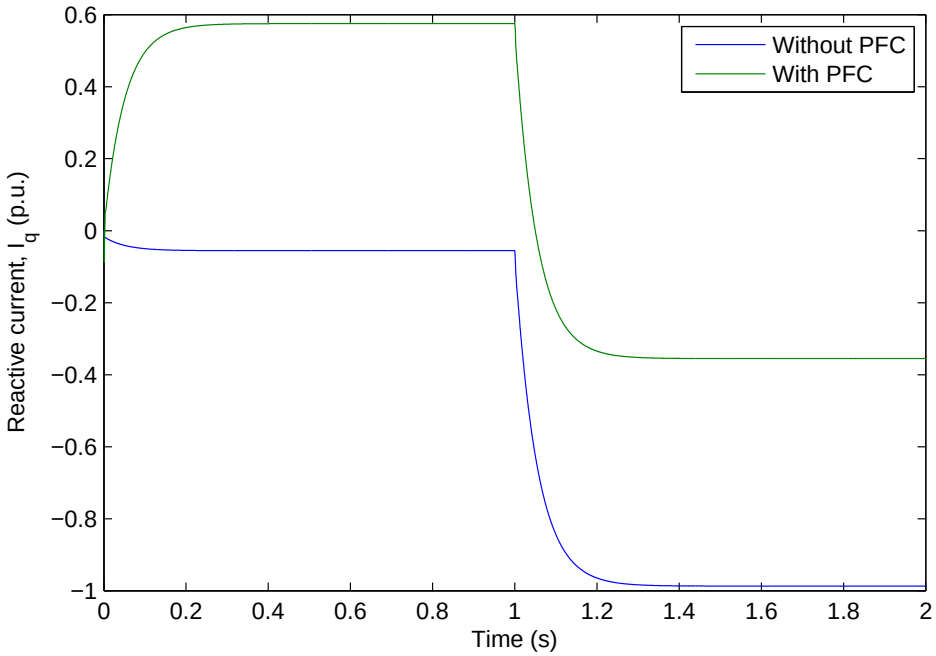

Figure 5.11: Reactive current supplied by the STATCOM connected to the 100 kVA when power factor correction capacitors are present, and without PFC for comparison.

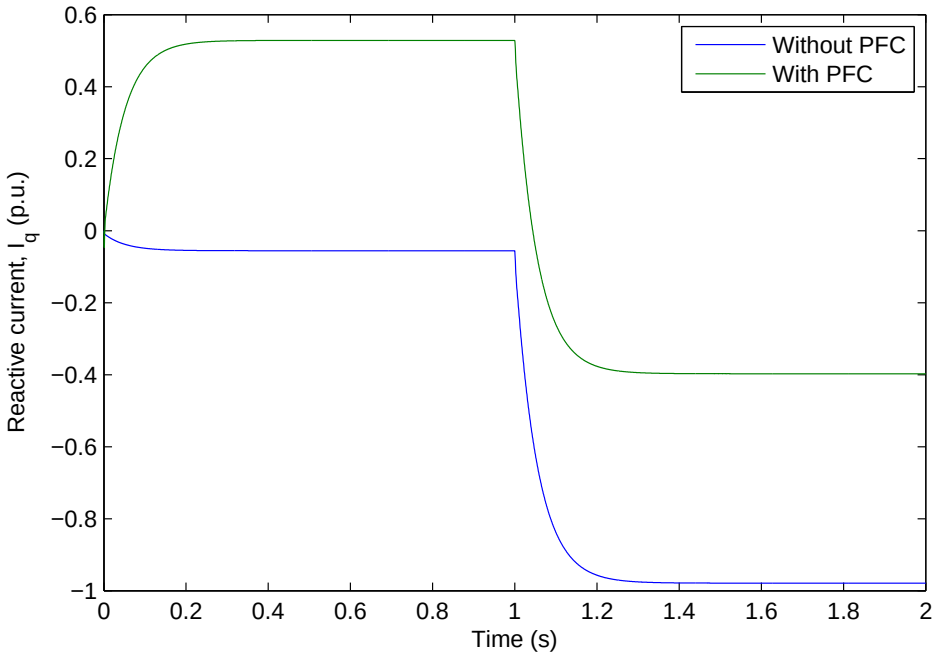

Figure 5.12: Reactive current supplied by the STATCOM connected to the 200 kVA when power factor correction capacitors are present, and without PFC for comparison.

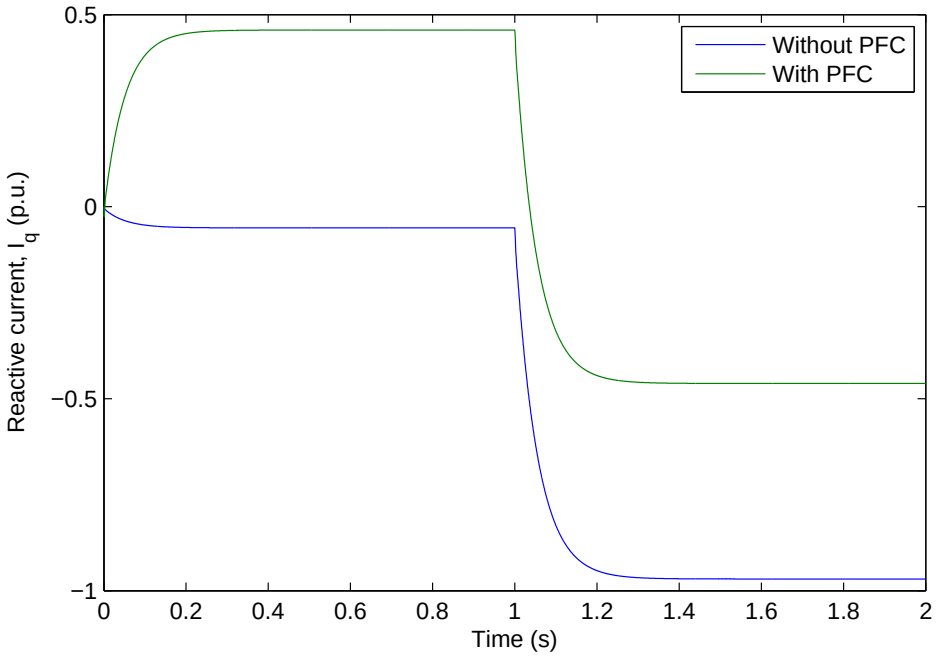

Figure 5.13: Reactive current supplied by the STATCOM connected to the 315 kVA when power factor correction capacitors are present, and without PFC for comparison.

regardless of the supply impedance. There are two key limitations of the control structure considered so far. First, the reactive power demand placed on the STATCOM can be very large, in some cases exceeding the rated current of the system. Second, the controller is not designed to allow multiple STATCOMs to operate in parallel, which limits the flexibility of the design considerably. In the following section the fixed reference controller will be replaced with a droop controller in order to address these shortcomings in the controller design.

5.2.2 Droop-controlled STATCOM

This section is concerned with the behaviour of a single droop-controlled STATCOM being used to regulate system voltage, which is proposed as a solution to the issues identified with the fixed-reference controller used in the previous section. The simulations performed in this section are similar to those performed in the previous section; however, droop feedback as described in Chapter 3 has been added so that the voltage set point is no longer constant, but varies depending on system loading. In these simulations, the STATCOM kVAr rating is taken to be 50 % of the system kVA rating and the STATCOM droop constant is set at 5 %.

Simulations were performed on the 100 kVA, 200 kVA and 315 kVA using the loads listed in Table 5.2 for systems having a STATCOM connected at either Zone 0 or Zone 4 as in the previous section. The voltages measured in each zone for each of the three systems are shown in Figure 5.14. The current injected to the 315 kVA system as a result of a step-change in load is shown in Figure 5.15. The voltage response for the same step-change in load can be seen in Figure 5.16.

Although the system voltage is no longer regulated to a constant value, it still remains well within the specified limits and the reactive current injected by the STATCOM has been significantly reduced compared to the fixed reference controller. One practical benefit of using a droop controller is that the

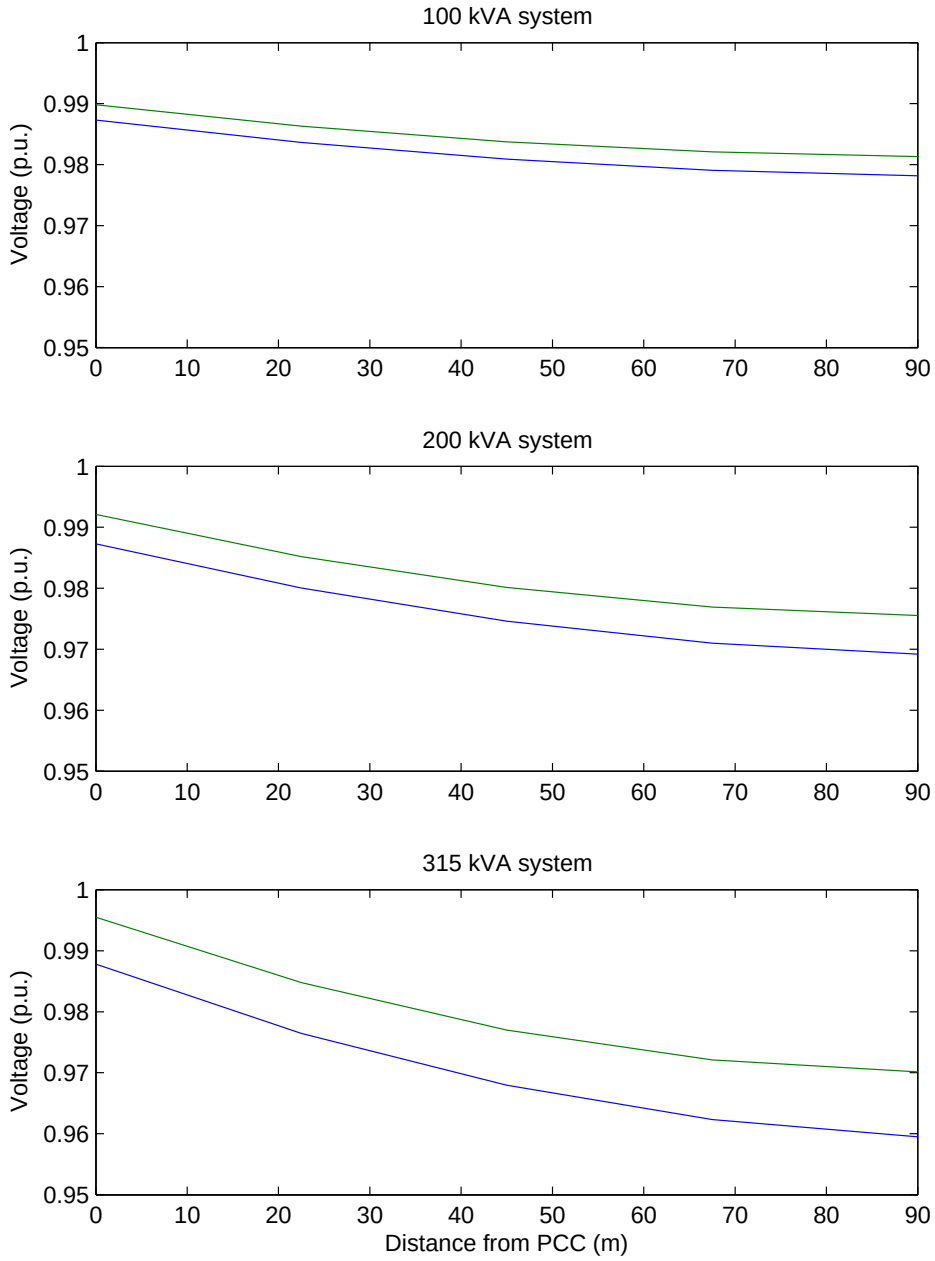

Figure 5.14: Voltage levels at different points along the line for 100 kVA, 200 kVA and 315 kVA systems with a droop controlled STATCOM at the PCC (blue) and at the end of the line (green).

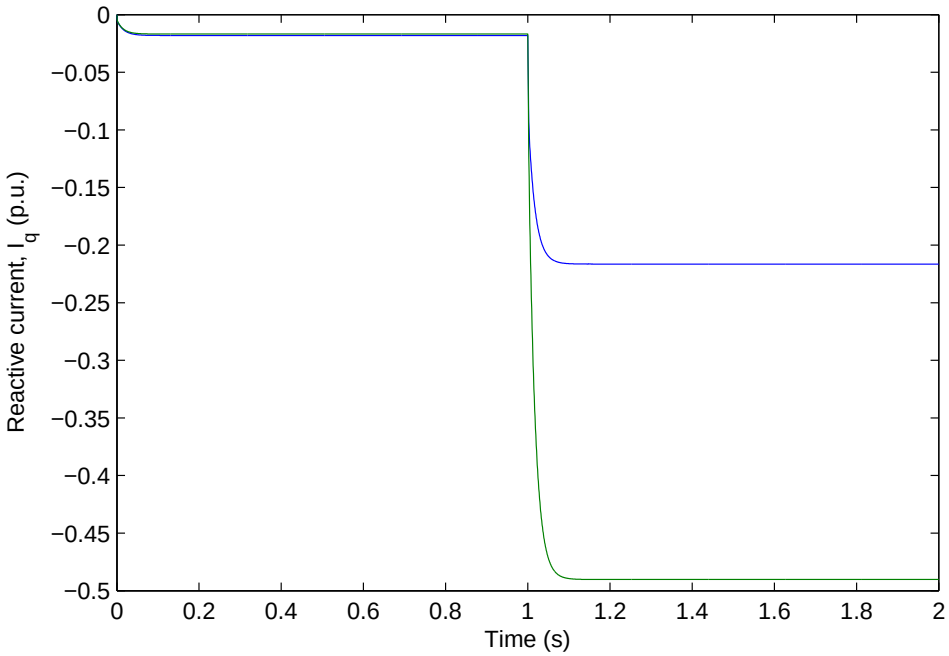

Figure 5.15: Reactive current response of the STATCOM when located at the PCC (blue) and at the end of the line (green) for a 315 kVA system.

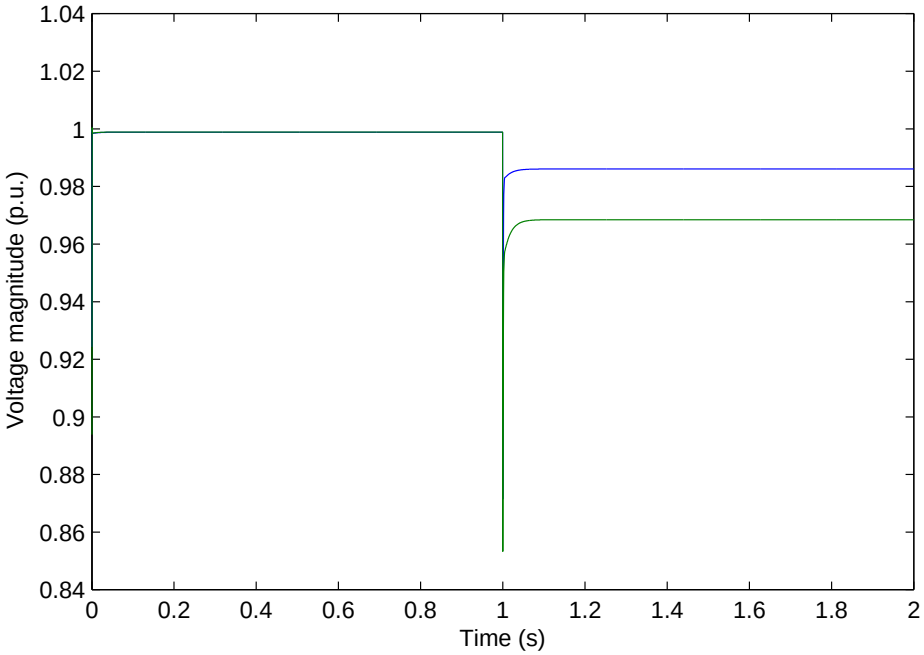

Figure 5.16: System voltage as measured by the STATCOM before and after a step load change on the 315 kVA system. The blue trace is for a STATCOM positioned at the PCC, the green for a STATCOM at the end of the line.

rating of the STATCOM may be reduced without any significant sacrifice in power quality. It should also be noted that compared to the non-droop controlled STATCOM the load step-change response time has been reduced, although the controller gains have not been changed. The droop-controlled STATCOM takes approximately 0.1 s to return to the voltage to steady-state, which is half the time taken for the original controller to return the voltage to 1 p.u. This is consistent with the results seen in Chapter 3.

In the previous section it was noted that the reactive current required by the STATCOM when positioned at the end of the line could exceed the rating of the system. By allowing the voltage to vary, the droop controlled STATCOM substantially reduces the reactive current demand. The key benefit of this reduction in current demand is that the rating, and therefore the size and cost, of the STATCOM may also be reduced.

This section has used simulation to demonstrate a droop-controlled STATCOM on a linear system. The important differences in behaviour between the droop-controlled STATCOM and the fixed-reference STATCOM have been highlighted. The benefits of using droop-control, even when only one STATCOM is present on the system have also been mentioned. All the work presented in this chapter so far has been concerned with simple linear systems supplied from a single source. In the next section, the effect of additional power sources will be considered. Subsequent sections shall only consider the fixed-reference controller but the work carried out should still be applicable to the droop-controlled STATCOM.

5.3 Studies of a system including distributed energy resources

The purpose of this section is to determine the effect of distributed energy resources on the performance of the impedance estimation algorithm and the overall behaviour of the STATCOM. Simulations were performed on

a system including models for distributed generation, connected at either Zone 0 or Zone 5. Two different models were used: a voltage source with an inductive output filter in series, which shall be referred to as a voltage-source DER, and a current source connected to an LC filter, which shall be referred to as a current-source DER. In both cases, the source voltage or current is varied so that a constant current is supplied to the system by the DER, in phase with the grid voltage at the point of connection. The DER configurations and control loops are shown in Figure 5.17. In the case of the voltage source DER, the output current is varied by controlling the source voltage. This is achieved using a single control loop. The control for the current source DER consists of an inner control loop, controlling the capacitor voltage by varying the source current, and an outer control loop which varies the output current by varying the capacitor voltage demand.

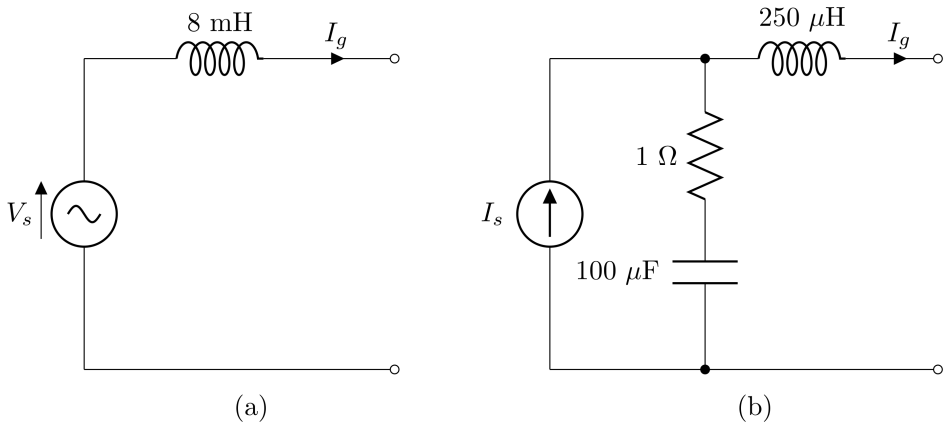

Figure 5.17: Simulation models used to represent DERs: (a) voltage source DER, (b) current source DER.

Simulations of a system with DERs installed were performed at various power levels. The simulations performed were similar to those in previous sections: a system with no STATCOM, a system with a STATCOM connected at Zone 0 and a system with STATCOM connected at Zone 4. For the results presented in this section, the STATCOM regulated the system voltage to a fixed value.

Figure 5.18 show the voltages measured in each zone for a system having light load and a high level (50 % of system rated power in these simulations) of generation provided by a voltage-source DER. The voltages when the system is fully loaded are shown in Figure 5.19. The reactance estimates calculated by the STATCOM for this case are shown in Figure 5.20 and the single frequency results are listed in Table 5.5. Finally the transient response of the STATCOM, both when tuned and untuned, is considered. The results are shown in Figure 5.21. Figure 5.22 is included to show the initial transient more clearly.

System	Ideal (Ω)	Estimated (Ω)
100 kVA	0.0762	0.0806
200 kVA	0.0387	0.0407
315 kVA	0.0249	0.0266

Table 5.5: Fundamental reactance estimates using extrapolation from 80 Hz and 120 Hz data when voltage source DERs are present in Zone 5.

As can be seen that the DERs cause the voltage to rise at the end of the line. For the lightly loaded 200 kVA and 315 kVA systems, the STATCOM must reduce the system voltage. When the system loading is increased the voltages measured in each zone initially drop in all cases as distance from the PCC increases, before rising again as the distance to the DER is reduced, resulting in an overall voltage profile that is almost flat. The impedance estimation results for the voltage source DER show that it is still possible for the STATCOM to accurately calculate the system reactance with the DERs installed. In addition, the tuned controllers continue to behave consistently once the initial transient caused by the connection of the DERs has settled, while the untuned controllers have variable settling times. The tuned controllers all return the voltage to 1 p.u. after 0.2 s following the transient, which is consistent with earlier results and the expected time-constant.

The transient following the initial connection of the DERs shows some oscillatory behaviour, although in all cases the ringing is quickly suppressed.

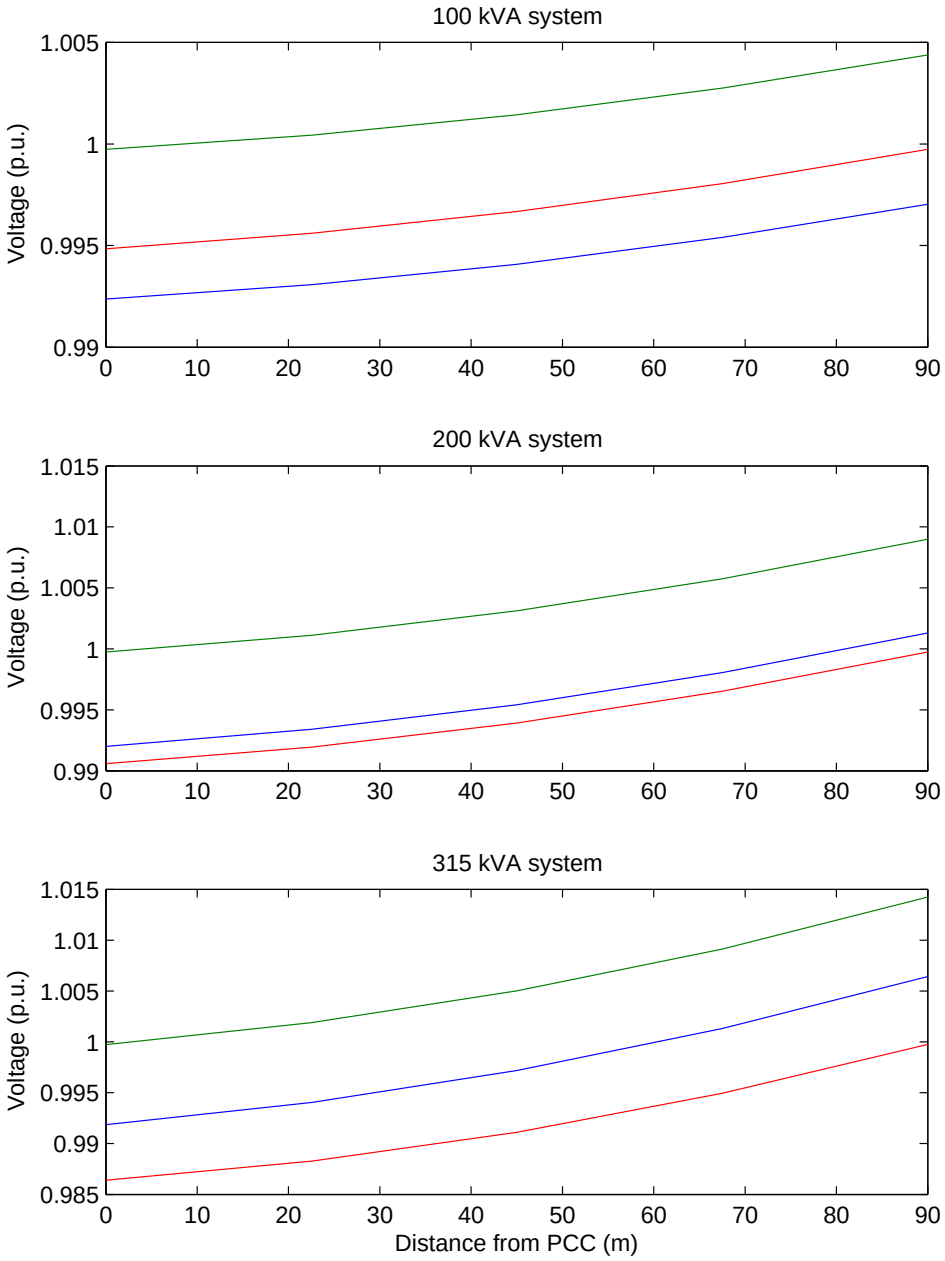

Figure 5.18: Voltages measured in each of the zones for the 100 kVA, 200 kVA and 315-kVA systems with light load and voltage-source type distributed energy resources installed at the end of the line. Each system was simulated with no voltage support (blue), voltage support at the PCC (green) and voltage support at the end of the line (red).

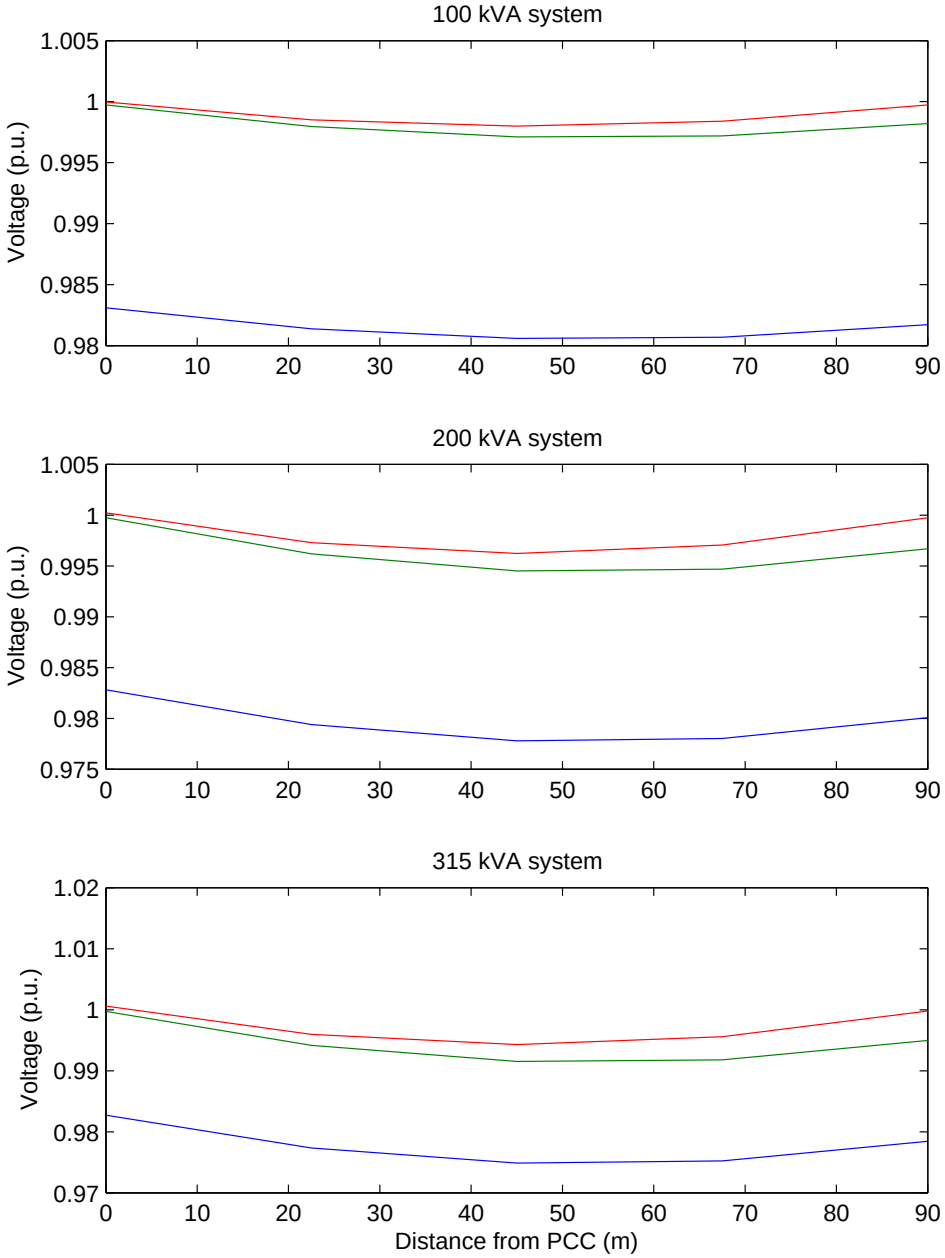

Figure 5.19: Measured voltages for a heavily loaded system with no voltage support (blue), voltage support at the PCC (green) and voltage support at the end of the line (red). A voltage source DER is installed at the end of the line.

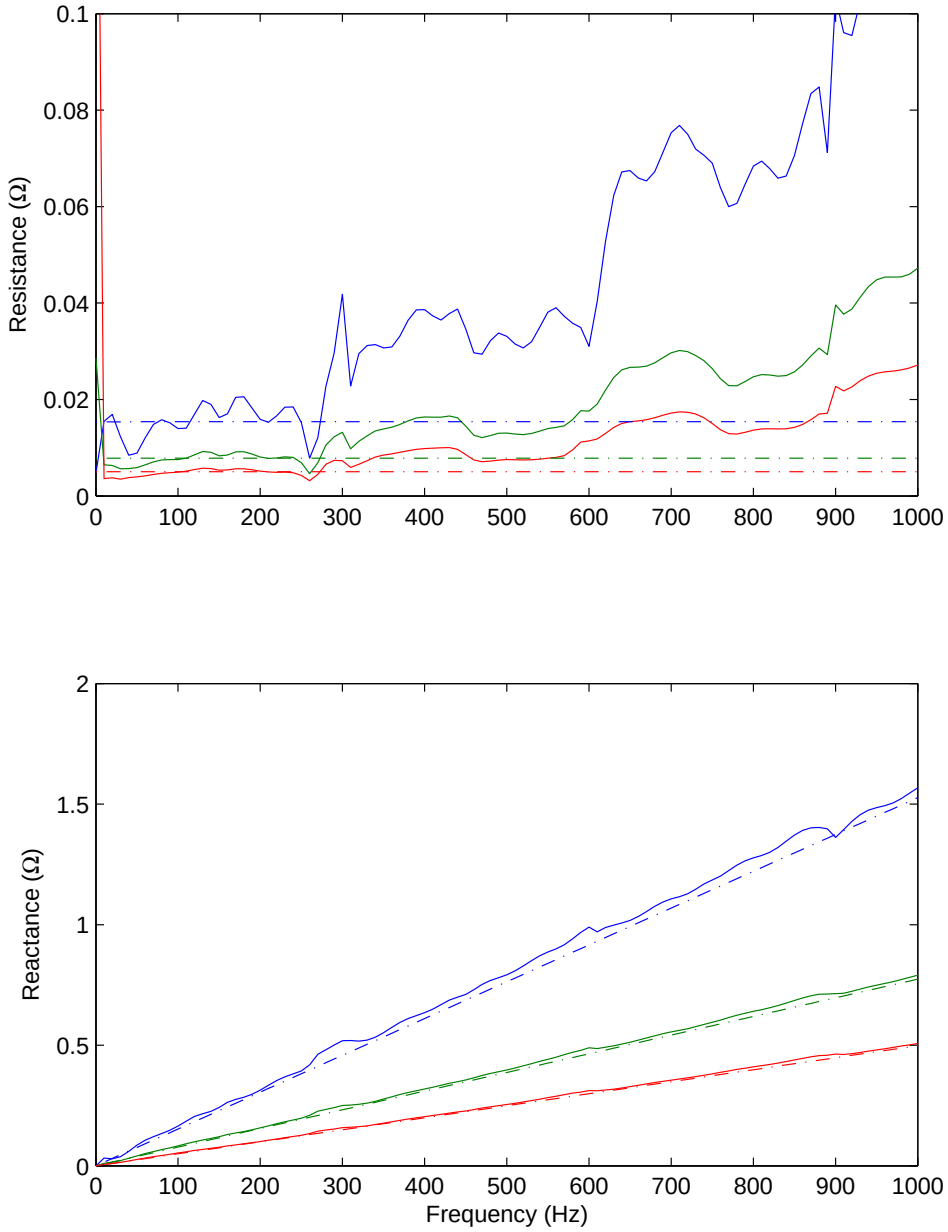

Figure 5.20: Reactance estimates for the 100 kVA, 200 kVA and 315 kVA systems with the voltage source DER model included at the end of the line.

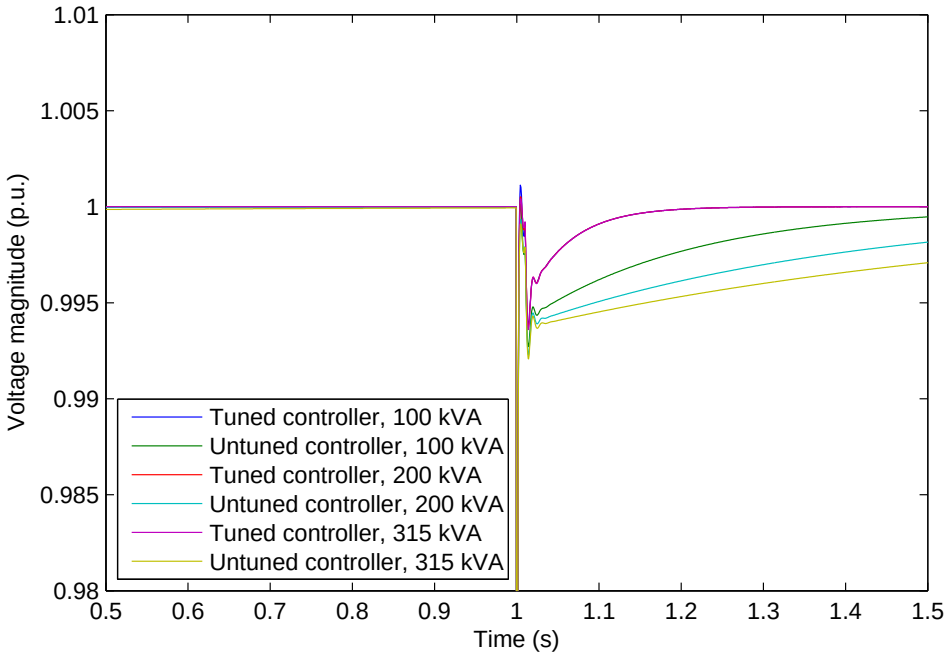

Figure 5.21: The transient voltage response caused by the connection of the voltage source DER as measured by the STATCOM for both tuned and untuned controllers.

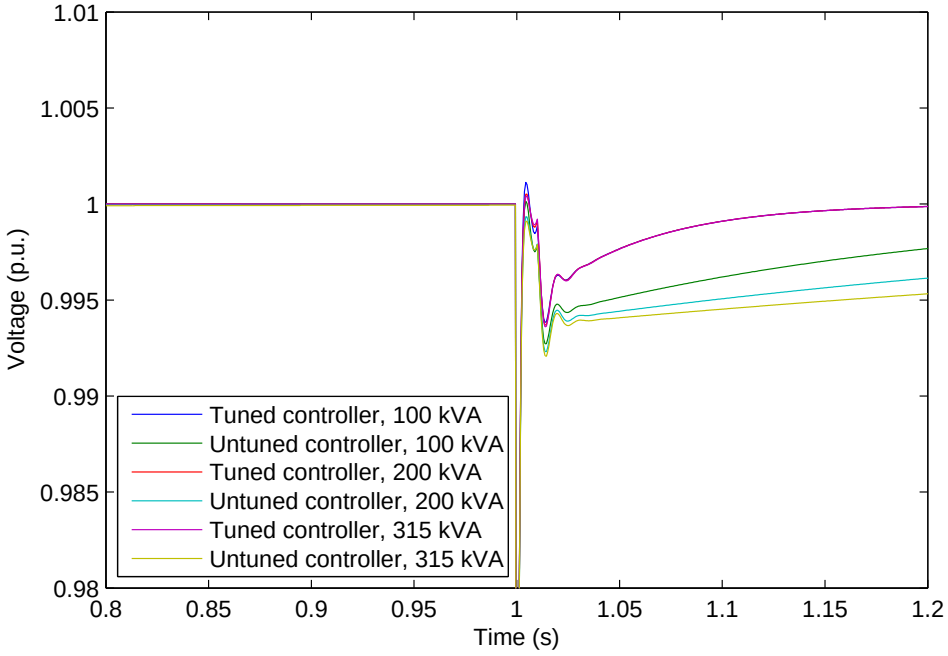

Figure 5.22: As previous figure, but zoomed on the transient.

This brief oscillation is caused by the connection of the DERs. Any small mismatch between the instantaneous system voltage and the voltage source within the DER model will cause a current to flow between them, resulting in the voltage disturbance seen. On real systems such transients could be caused by transformer inrush currents or small voltage differences between synchronous generator terminals and the grid. The precise properties of the disturbance on a real system will depend on the type and capacity of the DERs connected; the connection transient for a large DER could be quite severe if not properly managed.

System	Ideal (Ω)	Estimated (Ω)
100 kVA	0.0787	0.0783
200 kVA	0.0393	0.0385
315 kVA	0.0251	0.0248

Table 5.6: Fundamental reactance estimates using extrapolation from 80 Hz and 120 Hz data when current source DERs are present in Zone 5.

The simulations described above were repeated for systems with current source DERs installed at the end of the line. For the light-load, high-generation case, the voltages at various points along the line are shown in Figure 5.23. The high-load, high-generation case is shown in Figure 5.24. Reactance estimates are shown in Figure 5.25 and the transient response of the STATCOM is shown in Figure 5.26.

The system voltage profiles closely resemble those seen for the voltage source DER. This is to be expected as in steady state the two different DER types are supplying the same power (at unity power factor) to the system and therefore are expected to cause equal changes in the voltage regardless of filter configuration. The voltage transient resulting from the activation of the current-source DERs is very small. This is because it was necessary to limit the rate at which the current demand changed for the current-source DER model to 100 As^{-1} in order for the simulation to complete reliably. Therefore the STATCOM has time to respond to the variation in voltage before

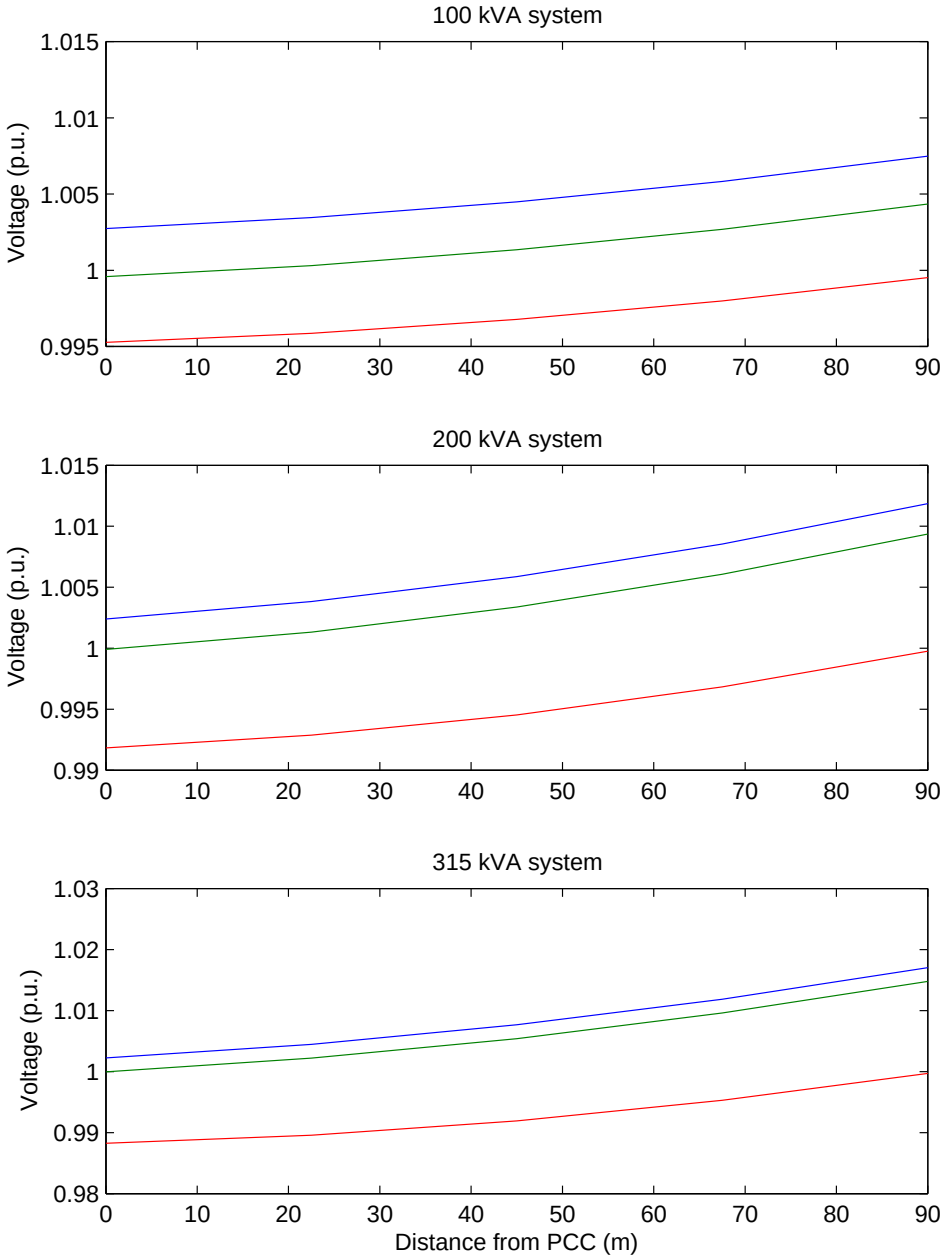

Figure 5.23: Voltages measured in each of the zones for each of the systems when lightly loaded. A current-source DER is installed at the end of the line. Each system was simulated with no voltage support (blue), voltage support at the PCC (green) and voltage support at the end of the line (red).

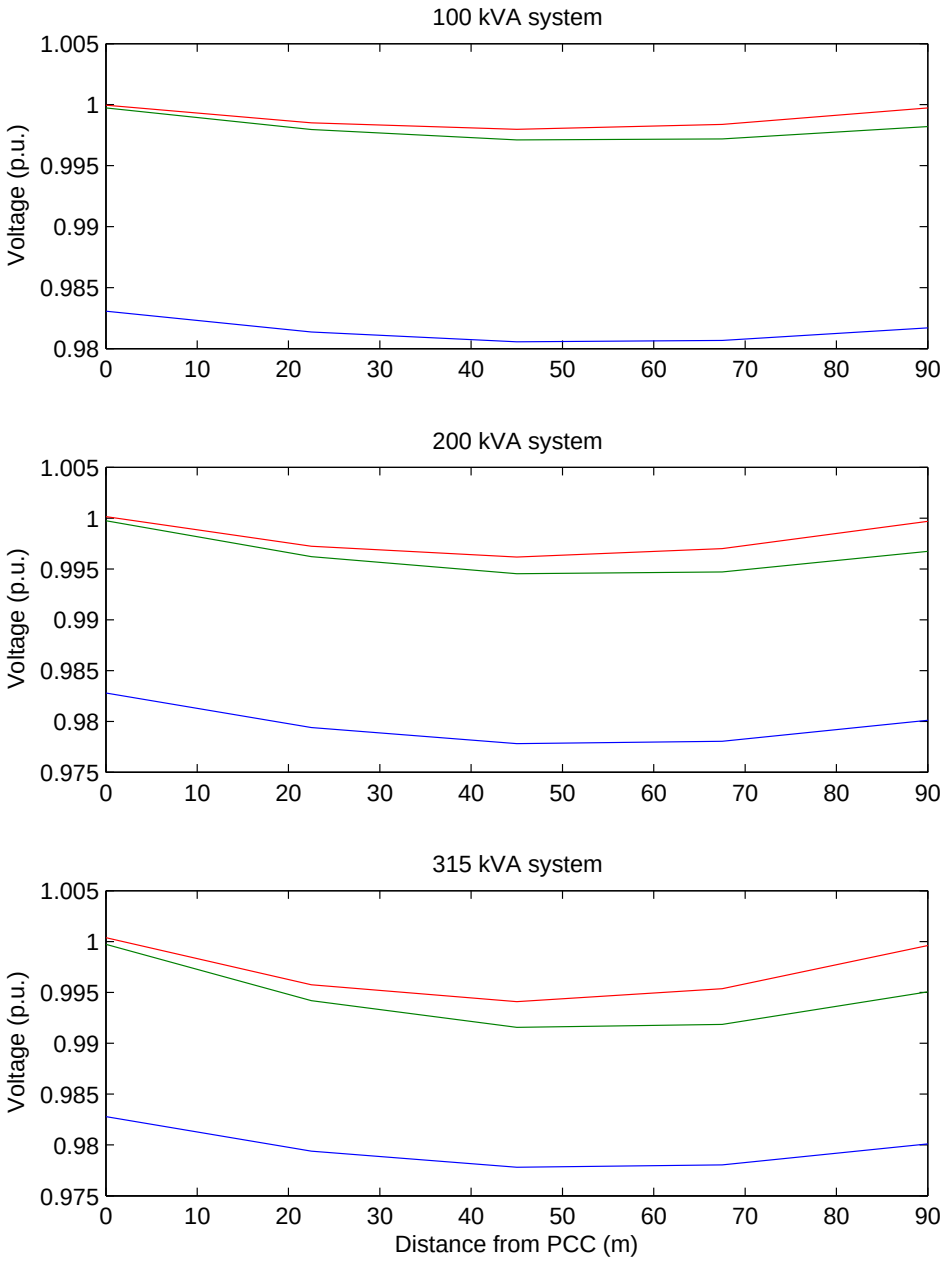

Figure 5.24: Measured voltages for a heavily loaded system with a current-source DER at the end of the line. Results are shown for no voltage support (blue), voltage support at the PCC (green) and voltage support at the end of the line (red).

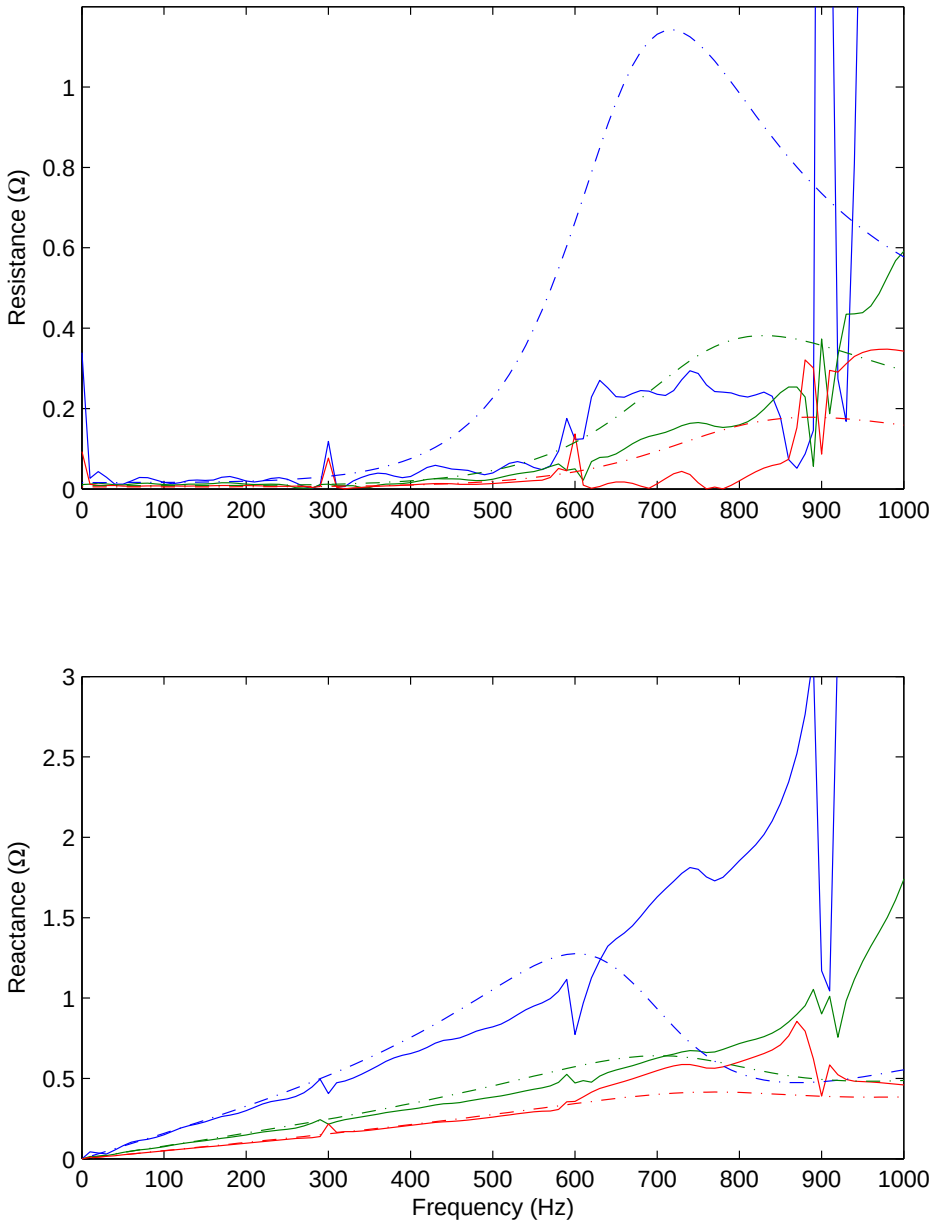

Figure 5.25: Reactance estimates for the 100 kVA, 200 kVA and 315 kVA systems. A current source DER is installed at the end of the line.

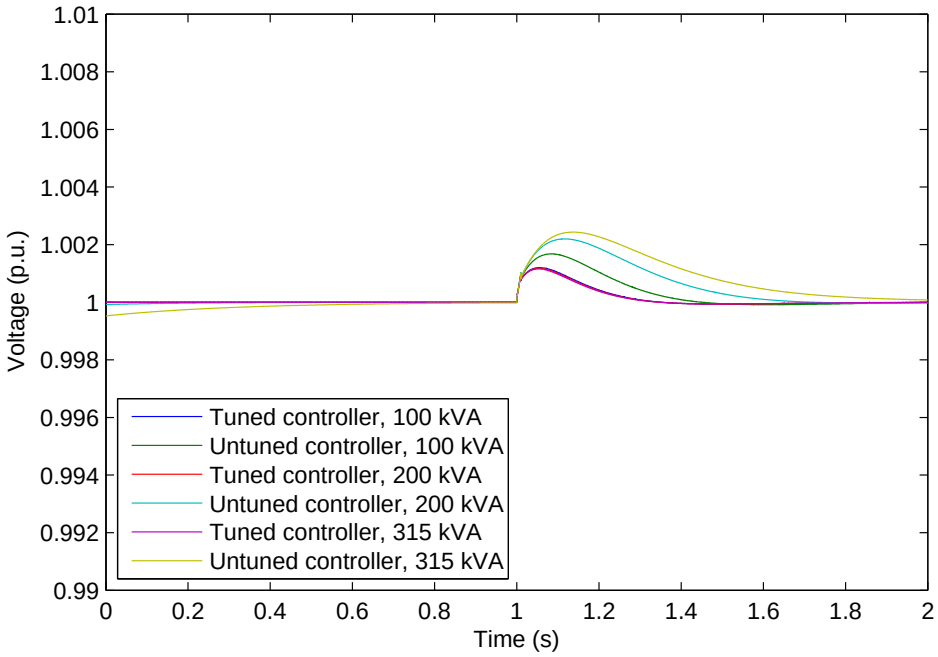

Figure 5.26: The transient voltage response measured on connection of the current-source DER, for both tuned and untuned controllers.

it becomes significant, resulting in only a small disturbance. It can still be seen that the settling times of the tuned controllers are all the same whereas the untuned controllers have varying settling times. The tuned STATCOMs now take slightly longer to return the voltage to 1 p.u., about 0.3 s, however, these results are not directly comparable with earlier results, since they do not show the response to a step change in voltage. Given the ramped, rather than stepped, change in DER output power, a slightly longer response time is to be expected.

Deterioration in the quality of the wideband impedance estimates can be seen at higher frequencies, starting between 300 Hz and 600 Hz for the different systems. The loss of accuracy is caused by the DER control response. The high-bandwidth capacitor voltage control suppresses the injection to prevent variation in the filter capacitor voltage. At low frequencies, the supply impedance dominates and the impedance estimates are not affected. At high frequencies, when the filter impedance becomes significant, the impe-

dance estimates become less accurate. The loss of accuracy at the higher frequencies does not affect the STATCOM tuning; at the low frequencies the estimation results still closely resemble the expected values, as can be seen in Table 5.6.

This section has considered the effect that DERs may have on the behaviour of the STATCOM and the impedance estimation algorithm. Two different models have been used to represent the DERs. It has been seen that a consistent voltage response can still be achieved on various systems by tuning the STATCOM voltage controller to the system reactance. It has also been seen that it is possible for the response of nearby controlled sources to affect the impedance estimation results.

5.4 The effect of harmonics and unbalance

The effect of unbalance and harmonics on the STATCOM control performance are considered in this section. The use of the DQ reference frame for control means that the STATCOM does not have any means of compensating for the effects of either harmonics or unbalance. Harmonics and unbalance are considered to have two possible sources: either loads on the system immediately surrounding the STATCOM or the supply itself. Regardless of the source, unbalance will result in a change in the relative amplitudes of the three system voltages and harmonics will result in distortion of the ideally sinusoidal voltage waveforms.

Harmonic load currents are caused by non-linear loads on the system. The most basic non-linear loads are bridge rectifiers with passive smoothing components on the DC-side, which may be a capacitor, inductor or combination of the two. Both inductively smoothed and capacitively smoothed rectifier circuits have been simulated. In this section, rectifiers with both types of smoothing are considered.

5.4.1 Load unbalance

During normal operation, load unbalance is typically caused by single-phase loads on the system. Unbalanced currents are drawn from the supply, resulting in unbalanced voltages being measured throughout the system, although the supply voltages remain the same. For the simulations in this section, the system loading was changed so that the resistive load connected to phase A was increased by 20 % compared with the restive load connected to phases B and C. The effect of this is that the current flowing through phase A will be decreased, resulting in a decreased drop in voltage for phase A. Current unbalance can typically reach much higher levels than the allowed level of voltage unbalance, and therefore 20 % decreased load on one phase may be considered a moderate rather than severe level of load unbalance.

Figure 5.27 shows the response of the STATCOM to a step change in load when unbalance is considered. The initial transient can be seen in more detail in Figure 5.28. The reactance estimation results are shown in Figure 5.29. Single frequency estimation results are listed in Table 5.7.

System	Ideal (Ω)	Estimated (Ω)
100 kVA	0.0785	0.0737
200 kVA	0.0393	0.0370
315 kVA	0.0251	0.0235

Table 5.7: Fundamental reactance estimates using extrapolation from 80 Hz and 120 Hz data when the load is unbalanced.

It can be seen that the system voltage has been affected. A high-frequency component has been superimposed onto the voltage magnitude calculated by the STATCOM. This is a sinusoidal component with a frequency of 100 Hz, and is caused by the asymmetric voltage drops on each phase resulting in different peak voltages. The impact of the unbalanced load appears to be limited. The STATCOM is still able to regulate the system voltage and the tuned controllers are still able to achieve consistent dynamics regardless of system impedance. The tuned controllers take approximately 0.2 *textrms* to

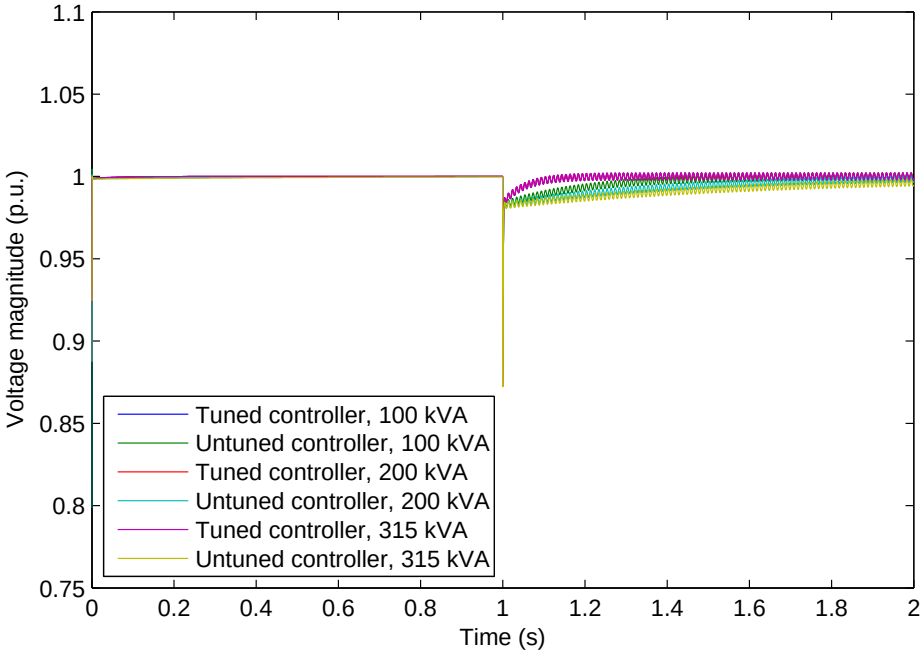

Figure 5.27: Transient voltage response of the STATCOM for a system with reduced loading on Phase A.

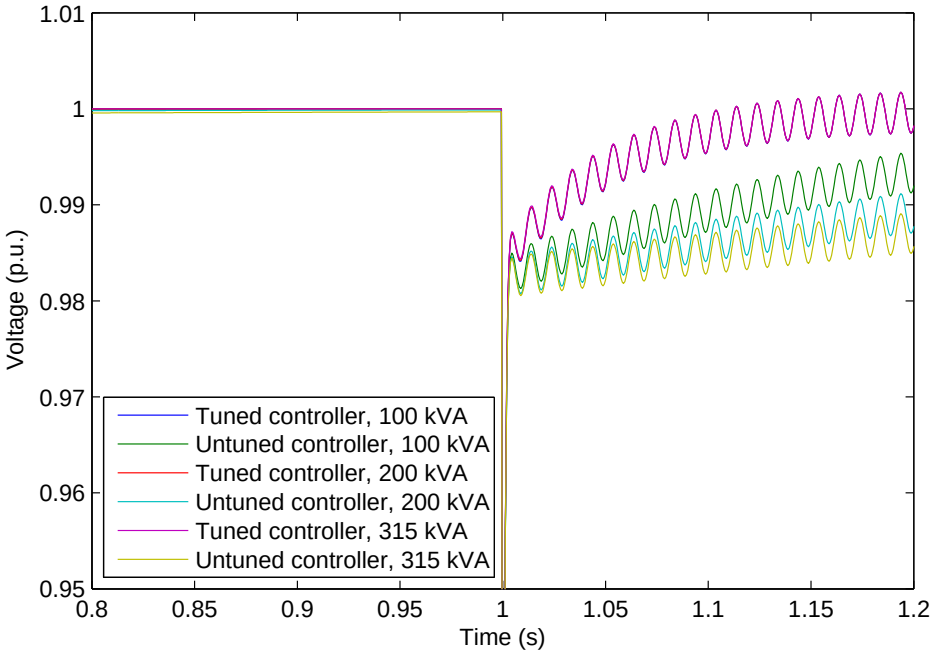

Figure 5.28: As previous figure, but zoomed on the transient.

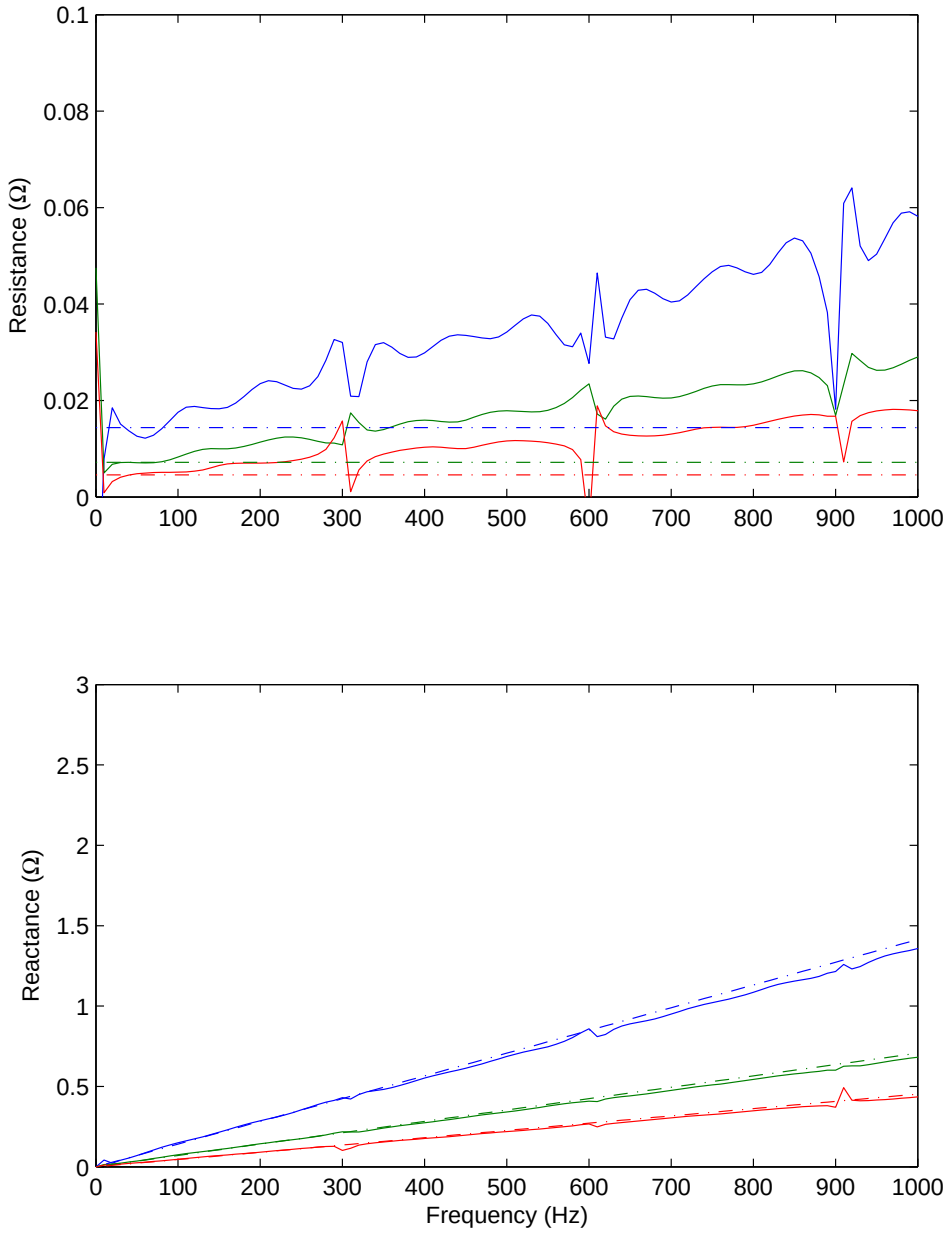

Figure 5.29: Results for the estimation of the system reactance when the loads are unbalanced.

return the voltage to steady-state, which is consistent with earlier results. The impedance estimation results show that the STATCOM continues to be able to identify the reactance of the system in the presence of an unbalanced load.

5.4.2 Supply unbalance

Unlike load unbalance which results in unbalanced currents and voltage drops, supply unbalance is seen as unbalanced supply voltages. Under normal conditions, unbalance in the supply should be limited, although the exact limits vary. For the purpose of this work it has been assumed that limits specified in the relevant British and European standard, as can be found in BS EN 50160 [15], are met, so that the worst case supply unbalance is no greater than 2 %. Supply unbalance was introduced into the simulations by increasing the amplitude of phase A relative to the other two phases.

As with load unbalance, the effect of supply unbalance on the system voltage calculated by the STATCOM and the effect on the transient behaviour was observed. Results are shown in Figures 5.30 and 5.31. As before, attempts to estimate the impedance of each phase of the system were made. Wideband results are shown in Figure 5.32 and single frequency estimates are listed in Table 5.8.

System	Ideal (Ω)	Estimated (Ω)
100 kVA	0.0785	0.0768
200 kVA	0.0393	0.0385
315 kVA	0.0251	0.0248

Table 5.8: Fundamental reactance estimates using extrapolation from 80 Hz and 120 Hz data when the supply is unbalanced.

It can be seen that the effect of the unbalanced supply voltage is greater than that of unbalanced load currents when considering the voltage calculations made by the STATCOM. However the controller continues to regulate the

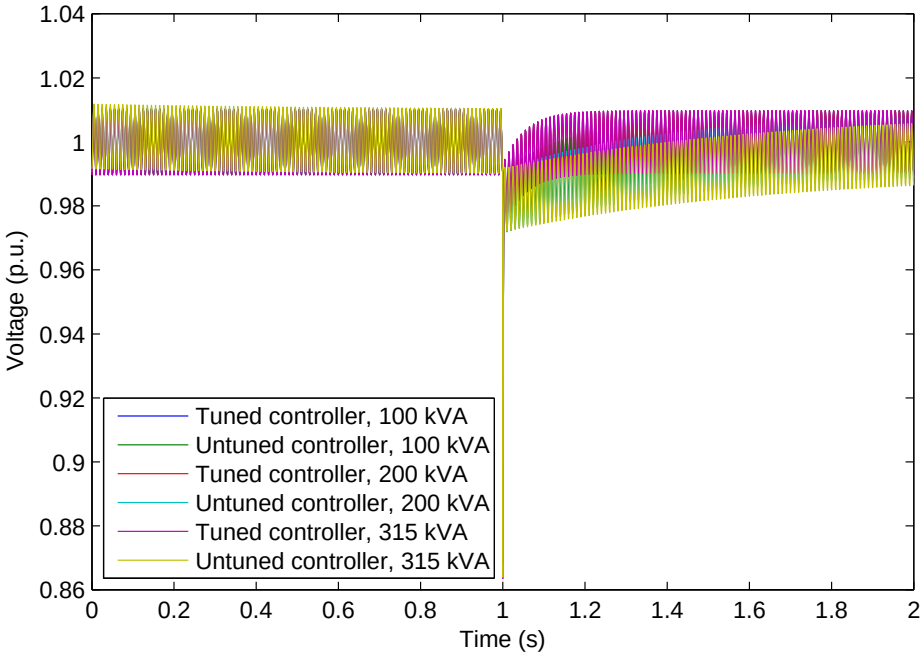

Figure 5.30: Transient voltage response of the STATCOM when the supply voltages are unbalanced.

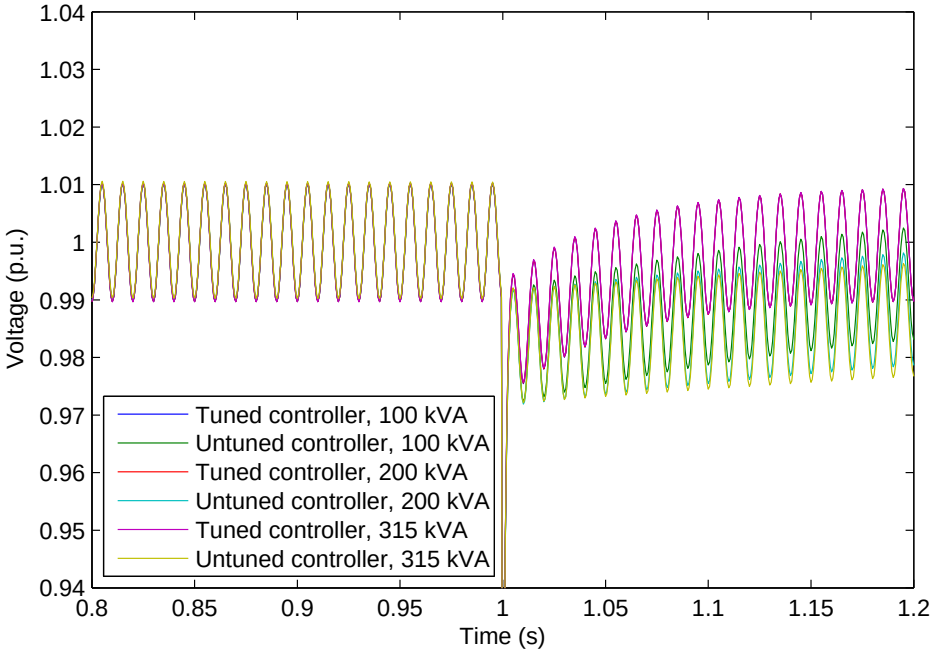

Figure 5.31: As previous figure, but zoomed on the transient.

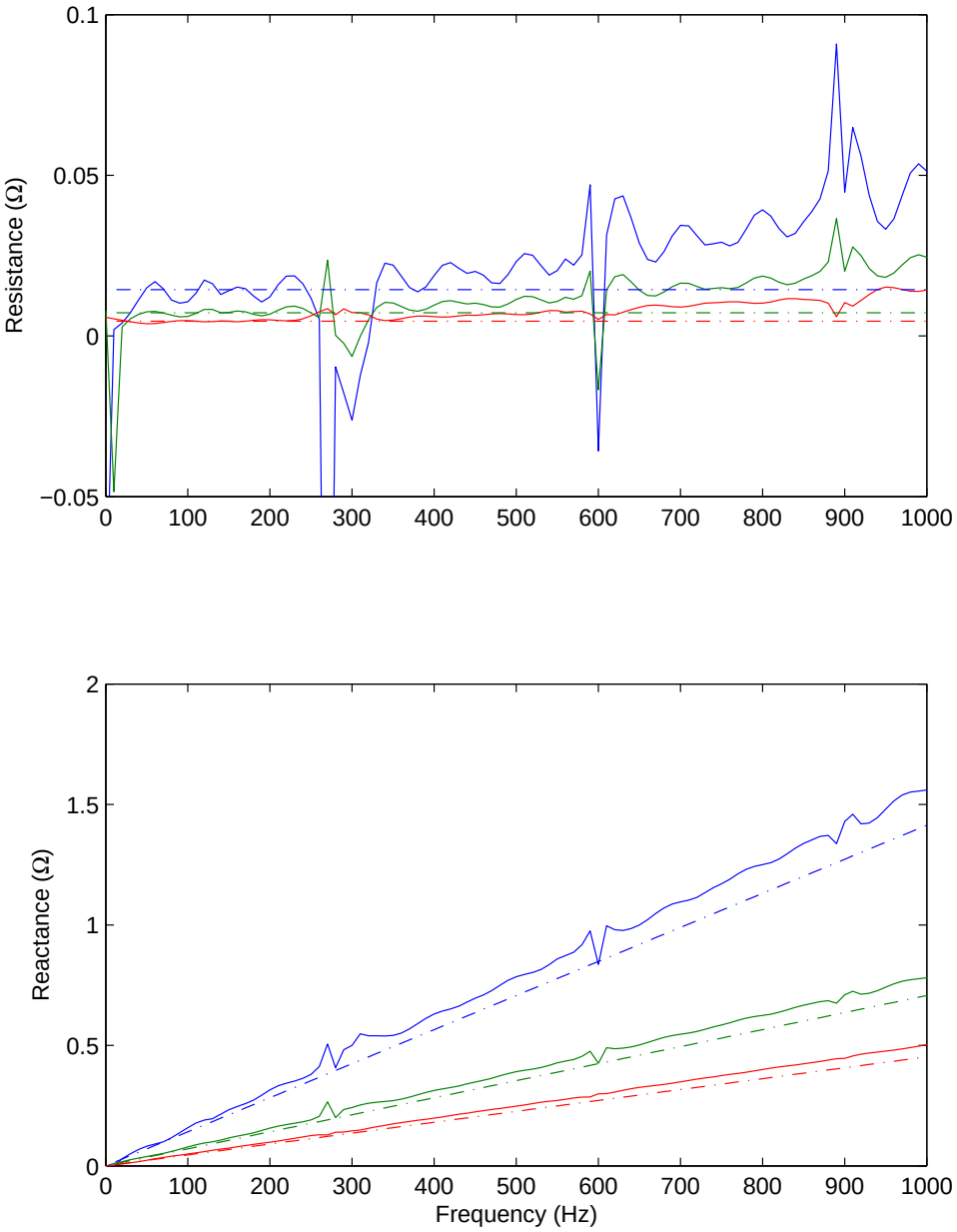

Figure 5.32: Reactance estimation results for the system when the supply voltages are unabalanced.

voltage effectively and when the controllers are tuned the dynamics of the STATCOM are consistent regardless of the impedance of the system. Although the high levels of distortion to present on the voltage waveforms make it difficult to determine exactly, the tuned controllers appear to return the voltage to steady-state after the expected 0.2 *textrms*. It can also be seen that the impedance estimation algorithm is not significantly affected by the supply unbalance.

5.4.3 Non-linear loads

Non-linear loads will result in harmonic currents being drawn from the supply. This will cause harmonic distortion to the voltages measured around the system. The specific harmonic currents and their magnitudes will vary depending on the exact nature of the non-linear load. To examine the effect of the harmonics, half of the loads at the PCC were replaced with a non-linear load of equal power rating. First an inductively smoothed rectifier was considered; this was followed by considering a capacitively smoothed rectifier.

Figure 5.33 shows the effect of the inductively smoothed rectifier on the STATCOM's voltage response, with the transient shown more clearly in Figure 5.34. Figure 5.35 shows the reactance estimated by the STATCOM for this case, with the single frequency results listed in Table 5.9. The voltage transient results for a capacitively smoothed rectifier are shown in Figures 5.36 and 5.37. The reactance estimates are shown in Figure 5.38 and listed in Table 5.10 for single frequency estimates.

High-frequency components appear superimposed on the voltages when the capacitively and inductively smoothed rectifiers are considered. Unlike the high-frequency component seen in the unbalanced case, this is not a single sinusoidal frequency, but a wide range of frequencies generated by the considerable harmonic distortion of the loads. The distortion appears to be worse for the capacitively smoothed rectifier. In both cases the STATCOM

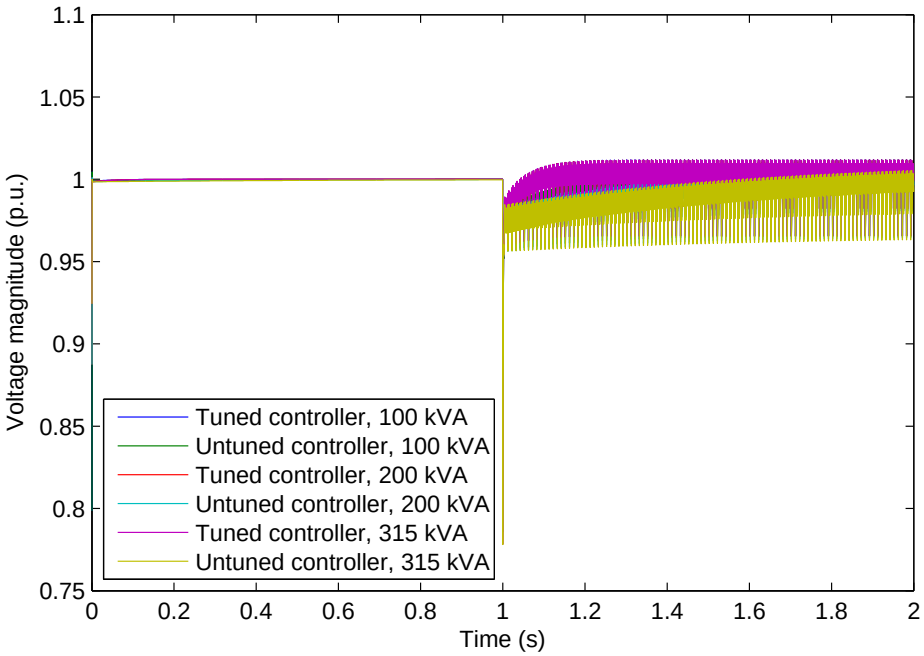

Figure 5.33: STATCOM transient voltage response for both tuned and untuned controllers when an inductively smoothed rectifier is installed at the PCC.

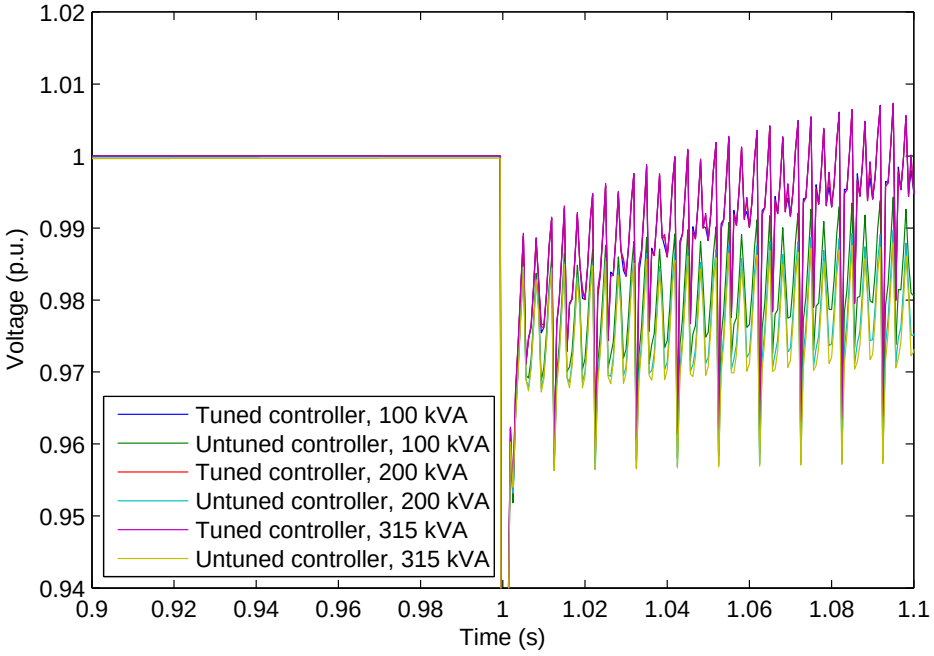

Figure 5.34: As previous figure, but zoomed on the transient.

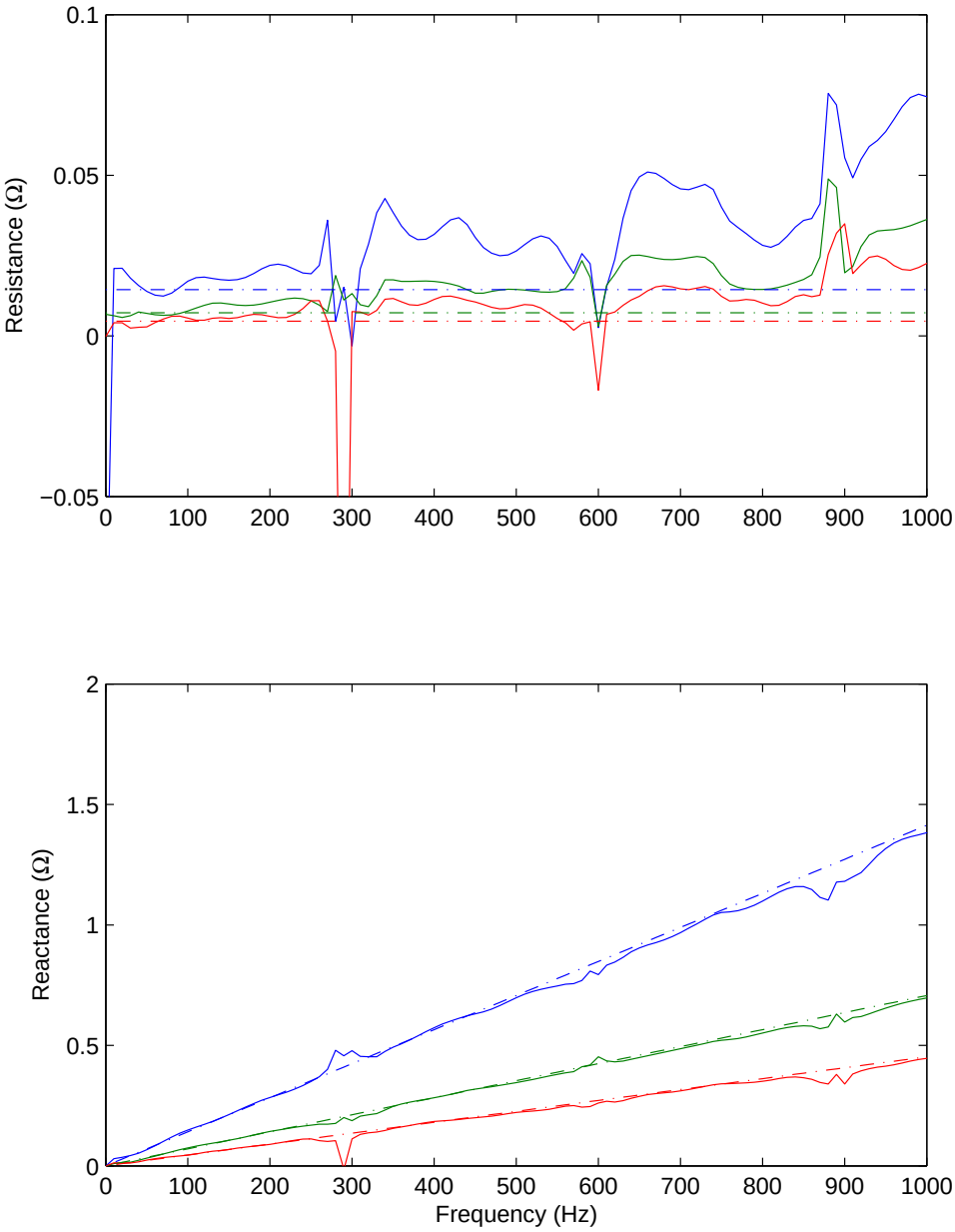

Figure 5.35: Results for the estimation of the system reactance when an inductively smoothed rectifier is installed at the PCC.

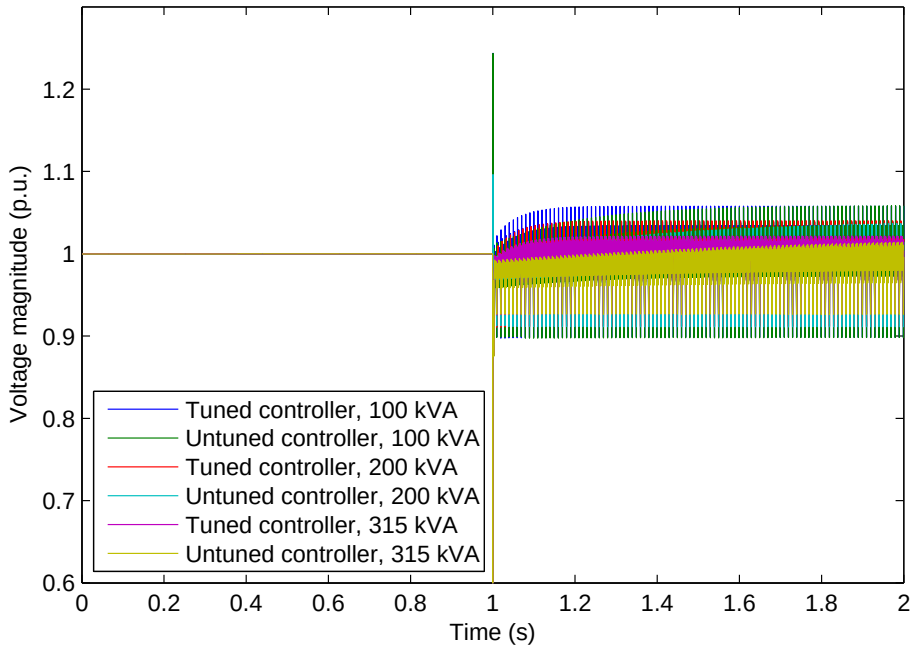

Figure 5.36: Response of both tuned and untuned controllers. A capacitively smoothed rectifier is installed at the PCC.

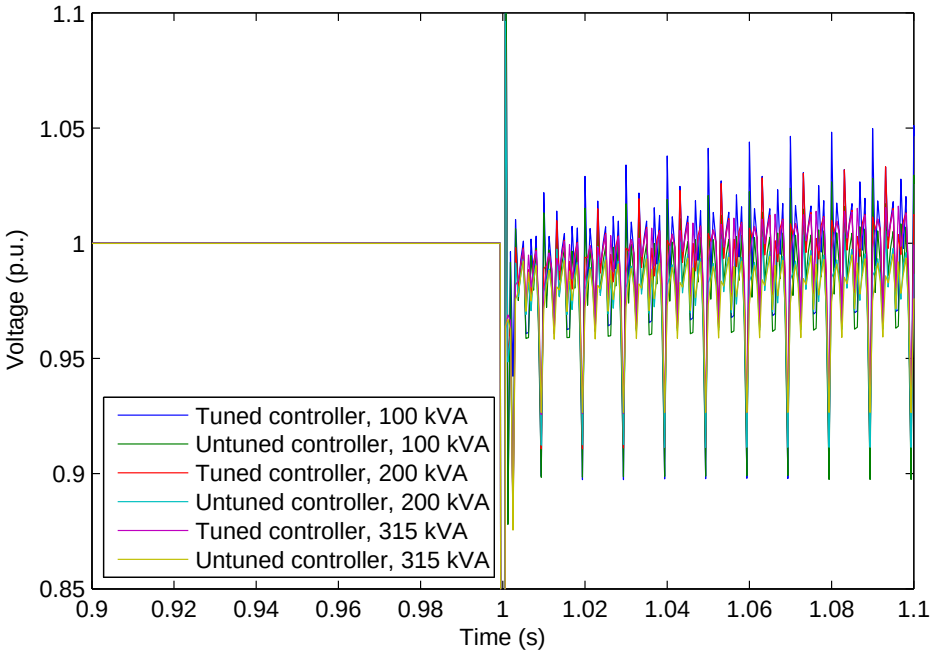

Figure 5.37: As previous figure, but zoomed on the transient.

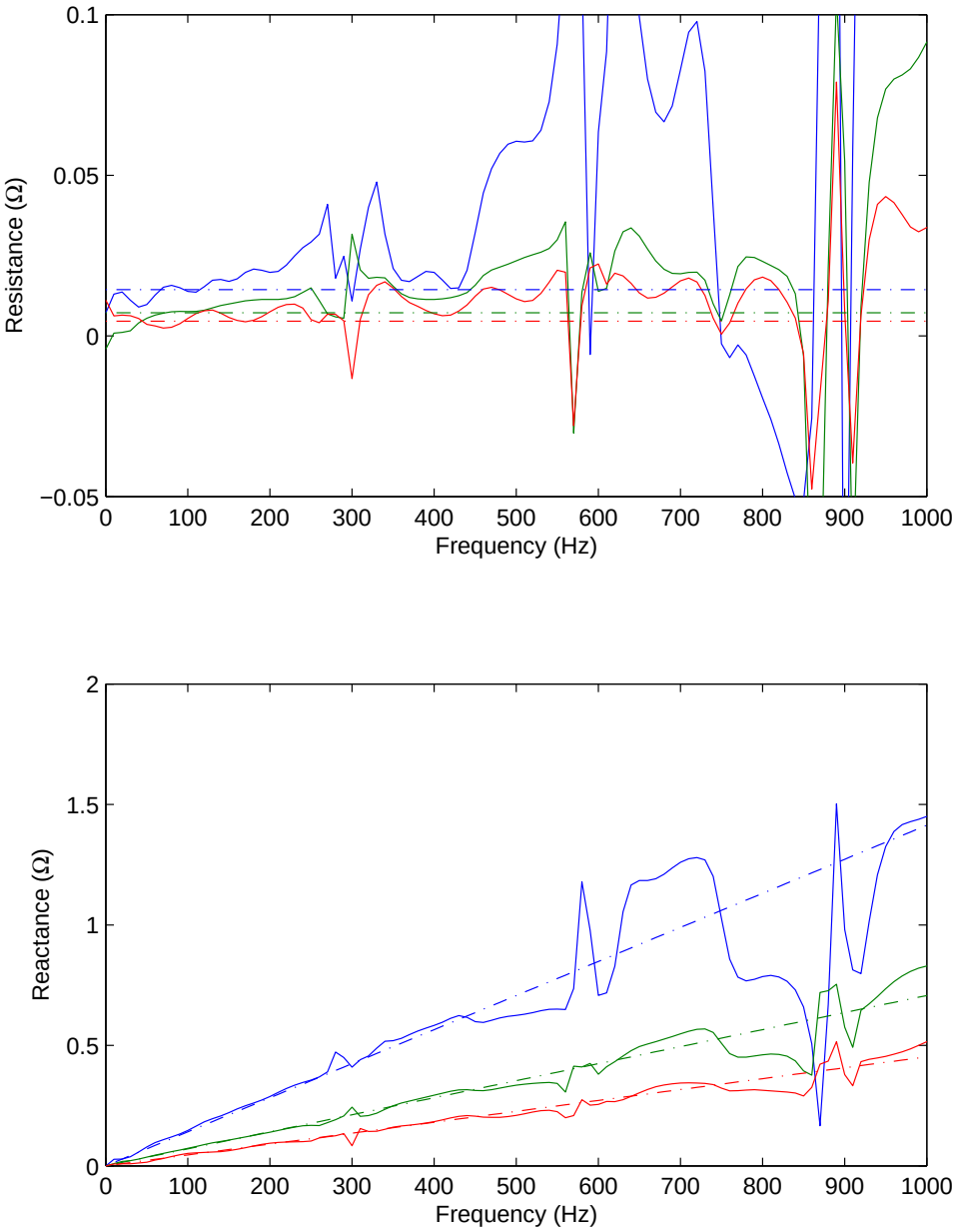

Figure 5.38: Estimation of the system reactance when the capacitively smoothed rectifier is installed at the PCC.

System	Ideal (Ω)	Estimated (Ω)
100 kVA	0.0785	0.0728
200 kVA	0.0393	0.0367
315 kVA	0.0251	0.0234

Table 5.9: Fundamental reactance estimates using extrapolation from 80 Hz and 120 Hz data when an inductively smoothed rectifier is present at the PCC.

System	Ideal (Ω)	Estimated (Ω)
100 kVA	0.0785	0.0756
200 kVA	0.0393	0.0367
315 kVA	0.0251	0.0237

Table 5.10: Fundamental reactance estimates using extrapolation from 80 Hz and 120 Hz data when a capacitively smoothed rectifier is present at the PCC.

continues to regulate the system voltage and the tuned controllers appear to have the expected dynamics, with the voltage returning to 1 p.u. after 0.2 s.

In the case of the inductively smoothed rectifier, the impedance estimation results appear to be largely unaffected by the presence of the non-linear load and the reactance may still be adequately identified. In the case of the capacitively smoothed rectifier, particularly for the 100 kVA system, the impedance estimation results are affected, particularly at the high frequencies. This is because the response of the rectifier when excited by the current injection is highly non-linear and contains a wide range of frequencies which causes difficulty in identifying the impedance. However, it is still possible to adequately identify the reactance at the fundamental since at low frequencies the supply impedance is small and therefore more significant than the effect of the rectifier load.

5.4.4 Supply harmonics

Harmonics may already be present on the supply, causing distorted voltage waveforms at the PCC. Like supply unbalance, under normal conditions, supply harmonics should be limited. As with the unbalanced supply case, the limits given in BS EN 50160 have been used to determine suitable levels of harmonic distortion in simulation. Supply harmonics were considered by adding additional voltage sources in series with the supply voltages. For each phase 5^{th} and 7^{th} harmonic voltage sources were added. The 5^{th} harmonic voltage was set at 5 % of the fundamental voltage while the 7^{th} harmonic voltage was set at 2 % of the fundamental. Transient voltage responses for each of the systems are shown in Figure 5.39 and Figure 5.40. Figure 5.41 shows the effect of supply harmonics on the reactance estimates. Single frequency estimation results are listed in Table 5.11.

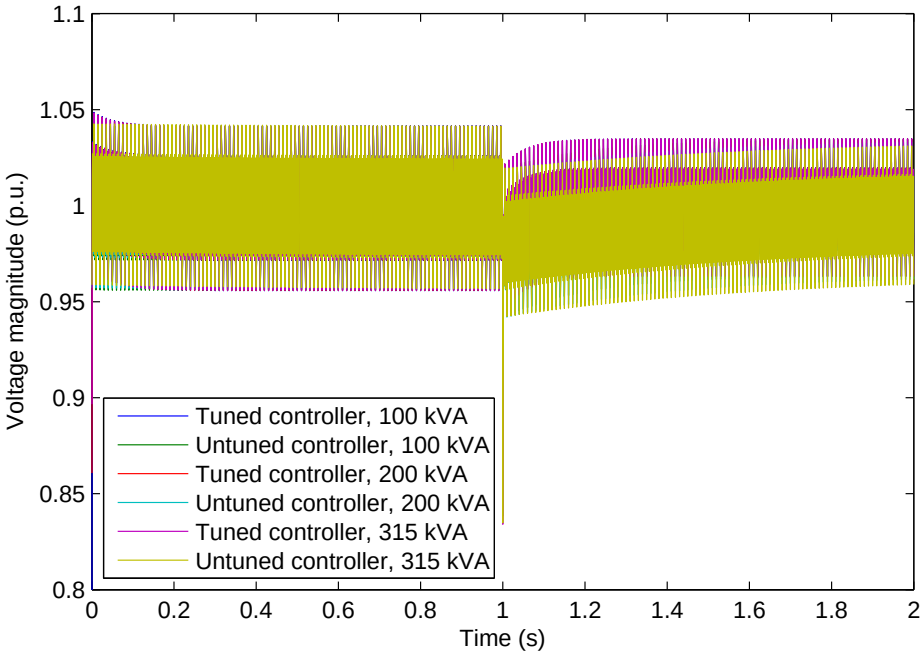

Figure 5.39: Transient voltage response of the STATCOM when harmonic distortion are present on the supply voltages. Both tuned and untuned controllers are considered.

The supply harmonics can be seen to cause considerable distortion to the

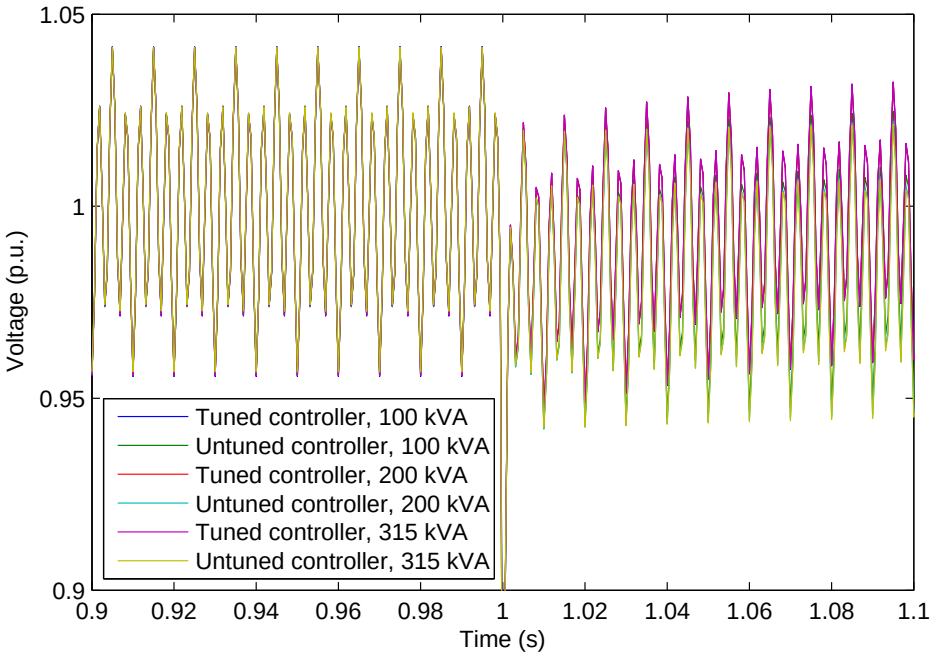

Figure 5.40: As previous figure, but zoomed on the transient.

System	Ideal (Ω)	Estimated (Ω)
100 kVA	0.0785	0.0740
200 kVA	0.0393	0.0372
315 kVA	0.0251	0.0241

Table 5.11: Fundamental reactance estimates using extrapolation from 80 Hz and 120 Hz data when the harmonic distortion is present on the supply.

system voltage, similar to the distortion caused by non-linear loads. Despite this, control of the voltage is still maintained and consistent controller dynamics may still be achieved using the tuned controllers. As expected, the settling time of the tuned controllers is 0.2 s. The impedance estimation results show that the STATCOM continues to be able to identify the system reactance when harmonic distortion is present on the supply. The largest errors appear at 300 Hz, 600 Hz and 900 Hz. As was explained in Chapter 4, this is because of partial cancellation of the three injections at these frequencies resulting in high estimation errors at these frequencies, and although

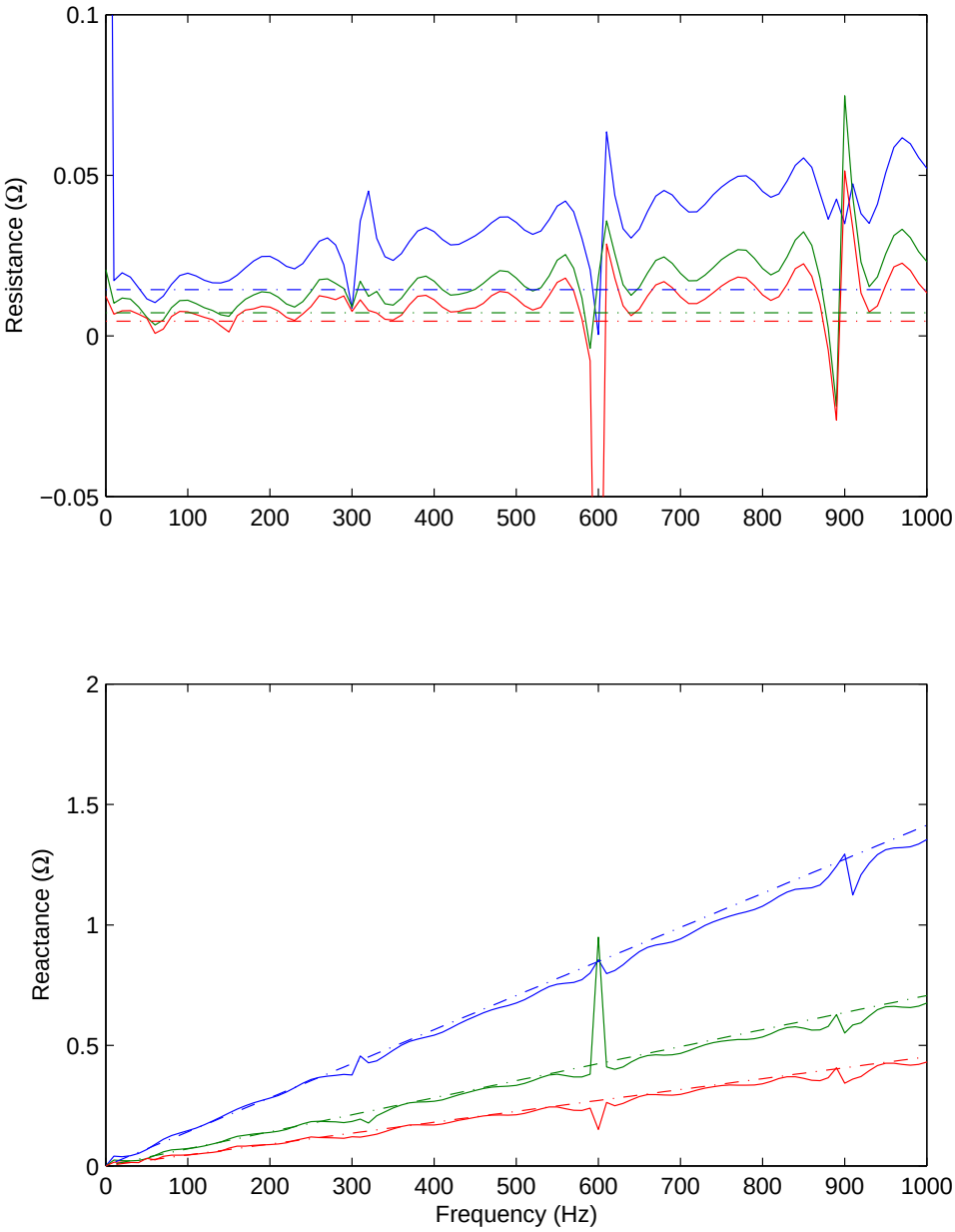

Figure 5.41: Estimation of the system reactance when supply harmonics are considered.

most clearly visible in these results, the phenomenon is not unique to this scenario.

5.5 Summary

In this chapter, a series of simulated studies have been used to explore the behaviour of a STATCOM using the proposed impedance identification method to tune the voltage controller. Initially it was shown that the reactance may be estimated for a simple linear system having only a single supply and that the information may then be used to achieve consistent controller dynamics regardless of system source impedance. Additional simulation was used to show that this is also the case when power factor correction capacitors are present at the PCC.

Simulations were also performed to examine the effect of DERs on both the STATCOM control and the impedance estimation algorithm. The ability of the STATCOM to regulate system voltage was unaffected by the presence of the additional supplies and the impedance estimation algorithm was able to continue estimating the fundamental reactance with sufficient accuracy.

Unbalanced loads and unbalanced supply voltages were considered. It was seen that the effect of unbalance on the performance of the STATCOM voltage support was minimal and that the quality of the impedance estimation did not suffer as a result of unbalance from either loads or the supply.

Finally the effect of non-linear loads and harmonic distortion of the supply voltages was considered. Results from these simulations suggest that problems could arise if the STATCOM is operated in the presence of certain types of non-linear load; the quality of impedance estimation results was affected by nearby capacitively smoothed rectifiers, although it does appear that the fundamental reactance may still be adequately identified.

In the next chapter, experimental tests are used to verify the STATCOM con-

trol scheme and demonstrate the practical implementation of a real-time tuning controller.

Chapter 6

Experimental evaluation

Simulated studies were described in the previous chapter to show the behaviour of the proposed STATCOM controller and the performance of the impedance estimation algorithm over a wide range of conditions. This chapter presents the experimental work that has been performed to demonstrate the proposed STATCOM control strategy and the on-line impedance estimation algorithm. This chapter consists of four subsequent sections; first, the experimental set-up is described and the design and purpose of the experimental tests is explained; second, a series of tests performed to evaluate the STATCOM performance on a single-source system are described and results are presented; third, the effect of including additional supplies is considered; the significance of the results presented to this work is then discussed. This chapter is specifically intended to validate the simulation work presented in the previous chapter. A direct comparison between experimental

and simulated results is therefore made.

6.1 Description of the experimental set-up

A laboratory-based power system, similar to the simulated system described in Chapter 5, has been designed and constructed. The design of the experimental power system is intended to be similar to the power system used for simulations in the previous chapter so that direct comparisons may be made between experimental and simulation results. The experimental power system is built around a laboratory based microgrid at the University of Nottingham [118] with the STATCOM implemented using a 90 kVA Triphase power converter. The experimental power system consists of a variable impedance supply connected to a main feeder which links five cabinets, each consisting of the switchgear and protection required to control the loads connected to that cabinet. The system is illustrated as a one-line diagram in Figure 6.1.

The system is powered from a set of busbars in the laboratory, fed from a 1000 kVA transformer, although the actual power available is limited to approximately 300 kVA. A second set of busbars are coupled to the first set through the variable impedance supply part of the experimental set-up, which consists of a set of three air-cored inductors with taps at 250 μH, 500 μH, 750 μH and 1 mH. A 100 A circuit breaker protects the supply, limiting the maximum power to approximately 70 kVA. The main feeder, which is sourced from the second set of busbars, consists of five-core steel wire armoured (SWA) cable with a conductor cross-sectional area of 16 mm^2. Using an impedance analyser [119], the cable inductance was found to be 0.8 μHm^{-1} and the resistance 2.3 mΩm^{-1}. The distance between each of the cabinets connected to the feeder is 10 m. Each of the cabinets is able to supply two loads, which may be controlled using the installed contactors. Resistor banks of various ratings were used as loads. For each of the experimental tests described in this chapter a multimeter was used to take voltage

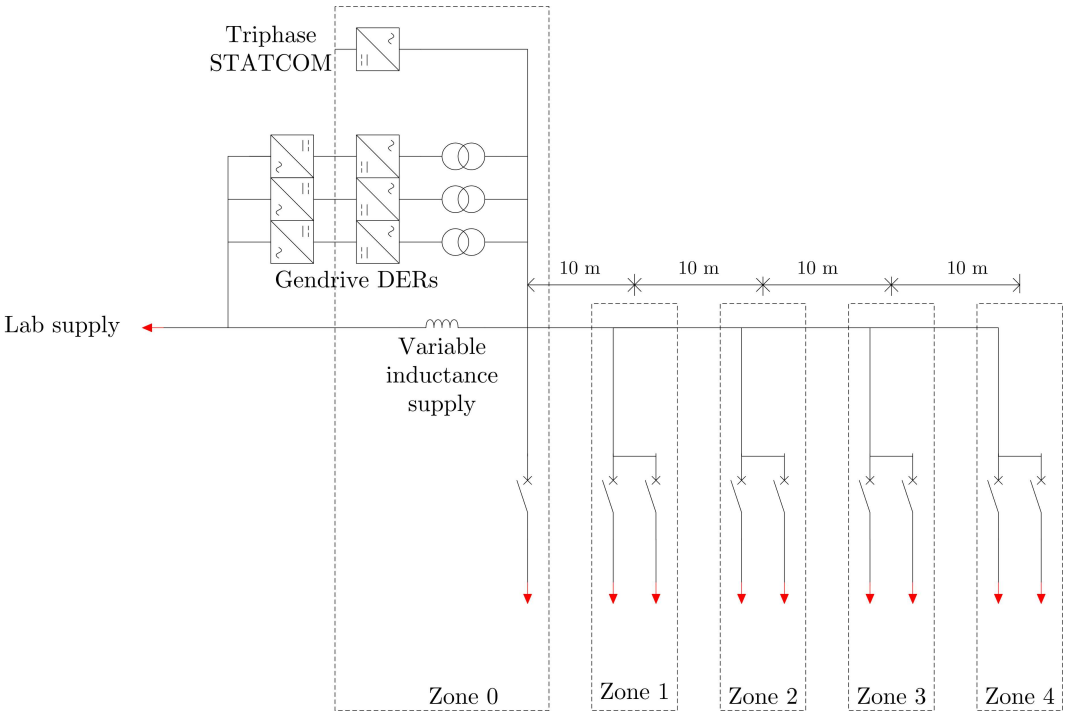

Figure 6.1: A single line diagram representing the experimental system in the laboratory.

measurements at the PCC, Zone 2 and Zone 4 and these were recorded manually. Table 6.1 lists the loads attached to each zone of the system. Figure 6.2 is a photograph showing the various elements of the experimental system.

Zone	Real power, P	Reactive power, Q
0	17.1 kW	5.97 kVAr
1	9.5 kW	0.8 kVAr
2	9.6 kW	0.17 kVAr
3	9.6 kW	0.17 kVAr
4	7.7 kW	80 VAr
	53.5 kW	7.22 kVAr

Table 6.1: Loading of the experimental power system.

The Triphase power converter used to implement the STATCOM is a 90 kVA power converter. The converter is controlled by a dedicated real-time PC and user interaction is provided through a second PC. The converter is programmed from within MATLAB using a dedicated Simulink toolbox, run-

ning on the user PC. The toolbox includes optimised DC-link voltage and AC current controllers, which meant that only the AC voltage controller and the AIE algorithm needed to be implemented to make use of the converter as a STATCOM. The current control loop included with the Triphase toolbox is high-bandwidth and non-linear. A simplified diagram of the power electronics for the Triphase power converter when configured as a STATCOM is shown in Figure 6.3 and the control hardware is shown in Figure 6.4.

Figure 6.2: Photographs of the experimental system showing the Triphase power converter (left), the Gendrive power converters (top right) and the zone switchgear cabinets (bottom right).

The laboratory infrastructure also includes three Gendrive Totus power converters [120], originally designed for use with wind turbines, but used to emulate generic sources of distributed generation for this work. Each of these power converters is capable of supplying up to 10 kVA. For the purposes of this work, the converters were restricted to supplying only real power and were limited to a total of 20 kW, or approximately 6.7 kW each, to prevent nuisance tripping of the MCBs protecting the converters, which was found to be a problem at higher power levels. The converters are connected

to the grid and to the experimental power system. Three 10 kVA transformers are installed between the converters and the experimental power system to provide galvanic isolation, which is required because they share a common supply. The Gendrive converters are connected to a control PC in the laboratory which provides the required power demands. The power supplied by the Gendrive converters is sourced from the supply busbars. Due to the physical arrangement of the laboratory it is only possible to connect the Triphase and Gendrive converters at the PCC of the experimental system.

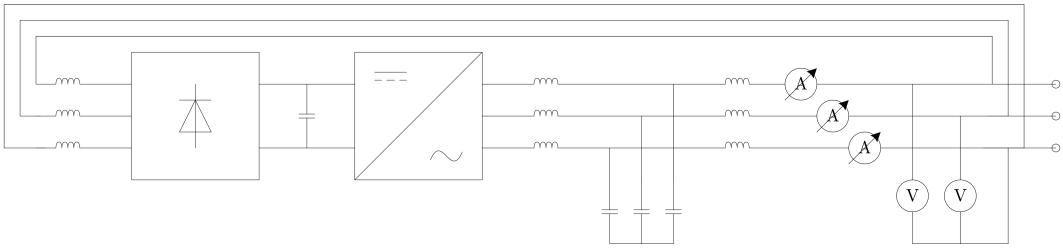

Figure 6.3: Simplified circuit diagram of the Triphase power converter.

6.2 Testing of a linear system

Similar to the simulation studies presented in the previous chapter, initial experimental testing was performed on a linear system with only a single power source. Evaluation of the basic STATCOM control was performed by applying a step change in load and comparing the response of a STATCOM which has been tuned to the system impedance with one which has not. Tuning is performed by adjusting the variable gain of the AC voltage controller based on the impedance estimated using the transient injection method. For all of the untuned controller tests presented in this chapter, the variable controller gain was set to 1. This is equivalent to the STATCOM being tuned to a 3.2 mH supply. The fixed gain is set to 20, as was the case with the simulation tests, which gives an expected controller time constant of 0.05 s.

The voltages measured at various points along the line for each of the sup-

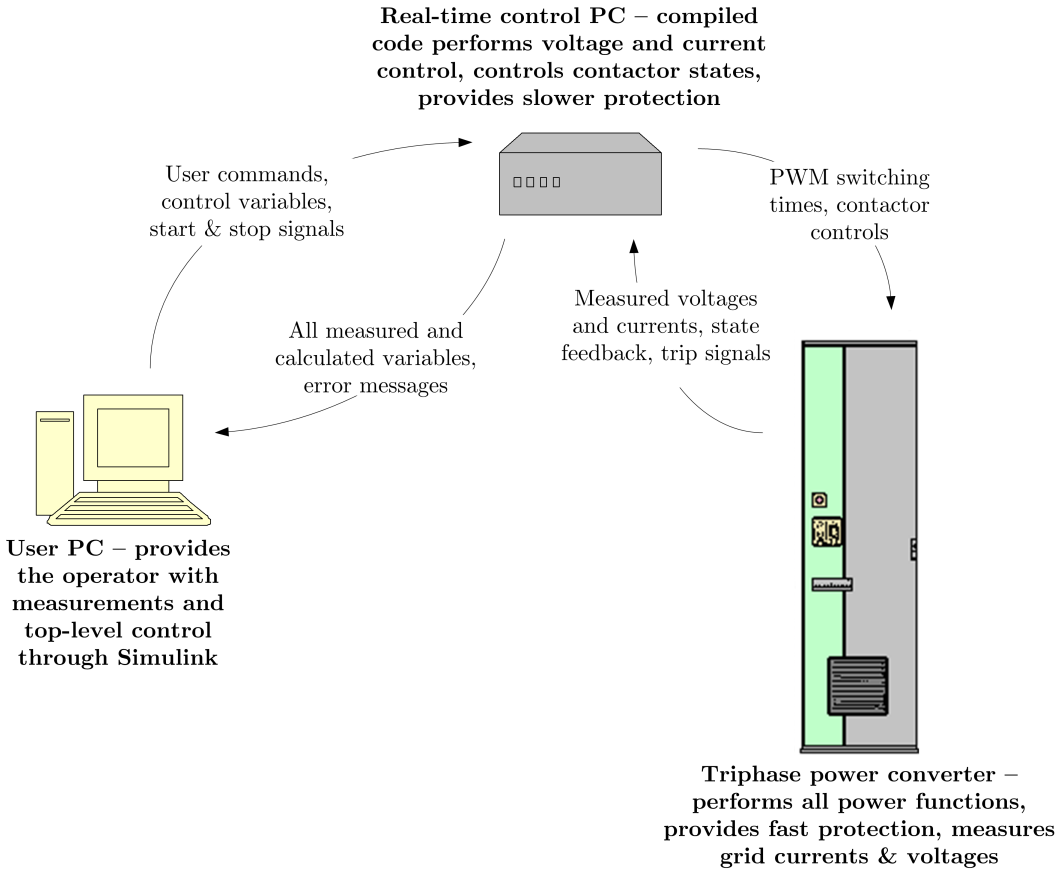

Figure 6.4: A top-level illustration of the control set-up for the Triphase power converter.

ply impedances while the system is operating at full load, both with and without the STATCOM, are shown in Figure 6.5. The response of each system to a step-change in load from no load to full load for each of the systems is shown in Figures 6.6–6.9. Impedance estimates calculated by the STATCOM tuning algorithm are listed in Table 6.2; wideband impedance estimates are shown in Figure 6.10.

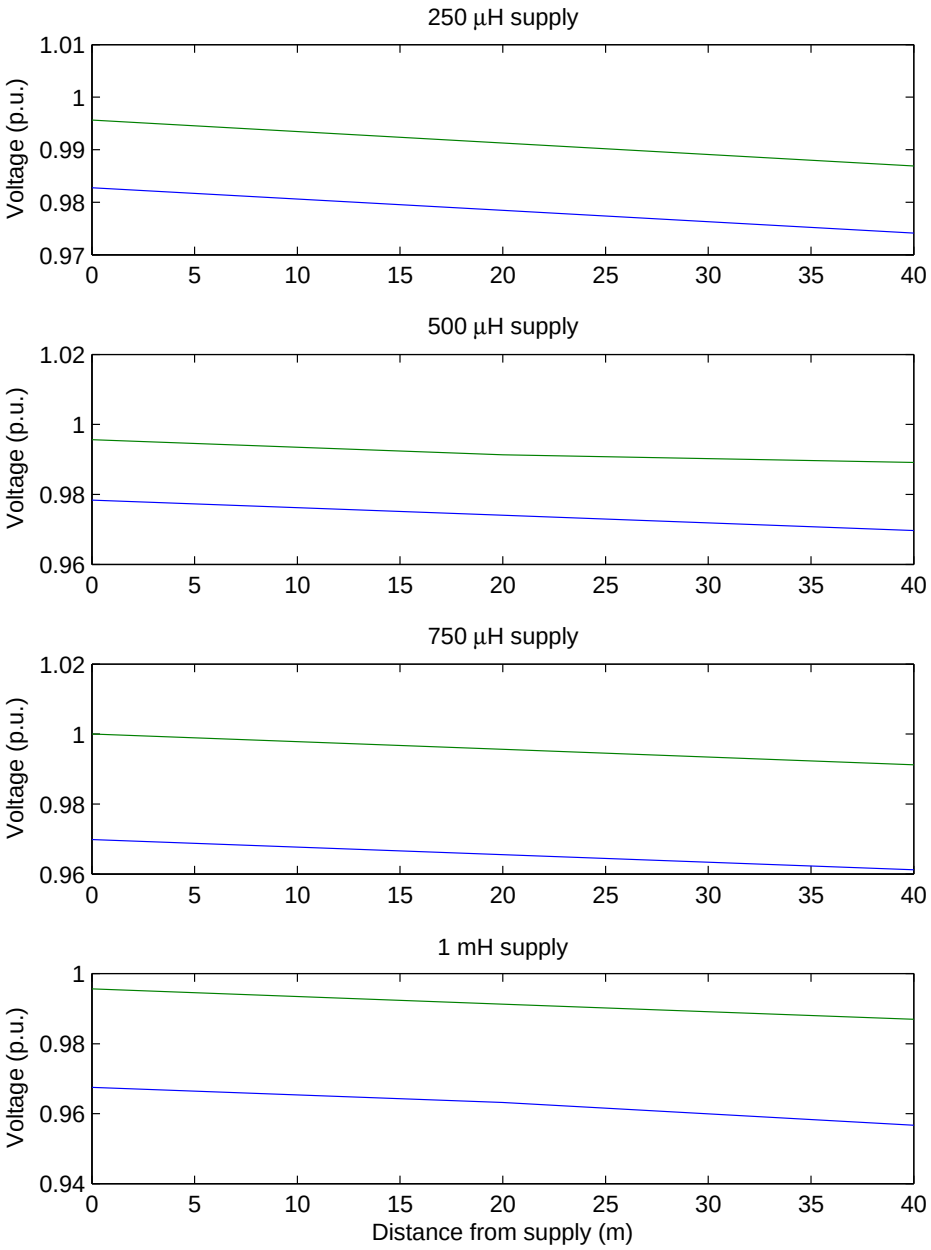

Figure 6.5: Voltage levels at different points along the line for each of the supply impedances. Voltages are shown for the system without STATCOM support (blue) and with STATCOM support (green).

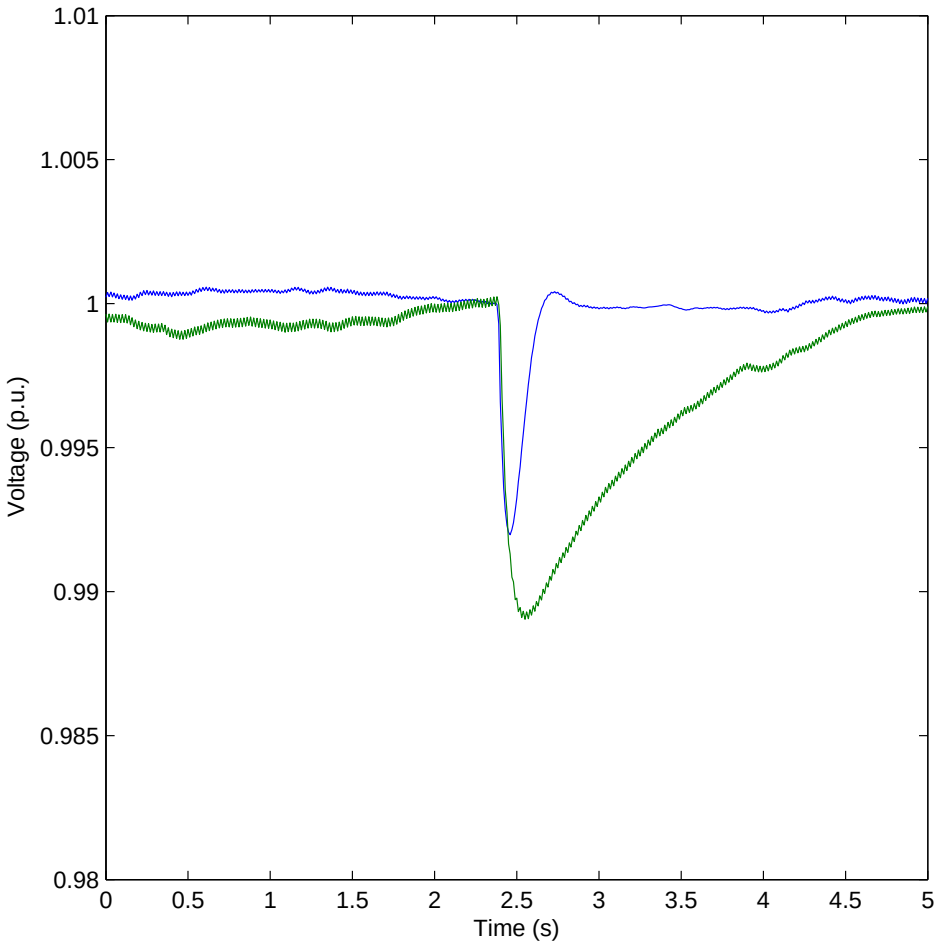

Figure 6.6: Experimental results showing a step change from no load to full load for the 250 μH system, both for an untuned STATCOM (green) and tuned STATCOM (blue).

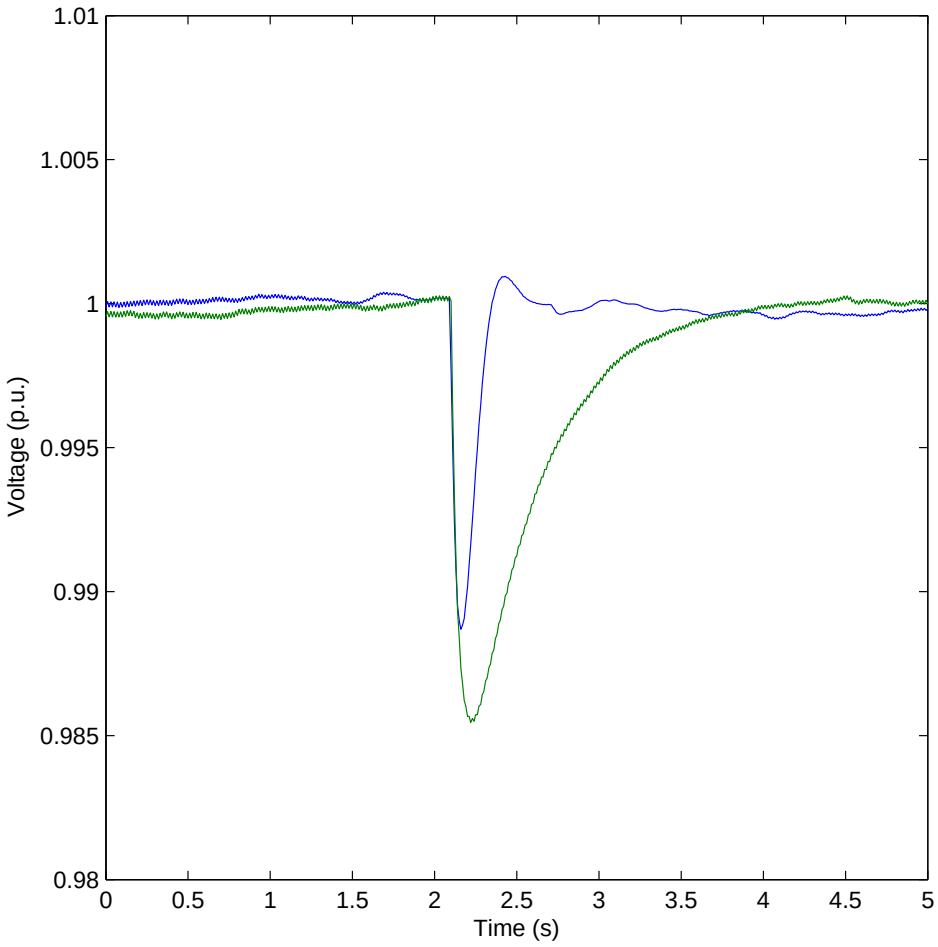

Figure 6.7: Experimental results showing a step change from no load to full load for the 500 μH system, both for an untuned STATCOM (green) and tuned STATCOM (blue).

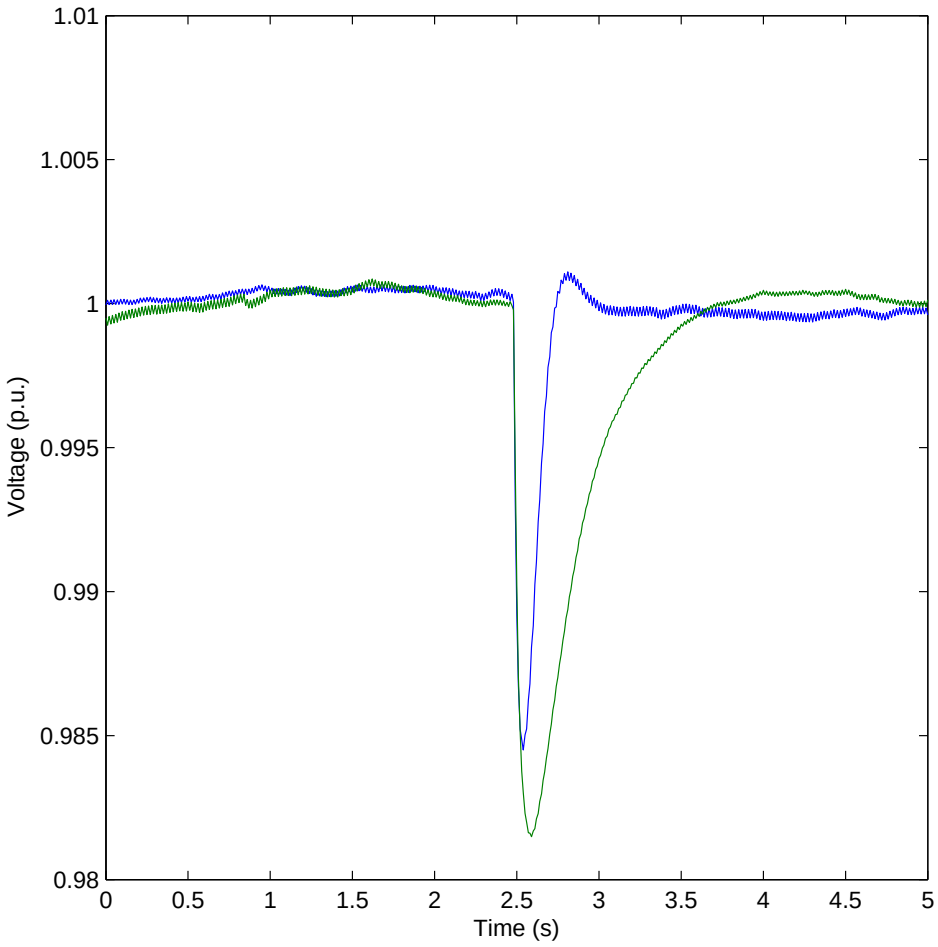

Figure 6.8: Experimental results showing a step change from no load to full load for the 750 μH system, both for an untuned STATCOM (green) and tuned STATCOM (blue).

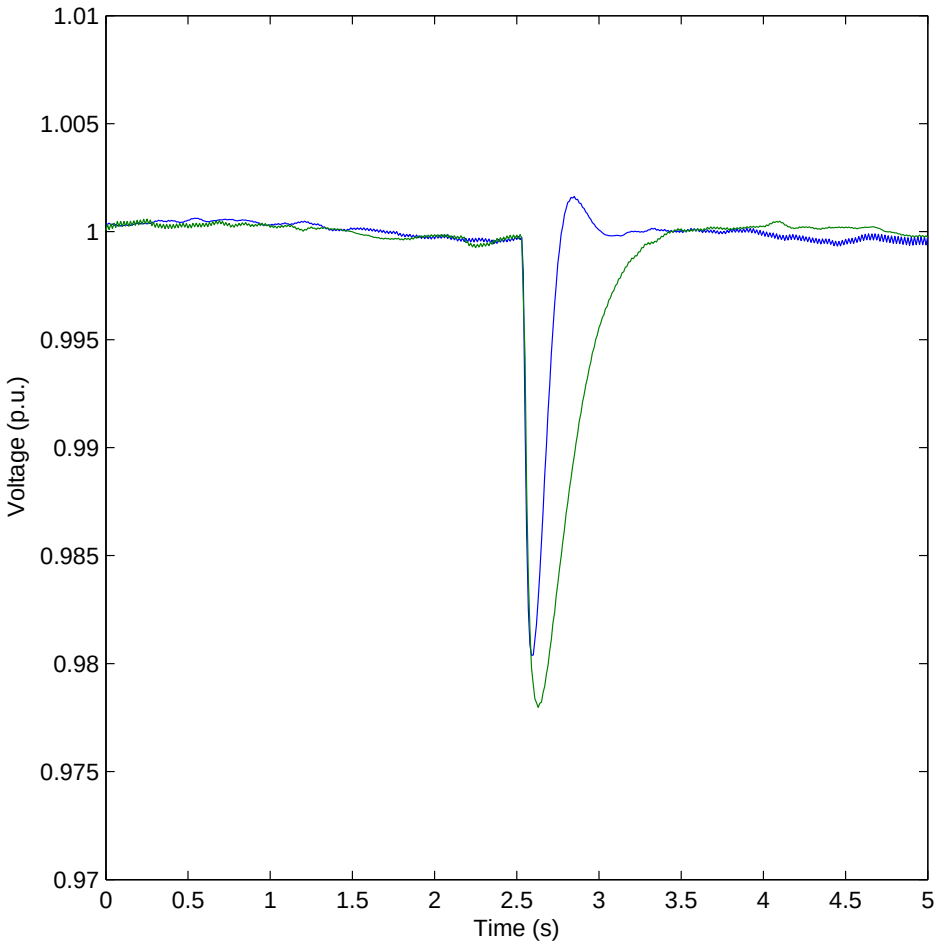

Figure 6.9: Experimental results showing a step change from no load to full load for the 1 mH system, both for an untuned STATCOM (green) and tuned STATCOM (blue).

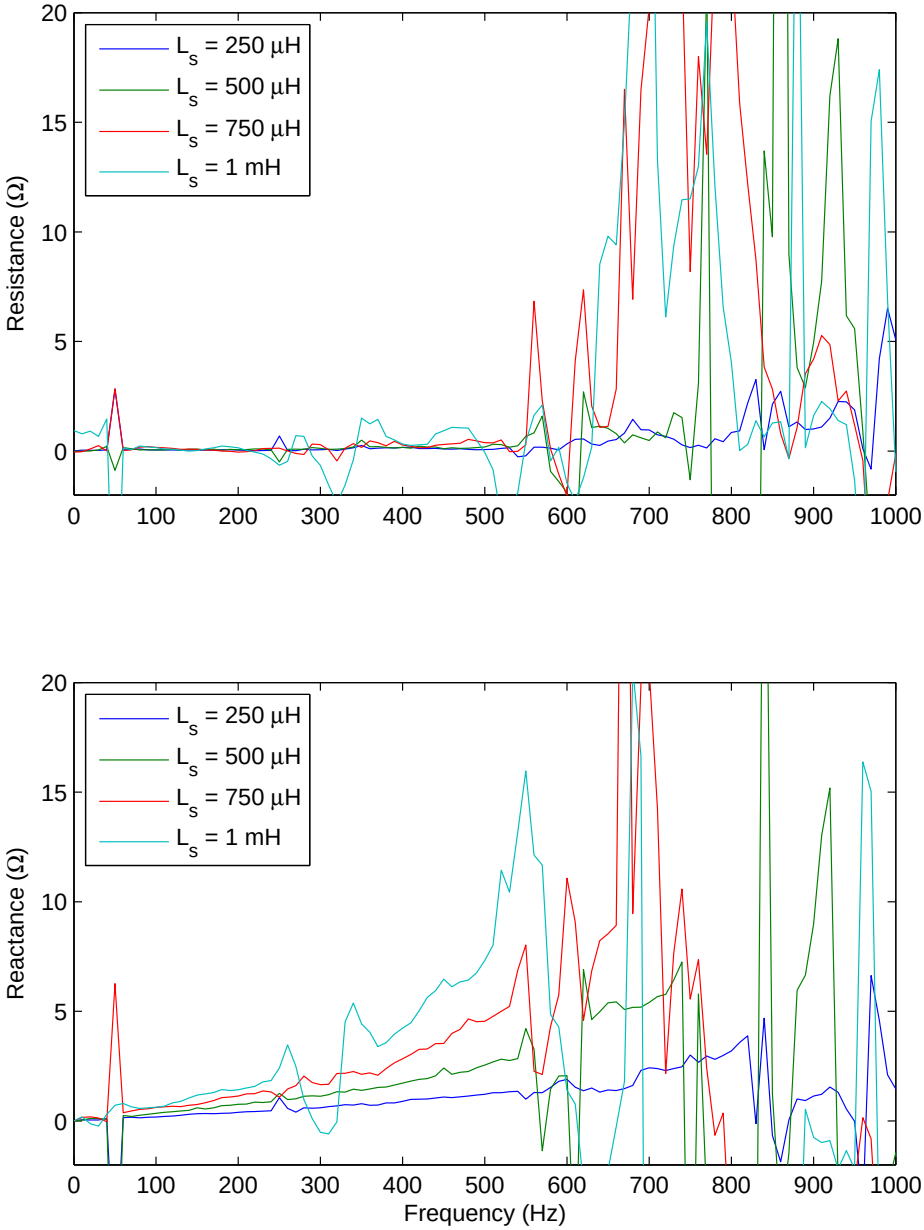

Figure 6.10: Impedance estimates for each of the four supply inductances.

Supply, L_s	Resistance, R	Reactance, X	Inductance, L
250 μH	0.020Ω	0.087Ω	277μH
500 μH	0.035Ω	0.155Ω	494μH
750 μH	0.047Ω	0.248Ω	789μH
1 mH	0.039Ω	0.322Ω	1.03mH

Table 6.2: Impedance estimates at the system fundamental frequency calculated by the STATCOM during testing of the linear system.

6.2.1 Discussion of linear results

It can be seen from the steady state voltages shown in Figure 6.5 that the voltage at the PCC is very slightly below 1 p.u. in each case when the STATCOM is connected. The discrepancy is less than 1 % and therefore may be considered small, but is still worth briefly considering. There are two possible explanations for this and both are likely to contribute to the discrepancy. First, it should be noted that the STATCOM terminals and the PCC are necessarily separated by a length of cable and therefore not necessarily at the same voltage. Second, there is likely a difference in calibration between the voltage transducers installed in the STATCOM and the multimeter used for voltage measurement at the PCC.

Considering the steady-state voltages for the systems with and without STATCOM support it can be seen that the majority of the voltage drop is caused by the load connected to the PCC. This is to be expected as the PCC load contributes almost one third of the total system load and over 80 % of the reactive power load. The difference in voltage drop between the two ends of the line is distributed almost linearly along the remaining length of the line. This was not expected as the total loading on the lengths of cable connecting the first zones is greater than the loading on the last length of cable. In addition, although the reactive power load is small, the cable is mostly resistive, and therefore it should be expected that real power loads and not reactive loads are the main cause of cable voltage drop. However, it is pos-

sible that the differences are too small to be accurately measured using the multimeter used. It is also possible that the limited number of measurement points used is insufficient to obtain an accurate voltage profile for the line.

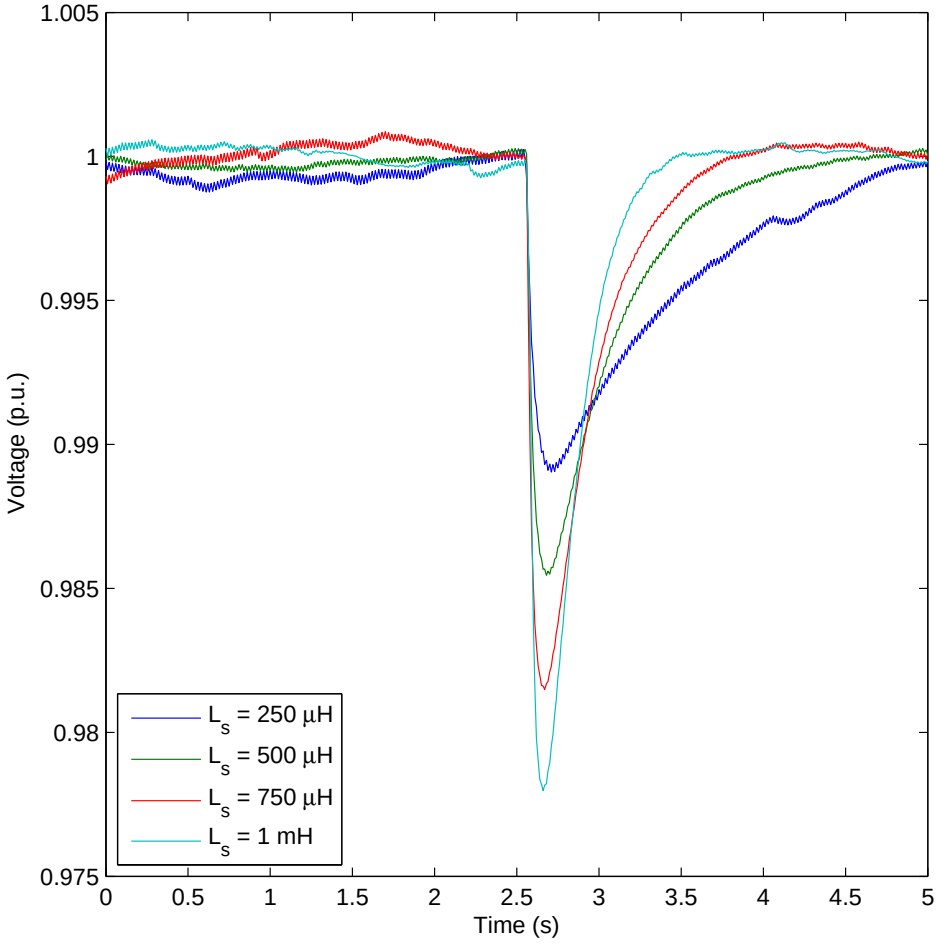

Figure 6.11: The untuned controller response to a step change in load.

The transient performance of the STATCOM AC voltage controllers is considered next. It can be seen that the response of the untuned controllers shown in Figures 6.6–6.9 varies considerably with varying supply impedance. This is shown more clearly in Figure 6.11, where the untuned response for each supply impedance setting is shown. The fastest response is achieved by the STATCOM connected to the 1 mH supply, which takes 0.8 s to return the voltage to 1 p.u. The slowest response is seen from the

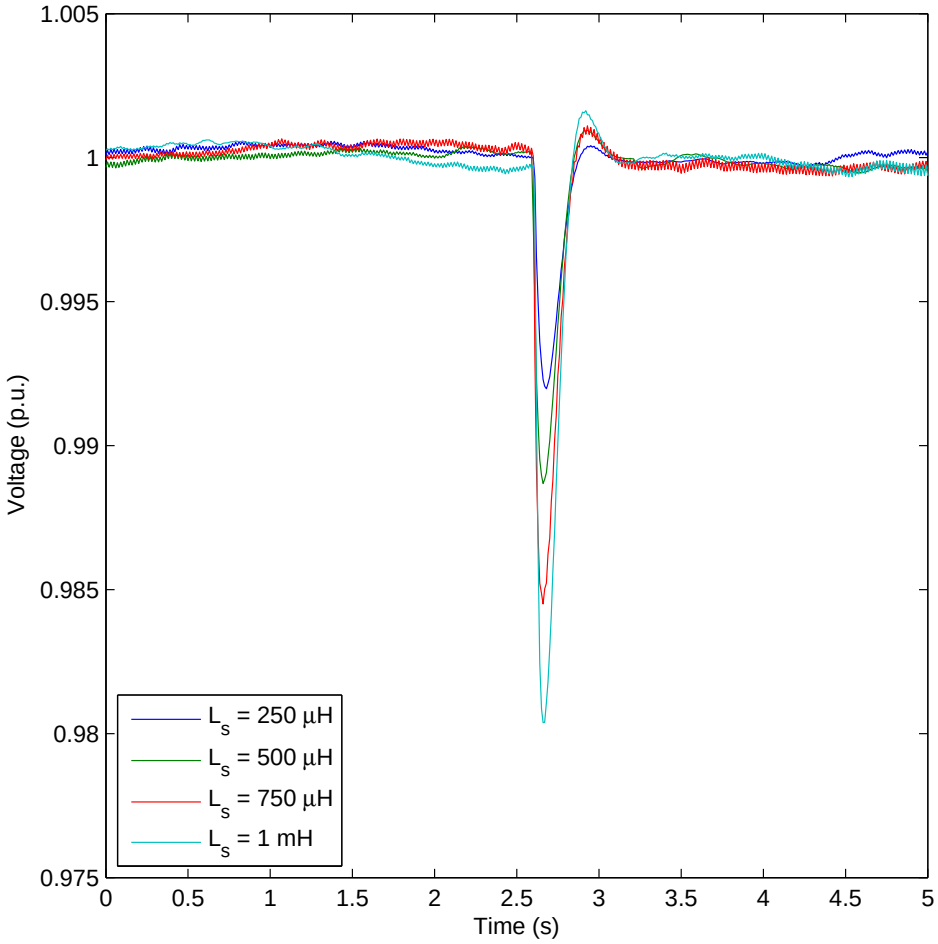

Figure 6.12: The tuned controller response to a step change in load.

STATCOM connected to the 250 μH supply, which reaches steady-state after about 2.5 S. The STATCOMs connected to the 500 μH and 750 μH supplies return the voltage to 1 p.u. after approximately 1.5 s and 2 s respectively. The step response of the tuned controllers can be seen in Figure 6.12. It can clearly be seen that the response of the tuned controllers to the step change in load is consistent regardless of supply setting. One unexpected feature of the tuned controller response is the overshoot which can clearly be seen. This will be discussed in more detail when comparisons are made between experimental and simulated results. The rise-time of the tuned controllers is 0.2 s, which is consistent with the expected controller time constant being 0.05 s, although the total settling time, which also includes recovery from the overshoot, is about 0.5 s.

6.2.2 Comparison with simulation results

In the previous section the performance of the STATCOM voltage controller was assessed by considering only the experimental results. In this section, the transient performance of the STATCOM controller will be compared with simulation results for a similar system. This comparison is intended to validate the simulation results presented in the previous chapter.

Figure 6.13 shows a comparison between the experimental results for the tuned response to a step change in load for the 250 μH supply inductance and the response seen when the same system is simulated. It can immediately be seen that the two responses are similar, although there are two notable differences which are discussed below.

It can be seen that the simulated results show a far larger initial drop in voltage. This is a consequence of the different filtering and sampling methods used as part of the data acquisition system. The experimental results are recorded from the value calculated by the Triphase for control purposes after filtering. This value is passed through a low-pass filter with a cut-off frequency of 20 Hz and the recorded value is sampled at 100 Hz. The lower

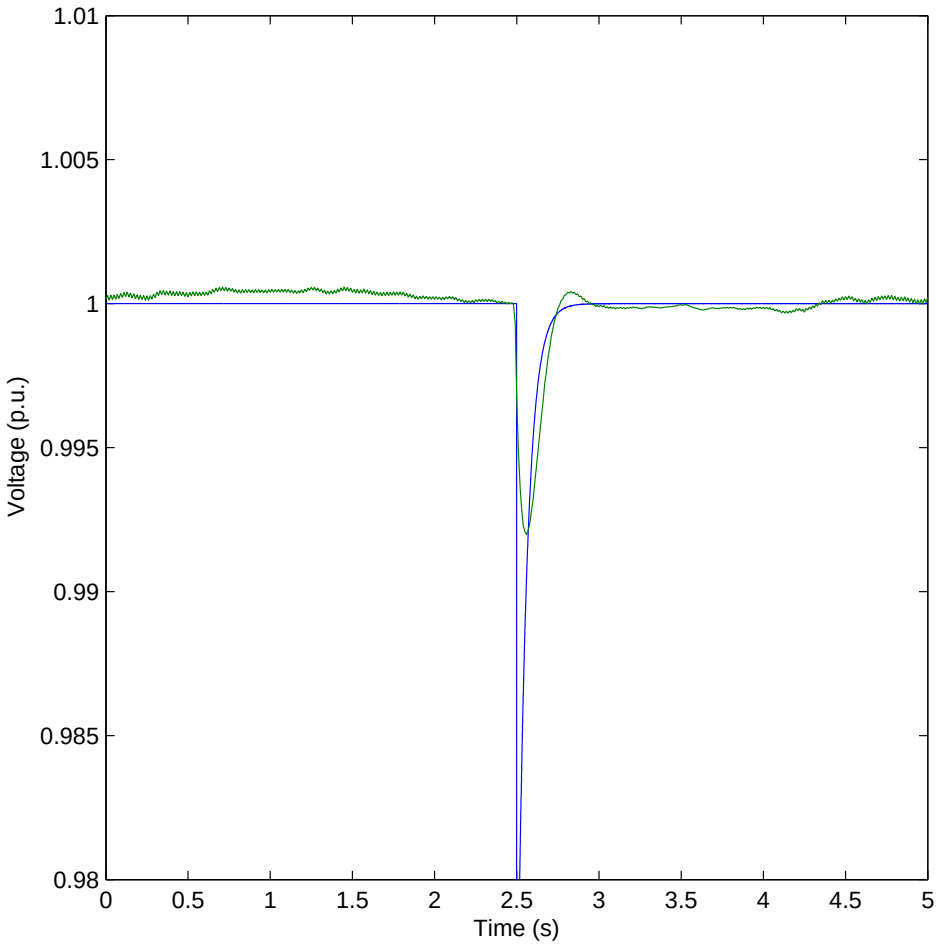

Figure 6.13: Comparison of the experimental (green) and simulated (blue) responses of controller for the system with a 250 μH supply inductance.

filter cut-off frequency for the experimental system was required as it was found that when the original filter cut-off frequency of 50 Hz was used the high-frequency content which is clearly present on the captured voltages made the results unusable. The lower cut-off frequency of the filter used on the Triphase results in the voltage control loop having a second order response overall. The simulated value is also calculated after the simulation has completed, from the three-phase voltages recorded during simulation, which are sampled at 16 kHz. As a result of the higher sampling frequency, it is possible to see the initial voltage drop more clearly in the simulated results.

A small amount of overshoot can be seen on the experimental results that is not present on the simulated results. It is possible that the stricter filtering requirements for the experimental system cause some of this variation; the settling time of the low-pass filter is comparable to the settling time of the control integrator, resulting in a controller with a second order response. It is also possible that the difference in the inner current control loop structure between simulated and practical implementations has some impact on the overall controller dynamics, although given that the difference in bandwidth between the AC voltage controller and the inner current control loop is large and therefore the two controllers should not interact significantly with each other, it is considered unlikely that this is the case.

6.3 Evaluating the effect of DERs

Additional work was carried out on the experimental system with the three Gendrive power converters connected and used to provide real power to the system. In order to comply with regulations governing the connection of distributed generation to the grid [98], the control of the Gendrive converters does not allow step changes in the power output. Therefore a step change in power demand results in the converters ramping the power output up or down to the new set point gradually, rather than attempting to

immediately change the injected power.

The tests performed on the linear system were repeated for the system with DERs included. Initially the system load was limited by only having Zones 3 and 4 connected. In these tests, the three DER converters are supplying the maximum 20 kW of power to the system. Voltages measured in various zones are shown in Figure 6.14. The testing of the effect of the DER power injection when loading is low was repeated with the system at full load. The resultant voltage profile can be seen in Figure 6.15. The response of each of the systems to the change in power injected by the Gendrive converters resulting from a step change in power demand is shown in Figures 6.16–6.18. The DERs all begin supplying power at $t = 2.5$ s. Results for the 250 μH supply inductance have not been included, because the transient is too small to reliably distinguish from background noise in those results. The fundamental impedance estimates for each of the four systems are listed in Table 6.3 and the wideband impedance estimate results are shown in Figure 6.19.

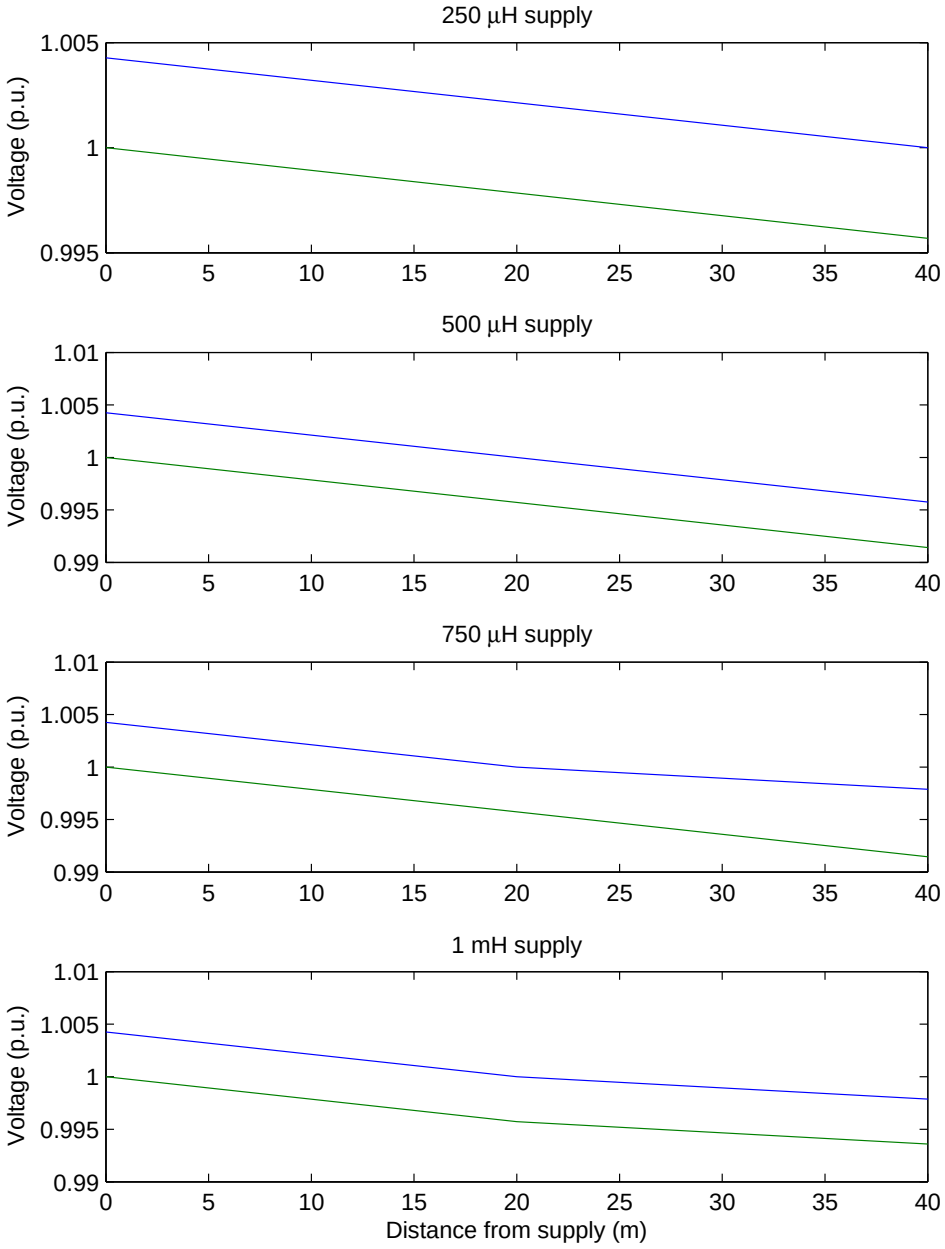

Figure 6.14: Voltage levels at different points along the line for each of the supply impedances when DERs are connected and the system load is low. Voltages are shown for the system without STATCOM support (blue) and with STATCOM support (green).

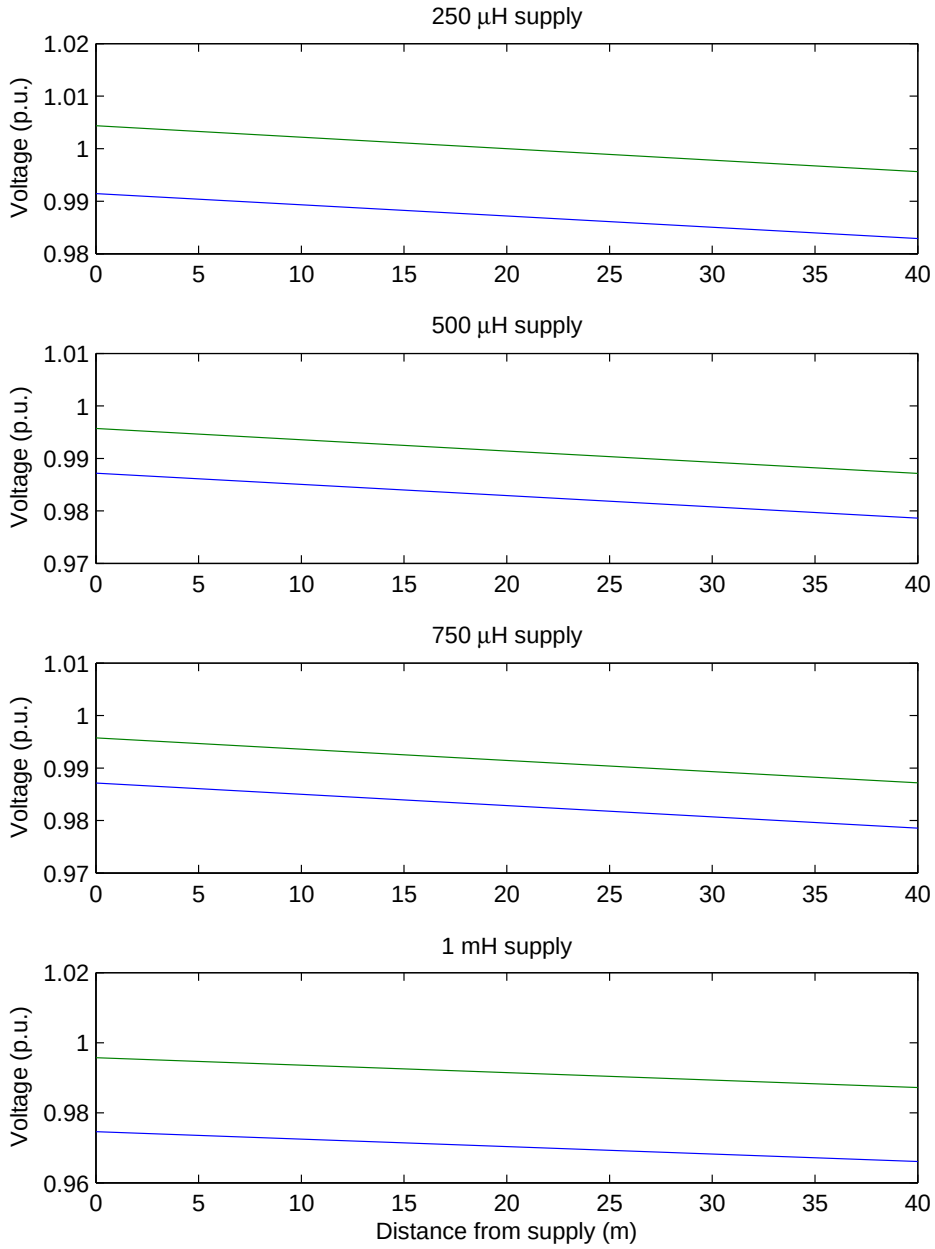

Figure 6.15: Voltage levels at different points along the line for each of the supply impedances when DERs are connected and the system is operating at full load. Voltages are shown for the system without STATCOM support (blue) and with STATCOM support (green).

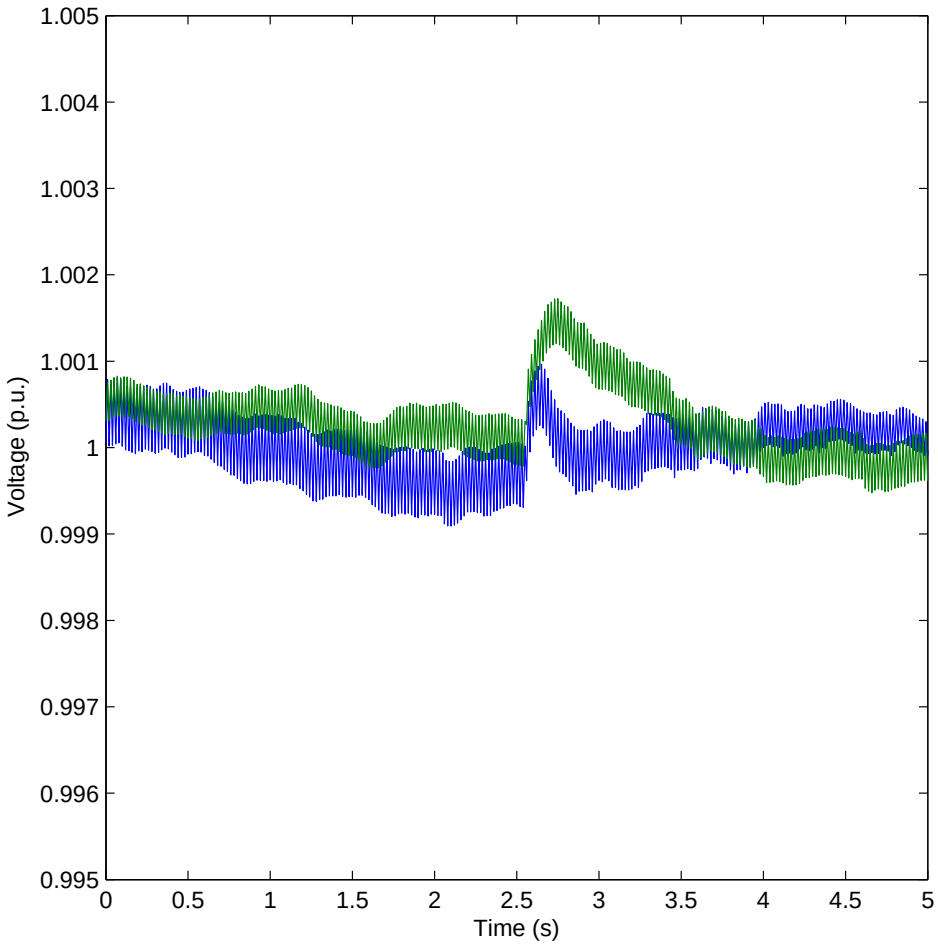

Figure 6.16: Experimental results showing an increase in DER injected power from 0 kW to 20 kW for the 500 μH system, both for an untuned STATCOM (green) and tuned STATCOM (blue).

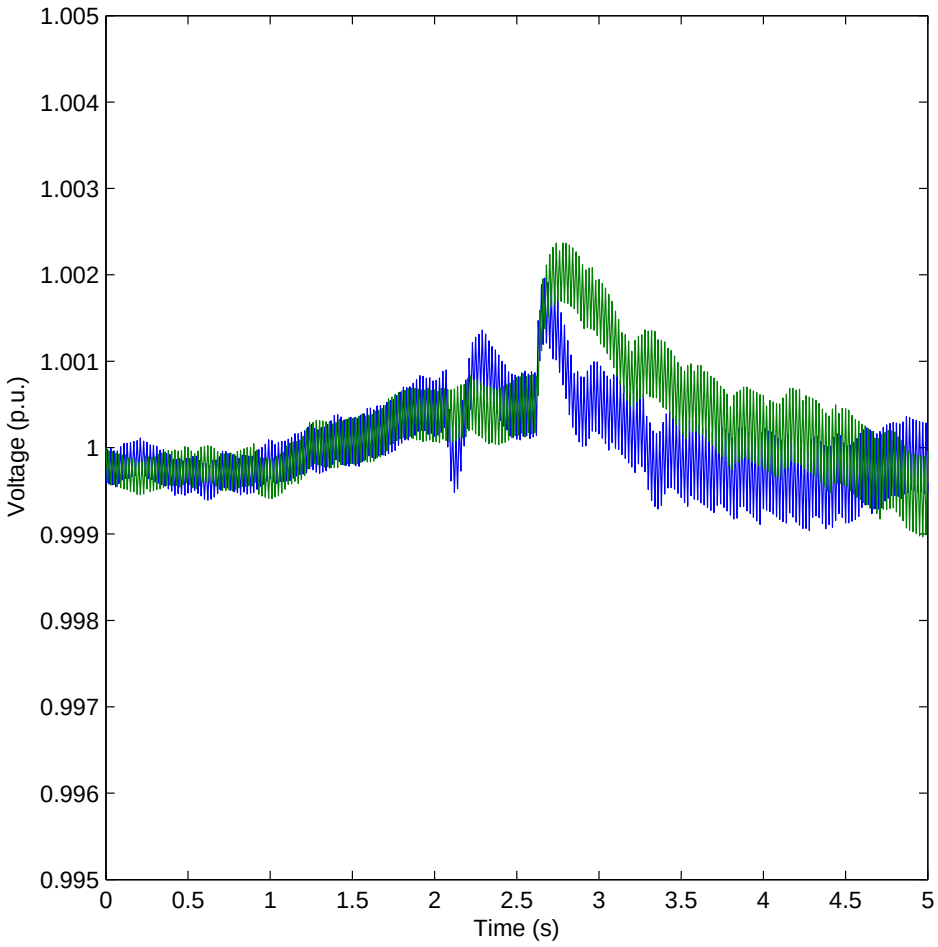

Figure 6.17: Experimental results showing an increase in DER injected power from 0 kW to 20 kW for the 750 μH system, both for an untuned STATCOM (green) and tuned STATCOM (blue).

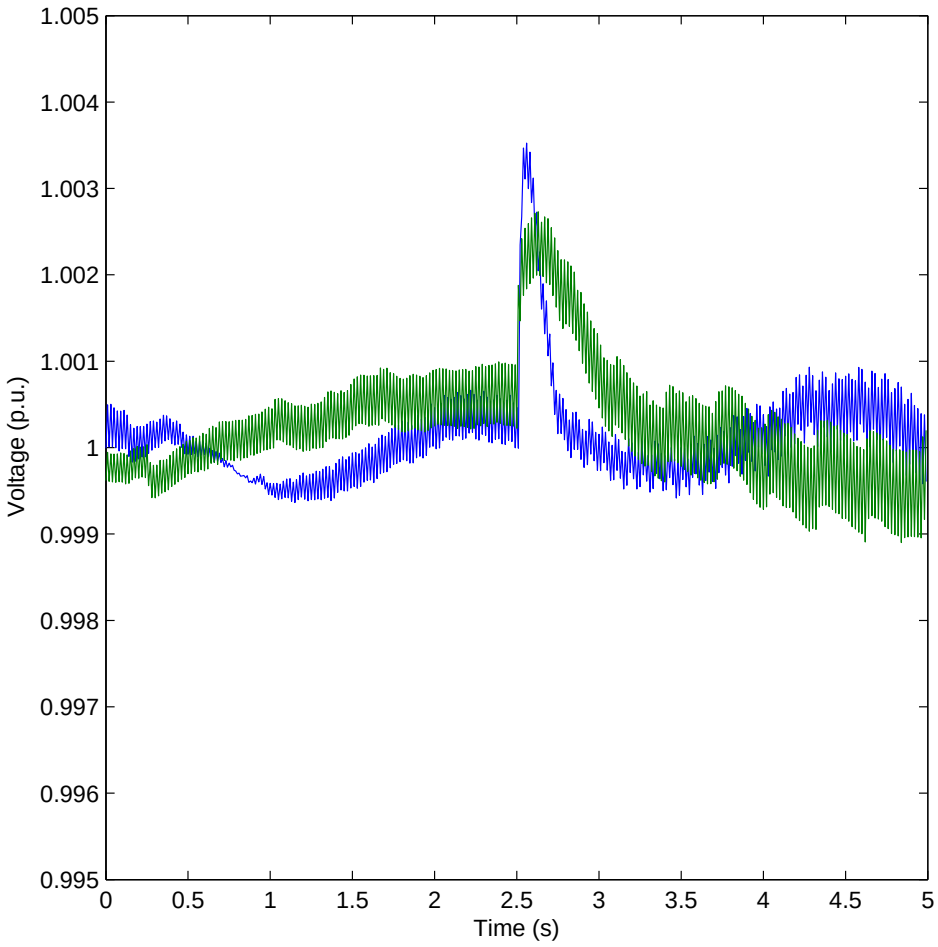

Figure 6.18: Experimental results showing an increase in DER injected power from 0 kW to 20 kW for the 1 mH system, both for an untuned STATCOM (green) and tuned STATCOM (blue).

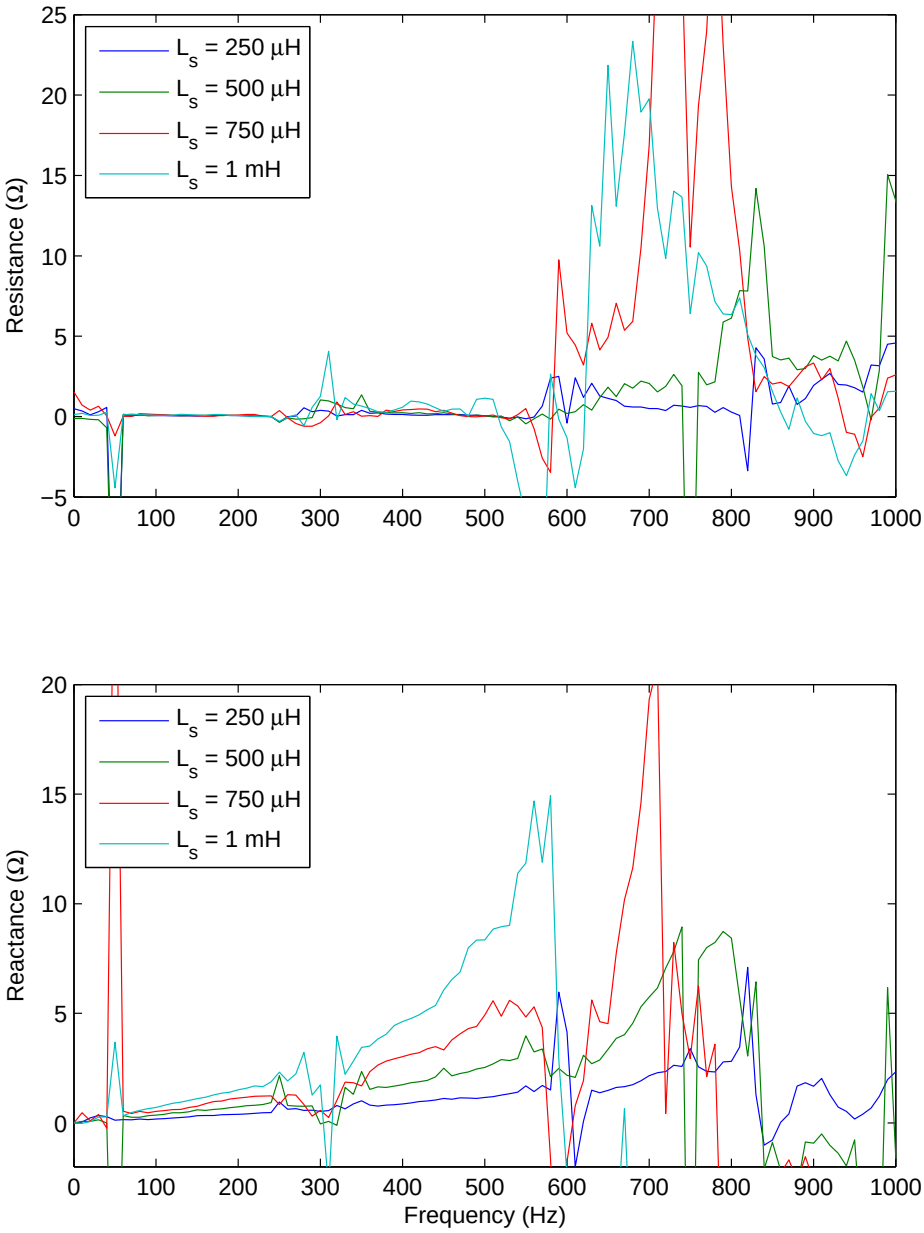

Figure 6.19: Impedance estimates for each of the four supply inductances when DERs are connected to the system.

Supply, L_s	Resistance, R	Reactance, X	Inductance, L
250 μH	0.014Ω	0.078Ω	248μH
500 μH	0.026Ω	0.149Ω	474μH
750 μH	0.038Ω	0.214Ω	682μH
1 mH	0.040Ω	0.296Ω	9.42mH

Table 6.3: Impedance estimates at the system fundamental frequency calculated by the STATCOM during testing of the system with the Gendrive power converters connected.

6.3.1 Discussion of results for the system with DERs

Two scenarios were considered. First, the system loading was light and the DERs were injecting maximum real power. It can be seen that when the STATCOM is not connected in this scenario a small rise in steady-state voltage at the PCC is observed. This is consistent with theory since the rise in voltage was expected to be small as the supply impedance is predominantly reactive for the systems considered. When the system is lightly loaded, the voltage drop along the first half of the line is greater than the voltage drop along the second half of the line for the 750 μH and 1 mH supply settings. This was expected for all voltage profiles, as was mentioned in the discussion of the system without DERs, so it is unclear why this effect is only seen in a limited number of results. A rise in voltage is also seen for each supply impedance when the system at full load with DERs but no STATCOM is compared with the system at full load with no DERs, although overall the voltage falls compared with the no-load case. This was to be expected and the rise in voltage is consistent with the rise observed when the system loading was light. When the STATCOM is connected the steady-state voltage at the PCC is effectively maintained close to 1 p.u. for both the lightly loaded and fully loaded systems, although, as was discussed above, there is a small discrepancy between the measured PCC voltage and the STATCOM voltage demand.

Considering the transient response of the STATCOM AC voltage controller to a change in DER output is slightly complicated by the fact that, as can be seen in Figures 6.16–6.18, the transient is of a comparable magnitude to other disturbances on the system and the noise and switching artefacts present on the measurements. The other disturbances are not caused by any identifiable piece of equipment within the laboratory used for testing. The source of these disturbances must therefore be an external one and cannot be controlled.

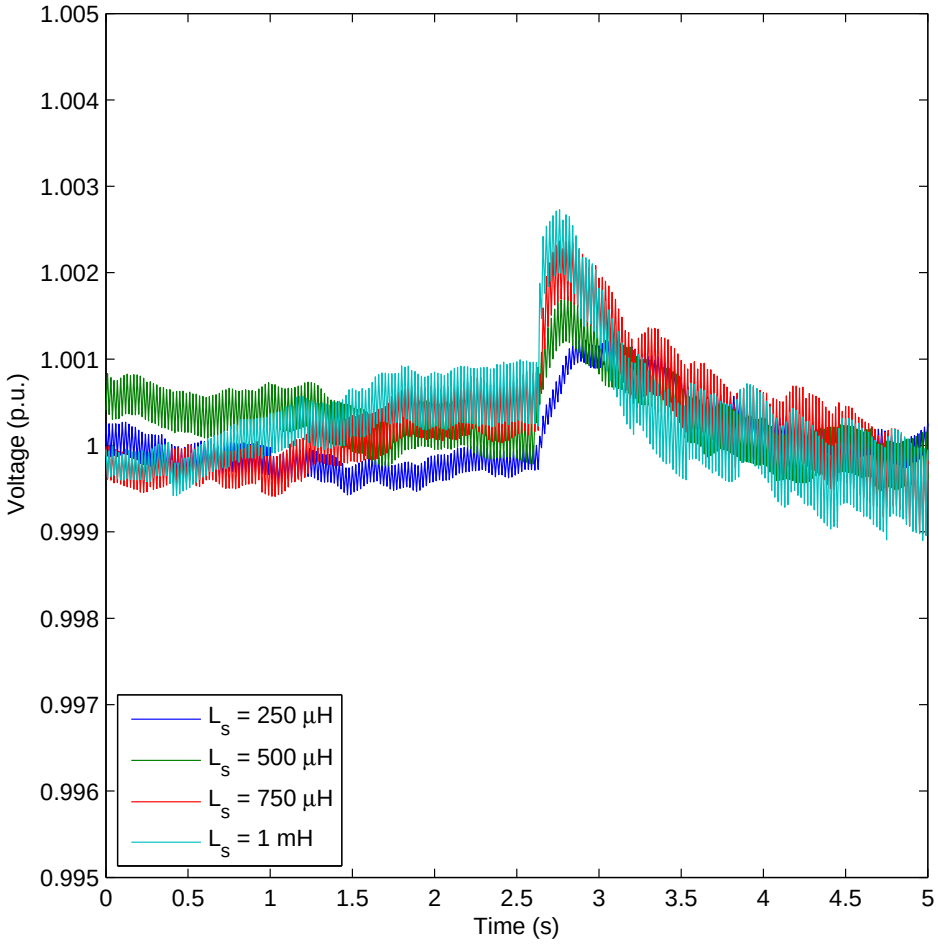

Figure 6.20: The untuned controller response to an increase in DER injected power.

The untuned STATCOM controllers seen in Figures 6.16–6.18 appear to show

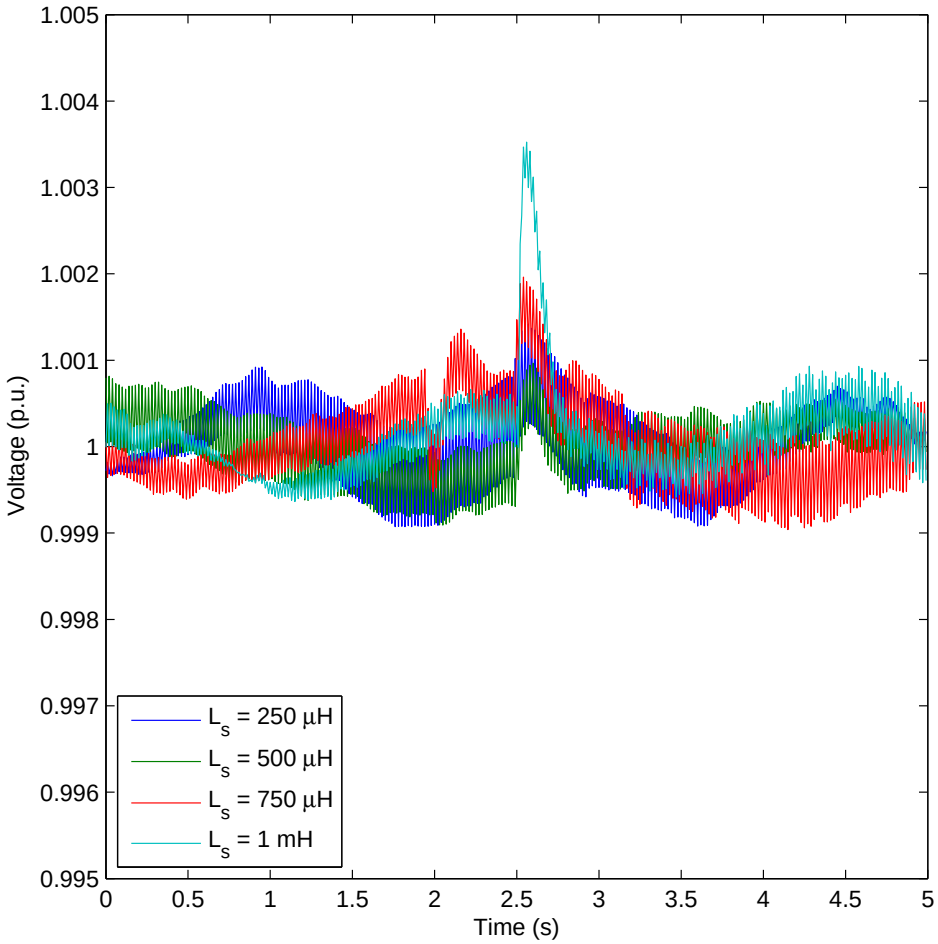

Figure 6.21: The tuned controller response to an increase in DER injected power.

some variation with supply impedance. Figure 6.20 attempts to show this more clearly, although the limited magnitude of the disturbance makes it difficult to observe the variation. It is difficult to make a good estimate of the controller settling times due to the high levels of noise on the results; however, the controller for STATCOM on the 500 μH system appears to return the voltage to steady-state between 1.5 s and 2 s after the initial transient, on the 750 μH system this is reduced to between 1 s and 1.25 s and roughly 0.75 s for the 1 mH system. Similar difficulty in comparing the transients is encountered when the tuned controllers are considered, as can be seen in Figure 6.21, although it does appear that the controller performs consistently when the supply impedance is varied. For these results, the settling-time appears to fall somewhere between 0.25 s and 0.4 s.

The impedance estimation results are similar to those for the system without DERs present. This is because the Gendrive converters are connected to the system through transformers which results in a relatively large inductance in series with the converter filter inductors. Consequently, the Gendrive converters present a relatively large impedance to the system and do not significantly affect the impedance estimation results. It should be noted that the actual values of the components used to construct the Gendrive output filter are not known and therefore it is difficult to assess how much of an effect the filter should have on the measured impedance. Detailed information regarding the internal control of the Gendrive converters is not available and it is therefore not possible to speculate about the effect, if any, the controllers might have on the impedance estimation.

6.3.2 Comparison with simulation results

Experimental and simulated results for the STATCOM response when the system includes DERs are shown in Figure 6.22. It would appear that the transients have similar shapes and settling times, although as was the case when only the experimental results were considered, the small size of the

experimental transient and the relatively high level of background noise makes it difficult to analyse the results in much depth.

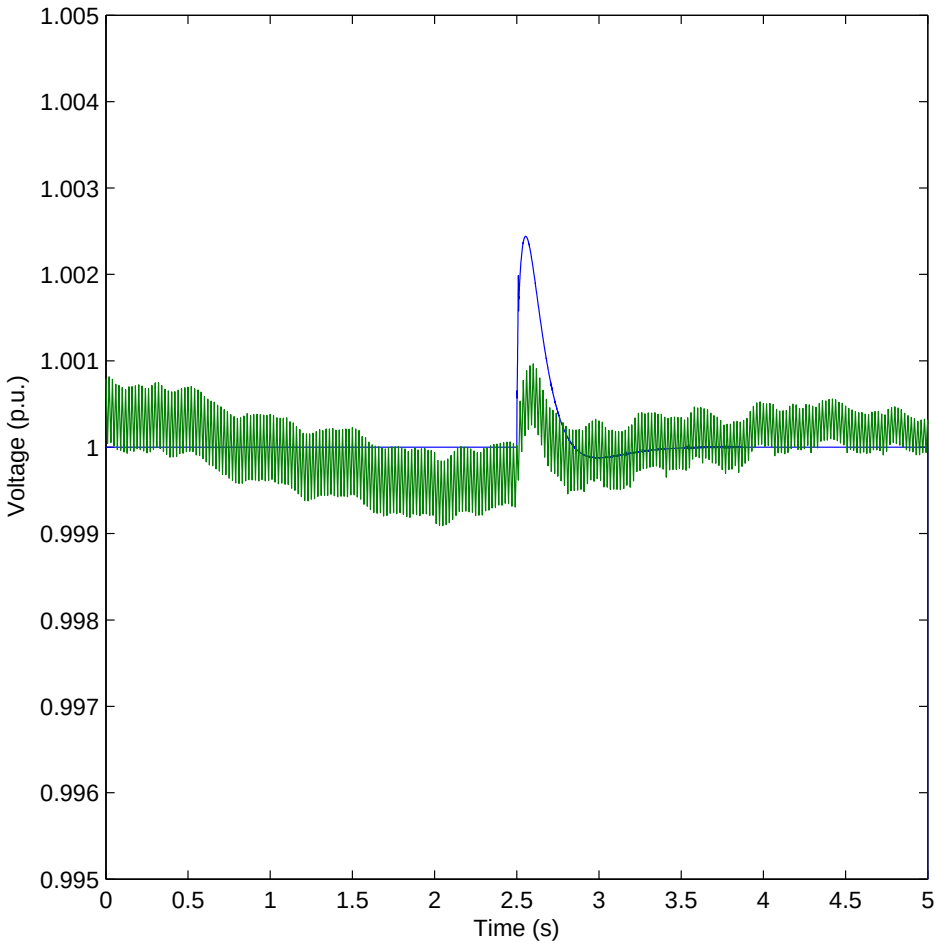

Figure 6.22: Comparison of the experimental (green) and simulated (blue) responses of controller for the system with a 500 μH supply inductance and DER power injection.

In both simulated and experimental results it can be seen that the STATCOM takes approximately 0.5 s to return the voltage to steady state following the start of the DER transient. However, the magnitude of the transient in simulation is approximately two times larger than that measured experimentally. This is likely due to differences between the ramp rates of the real and simulated DERs. The ramp rates for the Gendrive converters are not

available from the manufacturer. Therefore, in simulation, the maximum allowable ramp rate was used. However, given the consistency in settling times observed and the difficulty in determining a precise magnitude for the expected transient, there is sufficient overall similarity between the two results to suggest that the simulated behaviour is at least representative of the behaviour that may be expected in practice.

6.4 Summary

In this chapter, experimental results have been presented in order to validate the controller design and simulation work presented in earlier chapters. Experimental testing has been performed on a system with a variable supply impedance, both with and without DERs installed. It has been shown that tuning of the STATCOM AC voltage controller results in a consistent controller response to a change in system voltage.

Comparison of the experimental results with results obtained through simulation has shown general agreement and the experimental results would appear to validate the simulation work presented in the previous chapter. There are some differences between the simulation and experimental results, however these are small and can be reasonably explained. Some difficulty is encountered when examining the experimental results for a system with DERs. However, the experimental results still show reasonable similarity with the simulations and none of the results contradict the findings of the simulation studies.

When the response of the controller to a step change in load is considered, the results are clear. The tuned controllers show a consistent response regardless of supply impedance. When these results are compared with simulated results, the results are generally consistent. The results for a change in DER injected power are not so clear. Difficulties associated with analysing the results for these tests were encountered, due to the small size of the tran-

sient relative to the measurement noise and external interference (including switching events and harmonics present on the supply). Overall, it may be concluded that the experimental work has successfully validated the controller design and simulation results.

In the next chapter the applicability of the proposed STATCOM controller and impedance estimation algorithm to a system which includes standby generation for use during power outages is to be considered.

Chapter 7

Applicability to systems with standby generation

In previous chapters of this thesis the development of an adaptive STATCOM control scheme has been described and verified through simulation and experimental testing. This chapter is concerned with demonstrating the applicability of the scheme to critical power systems where back up generation is activated in the case of normal supply failure. Such a scenario is of interest to this work because it is an example of a situation where a change in supply impedance could be both large and sudden. In this chapter, simulations are presented showing the collapse and disconnection of the primary supply followed by the connection of a local backup generator. During normal operation the distribution system is supplied by from a low impedance supply. During emergency operation, when the system is supplied by the

backup generator, the source impedance is much higher. The changeover from normal to emergency operation may be viewed as a transition from a strong to a weak system. The behaviour of the STATCOM both with and without retuning of the AC voltage controller is considered to demonstrate the benefits of an adaptive control scheme in this scenario.

7.1 Modified model of the power system

The power system modelled in this chapter is a modified version of the 315 kVA system described in Chapter 5. The system supply model is modified to include an equivalent model for an 11 kV, 10 MVA distribution circuit. The 11 kV circuit includes a 2 MVA standby generator which may be connected in emergencies. The standby generator is connected to the 11 kV system rather than the 400 V system as it would be unusual to connect a generator larger than 250 kVA directly to the low voltage network [8, 103]. In addition, the generator terminal voltage is controlled and there would therefore be no benefit in using the STATCOM if the generator was connected at the PCC. Furthermore, the control of the STATCOM and the generator control would be likely to conflict, resulting in unpredictable or unstable operation. The distribution circuit is shown as a single line diagram in Figure 7.1. For the simulations conducted in this chapter, the 11 kV circuit has been represented as a 400 V equivalent circuit.

For the purposes of the simulations presented in this chapter, the transmission system is treated as an infinite bus and therefore simulated as an ideal voltage source in series with a small impedance, representing the secondary leakage reactance and winding resistance of the transformer connecting the transmission and distribution systems. The leakage inductance is 3.5 μH and the winding resistance is 0.16 mΩ. These values have been estimated using available information [10, 40, 103], assuming that the transformer leakage reactance is approximately 0.07 p.u. and that the transformer efficiency is 99 %. The transformers linking the 11 kV and 400 V circuits and

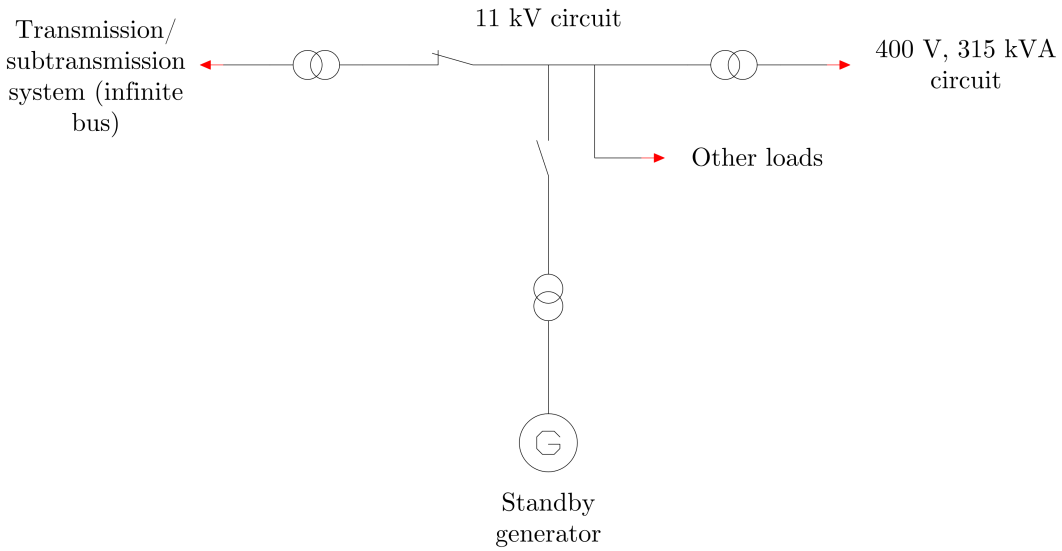

Figure 7.1: The simulated 11 kV circuit, represented as a single line diagram.

the transformer coupling the standby generator to the system are both simulated using the model shown in Figure 7.2. The circuit parameters used for simulation of these transformers are listed in Tables 7.1 and 7.2. For the purposes of these simulations, it has been assumed that the primary and secondary impedances are equal. The leakage reactances and winding resistances have been calculated assuming that the transformers have approximately 5 % impedance and are 99 % efficient [115].

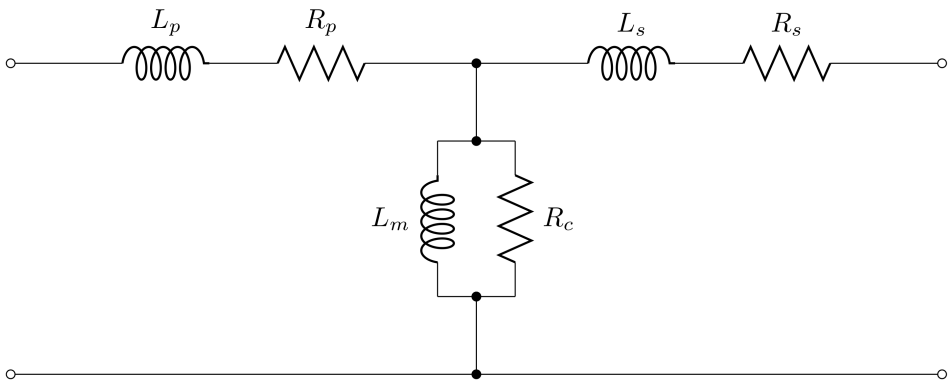

Figure 7.2: Equivalent circuit used to model transformers.

The backup supply is provided by a 2 MVA synchronous generator, which is electrically modelled as a voltage source with an inductance, L_g, and re-

Parameter	Value
L_s	40 μH
R_s	2.5 mΩ
L_p	40 μH
R_p	2.5 mΩ
L_m	61 mH
R_m	250 Ω

Table 7.1: Circuit parameters used for simulation of the 315 kVA, 11 kV/400 V distribution transformer.

Parameter	Value
L_s	12.5 μH
R_s	0.8 mΩ
L_p	12.5 μH
R_p	0.8 mΩ
L_m	10 mH
R_m	100 Ω

Table 7.2: Circuit parameters used for simulation of the 2 MVA, 11 kV/11 kV transformer connecting the synchronous generator to the system.

sistance, R_g, in series for each phase. The generator inductance is chosen so that the fundamental reactance is approximately 1.7 p.u., based on available data for generators of a similar size [121]. The generator resistance is chosen so that the generator losses are approximately 2 % at full load. This gives values for L_g and R_g of 470 μH and 5.2 mΩ respectively.

The control of the standby generator consists of two separate control loops; a speed control loop which is required to maintain the system frequency at 50 Hz and a voltage control loop, which maintains the voltage at the generator terminals at 1 p.u. The modelling of the generator dynamics and control is based on work originally presented by Jayamaha [122] and Agbedahunsi [123]. The dynamics of the generator have been considered in these simulations. The speed control loop includes a plant modelling the effect of the inertia, J, and mechanical losses, B, (friction and windage) of the generator. The lag associated with the generator's prime mover is also modelled (the prime move time constant is represented as τ_{pm}). The equivalent electrical torque, T_E, is calculated and fed into the speed control loop as a disturbance. The voltage control loop has been designed to be representative of the automatic voltage regulator (AVR) used to control the field winding of synchronous generators and includes a plant modelling the lags associated with the generator field winding and exciter (the field and exciter time constants are τ_f and τ_e respectively). The generator speed control loop is shown in Figure 7.3. The AVR loop is show in Figure 7.4

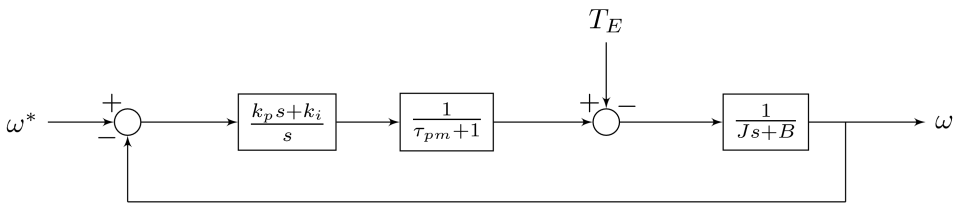

Figure 7.3: Generator speed control loop.

The generator speed control loop takes as its inputs the system frequency demand, which is a constant 50 Hz and the measured system frequency. The error is then used to control the rotational speed of the synchronous

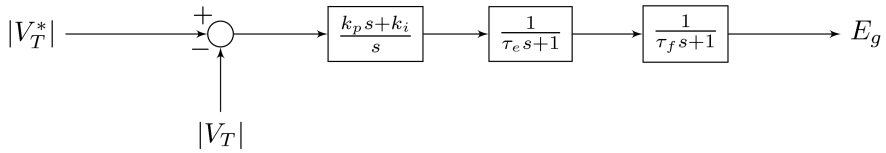

Figure 7.4: Generator AVR control loop.

generator, which, assuming a 2 pole machine is used, is the same as the electrical frequency of the system. The speed control loop plant consists of two transfer functions, one representing the prime mover dynamics and one representing the generator inertia and mechanical losses (friction and windage). A disturbance is added between the prime mover and the generator, representing the mechanical torque resulting from a change in electrical load. The controller gains have been calculated using the MATLAB Sisotool utility [124] to give a rise time of 0.1 s and a damping factor of 0.7. The resulting proportional and integral gains are 320 and 1600 respectively.

The inputs to the voltage control loop are the voltage demand and the measured terminal voltage of the generator. The voltage set point is typically set slightly above 1 p.u. to allow for some voltage drop between the source and load. For the purposes of this work, the voltage set point was 1.02 p.u. The plant for the voltage control loop is a combination of the field winding and exciter. This gives a second order plant, which may be controlled using a single PI controller. As before, the generator AVR gains were found using Sisotool utility. The gains were tuned to give a controller rise time 0.1 s and a damping factor of 0.7. The resulting proportional and integral gains are 6 and 30 respectively. The output of the AVR control loop is then used to determine the internal voltages of the generator. Tuning of the AVR gains is done assuming that the generator is operating under no load, which means that the internal and terminal voltages are equal and that the effect of the generator impedance on the dynamics of the control loop is ignored. As a consequence of this the dynamics of the AVR varies considerably depending on the generator loading.

7.1.1 Network collapse

Stability analysis of power networks and particularly analysis of system collapse is not trivial [40] and detailed consideration of the causes and dynamics of an unstable network falls outside of the scope of this work. For the purposes of the simulations presented in this chapter, network collapse is represented by a sudden drop in supply voltage from which the system does not recover, causing a disconnection of the supply. The supply voltage envelope used to represent voltage collapse is shown in Figure 7.5. The voltage envelope for the backup generator is also shown.

In addition to the collapse of the system voltage a number of other important events occur during the supply changeover period. These are the disconnection of loads, shut down of the STATCOM, the disconnection of the system from the supply, the connection of the system to the standby generator, the STATCOM returning to normal operation and the reconnection of loads. The sequence of events is as follows:

- At $t = 0$ s the system is operating normally.
- At $t = 0.33$ s and $t = 0.67$ s some of the loads on the 315 kVA circuit are switched on.
- At $t = 0.9$ s the supply voltage begins to collapse. The voltage falls steadily, reaching 0.1 p.u. at $t = 1.1$ s.
- At $t = 1.2$ s the loads disconnect from the system.
- At $t = 1.9$ s the STATCOM disconnects from the system.
- At $t = 3$ s the distribution system is disconnected from the transmission system.
- At $t = 3.8$ s the backup generator is connected.
- Between $t = 3.8$ s and $t = 4$ s the generator voltage is ramped up to 1.02 p.u.

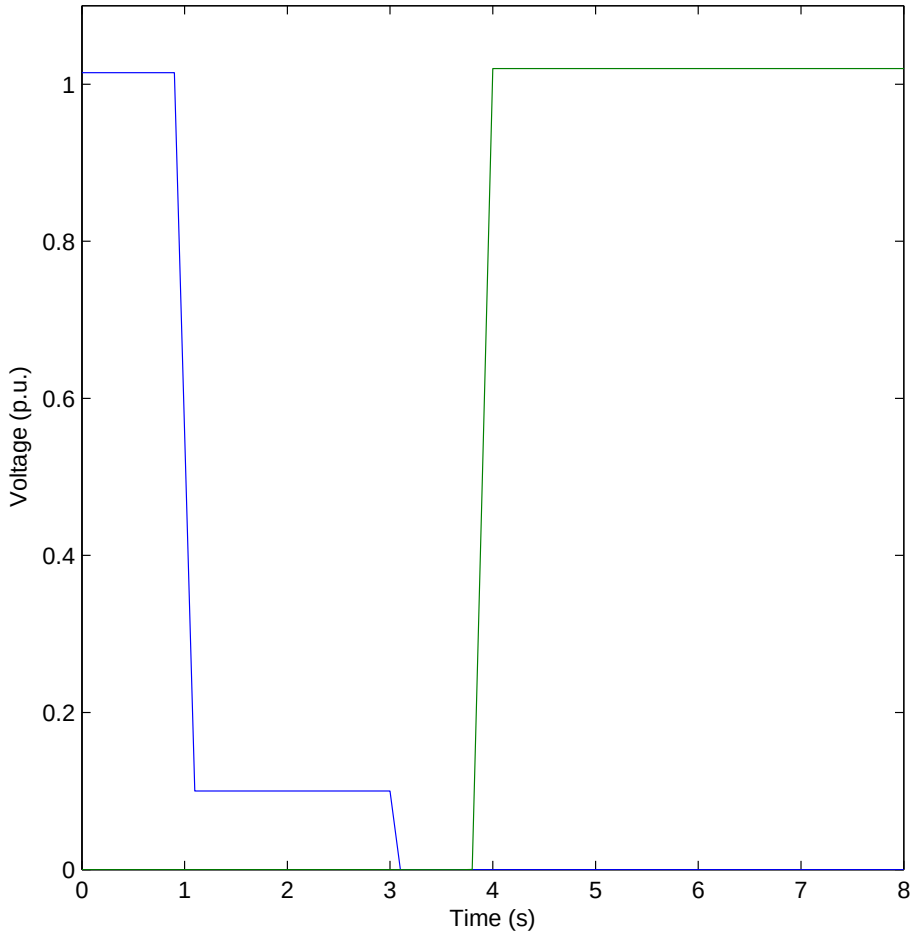

Figure 7.5: Voltage envelope for the main supply (blue) and the backup generator (green).

- At $t = 4.2$ s the STATCOM is reconnected but the controller is not enabled.
- Between $t = 4.2$ s and $t = 5$ s the impedance estimation algorithm is triggered and the STATCOM controller is retuned.
- At $t = 5$ s the STATCOM controller is enabled.
- At $t = 6.33$ s, $t = 6.67$ s and $t = 7$ s the loads on the 315 kVA system are reconnected.

The disconnection and reconnection of the STATCOM must be given some consideration here. In previous chapters, the STATCOM has been treated as though it has always been switched on and operating – i.e. the connection transient has been ignored. Making such a simplification is not possible in this chapter; the STATCOM must disconnect during the main supply outage and only reconnect once the system is operating again. For the purposes of this work, disconnection of the STATCOM is triggered after the maximum current has been continuously supplied for one second. The STATCOM will then cease supplying reactive power to the system and disconnect from the system. Once the system voltage recovers, the STATCOM will track the system voltage without enabling the AC voltage control (so that no current flows between grid and STATCOM) and reconnect. There is then a further one second delay before the STATCOM enables the AC voltage controller. This ensures that the STATCOM behaviour does not affect the recovery of the system.

The impedance estimation algorithm must be triggered at some point after the system has recovered in order for the controller to be correctly tuned to the new supply. This is triggered by the resetting of the STATCOM during the disconnection/reconnection cycle. The injection cycle then occurs once the system has recovered and reached a steady-state, but before the STATCOM control is enabled. This ensures that STATCOM is correctly tuned when the AC voltage controller is enabled.

7.2 Evaluation through simulation

Simulation results for four different scenarios are presented and discussed in this section. First, a system with no STATCOM connected is considered. Second, a system with a STATCOM is considered, with the AC voltage controller tuned to the normal supply. Third, the second scenario is considered again, but with the AC voltage controller tuned to the backup supply. Finally, the system with a STATCOM is considered, with the AC voltage controller undergoing a retuning cycle once the system has recovered. Results are presented below. Figures 7.6—7.9 show the results from each of the four scenarios. The figures have been annotated to highlight important transient events.

The STATCOM can be seen to raise the voltage very slightly while it continues operating during the sustained undervoltage condition. Although the response to normal load changes as the gain is varied is as expected, no significant differences are observed in the dynamic behaviour of the STATCOM during the voltage collapse. This is not unexpected, as the large voltage error causes the output of the STATCOM AC voltage controller to saturate almost immediately.

The total difference between no load and full load voltages at the PCC for the backup system when no STATCOM is connected is 0.025 p.u. The results from the system with no STATCOM show that the response of the generator AVR to a change in load is slightly oscillatory. When the STATCOM is operating, regardless of the gain, the oscillations are reduced, although the voltage settles faster for the STATCOM tuned to the main supply. When the STATCOM is tuned to the main supply, a large overshoot can be seen after the first change in load. This is also present when the STATCOM is tuned to the backup supply, although it is not as substantial. The response of the backup system with a STATCOM is shown more clearly in Figure 7.10, when the STATCOM is tuned to both the main supply and the backup supply.

The tuned response differs from the expected controller response. This re-

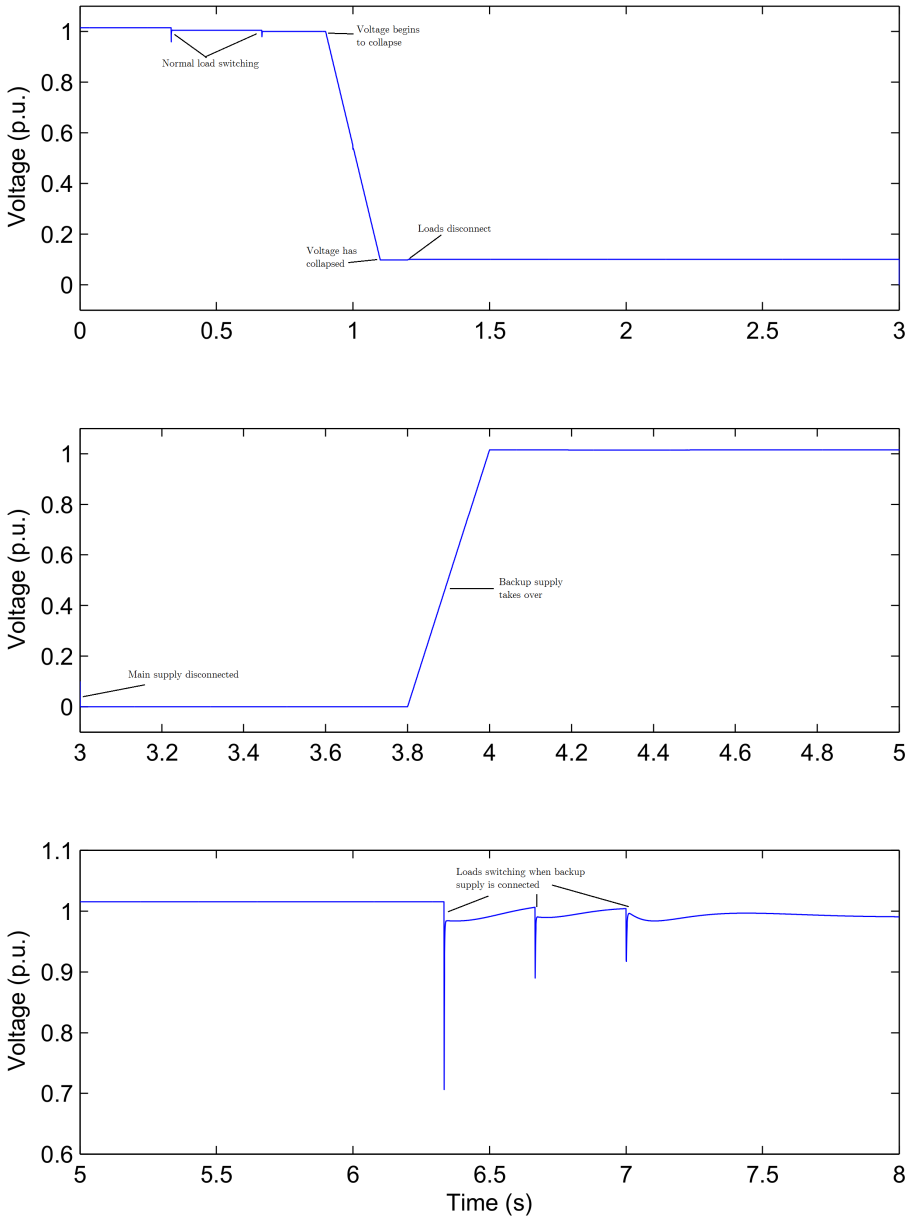

Figure 7.6: System voltage when no STATCOM is connected.

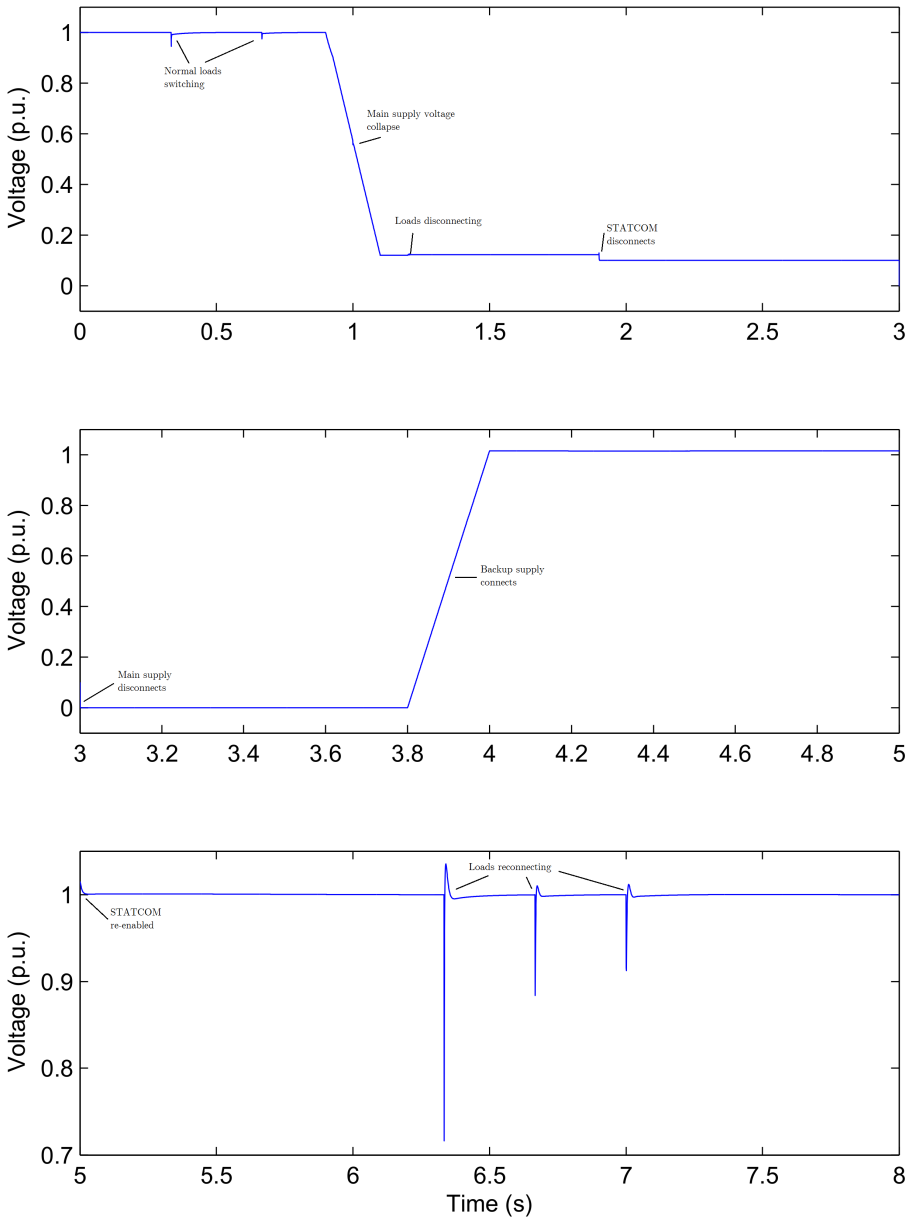

Figure 7.7: System voltage when a STATCOM tuned to the main supply is connected.

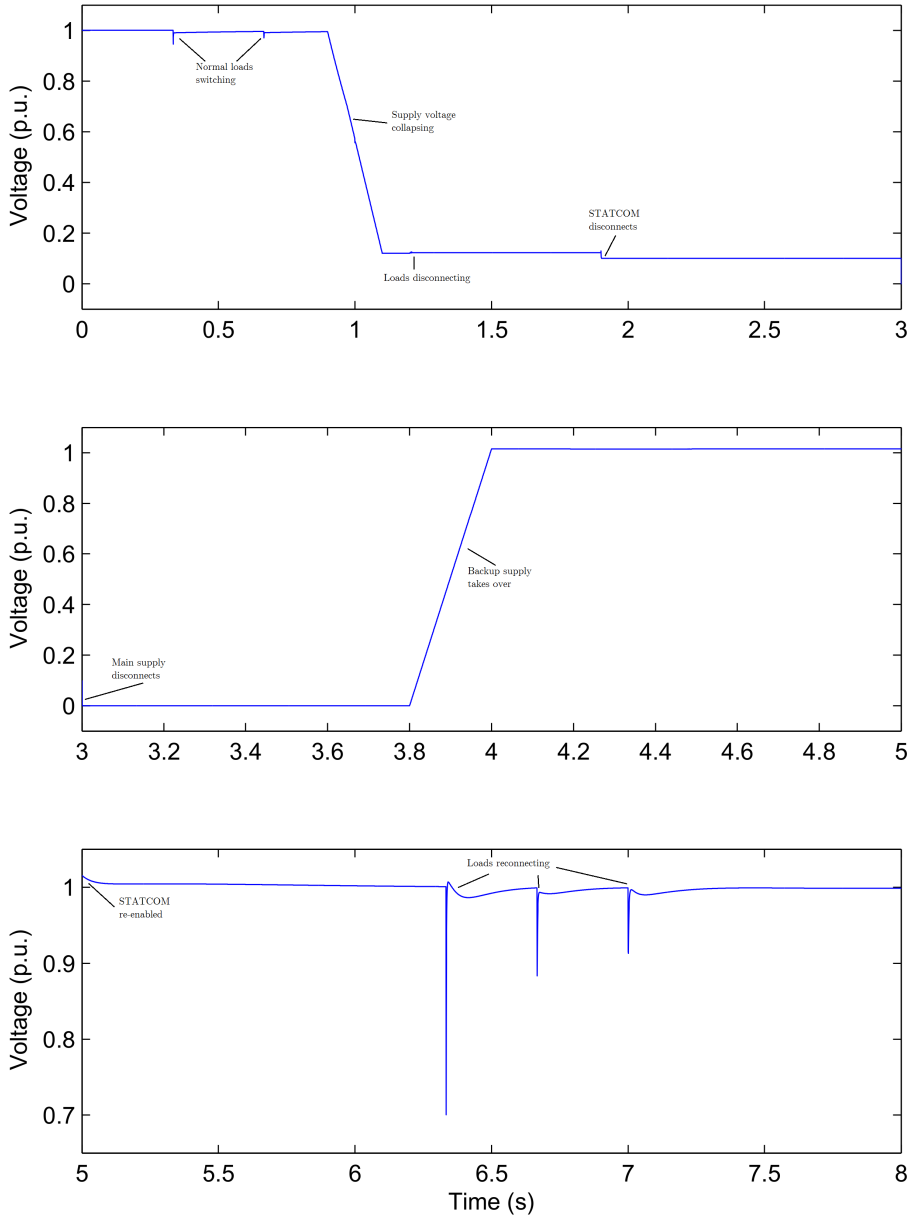

Figure 7.8: System voltage when a STATCOM tuned to the backup supply is connected.

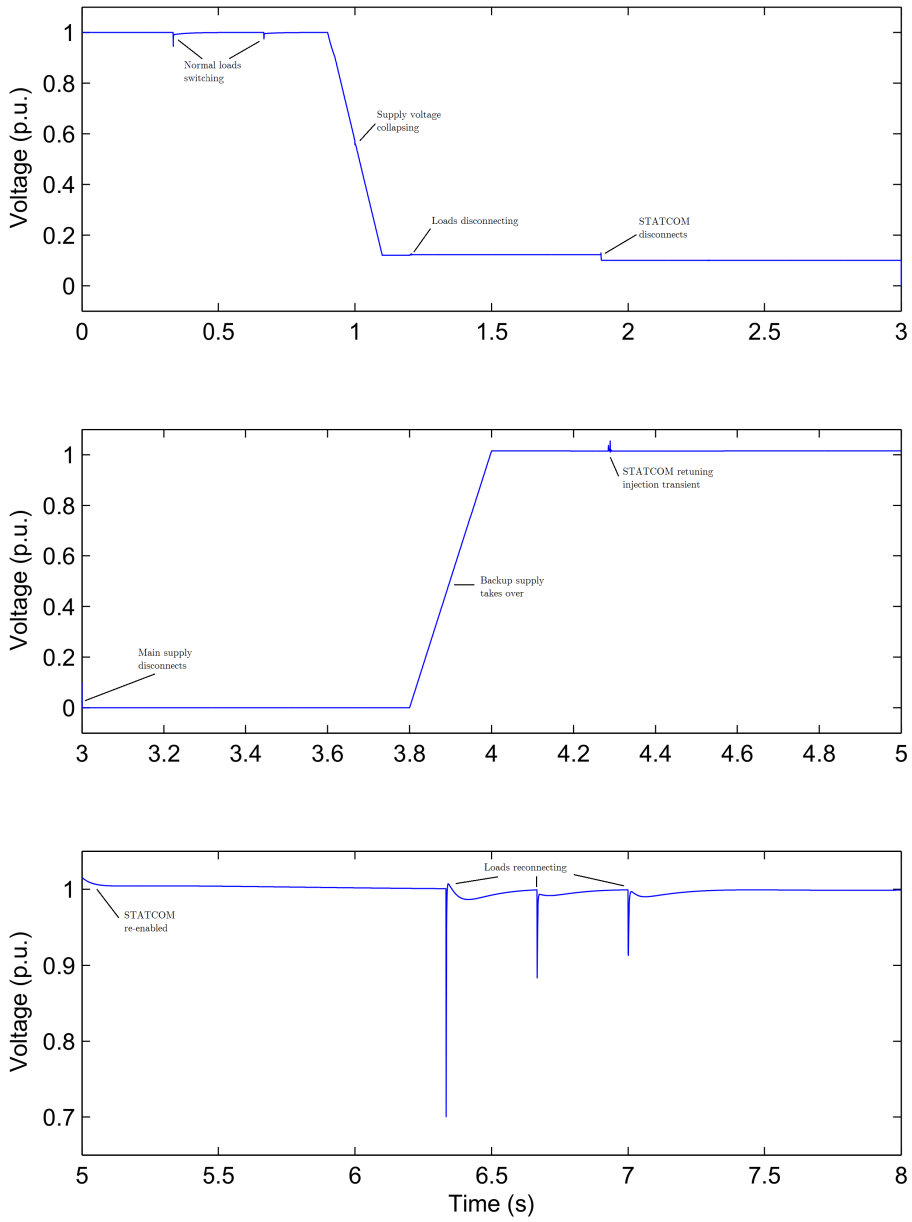

Figure 7.9: System voltage when a STATCOM is connected and retuned during the supply changeover.

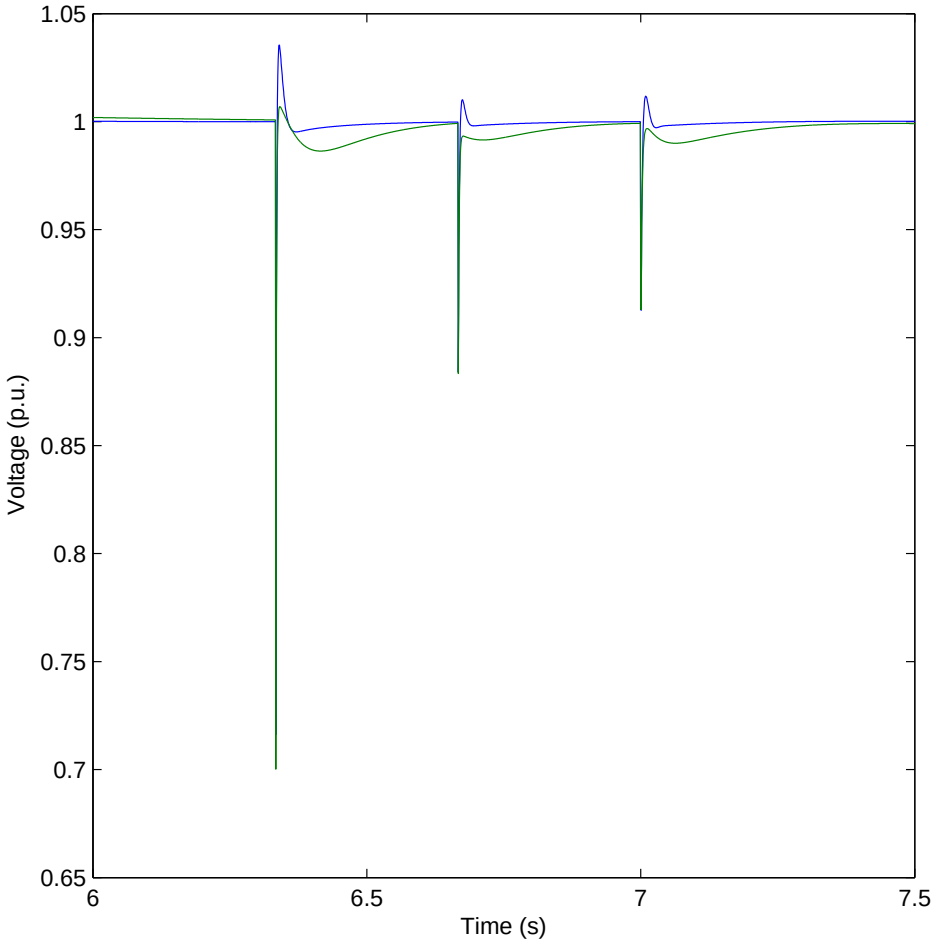

Figure 7.10: Voltage transients when the backup system is operating with STATCOM support. The STATCOM AC voltage controller is tuned to both the main supply (blue) and backup supply (green).

sult was not expected. The discrepancy is caused by the voltage control provided by the generator AVR conflicting with that provided by the STATCOM. In steady state the AVR maintains the generator terminal voltage at a fixed level regardless of the load current and as a result, although the actual physical impedance of the generator is large, the effective source impedance in steady state is close to zero. The impedance estimation method uses a transient too short to cause a response from the generator AVR and therefore does not identify the effective impedance, but the actual physical impedance of the system. The overall system voltage response is therefore determined by a combination of the STATCOM and AVR dynamics. The STATCOM AC voltage controller is designed to respond faster than the generator AVR and therefore the STATCOM dynamics are dominant during the initial transient. Although the conflict between the two voltage control loops causes some changes to the expected dynamic performance of the STATCOM, it does not appear to cause instability and neither controller fails to operate.

The injection used for retuning is just visible in Figure 7.9 between 4.2 s and 4.3 s. The wideband results of the impedance estimation are shown in Figure 7.11. It can be seen that the reactance estimates are accurate over the full range of frequencies but the resistance estimates are not. This is consistent with the results presented in previous chapters. At the fundamental, the resistance and reactance were estimated to be 16.2 mΩ and 0.182 Ω respectively. The impedance estimation does not appear to be affected by the generator dynamics, nor does the injection appear to cause any unexpected response from the generator.

7.2.1 Variation of the generator capacity

The results presented in this chapter have so far been inconclusive. The system remains stable regardless of whether the STATCOM is tuned to the main supply or the backup supply and neither response is a good match to earlier simulation results. In this section, the generator capacity is reduced

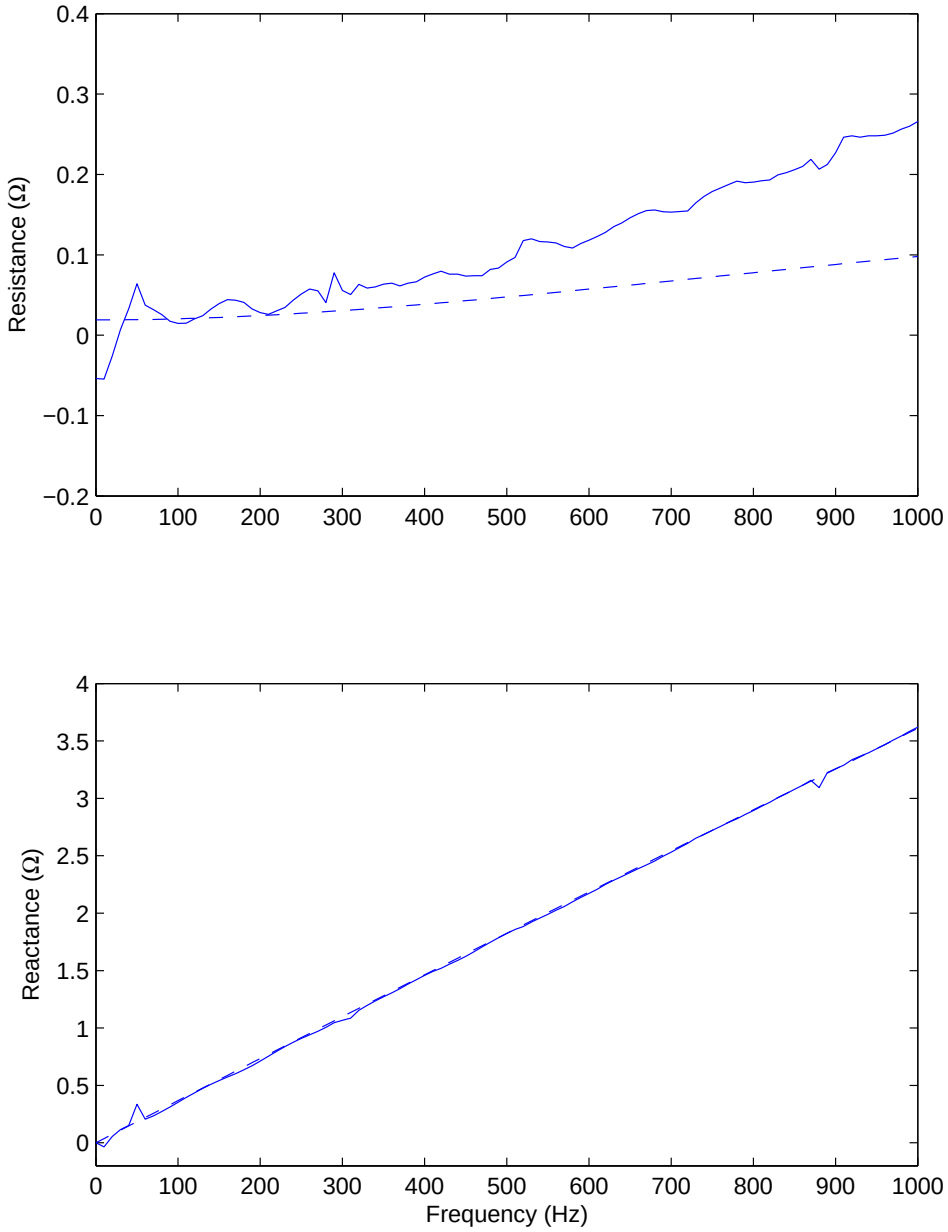

Figure 7.11: Wideband impedance estimates for the system with the standby generator connected. Dotted lines show the ideal resistance and reactance.

to 1 MVA. To achieve this, the generator impedances are doubled, the rotational inertia is halved and the generator speed controller gains adjusted to compensate. Simulation results are presented to demonstrate the effect this has on the transient response of the system, both with the original STATCOM AC voltage controller gain and with the gain adjusted after retuning.

The simulations performed with the 2 MVA generator were repeated with the 1 MVA generator model. Only the performance of the system with backup supply was considered since the system behaviour with the main supply connected was as expected in the previous simulations. The response of the system with no STATCOM, with the STATCOM tuned to the main supply and with the STATCOM tuned to the backup supply are shown in Figure 7.12. As was the case with the results for the 2 MVA generator simulations, the results are different to the results seen in earlier chapters. As before, this deviation from the expected results is caused by the conflict between the generator AVR and the STATCOM AC voltage control and the variability of the generator frequency. Similar to the previous case, the conflict between the two voltage control loops appears only to change the dynamic behaviour of the system and does not appear to cause any instability.

The effect of the reduced generator capacity is clear. The STATCOM tuned to the new supply impedance is now clearly preferable to the STATCOM tuned to the original supply impedance as the speed with which the controller attempts to respond when using the original gain risks making the system unstable. In all cases, as the system loading is increased, the voltage becomes more oscillatory. The most oscillatory response is observed when the STATCOM is tuned to the main supply. Although some ringing is still seen when no STATCOM is connected or when the STATCOM is tuned to the backup supply, it is much less severe. Furthermore, although the initial response of the tuned STATCOM is slightly more oscillatory than the response with no STATCOM, overall the system reaches steady state faster. ithout STATCOM support, the voltage fluctuates beyond the end of the simulation. In contrast, with the STATCOM tuned to the backup supply the

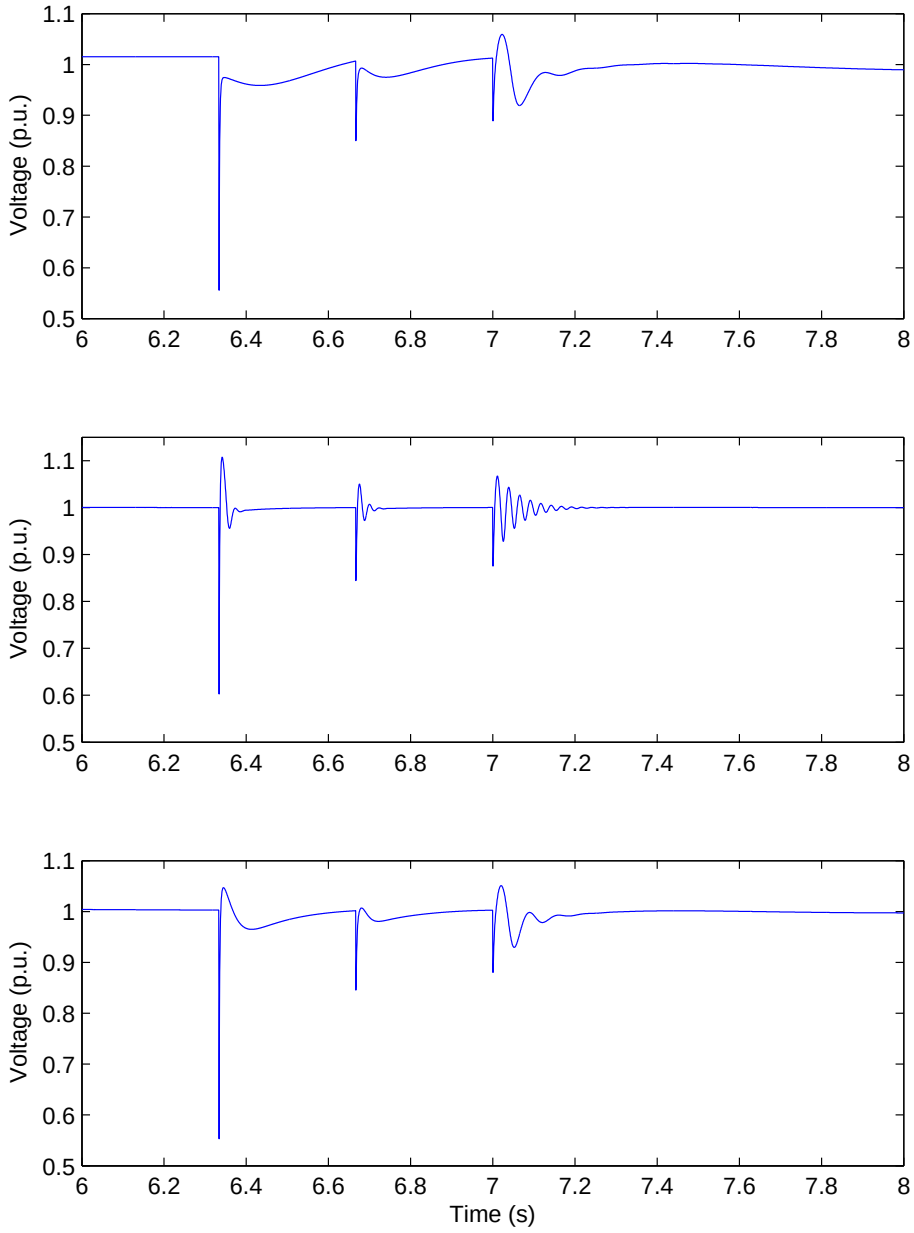

Figure 7.12: Results showing the system voltage response measured at the PCC when no STATCOM is installed (top), a STATCOM tuned to the main supply is installed (middle) and a STATCOM tuned to the backup supply is installed (bottom).

voltage takes a little longer than 0.2 s to return to 1 p.u.

In addition to the increased resonance, the transient voltage when the STATCOM is tuned to the main supply can be seen to exceed 10 % above nominal immediately after the first load change, which may be considered excessive. It should be noted that the STATCOM with the original controller gains is approaching the limit of stable operation. Any further reduction in the generator inertia or any increase in the controller gain could result in a response which is not just oscillatory, but which becomes unstable.

These results show that although the voltage response is not entirely consistent with the results from earlier simulation and experimental work, which considered only "strong" systems, there is still some benefit gained from retuning the STATCOM AC voltage controller and failure to do so could result in an excessively oscillatory, or possibly even unstable system. The importance of retuning increases with increased generator impedance and decreased generator inertia.

For completeness, the impedance estimation results for the system with a 1 MVA generator are shown in Figure 7.13. As with the previous results, close agreement is seen between estimated and ideal reactance and the resistance results are somewhat less accurate. As with the results for the 2 MVA generator, there is no evidence that the impedance estimation has been affected by the response of the generator AVR and so the results show the physical impedance and not the effective steady state impedance. As was stated previously, it can be seen that the quality of impedance estimates does not seem to be affected by the generator dynamics and the injection used for impedance estimation does not appear to have any effect on the behaviour of the generator.

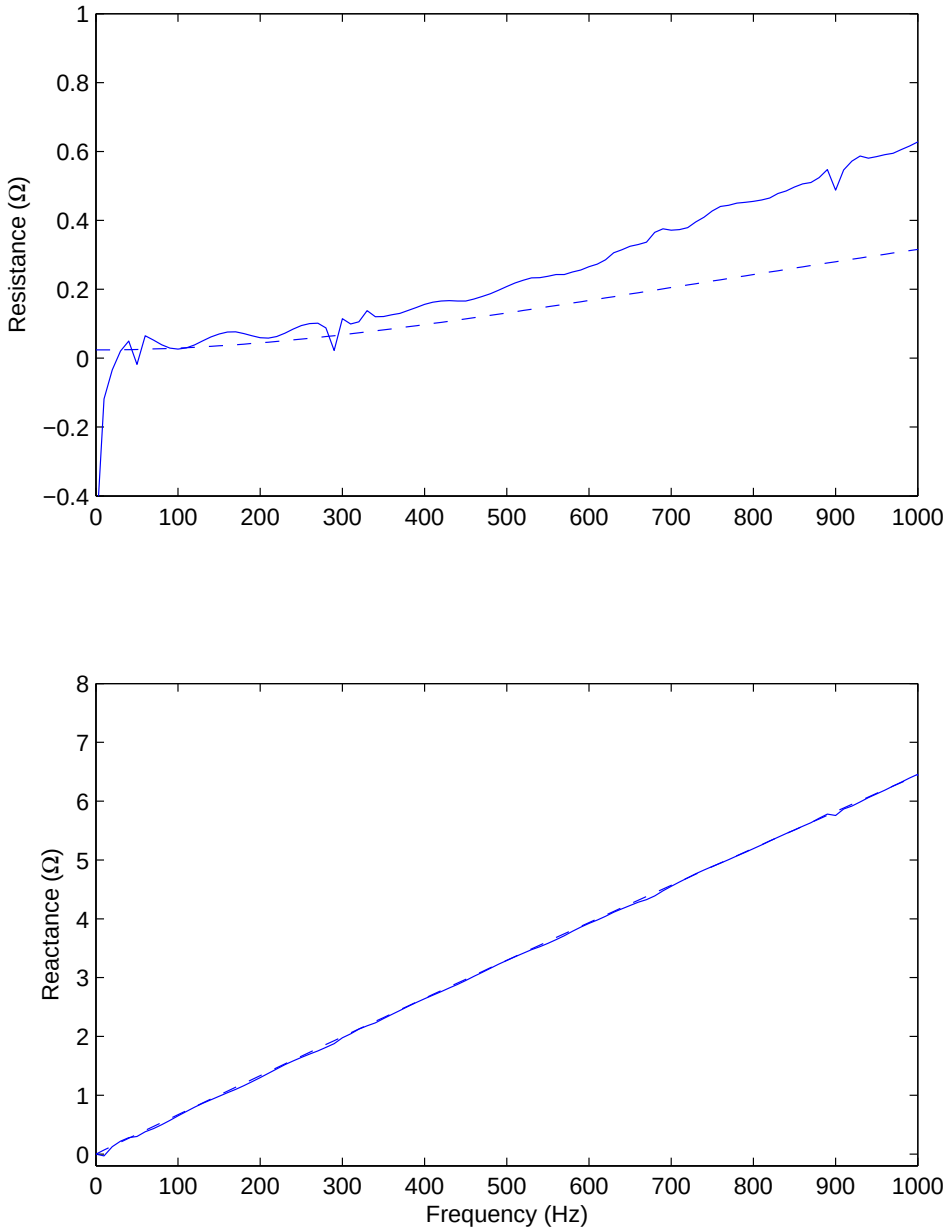

Figure 7.13: Wideband impedance estimation results for the system supplied by a 1 MVA generator. The dashed lines show ideal resistance and reactance.

7.3 Summary

This chapter has presented one particular application where tuning of the STATCOM voltage controller is potentially beneficial to the performance of the system. Specifically, the interactions between the STATCOM and a backup generator used to provide power in emergencies have been considered. The transition from normal operation to backup operation can be viewed as a transition from a strong system, with a low impedance source and good voltage and frequency stability to a weak system, with high source impedance and reduced stability.

Simulation results presented in this chapter show that the STATCOM can improve the response of the system during load transients, resulting in a shorter settling time than the generator AVR is able to achieve alone, but if the STATCOM AC voltage controller gain is set too high then the voltage stability of the system may be compromised. This shows that for weaker systems, the importance of retuning the voltage controller increases. Conflict between the generator AVR and the STATCOM AC voltage controller has been observed. The conflict affects the dynamic behaviour of the system, resulting in different voltage responses to those observed in earlier chapters of this work. In this chapter it has also been demonstrated that the impedance estimation algorithm used is able to function effectively on a weak system, where the system voltage and frequency are less stable than was the case in previous chapters.

Chapter 8

Conclusions and future work

This thesis has presented a STATCOM control method which utilises impedance estimation for the tuning of an AC voltage controller. This thesis has considered a suitable on-line impedance identification method, based on imposing short-term current transients on a power system, and a method of controlling the AC voltage magnitude of a power system through the injection of reactive power. The power systems considered in this work have all been distribution level systems, where voltage control has been limited in the past and where key assumptions used in the control of transmission systems are generally not valid. This chapter aims to conclude this work, with specific reference to the objectives stated in Chapter 1 and how they have been achieved. In addition, some of the limitations of this work are identified and possible future areas of research are identified.

8.1 Objective specific conclusions

In Chapter 1 the three objectives of this work were stated. They were:

1. To develop an AC voltage control strategy for STATCOMs installed on distribution networks using impedance estimation to tune the controller dynamics to the rest of the system.
2. To demonstrate the method both through simulation and experimentally.
3. To illustrate the applicability of this adaptive control scheme to a system which includes backup generation for use in times of power outages.

How each of these objectives has been addressed and the key findings of this work will now be considered.

8.1.1 Objective 1

The first objective has been addressed in Chapters 3 and 4. In Chapter 3 an AC voltage controller, generating a reactive current demand, was proposed based on consideration of the power flow equations. The reactive current demand is related to the desired change in voltage and the supply impedance, and therefore the supply impedance needs to be known in order to set the controller gain to an optimum value. To the best of the author's knowledge, impedance estimation has not been used to tune STATCOM voltage controllers in any previous works, and this may therefore be considered a novel contribution to knowledge from this thesis. In addition, the modification that has been made to the impedance estimation method, which involves generating a transient current demand rather than directly

manipulating the converter switching pattern in order to improve the impedance estimation algorithm, is new and has not been found in any other work reviewed by the author.

Basic simulations to demonstrate the controller behaviour were described and the effect of varying the supply resistance and reactance was considered. Unexpectedly it was found that, even at relatively low X/R ratios, the supply resistance has very little effect on the controller dynamics, and therefore, only knowledge of the supply reactance is required to set the controller gain. However, when the X/R ratio was reduced to less than unity, the controller behaviour becomes less consistent and it can be seen that the resistance considerably affects the controller dynamics. For this reason, further work is needed to apply the proposed control design to systems with an X/R ratio of less than one. Provided that the STATCOM is located close to a transformer, the X/R ratio is likely to be greater than one, even on distribution systems, where the cable resistance tends to be comparable to cable reactance.

The problem of identifying the supply impedance has been considered in Chapter 4. Initially, an existing transient current injection method based on directly manipulating the PWM switching pattern of a power converter was considered. However, it was found that the current control loop of some power electronic converters caused suppression of the injected signal, particularly at low frequencies. A novel modification was proposed to overcome this: rather than directly manipulating the converter PWM switching pattern, the desired transient current was added to the existing converter current demands, so that the current controller would not see the injection as an unwanted disturbance and the transient would not be suppressed.

Simulations were performed to demonstrate the efficacy of the improved injection method. The reactance estimates were found to be of a considerably higher quality than the resistance estimates for a simple RL supply, particularly at higher frequencies. However, the quality of the resistance estimates improved when a shunt capacitance was introduced to the supply

impedance. These results are consistent with earlier work using a transient injection method [125]. Experimental results were also presented. The experimental results are consistent with the results from simulation, although it was found that when the converter with an LCL output filter is used to estimate the impedance, the bandwidth of the impedance estimates is limited to a frequency dependent on both the supply impedance and the filter component values.

8.1.2 Objective 2

Objective 2 has been addressed, primarily through Chapters 5 and 6 of this work, although experimental demonstration of the impedance estimation method may also be found in Chapter 4.

Simulations were performed in order to evaluate the STATCOM controller behaviour. In Chapter 5, the simulations are described and the accompanying results are presented. The simulations are used to show the STATCOM controller and impedance estimation algorithm operating in a range of scenarios. The simulation results presented show that the impedance estimation algorithm is able to accurately identify the fundamental system reactance and that the AC voltage controller operates as expected in each of these scenarios. Using the impedance estimates to tune the AC voltage controller has been shown to produce a consistent step-response over a range of realistic supply impedances.

Unexpectedly, it was found that some DERs, specifically those that have been termed "current-source DERs" for the purposes of this work, may cause inaccurate results at higher frequencies. This is because the injection excites a response from the DER current controller, which attempts to suppress the injected current. However, at low frequencies the supply impedance dominates and therefore the controller response does not effect the impedance estimates. At higher frequencies, when the supply and DER output impedances become comparable, the controller response causes the

quality of the impedance estimation results to deteriorate.

Results from the experimental STATCOM are presented in Chapter 6. Experimental results were obtained for a systems with a range of supply impedances, both with and without additional power supplied from DERs. The results show that tuning the AC voltage controller using the impedance estimates results in a consistent controller response regardless of the supply impedance. In addition, it has been shown that the response obtained from the experimental STATCOM is consistent with the response obtained through simulation, with only a few minor differences, which are discussed in Chapter 6. The experimental results may therefore be regarded as having validated the simulation results, both for the AC voltage controller and for the impedance estimation algorithm.

8.1.3 Objective 3

Objective 3 was addressed in Chapter 7. A STATCOM connected to a system that may be supplied from a standby generator during times when the normal supply is unavailable was considered. Simulations were performed in order to evaluate the system behaviour. Both the electrical characteristics and the mechanical behaviour of the standby generator were modelled. When the supply is lost and the generator takes over, the system effectively transitions from a strong, low impedance system to a weak, high impedance system. As a result, it is necessary for the STATCOM controller to retune. No previous work has been found specifically investigating the interactions between a STATCOM and backup generator on a distribution system and therefore the work performed in order to complete this objective is also presented as a novel contribution to knowledge.

Initial results were inconclusive. This is because the AVR associated with the standby generator provides good voltage control, resulting in a well regulated supply. The simulations were repeated with the generator rating reduced. It was found that retuning the STATCOM controller following

the supply interruption resulted in a less oscillatory response than if the controller was not retuned and in a faster voltage settling time than if no STATCOM was used to support the system voltage.

One interesting and unexpected finding from Chapter 7 is that the performance of the AC voltage controller is different from earlier simulations and experimental results. This is because the system voltage is affected by both the STATCOM voltage control and the generator AVR. The two methods of controlling the voltage interact, and the result is that the system voltage response deviates from the expected response. It should also be noted that, unlike earlier simulations and experimental work, load changes have a non-negligible effect on the system frequency, and this may cause further interactions with the STATCOM voltage controller which should be investigated thoroughly as part of any future work.

In addition to demonstrating that the AC voltage controller continues to operate effectively, it has also been shown that the system impedance may still be accurately identified in the presence of the standby generator. However, a distinction should be made between the transient impedance measured by the impedance estimation algorithm and the steady-state impedance, which takes the effect of the generator AVR into account.

8.2 Limitations and recommendations for further work

There are several limitations to this work and several unexpected findings which have been noted but not investigated further. This section aims to identify the weaknesses of the this work and to suggest potential areas of future investigation.

The AC voltage controller used in this work consists of an integrator with variable gain. The pole introduced by the integrator is intended to can-

cel the zero associated with the system reactance. While this approach has been found to be adequate for the needs of this work, integral controllers tend to be slow compared to other controller designs and lack any inherent damping, which can lead to an oscillatory control response if sufficient damping is not provided by the system resistance. It is therefore desirable for a more robust controller to be found. There is no immediately obvious way of choosing gains for a PI controller from the power-flow equations describing the relationship between reactive power and voltage. Considering the non-linear nature of these equations, it may be worthwhile investigating a non-linear controller design. Model predictive control could be a suitable non-linear alternative to the controller presented in this work. There are also other potential benefits of revising the controller design, such as providing damping of oscillations produced by large power swings, or optimising the controller to reduce short-term transients.

In Chapter 4 it was found that the useful bandwidth of the injection used for impedance estimation was limited by a combination of the supply reactance and power converter filter when an LCL type filter was used to couple the converter to the grid. This work was only concerned with the impedance at the fundamental, well below the cut-off frequencies observed in this work. Knowledge of the impedance at higher harmonics may be useful for other applications, such as control of active filters, and it is therefore useful to overcome this limitation if possible. One possible means of achieving this may be to increase the current controller bandwidth. However, this is likely to require an increase in the switching frequency of the converter, resulting in increased losses and additional design challenges, and therefore may not be a practical solution and further consideration of the problem is required.

It was observed in Chapter 5 that the controllers in nearby active sources and loads may result in suppression of the injections used for impedance estimation. In this work, this was limited to higher frequencies and therefore was not of any particular concern. There are situations however, such as isolated microgrids powered predominantly by power electronic converters, where the impedance estimation algorithm described in this work may

not be effective in identifying the source impedance. In Chapter 7 it was found that the dynamics of controlled sources may result in a different effective impedance when the system is operating in steady-state to the estimate obtained through impedance estimation. Both these results suggest that the impedance estimation method described may have limited usefulness when used on systems with a large number of controlled sources and loads and further investigation is required to develop a method capable of system identification in this instance.

This work has focused on voltage control for balanced, three-phase systems. Although unbalance has been briefly considered, it has been assumed throughout this work that the supply impedance itself is balanced. Single-phase supplies have not been considered. It should be possible to use the STATCOM to help balance the three-phase voltages and this may be investigated as part of any future work. This will probably require a neutral conductor to be connected to the STATCOM and that modifications are made to the control in order to allow independent control of the current in each phase. It should also be possible to construct a single-phase STATCOM, which may be used on single-phase systems, or in situations where unbalance is expected to be unusually high, such as if the STATCOM is installed in a small and relatively remote residential area.

The scope of this work was limited to systems with an X/R ratio of greater than one. It is possible that some distribution systems may have lower X/R ratios, particularly remote areas connected to the rest of the grid using long lengths of cable, and further investigation is required to determine the effectiveness of using a STATCOM on such systems. Furthermore, it is likely that the controller developed as part of this work would have to be redesigned to work optimally on such systems. A few previous works by other authors have investigated the use of real power and energy storage in supporting weak grids [122, 123]. In addition to extending this work to cover systems with very low X/R ratios, it may be worth considering combining the STATCOM control and impedance estimation from this thesis with the real power control methods in those earlier works so that both real and reactive power

support can be provided to particularly weak and lossy systems.

Appendix A

Grid synchronisation and the dq transformation

Accurate grid synchronisation is required in order to connect the STATCOM described in this work to the grid. To achieve this, a reference phase must be obtained from the grid voltages. In addition, the magnitude of the grid voltage must be known so that the converter voltages may be precisely matched to the grid voltages when no real or reactive power flow between the grid and converter is required.

The grid voltage magnitude, $|V|$, may be derived from the three-phase grid voltages, V_a, V_b and V_c, using (A.1):

$$|V| = \frac{1}{\sqrt{3}}\sqrt{V_a^2 + V_b^2 + V_c^2} \tag{A.1}$$

The grid phase, θ may be found by first applying the $\alpha\beta$ transform to the three-phase grid voltages, as in (A.2), and then applying (A.3) to the two-phase voltages, V_α and V_β.

$$\begin{pmatrix} V_\alpha \\ V_\beta \end{pmatrix} = \begin{pmatrix} 1 & -\frac{1}{2} & -\frac{1}{2} \\ 0 & \frac{\sqrt{3}}{2} & \frac{\sqrt{3}}{2} \end{pmatrix} \begin{pmatrix} V_a \\ V_b \\ V_c \end{pmatrix} \tag{A.2}$$

$$\theta = \mathrm{Arg}(V_\alpha + jV_\beta) \tag{A.3}$$

The dq transformation has been used throughout this work to simplify the control. The dq transformation translates three-phase quantities from a stationary frame of reference to a rotating frame of reference. The output of the dq transformation is two quantities describing the magnitude of the direct (in-phase) and quadrature (90° out of phase) components of a three-phase system, relative to a reference phase. Using the reference phase derived from the grid voltages, the current and voltages quantities used for control may be translated to two constant values, rather than the three time-varying values when a stationary frame of reference is used, and these will be synchronised to the grid voltages. This significantly simplifies the STATCOM control structure.

The dq transformation is described in (A.4):

$$T_{a,b,c\to d,q} = \sqrt{\frac{3}{2}} \begin{pmatrix} \cos(\theta) & \cos(\theta - \frac{2\pi}{3}) & \cos(\theta + \frac{2\pi}{3}) \\ -\sin(\theta) & -\sin(\theta - \frac{2\pi}{3}) & -\sin(\theta + \frac{2\pi}{3}) \end{pmatrix} \tag{A.4}$$

When the dq transformation is applied to the STATCOM converter currents using an accurate phase reference, the resulting d-axis current is associated only with real power flow between the converter and the grid, whereas the

q-axis current is associated only with reactive power flow. This decoupling of the d-axis and q-axis currents is critical to the control structure used in this work.

Appendix B

Impedance estimation using MATLAB

This appendix presents the MATLAB code used for impedance estimation.

The fundamental (50 Hz) grid impedance estimation using Goertzel's algorithm is performed using the code below. The code is used for both the simulated and experimental implementations of the STATCOM. The function used takes as input the three-phase voltage and current samples for the current sampling period (`V_g`, `I_g`), the present time (`t`), the calculated grid voltage phase angle (`theta_grid`) and an enable signal (`en`). The function outputs are an injection enable signal (`EnInj`), the estimated grid resistance (`Rgrid`) and the estimated grid reactance (`Xgrid`).

```
function [EnInj, Rgrid, Xgrid] ...
  = zest(theta_grid, t, Vg, Ig, en)

% first injection start time:
persistent t_start;
% frequency domain current, 80hz, 120hz:
persistent I_80 I_120;
% frequency domain voltage, 80hz, 120hz:
persistent V_80 V_120;
% resistance/reactance, 50hz:
persistent R50 X50;
% initialise variables:
if isempty(R50)
    t_start = 1.0;
    I_80 = [0+0j 0+0j 0+0j];
    I_120 = [0+0j 0+0j 0+0j];
    V_80 = [0+0j 0+0j 0+0j];
    V_120 = [0+0j 0+0j 0+0j];
    R50 = 0.1;
    X50 = 0.1;
end

% split input vectors
Va=Vg(1);
Vb=Vg(2);
Vc=Vg(3);
Ia=Ig(1);
Ib=Ig(2);
Ic=Ig(3);

if en~=0 % if enabled
 if t_start<t-0.1 % if injection cycle has finished:
```

```
  t_start=t_start+2.0; % set trigger time for next injection
  % calculate 50hz R and X
  R50=1/1.732(sum(real(V_80/I_80)) ...
    +sum(real(V_120/I_120)))/6;
  X50=1/1.732*(sum(imag(V_80/I_80)) ...
    +sum(imag(V_120/I_120)))/6;
  % scaling: 1.732 = sqrt(3)
  I_80 = [0+0j 0+0j 0+0j]; % reset vectors to zero
  I_120 = [0+0j 0+0j 0+0j];
  V_80 = [0+0j 0+0j 0+0j];
  V_120 = [0+0j 0+0j 0+0j];
 end
 if t>t_start % if the injection cycle is currently active:
  % Goertzel's algorithm at 80hz and 120hz
  exp80=exp(-2j*pi*80*(t-t_start));
  exp120=exp(-2j*pi*120*(t-t_start));
  I_80=I_80+exp80*[Ia Ib Ic];
  I_120=I_120+exp120*[Ia Ib Ic];
  V_80=V_80+exp80*[Va Vb Vc];
  V_120=V_120+exp120*[Va Vb Vc];
 end
 if (t>t_start+0.08)&&(t<t_start+0.0994375)
  % if it is time to inject:
  EnInj = 1; % enable the injection
 else
  EnInj = 0; % otherwise, disable
 end
else % if impedance estimation is disabled:
 EnInj = 0; % disable injection
 if (t_start<t-0.1) ...
   &&(theta_grid>3.1318)||(theta_grid<-3.1318)
  % reset trigger time if trigger time has passed
  t_start=t+1.0;
```

```
 end
end

% output impedance estimates
Rgrid=R50;
Xgrid=X50;
```

Wideband impedance estimation is achieved using the MATLAB function below. Wideband impedance estimation is only performed in the MATLAB workspace on data captured from simulations or experimental tests. The wideband impedance estimation algorithm takes as input a 3×1600 element matrix for both voltage and current (`v`, `i`), and outputs a frequency vector (`f`), and a complex impedance vector (`Z`).

```
function [f, Z] = estimate(v, i)

% calculate fast fourier transform of voltages and currents
fV = fft(v);
fI = fft(i);

% calculate impedance of each phase
Z3 = fV./fI;

% calculate average single phase impedance
Z = (Z3(1,:)+Z3(2,:)+Z3(3,:))./3;

% generate frequency vector (0-16khz)
f = 0:10:15990;
```

References

[1] The Institution of Engineering and Technology, "Electricity networks: Handling a shock to the system," 2013.

[2] The European Parliament and The Council of the European Union, "Directive 2009/28/ec of the european parliament and of the council," *Official Journal of the European Union*, vol. L. 140, pp. 16–62, 2006.

[3] Department of Energy and Climate Change, *Digest of United Kingdom Energy Statistics 2014*. 2014.

[4] H. Farhangi, "The path of the smart grid," *Power and Energy Magazine, IEEE*, vol. 8, pp. 18–28, January 2010.

[5] The Institution of Engineering and Technology, "What is a smart grid?," 2013.

[6] The Institution of Engineering and Technology, "Distributed generation," 2006.

[7] The Institution of Engineering and Technology, "Electricity storage," 2012.

[8] N. Jenkins, R. Allan, P. Crossley, D. Kirschen, and G. Strbac, *Embedded Generation*. IET, 2000.

[9] L. Ding, Z. Pan, W. Cong, and J. Pang, "An integrated automatic control system for distributed generation hierarchical islanding," in *Power System Technology, 2006. PowerCon 2006. International Conference on*, pp. 1–6, Oct 2006.

[10] M. R. Patel, *Introduction to Electrical Power and Power Electronics*. CRC Press, 2013.

[11] M. Ropp, J. Newmiller, C. Whitaker, and B. Norris, "Review of potential problems and utility concerns arising from high penetration levels of photovoltaics in distribution systems," in *Photovoltaic Specialists Conference, 2008. PVSC '08. 33rd IEEE*, pp. 1–6, May 2008.

[12] W. Jewell, R. Ramakumar, and S. Hill, "A study of dispersed photovoltaic generation on the pso system," *Energy Conversion, IEEE Transactions on*, vol. 3, pp. 473–478, Sep 1988.

[13] D. Garrett and S. Jeter, "A photovoltaic voltage regulation impact investigation technique. i. model development," *Energy Conversion, IEEE Transactions on*, vol. 4, pp. 47–53, Mar 1989.

[14] M. Thomson and D. G. Infield, "Impact of widespread photovoltaics generation on distribution systems," *IET Journal of Renewable Power Generation*, vol. 1, pp. 33—40, 2007.

[15] British Standards Institute, "BS EN 50160:2010; Voltage characteristics of electricity supplied by public electricity networks," December 2010.

[16] Y. Hou, J. Magnusson, G. Engdahl, and L. Liljestrand, "Impact on voltage rise of pv generation in future swedish urban areas with high pv penetration," in *Energy Conference (ENERGYCON), 2014 IEEE International*, pp. 904–911, May 2014.

[17] R. Tonkoski, D. Turcotte, and T. El-Fouly, "Impact of high pv penetration on voltage profiles in residential neighborhoods," *Sustainable Energy, IEEE Transactions on*, vol. 3, pp. 518–527, July 2012.

[18] A. Canova, L. Giaccone, F. Spertino, and M. Tartaglia, "Electrical impact of photovoltaic plant in distributed network," *Industry Applications, IEEE Transactions on*, vol. 45, pp. 341–347, Jan 2009.

[19] C. Masters, J. Mutale, G. Strbac, S. Curcic, and N. Jenkins, "Statistical evaluation of voltages in distribution systems with embedded wind

generation," *Generation, Transmission and Distribution, IEE Proceedings-*, vol. 147, pp. 207–212, Jul 2000.

[20] E. Vittal, M. O'Malley, and A. Keane, "A steady-state voltage stability analysis of power systems with high penetrations of wind," *Power Systems, IEEE Transactions on*, vol. 25, pp. 433–442, Feb 2010.

[21] P. Trichakis, P. Taylor, P. Lyons, and R. Hair, "Predicting the technical impacts of high levels of small-scale embedded generators on low-voltage networks," *Renewable Power Generation, IET*, vol. 2, pp. 249–262, December 2008.

[22] S. Eftekharnejad, V. Vittal, G. Heydt, B. Keel, and J. Loehr, "Impact of increased penetration of photovoltaic generation on power systems," *Power Systems, IEEE Transactions on*, vol. 28, pp. 893–901, May 2013.

[23] K. Kawabe and K. Tanaka, "Impact of dynamic behavior of photovoltaic power generation systems on short-term voltage stability," *Power Systems, IEEE Transactions on*, vol. PP, no. 99, pp. 1–9, 2015.

[24] M. Yagami, S. Ishikawa, Y. Ichinohe, K. Misawa, and J. Tamura, "Transient stability analysis of power system with photovoltaic systems installed," in *Renewable Power Generation Conference (RPG 2014), 3rd*, pp. 1–6, Sept 2014.

[25] Y. T. Tan and D. Kirschen, "Impact on the power system of a large penetration of photovoltaic generation," in *Power Engineering Society General Meeting, 2007. IEEE*, pp. 1–8, June 2007.

[26] M. Hossain, H. Pota, M. Mahmud, and R. Ramos, "Investigation of the impacts of large-scale wind power penetration on the angle and voltage stability of power systems," *Systems Journal, IEEE*, vol. 6, pp. 76–84, March 2012.

[27] X. Feng and T. Wei, "Study on voltage quality of distribution network with high penetration of dg," in *Power System Technology (POWERCON), 2010 International Conference on*, pp. 1–7, Oct 2010.

[28] N. Kasmas and S. Papathanassiou, "Evaluation of the voltage change factor ku for dg equipped with synchronous generators," *Renewable Power Generation, IET*, vol. 2, pp. 102–112, June 2008.

[29] J.-H. Choi and J.-C. Kim, "Advanced voltage regulation method of power distribution systems interconnected with dispersed storage and generation systems," *Power Delivery, IEEE Transactions on*, vol. 16, pp. 329–334, Apr 2001.

[30] Y. Liu, J. Bebic, B. Kroposki, J. de Bedout, and W. Ren, "Distribution system voltage performance analysis for high-penetration pv," in *Energy 2030 Conference, 2008. ENERGY 2008. IEEE*, pp. 1–8, Nov 2008.

[31] N. Daratha, B. Das, and J. Sharma, "Coordination between oltc and svc for voltage regulation in unbalanced distribution system distributed generation," *Power Systems, IEEE Transactions on*, vol. 29, pp. 289–299, Jan 2014.

[32] K. Alobeidli and M. El Moursi, "Novel coordinated secondary voltage control strategy for efficient utilisation of distributed generations," *Renewable Power Generation, IET*, vol. 8, pp. 569–579, July 2014.

[33] Y. Agalgaonkar, B. Pal, and R. Jabr, "Distribution voltage control considering the impact of pv generation on tap changers and autonomous regulators," *Power Systems, IEEE Transactions on*, vol. 29, pp. 182–192, Jan 2014.

[34] P. Douglass, R. Garcia-Valle, J. Ostergaard, and O. Tudora, "Voltage-sensitive load controllers for voltage regulation and increased load factor in distribution systems," *Smart Grid, IEEE Transactions on*, vol. 5, pp. 2394–2401, Sept 2014.

[35] S. Hietpas and M. Naden, "Automatic voltage regulator using an ac voltage-voltage converter," *Industry Applications, IEEE Transactions on*, vol. 36, pp. 33–38, Jan 2000.

[36] M. Vaziri, M. Afzal, M. Zarghami, A. Yazdani, S. Vadhva, and F. Tavatli, "Voltage impacts of dg on distribution grid with voltage regulators and svcs," in *Green Technologies Conference, 2013 IEEE*, pp. 322–329, April 2013.

[37] FACTS Terms & Definitions Task Force, "Proposed terms and definitions for flexible ac transmission system (facts)," *Power Delivery, IEEE Transactions on*, vol. 12, pp. 1848–1853, Oct 1997.

[38] K. Tsunedomi, S. Tamura, T. Omori, Y. Imazu, T. Sodeyama, D. Cheung, M. Parr, and S. Gough, "Effectiveness of d-svc on rural networks," in *Electricity Distribution (CIRED 2013), 22nd International Conference and Exhibition on*, pp. 1–4, June 2013.

[39] W. Wong, D. Osborn, and J. McAvoy, "Application of compact static var compensators to distribution systems," *Power Delivery, IEEE Transactions on*, vol. 5, pp. 1113–1120, Apr 1990.

[40] J. C. Das, *Power System Analysis: Short Circuit Load Flow and Harmonics*. CRC Press, 2011.

[41] D. Kulkarni and G. Udupi, "Optimized operation of svc for minimal harmonics at distribution level," in *Information and Communication Technology in Electrical Sciences (ICTES 2007), 2007. ICTES. IET-UK International Conference on*, pp. 469–474, Dec 2007.

[42] A. Mahyavanshi, M. A. Mulla, and R. Chudamani, "Reactive power compensation by controlling the DSTATCOM," *International Journal of Emerging Technology and Advanced Engineering*, vol. 2, no. 11, pp. 212–218, 2012.

[43] W. Freitas, E. Asada, A. Morelato, and W. Xu, "Dynamic improvement of induction generators connected to distribution systems using a dstatcom," in *Power System Technology, 2002. Proceedings. PowerCon 2002. International Conference on*, vol. 1, pp. 173–177 vol.1, Oct 2002.

[44] P. Mitra and G. Venayagamoorthy, "Real time implementation of an artificial immune system based controller for a dstatcom in an electric ship power system," in *Industry Applications Society Annual Meeting, 2008. IAS '08. IEEE*, pp. 1–8, Oct 2008.

[45] R. Grunbaum, "Svc light: a powerful means for dynamic voltage and power quality control in industry and distribution," in *Power Electronics and Variable Speed Drives, 2000. Eighth International Conference on (IEE Conf. Publ. No. 475)*, pp. 404–409, 2000.

[46] J. Clouston and J. Gurney, "Field demonstration of a distribution static compensator used to mitigate voltage flicker," in *Power Engineering Society 1999 Winter Meeting, IEEE*, vol. 2, pp. 1138–1141 vol.2, Jan 1999.

[47] B. Muni, S. Rao, J. Vithal, S. Saxena, S. Lakshminarayana, R. Das, G. Lal, and M. Arunachalam, "Development of $\pm$ 500 kVAR DSTATCOM for distribution utility and industrial applications," in *TENCON 2003. Conference on Convergent Technologies for the Asia-Pacific Region*, vol. 1, pp. 278–282 Vol.1, Oct 2003.

[48] C. Hochgraf and R. Lasseter, "Statcom controls for operation with unbalanced voltages," *Power Delivery, IEEE Transactions on*, vol. 13, pp. 538–544, Apr 1998.

[49] H. F. Wang, "Application of damping torque analysis to statcom control," *Electrical power and energy systems, International journal of*, vol. 22, pp. 197–204, 2000.

[50] A. Safari, A. Ahmadian, and M. A. A. Golkar, "Controller design of statcom for power system stability improvement using honey bee mating optimization," *Journal of Applied Research and Technology*, vol. 11, pp. 144–155, 2013.

[51] G. Kumaravel and C. Kumar, "Design of self tuning pi controller for statcom using bats echolocation algorithm based neural controller," in *Advances in Engineering, Science and Management (ICAESM), 2012 International Conference on*, pp. 276–281, March 2012.

[52] Y. Xu and F. Li, "Adaptive pi control of statcom for voltage regulation," in *PES General Meeting & Conference Exposition, 2014 IEEE*, pp. 1–10, July 2014.

[53] H. Wang, "Phillips-heffron model of power systems installed with statcom and applications," *Generation, Transmission and Distribution, IEE Proceedings-*, vol. 146, pp. 521–527, Sep 1999.

[54] W. Heffron and R. Phillips, "Effect of a modern amplidyne voltage regulator on underexcited operation of large turbine generators [includes discussion]," *Power Apparatus and Systems, Part III. Transactions of the American Institute of Electrical Engineers*, vol. 71, pp. 692–697, Jan 1952.

[55] K. Bollinger and R. Lalonde, "Tuning synchronous generator voltage regulators using on-line generator models," *Power Apparatus and Systems, IEEE Transactions on*, vol. 96, pp. 32–37, Jan 1977.

[56] A. Ibrahim, B. Hogg, and M. Sharaf, "Self-tuning automatic voltage regulators for a synchronous generator," *Control Theory and Applications, IEE Proceedings D*, vol. 136, pp. 252–260, Sep 1989.

[57] J. Finch, K. Zachariah, and M. Farsi, "Turbogenerator self-tuning automatic voltage regulator," *Energy Conversion, IEEE Transactions on*, vol. 14, pp. 843–848, Sep 1999.

[58] P. Hart, "An experimental study of short-circuit currents on a low-voltage system," *Industry Applications, IEEE Transactions on*, vol. 24, pp. 940–946, Sep 1988.

[59] Z. Staroszczyk and K. Mikolajuk, "Time-dependent power systems impedance-interpretation and measuring problems," in *Instrumentation and Measurement Technology Conference, 1999. IMTC/99. Proceedings of the 16th IEEE*, vol. 2, pp. 795–800 vol.2, 1999.

[60] Z. T. Staroszczyk, "Smart grids instrumentation-obtaining subgrid

impedance information," *International Transactions on Electrical Energy Systems*, 2015.

[61] A. Knop and F. Fuchs, "High frequency grid impedance analysis by current injection," in *Industrial Electronics, 2009. IECON '09. 35th Annual Conference of IEEE*, pp. 536–541, Nov 2009.

[62] J. Wang, M. Sumner, D. W. P. Thomas, and R. D. Geertsma, "Fast dault detection and location for a marine power ststem using system power converters and active impedance estimation," in *Power Electronics, Machines and Drives (PEMD), 4th IET Conference on*, April 2008.

[63] M. Sumner, A. Abusorrah, D. Thomas, and P. Zanchetta, "Improved power quality control and intelligent protection for grid connected power electronic converters, using real time parameter estimation," in *Industry Applications Conference, 41st IAS Annual Meeting*, (Tampa, FL,), pp. 1709–1713, 2006.

[64] P. D. Hopewell, N. Jenkins, and A. D. Cross, "Loss-of-mains detection for small generators," *IEE Proc.-Electric Power Applications*, vol. 143, no. 3, pp. 1350–2352, 1996.

[65] L. Asiminoaei, R. Teodorescu, F. Blaabjerg, and U. Borup, "A digitally controlled pv-inverter with grid impedance estimation for ens detection," *IEEE Transactions on Power Electronics*, vol. 20, no. 6, pp. 1480–1490, 2005.

[66] D. Crevier and A. Mercier, "Estimation of higher frequency network equivalent impedances by harmonic analysis of natural waveforms," *IEEE Transactions on Power Apparatus and Systems*, vol. 97, no. 2, pp. 424–431, 1978.

[67] D. Rizy, E. Gunther, and M. McGranaghan, "Transient and harmonic voltages associated with automated capacitor switching on distribution systems," *Power Systems, IEEE Transactions on*, vol. 2, pp. 713–723, Aug 1987.

[68] A. de Oliveira, J. C. de Oliveira, and J. W. Resende, "Practical approaches for ac system harmonic impedance measurements," *IEEE Transactions on Power Delivery*, vol. 6, no. 4, pp. 1721–1726, 1991.

[69] A. Morched and P. Kundur, "Identification and modelling of load characteristics at high frequencies," *Power Systems, IEEE Transactions on*, vol. 2, pp. 153–159, Feb 1987.

[70] A. Girgis and R. McManis, "Frequency domain techniques for modeling distribution or transmission networks using capacitor switching induced transients," *Power Delivery, IEEE Transactions on*, vol. 4, pp. 1882–1890, Jul 1989.

[71] M. Nagpal, W. Xu, and J. Sawada, "Harmonic impedance measurement using three-phase transients," *IEEE Transactions on Power Delivery*, vol. 13, no. 1, pp. 272–277, 1998.

[72] M. Bridgeman, N. MacLeod, S. Tennakoon, and R. Morrison, "The resonance damping effect associated with linear shunt loads and single-phase converters," in *Harmonics and Quality of Power, 2000. Proceedings. Ninth International Conference on*, vol. 2, pp. 535–540 vol.2, 2000.

[73] E. W. Palmer and G. F. Ledwich, "Three phase harmonic modelling of power system loads," *IEE Proc.-C Generation, Transmission and Distribution*, vol. 140, no. 3, pp. 206–212, 1993.

[74] C. Xie, S. Tennakoon, R. Langella, D. Gallo, A. Testa, and A. Wixon, "Harmonic impedance measurement of 25 kv single phase ac supply systems," in *Harmonics and Quality of Power, IEEE Ninth international conference on,*, 2000.

[75] K. Jia, D. Thomas, and M. Sumner, "A new single-ended fault-location scheme for utilization in an integrated power system," *Power Delivery, IEEE Transactions on*, vol. 28, pp. 38–46, Jan 2013.

[76] K. Jia, D. Thomas, and M. Sumner, "A new double-ended fault-location scheme for utilization in integrated power systems," *Power Delivery, IEEE Transactions on*, vol. 28, pp. 594–603, April 2013.

[77] M. B. Harris, A. W. Kelley, J. P. Rhode, and M. E. Baran, "Instrumentation for measurement of line impedance," in *IEEE Proc. of Ninth Annual Applied Power Electronics Conference and Exposition*, pp. 887–893, 1994.

[78] J. P. Rhode, A. W. Kelley, and M. E. Baran, "Line impedance measurement: A nondisruptive wideband technique," in *Industry Applications Conference, Thirtieth IAS annual meeting*, pp. 2233–2240, 1995.

[79] J. P. Rhode, A. W. Kelley, and M. E. Baran, "Complete characterisation of utilization-voltage power system impedance using wideband measurement," in *Industrial and Commercial Power Systems Technical Conference*, pp. 123–130, 1996.

[80] A. V. Timbus, R. Teodorescu, F. Blaabjerg, and U. Borup, "Online grid measurement and ens detection for pv inverter running on highly inductive grid," *IEEE Power Electronics Letters*, vol. 2, no. 3, pp. 77–82, 2004.

[81] L. Asiminoaei, R. Teoderescu, and F. Blaabjerg, "A new method of on-line grid impedance estimation for pv inverter," in *19th Annual IEEE Applied Power Electronics Conference and Exposition*, pp. 1527–1533, 2004.

[82] L. Asiminoaei, R. Teodorescu, F. Blaabjerg, and U. Borup, "Implementation and test of an online embedded grid impedance estimation technique for pv inverters," *IEEE Transactions on Industrial Electronics*, vol. 52, no. 4, pp. 1136–1144, 2005.

[83] A. V. Timbus, R. Teodorescu, F. Blaabjerg, and U. Borup, "Online grid impedance measurement suitable for multiple pv inverters running in parallel," in *Twenty-First Annual IEEE Applied Power Electronics Conference and Exposition*, pp. 907–911, 2006.

[84] M. B. Hughes, R. W. Leonard, and T. G. Martinich, "Measurement of power system subsynchronous driving point impedance and comparison with computer simulations," *IEEE Transactions on Power Apparatus and Systems*, vol. 103, no. 3, pp. 619–630, 1984.

[85] Z. Staroszczyk, "Problems in real-time wide-band indentification of power systems," in *IEEE Instrumentation and Measurement Technology Conference*, (St Paul, Minnesota,), pp. 779–784, 1998.

[86] W. Wang, E. E. Nino, and W. Xu, "Harmonic impedance measurement using a thyristor-controlled short circuit," *IET Generation, Transmission and Distribution*, vol. 1, no. 5, pp. 707–713, 2007.

[87] B. Palethorpe, M. Sumner, and D. W. P. Thomas, "System impedance measurement for use with active filter control," in *Power Electronics and Variable Speed Drives, Eighth International Conference on*, IEE, 2000.

[88] M. Sumner, B. Palethorpe, D. Thomas, P. Zanchetta, and M. C. D. Piazza, "Estimation of power supply harmonic impedance using a controlled voltage disturbance," in *Power Electronics Specialist Conference, IEEE 32nd Annual*, 2001.

[89] M. Sumner, B. Palethorpe, D. Thomas, P. Zanchetta, and M. di Piazza, "A technique for power supply harmonic impedance estimation using a controlled voltage disturbance," *IEEE Transactions on Power Electronics*, vol. 17, no. 2, pp. 101–109, 2002.

[90] M. Sumner, B. Palethorpe, and D. W. P. Thomas, "Impedance measurement for improved power quality – part 1: the measurement technique," *IEEE Transactions on Power Delivery*, vol. 19, no. 3, pp. 1442–1448, 2004.

[91] M. Sumner, B. Palethorpe, and D. W. P. Thomas, "Impedance measurement for improved power quality – part 2: a new technique for stand-alone active shunt filter control," *IEEE Transactions on Power Delivery*, vol. 19, no. 3, pp. 1457–1463, 2004.

[92] P. García, J. M. Guerrero, J. García, Ángel Navarro-Rodríguez, and M. Sumner, "Low frequency signal injection for grid impedance estimation in three phase systems," in *Energy Conversion Congress and Exposition (ECCE), 2014 IEEE*, 2014.

[93] S. Neshvad, S. Chatzinotas, and J. Sachau, "Online determination of grid impedance spectrum through pseudo-random excitation of a pulse width modulator," in *International Conference on Renewable Energies and Power Quality (ICREPQŠ14)*, 2014.

[94] R. Mutagi, "Pseudo noise sequences for engineers," *Electronics Communication Engineering Journal*, vol. 8, pp. 79–87, April 1996.

[95] U. Tewari, S. Neshvad, D. Goldbach, and J. Sachau, "Verification and implementation of pseudo-random-binary-sequences for online determination of grid impedance spectrum," in *International Conference on Renewable Energies and Power Quality (ICREPQŠ15)*, 2015.

[96] M. P. Kaźmierkowski, F. Blaabjerg, and R. Krishnan, *Control in Power Electronics: Selected Problems*. Academic Press, 2002.

[97] M. Prodanović and T. Green, "Control and filter design of three-phase inverters for high power quality grid connection," *Power Electronics, IEEE Transactions on*, vol. 18, pp. 373–380, Jan 2003.

[98] Energy Networks Association, "Engineering recommendation g83/2," August 2012.

[99] T. C. Green, R. W. Silversides, and Tüth, "Power electronics in distribution system management," in *HubNet Position Paper Series*, 2015.

[100] N. Dinic, B. Fox, D. Flynn, L. Xu, and A. Kennedy, "Increasing wind farm capacity," *Generation, Transmission and Distribution, IEE Proceedings-*, vol. 153, pp. 493–498, July 2006.

[101] E. Lourenco, T. Loddi, and O. Tortelli, "Unified load flow analysis for emerging distribution systems," in *Innovative Smart Grid Technologies Conference Europe (ISGT Europe), 2010 IEEE PES*, pp. 1–7, Oct 2010.

[102] I. of Electrical and E. Engineers, "Ieee recommended practice for electric power systems in commercial buildings (ieee std 241-1990)," December 1990.

[103] L. Freris and D. Infield, *Renewable Energy in Power Systems*. John Wiley & Sons, 2008.

[104] J.-W. Kim, H.-S. Choi, and B. H. Cho, "A novel droop method for converter parallel operation," *Power Electronics, IEEE Transactions on*, vol. 17, pp. 25–32, Jan 2002.

[105] Q.-C. Zhong, "Robust droop controller for accurate proportional load sharing among inverters operated in parallel," *Industrial Electronics, IEEE Transactions on*, vol. 60, pp. 1281–1290, April 2013.

[106] Y. Zhu, F. Zhuo, B. Liu, and H. Yi, "An enhanced load power sharing strategy for low-voltage microgrids based on inverse-droop control method," in *Power Electronics Conference (IPEC-Hiroshima 2014 - ECCE-ASIA), 2014 International*, pp. 3546–3552, May 2014.

[107] National Grid Electricity Transmission Plc, "The grid code," 2014.

[108] Agilent Technologies, "The fundamentals of signal analysis (application note 243)," 1994.

[109] G. Goertzel, "An algorithm for the evaluation of finite trigonometric series," in *The American Mathematical Monthly*, vol. 65, 1958.

[110] V. Diana, M. Sumner, P. Zanchetta, and M. Marinelli, "Non-invasive power system impedance monitoring for improved power quality," in *Power Electronics, Machines and Drives, 2004. (PEMD 2004). Second International Conference on (Conf. Publ. No. 498)*, pp. 265–268, 2004.

[111] Triphase NV, "Pm90f60c 90 kw power module with 2 x 3-phase ac/dc interface." Webpage, 2013. *http://www.triphase.be/products/PM/90/F60*, Accessed 27 May 2015.

[112] Hammond Power Solutions, *HPS Centurion R Reactors*.

[113] MTE Corporation, *RL Line/Load Reactors: Selection table, technical details & product application guide*, 2008.

[114] Marcus Transformer of Canada Ltd, *Three phase line reactor type MLR open style*.

[115] Siemens AG, *Totally Integrated Power*. Siemens AG, 2nd ed., 2005.

[116] T. Haggis, *Network Design Manual*. EOn Central Networks, 2006.

[117] British Standards Institute, "Bs 5467:1997+a3:2008 electric cables. thermosetting insulated, armoured cables for voltages of 600/1000 v and 1900/3300 v," December 2010.

[118] R. Davies, A. Fazeli, S. P. Oe, M. Sumner, M. Johnson, and E. Christopher, "Energy management research using emulators of renewable generation and loads," in *Innovative Smart Grid Technologies (ISGT), 2013 IEEE PES*, pp. pp.1–6, February 2013.

[119] Newton's 4th Ltd, "Lcr active head and impedance analysis interface." Webpage., 2010. *http://www.newtons4th.com/wp-content/uploads/2010/02/LCRActiveHead-IAI1.pdf*, Accessed 1 June 2015.

[120] Gendrive Ltd, "Totus wind product information." Webpage, 2005. *http://www.gendrive.co.uk/products/* , Accessed June 2013 (Currently unavailable).

[121] J. M. Gers and E. J. Holmes, *Protection of Electricity Distribution Networks*. The Institute of Engineering and Technology, 2 ed., 2004.

[122] P. C. Jayamaha, *Energy Storage for Frequency Support in Weak Grids*. PhD thesis, University of Nottingham, 2014.

[123] A. T. Agbedahunsi, *Frequency Control for Microgrids using Enhanced STATCOM and Supercapacitor Energy Storage*. PhD thesis, University of Nottingham, 2013.

[124] Mathworks, "Siso design tool." Webpage, 2015. *http://uk.mathworks.com/help/control/getstart/siso-design-tool.html*, Accessed 2 June 2015.

[125] B. Palethorpe, *A novel system Impedance measurement for power system Analysis and improvement in power quality*. PhD thesis, University of Nottingham, 2002.